

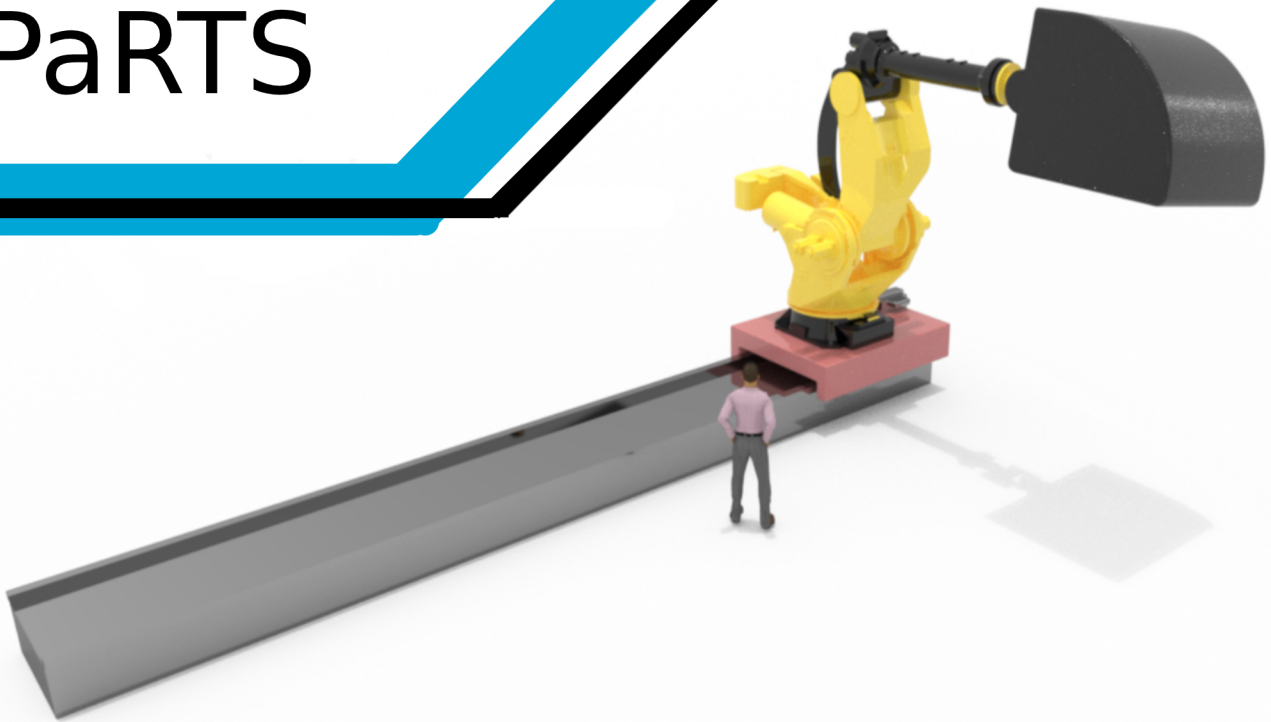
# Final Report

Flight Simulator for Upset Prevention & Recovery Training

## DSE Group 11

June 29, 2020

# UPaRTS





# Final Report

## Flight Simulator for Upset Prevention & Recovery Training

by

DSE Group 11

under guidance of

Tutor Olaf Stroosma  
Coaches Sung-Hoon Mok  
Xiaodong Li

Student number	Surname, Given name
4367138	Bakker, Roemer
4656970	Bettini, Andrea
4545788	Bouwmeesters, Max
4663217	El-Kebir, Hamza
4651715	Hoefnagel, Kaj
4537882	Kho, Kevin
4662792	Origer, Sebastien
4645626	Tuna, Afonso
4540050	Weijers, Jacques
4663861	van Woerkom, Quirijn

*This document has been issued on June 29, 2020.*

# Executive Overview

In 2019, the International Air Transport Association (IATA) issued a report on Loss of Control In-flight (LOC-I), establishing that LOC-I is the leading cause of aviation-related fatalities. Recent fatal accidents such as Air France 447 and Turkish Airline 1951 show that LOC-I remains a problem in present-day aviation. The prevalence of these accidents serves to show that pilots are ill-prepared to deal with LOC-I, as attested by the IATA report. This proves that there is indeed a material need to provide pilots with the proper means to train in prevention of, and recovery from aircraft upsets.

To address this need, this project ventured to develop a novel solution for upset prevention and recovery training (UPRT). Previous project reports have focused on identifying requirements and developing a base architecture. The present report provides a comprehensive overview of the conceptual design, with analyses on training systems and individual subsystems. With this, the necessary groundwork is laid to show that this endeavour is indeed feasible within the stakeholder requirements.

## Previous Reports

In previous reports, top-level stakeholder requirements have been analysed and complemented with additional key requirements. From these requirements, a functional analysis yielded a number of essential functions, allowing additional requirements to be derived, as established in the baseline report[1]. These set the stage for three design candidates: a Stewart platform, a centrifuge, and a robotic arm. Based on a comprehensive trade-off in the baseline report[2], the robotic arm was deemed the best solution.

## Market Analysis

To determine if this simulator is a viable product market-wise, a market analysis was performed. The target market of this simulator will be airliners and training centres which need to train pilots for the A320 family. Based on research on the amount of pilots there will be a yearly simulator demand between 7 and 19. In terms of competition, regular simulators are currently the biggest threat, hence a hard push for regulation change and/or achieving Level D certification is recommended. A SWOT analysis was performed to find the Strengths, Weaknesses, Opportunities and Threats of this project; while this design has many strengths, the biggest weakness was identified to be the possible lack of a Level D certification. After a cost analysis, a price was estimated with a positive return of investment. In the end it is concluded that the simulator is viable in the market.

## Training Systems

To set the framework on the training capabilities of the system, an in-depth study into training systems was carried out. Loss of control in-flight is the leading cause of fatalities in aviation, and such scenarios are most often induced due to improper training or the application of incorrect procedures. To understand why pilot skills were lacking in these incidents, a critical look was taken at the current regulations for pilot training, in particular UPRT. From this study, it was found that training gaps are still present in current regulation, in particular considering UPRT continuity and the effect of startle and surprise on pilot performance. To bridge these gaps in the system, some training objectives were set, namely the inclusion of UPRT scenarios in the regular proficiency checks undertaken by pilots, and the introduction of distraction elements during the simulator training sessions. In accordance with these objectives, a training envelope for the system was drafted, featuring several key UPRT scenarios, such as stall at different altitudes and configurations, as well as the within-the-envelope scenarios carried out during proficiency checks, as required by the regulations. To support the training objectives, the system ships with proof-of-concept training guides, both for the instructor as well as the pilot, ensuring the system capabilities are fully explored. To offer a consolidated system, providing operators with the capability of performing proficiency checks along with UPRT exercises, the system will be required to achieve Level D qualification or equivalent. For this to occur, due diligence must be carried out, ensuring the applicable acceptable means of compliance are adhered to. While this is not pursued at this stage in the project, ensuring such a qualification is obtained will be a key part of the post-DSE activities.

## Structures

The structural analysis mainly revolved around the structural feasibility given the budgets and requirements. First, the structural functions and requirements are derived, followed by updated

internal- and external views of the concept to aid later analysis.

Before a structural analysis can be performed, the exact forces at the base and end of the robot arm first need to be known. These are found by using the Denavit-Hartenberg convention to define several frames along the robot arm. These can then be used to convert joint angles, velocities, accelerations and inertia to total accelerations and forces. These inputs are largely obtained from the kinematics department, except for the inertias, which are estimated. Since the kinematics depend on the cabin mass, the structural cabin mass is found using an iterative process. The structural cabin mass includes two parallel hollow aluminium beams, a carbon fibre outer shell and a structure to connect to the robot arm end effector. It is also confirmed that the standard end effector of the robot arm is able to support the robot arm under all loading conditions. Additionally, based on the critical forces and moments at the base of the robot arm, the floor loading is found.

The cabling to both the external motion system and the cabin is also considered; both in terms of power and in terms of data handling. A one-degree-of-freedom cable carrier to the carriage and two three-degrees-of-freedom cable carriers to the cabin are found to be sufficient. Reliability and safety are ensured by safety factors and frequent inspections. Daily test runs and monthly maintenance can be performed within the one hour of downtime per day, yearly maintenance is expected to fit within the two weeks of yearly downtime. Furthermore, a number of safety features such as emergency buttons, an emergency computer and a backup battery are implemented.

Finally, the code used for the structural analyses is verified by means of hand calculations and future validation plans are presented. Additionally, the sensitivity of the numbers found is analysed.

## **Kinematics**

Since the vestibular cueing requirements have a significant bearing on mission success, as well as on the final choice of hardware, the motion cueing system was sized through an analysis of the motion cueing hardware; at the centre of this effort lies the robotic arm kinematics. To enable this analysis, a number of cueing requirements were derived from aeromechanical considerations, which included an analysis of simulation and flight data. The motion cueing system was previously determined to be comprised of a linear rail, a robotic arm, and a sustained motion cueing seat (or g-seat). These were then analysed to deduce their motion capabilities, leading to the conclusion that the top-level requirements are indeed met.

Then, to study the feasibility of online motion planning, a thorough analysis of a potential motion cueing framework was conducted. This led to a firmly grounded affirmation of the feasibility of a real-time motion cueing algorithm that takes advantage of all motion cueing capabilities afforded by the linear rail, robotic arm, and g-seat. This analysis was complemented by an in-depth verification and sensitivity analysis, as well as recommendations for future validation efforts.

## **Aural Cueing**

During the design of the aural system a distinction was made between two main functions: providing the flight crew with flight sounds and allowing communication between the pilot and the instructor, ATC and the offboard pilot. The flight sounds, among other engine noise, airframe noise and also warning sounds, will be provided to the flight crew with a multi-speaker sound system which is able to source the audio from multiple locations. The flight crew will also wear headsets for communication. All the different components of the aural system will be connected by Ethernet cables which results in a system that is called Dante (Digital audio network through Ethernet). The use of Dante ensures a high-quality, low latency, multiple channel aural system that mainly consist of off-the-shelf components and that can easily be extended or upgraded.

## **Visual Cueing**

In terms of visual cueing the high-end VR market was investigated for options. Mass and power were identified as insignificant parameters in case of the VR headset. As a result, cost budget and visual fidelity, resolution, field-of-view and refresh rate were the defining parameters in the comparison of the different high-end VR headsets: the latter of these parameters were a result of motion sickness and simulation immersiveness considerations, which led to the Pimax 8K PLUS as choice for the VR glasses. Some uncertainty still remains with regards to Level D certification requirements and instrument legibility. Pursuing Level D certification would require a change in the acceptable means of compliance which is unlikely, whereas improving legibility would require a higher amount of pixels-per-degree (PPD), which may require a different headset. The latter, while possible, does not have any ramifications for the remainder of the design due to the relatively low weight, power and cost required for each of the headsets in comparison to the other subsystems. Hence, the sizing results for the visual cueing system stand firm.

## Haptic Cueing

As for haptic cueing, based on requirements flowing forth from the choice of visual system, a pair of motion capturing gloves were selected (the Manus Prime One). This choice was motivated largely by the need for millimetre-level precision to allow for interaction with instruments and also the refresh rate. The latter was influenced by the risk of motion sickness that can result from a mismatch between the proprioceptive and visual senses, which can be avoided through use of a sufficiently high refresh rate. To allow for operation as in the real aircraft, a number of essential instruments is included, such as full replicas of the throttle lever, sidestick and pedals, as well as a number of instrument panels. These results hold firm except for a possible change of preferred aircraft family: were the customer to decide that they prefer a Boeing over an Airbus system, the consequential implementation of control loading could, through an increase in mass, affect other systems.

## System Overview

With all the subsystems now defined, it is possible to present an overview of the system as a whole. The system will have three main components: the onboard cabin, the IOS and the off-board cabin. The onboard cabin is mounted to the robotic arm and the rail system and will be located in the middle of the facility. The IOS, located in the corner of the facility, will allow the instructor/operator to control the simulator and communicate with the flight crew. Finally, The offboard cabin, which houses the secondary pilot, will be a copy of the onboard cabin, but will not include the robotic arm, the railsystem and the g-seat and will be located next to the IOS.

Both the (onboard) mass and power estimations are well within the budgets which leaves enough space for future design iterations and also leads to compliance of several requirements. Furthermore, the CO<sub>2</sub> emission reduction compared to in-aircraft training is currently estimated on 89%, which complies with the minimum of 80% set by the customer. The key requirements, training pilots for upset prevention and recovery, are very close to be verified due to the extensively defined training curriculum and the subsystems providing the motion, visual, haptic and aural cues. Validation will be performed when the system has been prototyped or fully sized and will, therefore, be included in the post-DSE activities.

Finally, a sensitivity analysis was performed to get an idea on how sensitive the simulator is to design- and requirement changes. From this analysis can be concluded that the simulator is not very sensitive in terms of cost, weight or power, but is sensitive relative to the (equivalent to) EASA level D certification, since this will lead to design and objective changes as discussed earlier.

## System Logistics

To ensure the design can be translated into a manufacturable, feasible product, the system logistics must be taken into account. In terms of manufacturability, a production plan was drafted, detailing the necessary steps, and their timeline, to build a full product. Integrating the system into the customer's premises is also of high importance, given the specificity of the equipment, and so certain preparations must be made in that sense. Ultimately, the system components shall be built in different locations, according to the chosen suppliers, with the final product being assembled and integrated at the client's location. Once the system is assembled, integration into the customer's operations is facilitated due to some similarities with conventional FSTD's, but will still require adequate personnel training and adaptation of training materials. Given standard training scenarios, the training throughput of the system is expected to be comparable to that of conventional systems. Maintenance and upgradability are also considered, with regular checks and repairs being carried out daily, and larger changes in bi-yearly downtime. Finally, end-of-life processes were drafted, with a special focus on repurposing and recycling, adhering to the project's environmental sustainability goals.

## Sustainability

The sustainability department took into account all concerns related to environment, economic and social sustainability which had been compiled over the course of the project. The process of identifying, measuring and mitigating sustainability-related issues has been embedded in a continuous, integral and intrinsic process. Through the described process the requirements, goals and concerns related to sustainability were carefully analysed which triggered design changes and choices throughout the team. It can thus confidently be said that the main requirements in terms of sustainability can be met: in particular, the 80% CO<sub>2</sub>-reduction goal is satisfied with a considerable margin. It can be concluded that there is then confidence that no sustainability concerns are left at risk of remaining unaddressed at this stage of the design.

---

## **Risk Assessment**

The risk department performed an iteration which yielded the current, most relevant risks. Processing these risks has been performed in a continuous matter throughout this project by consulting each department and discussing the risks that emerged and the ones which were mitigated through design choices. The risk of negative pilot training (R-S-1) persisted since the early start of this project. Hence, it is likely to be considered a major risk until further design stages. The training curriculum will be restricted in such a way that high fidelity motion can be guaranteed and experienced pilots will test the flight simulator to assure representative training. The other risks have already been accounted for and mitigation solutions exist such that none of them pose a high threat to the project. Alongside the previously identified risks, new risks have emerged in this phase: those have been identified and have been given priority in the post-DSE phase.

## **Post DSE**

Post DSE describes the future trajectory of the product to be able to get it into service. Four phases are described for a total of 134 weeks. These phases are the detailed design phase, testing phase, production phase and the delivery phase. During these phases the design aspect and the business aspect are tackled. The design phase mainly describe the goals and actions that must be taken to create the desired product while the business aspect looks more at the financial and administrative side. The main goal of the business aspect is to make sure that the design aspect can continue unhindered by providing the necessary monetary tools and services.

## **Conclusion**

In conclusion, this project has endeavoured to design a market-viable flight simulator training device capable of meeting an ever-growing need for upset prevention and recovery training. This project objective was met, as shown in this report, by way of a rigorous conceptual design process, taking into account marketability, training systems, cueing, and structural and environmental safety. For future work, while there remain tasks that need to be completed, it is safe to conclude that a solid foundation has been laid from which the mission need can be served in the future.

# Acknowledgements

We are extremely grateful to everyone who contributed to this project. In particular, we would like to thank Dr Sunjoo Advani and dr. ir. Mark Wentink for generously sharing their time and expertise to answer our questions and attend our reviews. We would also like to thank Anique Altena for answering all our questions and providing extensive feedback from the project management and systems engineering point of view. Furthermore, we would like to thank our coaches Xiaodong Li, MSc and Dr Sung-Hoon Mok for attending all our meetings, answering questions and providing extensive feedback. Additionally, we would like to thank the Design Synthesis Exercise organising committee for organising a smooth, online exercise.

Finally, our greatest gratitude goes to our principle tutor ir. Olaf Stroosma, who has kindly allocated a great deal of his time to: set up this project, meet with us multiple times per week, respond to our emails, provide feedback on our draft reports, grade our final reports and attend our review sessions.

# Contents

<b>1</b>	<b>Introduction</b>	<b>2</b>
1.1	Changes	2
<b>2</b>	<b>Lightweight Concept Second Iteration</b>	<b>3</b>
2.1	Previous Concept Analysis	3
2.2	Motion System Iteration Possibilities	4
2.3	Iteration Selection	8
2.4	Updated Budgets	9
<b>3</b>	<b>Financial and Market Analysis</b>	<b>12</b>
3.1	Target Market	12
3.2	Market Size	12
3.3	Competition	13
3.4	SWOT Analysis	14
3.5	Cost estimate	16
3.6	Return on investment	19
<b>4</b>	<b>Training Systems</b>	<b>20</b>
4.1	An overview on pilot training	20
4.2	Training breakdown	25
4.3	Training guides	28
4.4	Final considerations	30
<b>5</b>	<b>Subsystem Design</b>	<b>31</b>
5.1	Functional Analysis Overview	31
5.2	Updated System Interface Diagrams	31
5.3	Structural Characteristics	45
5.4	Aeromechanics	65
5.5	Robotic Motion Kinematics	77
5.6	Aural Cueing	92
5.7	Visual Cueing	98
5.8	Haptic Cueing	103
5.9	System Overview	108
<b>6</b>	<b>System Logistics</b>	<b>114</b>
6.1	Production Plan	114
6.2	Operations and Logistics	116
<b>7</b>	<b>Sustainability</b>	<b>121</b>
7.1	Implementation of Sustainability	121
7.2	Contribution of the product to Sustainability	122
<b>8</b>	<b>Technical Risk Assessment</b>	<b>127</b>
8.1	Framework for Risk Management	127
8.2	Risk requirement compliance	128
8.3	Risk Analysis	130
<b>9</b>	<b>Future Plans</b>	<b>134</b>
9.1	Design Considerations	134
9.2	Business Considerations	134
9.3	Future Project Logic	134
<b>10</b>	<b>Conclusion</b>	<b>137</b>
<b>11</b>	<b>Recommendations</b>	<b>138</b>
	<b>Bibliography</b>	<b>139</b>

# Acronyms

<b>ADIRU</b> Air Data Inertial Reference Unit.	<b>NASA</b> National Aeronautics and Space Administration.
<b>AOA</b> Angle of attack.	<b>NLR</b> Nederlands Lucht- en Ruimtevaartcentrum; Netherlands Aerospace Centre.
<b>AR</b> Augmented reality.	<b>NONONE</b> Not equal to one.
<b>ASI</b> Airspeed Indicator.	<b>OAT</b> Outside Air Temperature.
<b>ATC</b> Air Traffic Control.	<b>OEM</b> Original Equipment Manufacturer.
<b>ATO</b> Approved Training Organisation.	<b>PF</b> Pilot Flying.
<b>ATPL(A)</b> Airline Transport Pilot License (Aircraft).	<b>PFD</b> Primary Flight Display.
<b>AvGas</b> Aviation Gasoline.	<b>PM</b> Pilot Monitoring.
<b>CAT</b> Clear Air Turbulence.	<b>PPD</b> Pixels Per Degree.
<b>CFD</b> Computational Fluid Dynamics.	<b>PPL</b> Private Pilot License.
<b>CG</b> Centre of gravity.	<b>QNH</b> Altimeter pressure setting.
<b>CPL</b> Commercial Pilot License.	<b>QRH</b> Quick Reference Handbook.
<b>DC</b> Direct Current.	<b>RAMS</b> Reliability, Availability, Maintainability, Manufacturability, and Safety.
<b>DLR</b> Deutsches Zentrum für Luft- und Raumfahrt; German Aerospace Centre.	<b>RBM</b> Risk before mitigation.
<b>DOF</b> Degree-of-freedom.	<b>RBS</b> The DLR Robotic Motion Simulator.
<b>EASA</b> European Aviation Safety Agency.	<b>RDT</b> Requirement Discovery Tree.
<b>EE</b> End Effector.	<b>RMS</b> Root Mean Square.
<b>FCOM</b> Flight Crew Operating Manual.	<b>ROI</b> Return on Investment.
<b>FDR</b> Flight Data Recorder.	<b>RWM</b> Risk with mitigation.
<b>FFS</b> Full Flight Simulator.	<b>SD</b> Spatial Disorientation.
<b>FPS</b> Frames Per Second.	<b>SEP</b> Safety & Emergency Procedures.
<b>FSTD</b> Flight Simulation Training Device.	<b>SOP</b> Standard Operating Procedures.
<b>FTD</b> Flight Training Device.	<b>SPL</b> Sound Pressure Level.
<b>GTM</b> Generic Transport Model.	<b>TCAS</b> Traffic Collision Avoidance System.
<b>HLD</b> High-lift Devices.	<b>TOGA</b> Take-off/go around thrust.
<b>HW/SW</b> Hardware/Software.	<b>UPRT</b> Upset Prevention and Recovery Training.
<b>IFR</b> Instrument Flight Rules.	<b>VMC</b> Visual Meteorological Conditions.
<b>IK</b> Inverse Kinematics.	<b>VNAV</b> Vertical Navigation.
<b>ISA</b> International Standard Atmosphere.	<b>VR</b> Virtual reality.
<b>LOC-I</b> Loss of control in-flight.	<b>VRAM</b> Video Random Access Memory.
<b>MCC</b> Multi-Crew Coordination.	<b>VSI</b> Vertical Speed Indicator.
<b>MCDU</b> Multi-Function Control and Display Unit.	
<b>MCT</b> Maximum Continuous Thrust.	

# List of Symbols

Symbol	Description	Unit	Symbol	Description	Unit
<i>Numbers:</i>			$q$	Joint parameter	rad
1	Heaviside unit step function	-	$q_{(\bullet\bullet)}$	Distributed loading along the $\langle\bullet\bullet\rangle$ -direction	$\text{N m}^{-1}$
<i>Alphabet:</i>			$q$	Joint state	rad
$A$	Amplitude, Maximum acceleration	$\text{m s}^{-2}$	$q_k$	Generalised forces	-
$A_0$	Enclosed Area	$\text{m}^2$	$r$	Length of the normal between the two axes, Cylinder radius	m,
$a$	Linear acceleration	$\text{m s}^{-2}$	$T$	Period, manoeuvring time	s,
$C_{rr}$	Frictional Coefficient	-	$\mathcal{T}$	Test space of end effector	-
$\text{DB}_{\mathcal{K}',\mathcal{Q}}$	Database mapping end effector state to joint state	-	$t$	Time, Torque, Thickness	s, N m, mm
$d$	Distance, Length of normal between the two axes	m, m	$u, u$	Control input	-
$E$	Energy	J	$V_{(\bullet\bullet)}$	Shear force along the $\langle\bullet\bullet\rangle$ -direction	N
$\hat{e}_i$	Unit vector in $i$ direction	-	$V_e$	Volume of motion freedom space	-
$F_a$	Force	N	$v$	Velocity	$\text{m s}^{-1}$
$F_{g\text{-seat}}$	Minimum that the padding of the g-seat exerts on the person	N	$W$	Weight, Beam width	N, m
$f$	Force	N	$\mathbf{W}$	Velocity tensor	-
$g$	Gravitational acceleration	$\text{m s}^{-2}$	$w$	Measure of manipulability, Width	- m
$H$	Acceleration Tensor, Beam height	$\text{m}$	$x, x$	State	-
$I_{(\bullet\bullet)}$	Area moment of inertia along the $\langle\bullet\bullet\rangle$ -axis, Mass moment of inertia along the $\langle\bullet\bullet\rangle$ -axis	$\text{m}^4$ , $\text{kg m}^2$	$x_g$	Distance to center of gravity in $x$ -axis	m
$I$	Cabin noise isolation	dB	$x_{g\text{-seat}}$	Displacement of the g-seat padding	m
$J$	Jacobian matrix, Lagrange energy	$\text{W}$	$x_{\text{vert}}$	Vertical displacement of the g-seat	m
$J_0$	Euler inertia matrix	-	$y_g$	Distance to centre of gravity in $y$ -axis	m
$J$	Cost function	-	$z_g$	Distance to centre of gravity in $z$ -axis	m
$\mathcal{K}$	Space of kinematically feasible end effector states	-	<i>Greek:</i>		
$L$	Sound pressure level, Beam length	dB, m	$\alpha$	angle about $x_n$ from $z_{n-1}$ to $z_n$	rad
$l$	Length	-	$\Gamma$	Gamma function	-
$M_{(\bullet\bullet)}$	Moment along the $\langle\bullet\bullet\rangle$ -axis	N m	$\theta$	Pitch angle, angle about joint $n - 1$ $z$ -axis from $x_{n-1}$ -axis to $x_n$ -axis, defined positive counter-clockwise	rad, rad
$M$	Denavit-Hartenberg transformation matrix	-	$\Lambda$	Triangular function	-
$m$	Component mass	kg	$\Lambda^*$	Modified triangular function	-
$n$	Load factor	-	$\mu$	Tuning parameter	-
$P$	Power	W	$\xi$	Distributed moment	$\text{N m m}^{-1}$
$P_{\text{max}}$	Maximum power of g-seat	W	$\sigma$	Singular value, Normal stress	$\text{N m}^{-2}$
$P_{\text{mode}}$	Power of the mode that is selected on the g-seat	W	$\tau_{(\bullet\bullet)}$	Shear stress along the $\langle\bullet\bullet\rangle$ -plane	$\text{N m}^{-2}$
$P_{\text{nom}}$	Nominal power of g-seat	W	$\tau_{g\text{-seat}}$	Time constant for power of g-seat	s
$Q_k$	Generalised coordinates	-	$\Phi$	Force tensor	-
$Q$	First moment of area	$\text{m}^3$	$\phi$	Roll angle, Robot arm angle	rad, rad
$\mathcal{Q}$	Space of kinematically feasible joint states	-	$\psi$	Yaw angle	rad
			$\omega$	Angular velocity	$\text{rad s}^{-1}$

# 1 Introduction

As established in [1–3] and in [4], Loss of Control In-flight (LOC-I) is the leading cause of fatalities in commercial aviation. Consequently, there is a need for solutions to prevent and to recover from LOC-I. One solution is to provide additional pilot training, particularly upset prevention and recovery training (UPRT). This project presents one way to provide this training by designing a flight simulator system capable of reproducing conditions experienced in upset events. In the previous report [2], a trade-off of the flight simulator concepts was carried out by sizing the three concepts and assessing their feasibility, strengths and weaknesses. Out of the three concepts proposed, the report concludes that the robotic arm was the best design. In this report, further analysis of the robotic arm is carried out.

This report starts by providing an overview of the second design iteration, followed by the market analysis and the training systems. The subsystem sizing is then detailed, providing an account of the system interfaces, the structures, aeromechanics, robotic kinematics, aural cueing, visual cueing, and haptic cueing. Then, the system logistics are defined, from where a sustainability analysis and risk assessment can be conducted. Finally, the post-DSE activities are defined, and the project is concluded.

The following segment gives the Mission Need Statement (MNS), and the Project Objective Statement (POS), as was established in the first project report [3].

**MNS** Provide safe and effective training for pilots to prevent and recover from aircraft upsets.

**POS** Design a flight simulator to realistically train pilots in the prevention of, and recovery from upsets by 10 students over 10 weeks.

## 1.1. Changes

During the design process it was discovered that some requirements as proposed in [2] led to problems during the design process. These problem have been discussed with the client, which resulted in several relaxations in the last three requirements presented in Tab. 1.1. Note that the requirements were changed during the second iteration and are therefore only taken into account from Sec. 2.3 onward.

First, it was required that the system was capable of generating a sustained motion cue of 3.5 g, resulting in unsafe jerk values. Therefore, in consultation with the client, a revised requirement set the range of g-forces from -1.0 g to +2.5 g. Secondly, the combination of sustained g-forces and the environmental constraint of an 80% reduction of emissions was found to be incompatible. The sustained g-forces were found to be feasible only in centrifuge-like designs, making the sustainability requirement infeasible in the context of power generation. The client then deemed that the g-forces do not have to be sustained and can be simulated as onset cues. Lastly, the onboard power requirement was found to have no relevant basis on the client side — it was an assumed reasonable power budget for a concept the client had in mind. This has been altered to be in line with a feasible power budget.

It should be also noted that during the design phase, the floor loading requirement was further quantified after carrying out the floor loading analysis; the resulting maximum floor loading was found to be  $11.97 \text{ kN m}^{-2}$ .

Table 1.1: Requirement updates

Original		Modified	
Identifier	Requirement	Identifier	Requirement
<b>UPaRTS-SH-SO-19</b>	The simulator floor loading shall not exceed <TBD> $\text{N/m}^2$ .	<b>UPaRTS-SH-SO-19</b>	The simulator floor loading shall not exceed $11.97 \text{ kN m}^{-2}$ . [Subsec. 5.3.2]
<b>UPaRTS-SH-SO-21</b>	The simulator shall provide onset g-forces at 70% of the real aircraft.	<b>UPaRTS-SH-SO-22</b>	The simulator shall provide onset g-forces at 70% of +2.5 and -1. [[5]]
<b>UPaRTS-SH-SO-07</b>	The simulator shall represent a two-pilot single aisle airliner of comparable specifications as a Boeing 737 or Airbus A320.	<b>UPaRTS-SH-SO-23</b>	The simulator shall represent a two-pilot single aisle airliner of comparable specifications as a Airbus A320. [client individual meeting]
<b>UPaRTS-SH-SO-08</b>	The power budget of the on-board of the system shall not exceed 2 kW.	<b>UPaRTS-SH-SO-24</b>	The power delivered to the onboard cabin shall be feasible regardless of the amount. [[6]]

# 2 Lightweight Concept Second Iteration

Each concept proposed in the previous report was thought of as a first iteration. This chapter treats possible second iterations that can be undertaken, providing trade-offs regarding the utility of each design. The result of this endeavour is a final second iteration which the remainder of this report will draw from.

## 2.1. Previous Concept Analysis

In this section, the main strengths and weaknesses of the various aspects of each concept are tabulated. This table is used to assist in generating iteration possibilities by considering the weaknesses of the light-weight aspect; it is then attempted to ameliorate existing concepts by combining them with favourable aspects of contending concepts. This table is shown below (Tab. 2.1):

Table 2.1: Strength and weakness table for each concept from the midterm report [2]

Concept	Feature	Strengths	Weaknesses
<b>Conventional</b>	Motion system	✓ Low power	✗ g-loads not sustained ✗ Limited motion range
	Visual system	✓ Excellent visual cues	✗ High mass ✗ High power
	Aural system	✓ Directional sound	✗ High power ✗ High mass
	Second pilot	✓ Identical to in-aircraft	✗ High cabin mass ✗ High cabin power
	IOS	✓ Direct pilot contact	✗ Onboard power ✗ Onboard mass ✗ Onboard (de)briefings ✗ Normal displays
<b>True-to-Life</b>	Motion system	✓ Sustained g-loads	✗ Sustainability requirement cannot be met
	Visual system	✓ Low mass ✓ Low power	✗ Visual cues of low quality
	Aural system	✓ Directional sound	✗ High power ✗ High mass
	Second pilot	✓ Identical to in-aircraft	✗ High cabin mass ✗ High cabin power
	IOS	✓ Offboard (de)briefing ✓ No onboard power ✓ No onboard mass	✗ Indirect pilot contact ✗ Normal displays
<b>Lightweight</b>	Motion system	✓ Wide motion range ✓ Low power	✗ g-loads not sustained
	Visual system	✓ Good visual cues ✓ Very low power ✓ Very low mass	
	Aural system	✓ Low mass ✓ Low power	✗ Incorrect auditory spatial perception
	Second pilot	✓ No cabin power ✓ No cabin mass	✗ Virtually projected pilot
	IOS	✓ Offboard (de)briefings ✓ AR visuals for instructor ✓ No onboard power ✓ No onboard mass	✗ Indirect pilot contact

As can be seen in Tab. 2.1, the haptic system is not included: this is because the differences between the three concepts are negligible in this regard. On the other hand, the motion system, visual system, the aural system, second pilot integration and the IOS all have noticeable differences between the concepts and are therefore included in Tab. 2.1. To properly identify second iteration possibilities of the motion system, a comprehensive analysis is carried out. This analysis is presented in Sec. 2.2.

Although the visual cues of the conventional system are slightly better than the robotic system, the higher power and mass offsets this advantage; therefore virtual reality (VR) is chosen instead. Similarly, the benefits of having a second pilot physically present are outweighed by the mass and cost increase, therefore the second pilot is virtually projected. Due to payload constraints, the instructor and operator station (IOS) with its augmented reality (AR) features is located outside the cockpit. Finally, due to the advantages posed by a 5.1 surround sound system over the headset, the surround sound system is chosen.

In addition, the air-conditioning unit was removed. As stated in the midterm report [2], the

cabin movement grants sufficient airflow for cooling. Otherwise, low-powered fans can be added for additional flow. A g-seat was also added to allow for necessary vibrations as required by UPARTS-SYS-AM-USP-4. Finally, the processing unit was placed off-board.

## 2.2. Motion System Iteration Possibilities

For the motion system, three possible avenues are identified: further development of the linear rail concept, the use of a circular rail system, and a concept with no rail system. The latter can be divided further into a ceiling-mounted system or a floor-mounted system. Each of these will be analysed in due detail. In addition, this section provides further details on the attainability of the g-loading requirements, and whether the iterations are feasible or not.

### 2.2.1. Linear Rail

This concept considers the robot arm on a linear rail system. Combining the restricted floor area and the length of the robot arm, a maximum track length was calculated. The robot arm extends a maximum of 4.7 m (FANUC M-2000iA/1700) and the cabin extends another 1.5 m<sup>1</sup>. The floor area restriction is 20 × 20 m<sup>2</sup>, hence the longest possible track would be 10.75 m from one corner to the opposite corner. This is represented in Fig. 2.1.

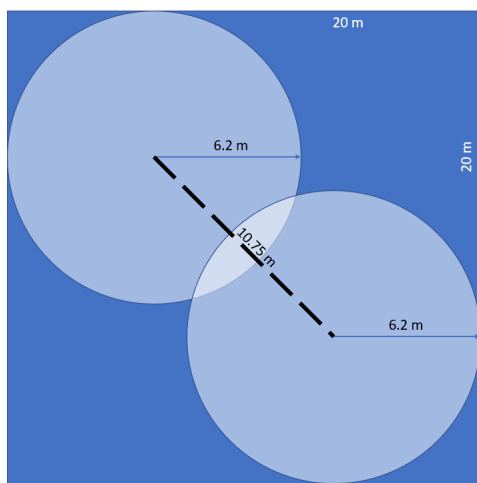


Figure 2.1: Possible track length for a linear rail system

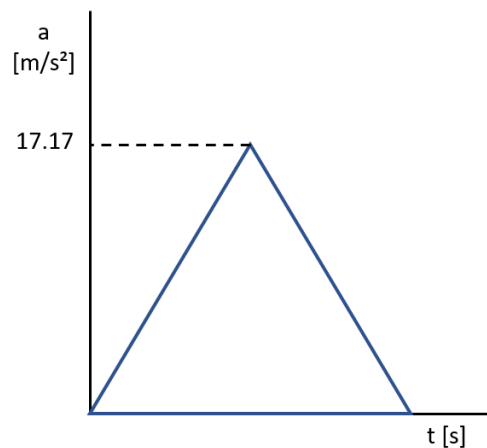


Figure 2.2: Approximation of the process of obtaining g forces

With the track length determined, the possibilities for obtaining the desired g-forces through braking can be sized. The maximum velocity of the rail (Güdel TMF-6) is  $0.75 \text{ m s}^{-1}$  and the g-loading cueing requirement is 1.75 g ( $17.17 \text{ m s}^{-2}$ ). In order to find if this is feasible, the resulting jerk due to braking is analysed. Considering the acceleration profile in Fig. 2.2, the average acceleration over the total period of time is  $8.58 \text{ m s}^{-2}$ , giving a time to standstill of  $V_{\text{max}}/a_{\text{avg}} = 0.75/8.58 = 0.087 \text{ s}$ . The peak acceleration occurs at the halfway mark, hence the jerk is at least  $a_{\text{max}}/t_{\text{int}/2} = 17.17/(0.087/2) = 393 \text{ m s}^{-3}$ . This jerk is exceptionally high, therefore the initial concept is not deemed viable on the grounds of personal safety.

Furthermore, an issue regarding cueing latency, i.e. the time lag between a command cue and the execution thereof, is identified. To account for the time required to attain a certain motion cue, it is important to also consider the frequency at which such cues can be generated. This property is dictated by the maximum velocity: a low maximum velocity allows cues to be staged in rapid succession, but will also decrease the time for which they can be sustained. For an increased velocity, a longer sustained cue can be attained, at the expense of the braking system, which introduces a higher jerk, and a diminished cueing frequency.

To modify the system such that this jerk is acceptable, a few changes can be made. First of all, the maximum starting velocity should be increased. Secondly, the required g-forces can be reduced. This second change may cause the system to violate the stakeholder requirement, required separate solutions to be sought.

**Velocity Change** In order to increase the starting velocity of the robot arm, increasing the time of sustained loading and reducing the jerk on braking down to appropriate levels, the track length itself must ideally be increased. The reason for this is to minimise jerk of the cabin, which should ideally be imperceptible. Attempting to do so brings about several detriments. A major disadvantage

<sup>1</sup> Fanuc.co.jp: FANUC Robot M-2000iA

is cueing latency, which, as discussed above, will largely detract from the cueing performance of the system, as the onset time for vestibular cues becomes unacceptably high. Therefore, an increase in velocity will impart a severe dent in cueing performance, and is therefore disregarded as a viable option.

**Reduced g-force on the rail** In an effort to decrease the jerk of the linear rail, a possibility is to lower the rail's acceleration requirement. In light of the foregoing discussion, this seems to be the most viable option. Therefore, part of the vestibular cueing requirements must be delegated to separated systems, such as the bespoke robotic arm and a separate motion cueing solution, i.e. the sustained motion cueing seat, or 'g-seat' for short.

A g-seat is a special type of seat which evokes the sense of controlled accelerations on the pilot. Additionally, vibrational cues are supported by this device. However, one of the disadvantages of a g-seat lies in its high power consumption. For this reason, power delivery to the cabin needs to be reconsidered. A representative series of a g-seats is produced by MOOG, capable of providing up to 9 g but requiring 3 kW of power continuously<sup>2</sup>.

**Verification** All calculations for the linear rail concept were performed by means of a spreadsheet software. These calculations were checked step by step through hand calculations. Two team members did this separately from each other to prevent mistakes.

### 2.2.2. Circular Rail

The circular rail concept concerns two different solutions. There is the 'infinite-rail' concept where the simulator will have a low velocity such that the centrifugal force is also low and will brake to obtain the onset g-loading. Then, there is the sustained g-loading rail system, where by varying the length of the arm, the g-loading will vary.

**Subconcept A: Sustained g-loading rail system** One possible manner to sustain the required g-loading is by exploiting centrifugal accelerations caused by travelling in a circle. By varying the centrifugal radius using the reach of the robot arm, different loading schemes can be found. At the rail, the cabin will have a maximum sustained load while at a radius that coincides with the circular origin the acceleration will be equal to zero. Emphasis is placed on the jerk value that the cabin experiences when aiming for different g-requirements. The required velocity can be calculated by taking the force equilibrium normal to the tangential direction of travel, resulting in the following equation:

$$1.75 g = \frac{v^2}{r} \quad (2.1)$$

With both velocity  $v$  and track radius  $r$  being free variables, a first estimate constraint for  $r$  is the robotic arm reach, which is in the order of 5.0 m. This value is based on the reach of the arm combined with the cabin with a contingency margin. Therefore, by Eq. 2.1,  $v = 11.7 \text{ m s}^{-1}$ . To get a first estimate of the viability of the power and time required to accelerate to this maximum speed, consider an energy balance:

$$E_{\text{translational}} + E_{\text{rotational}} + E_{\text{losses}} = E_{\text{generated}}, \quad (2.2)$$

where  $E_{\text{translational}}$  is the translational energy of the system,  $E_{\text{rotational}}$  is the rotational energy of the system,  $E_{\text{losses}}$  is the losses due to friction, and  $E_{\text{generated}}$  is the energy generated. Expanding upon Eq. 2.2:

$$\frac{1}{2} v^2 \left( m + \frac{I}{r^2} \right) + C_{rr} m g d = P t, \quad (2.3)$$

where  $m$  is the mass of the system,  $I$  is the mass moment of inertia around the robotic arm's axis of rotation,  $C_{rr}$  is the rolling friction coefficient,  $d$  is the distance travelled around the rail,  $t$  is the time required to meet the energy balance, and  $P$  is the power input. Assuming constant tangential acceleration,  $d = \frac{1}{2} a t^2$ . Being constrained by  $v$  due to the g-requirement, the acceleration kinematic term can be rewritten as  $a = \frac{v}{t}$ , therefore:  $d = \frac{1}{2} v t$ . Rearranging Eq. 2.3:

$$\frac{1}{2} v^2 \left( m + \frac{I}{r^2} \right) + C_{rr} \frac{1}{2} m g v t = P t. \quad (2.4)$$

Ultimately, both  $P$  and  $t$  are free variables, where  $P$  is constrained by the sustainability requirement. However the energy balance is still manageable as the time required to meet it adjusts for the power input accordingly. This has no impact on operations other than on the start up time; a long start up time corresponds to higher frictional losses. For a power of 30 kW<sup>3</sup>, this will lead to a

<sup>2</sup>MOOG: G-SEATS

[cited 2020-06-02]

<sup>3</sup>This is equal to the sustainability limit minus the onboard power and the robot power.

spin-up time of 62.5 s.

The rate of change of the radius of the arm, is one of the most important characteristics considered. For all these manoeuvres the FANUC M-2000iA/1700L is considered<sup>1</sup>. Considering the ultimate case where the arm is fully horizontal (maximum change of radii), a jerk of  $0.34 \text{ gs}^{-1}$  is found.

Achieving the velocity calculated with Eq. 2.1 using commercial carriages is not feasible. More concerning for this design is the maximum jerk level. The change of radius of the circle by the robot arm amounts to a jerk level of  $0.34 \text{ gs}^{-1}$  at most when considering robotic arms on the market. A factor of 10 or more is required to facilitate a realistic jerk level [2], and it is believed, even with an in-house design, that this is not feasible. Therefore, this whole concept is deemed infeasible.

**Subconcept B: Translational acceleration** Contrary to the linear rail system, the circular rail presents an infinite track on which motion can occur. Here, the same analysis as for a linear rail is carried out, neglecting the constraints imposed by a linear rail segment, while taking into account the effect of centrifugal accelerations.

To this end, an off-the-shelf linear unit is analysed. This system, the Güdel TMF-6<sup>4</sup>, has a maximum velocity  $0.75 \text{ m s}^{-1}$ , and an acceleration time from rest of 1.16 s. Given these numbers, it can be shown that:

$$t_{\text{braking}} = -\frac{v_{\text{max}}}{a_{\text{braking}}} = -\frac{0.75 \text{ m s}^{-1}}{-1.75 \cdot 9.80665 \text{ m s}^{-2}} = 4.4 \text{ ms.} \quad (2.5)$$

Given this braking time, the maximum jerk is found to be  $392 \text{ m s}^{-3}$ . One of the main drawbacks of this design is the time required to attain the maximum velocity. To investigate the severity of the 1.16 s acceleration time, a Fourier analysis of the bespoke model upset event (see [2]) was performed. The results are shown in Fig. 2.3:

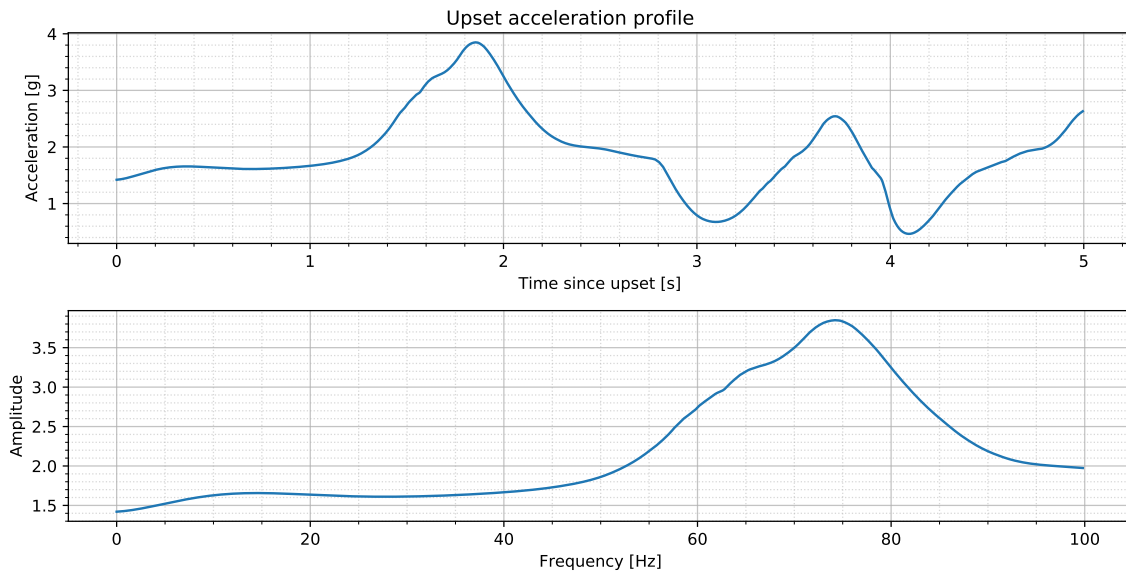


Figure 2.3: Upset acceleration profile and Fourier analysis

In this figure, it can be seen that the dominant frequency lies at about 74.2 Hz, which can likely be attributed to stall buffeting [7]. Beyond that, in the lower frequency range, the dominant frequency is 14.4 Hz, which would be the desired frequency of manoeuvres that are to be carried out by the robot arm system. Such a frequency would be in the operational range of the linear unit, provided that appropriate washout filters are applied and cues are limited in magnitude.

The problem with this concept, however, is the average human acceleration perception threshold: laterally, this is  $6.5 \text{ cm s}^{-1}$  and anterior-posterior (longitudinally) this is  $8.5 \text{ cm s}^{-1}$  [8]. Using the previously discussed maximum velocity of  $0.75 \text{ m s}^{-1}$  and a radius of  $3.8 \text{ m}$ <sup>5</sup>, a centripetal acceleration of  $0.15 \text{ m s}^{-2}$  is found. This exceeds both the lateral and longitudinal threshold and is therefore not acceptable.

To mitigate this problem, the only solution is to lower the maximum velocity, thereby lowering the unwanted centrifugal acceleration below its perception limit. This, however, brings with it a number

<sup>4</sup> Güdel AG: Linear Traversing Axis TMF

[cited 2020-06-02]

<sup>5</sup>This is based off of the total available area of 20 m by 20 m and an arm-with-cabin radius of 6.2 m

of negative consequences: for one, the time over which accelerations can be sustained will have to be lowered, or the accelerations themselves will have to be lowered. This detracts from motion cueing fidelity at large, making the advantages of a diminished centrifugal acceleration pale in comparison.

**Verification** For both subconcepts, the computations described above rely on elementary classical mechanics, making the verification procedure rather straightforward. To ascertain the validity of the results, additional analysis was performed through Lagrangian mechanics; naturally this yielded identical results. Finally, the Fourier analysis was performed by means of SciPy Fast Fourier Transform (FFT) routines, which have been verified in greater depth in Subsec. 5.4.5.

### 2.2.3. Static Robot arm

The third possible solution is to use no rail at all. Onset g-forces are briefly generated just by the robot arm. If the arm is floor-mounted, its blind spot due to its base limits the motions that can be utilised to generate the high-acceleration loads, the most extreme of which will occur in upward direction relative to the floor. It makes up for this in simplicity and relatively straight-forward installation. Producing sustained loads is not possible, but the possibilities in terms of one-to-one recreation of attitudes is vastly superior to the classic hexapod simulator, and the range of motion is similarly more extensive [9]. The exact range in terms of accelerations reachable within the limits of the arm joints can only be determined through a full kinematic simulation, and so it cannot be determined if this concept would be preferable over the rail concept. This will also determine the viability of this concept in terms of meeting the accelerations requirements as set by the customer (the current state of which is described Sec. 1.1).

To maximise the forces generated using as little power as possible, a slingshot manoeuvre is implemented whereby brief centripetal forces are also generated. However, in a classic floor-mounted robot arm these would point in the opposite direction of gravity and be generated upwards. Also, the highest g-forces encountered will be in the downward direction [2]. Mounting the robot arm to the ceiling means a slingshot manoeuvre makes use of both gravitational and centripetal g-forces in the downward direction. When the cabin is approximately at the bottom, gravity and centripetal force align and the 1.8g are reached after which it washes out. A sketch of the concept with coordinate system and angle definitions is shown in Fig. 2.4.

**Required power** In order to determine the required power of the system, the critical case, which is reaching 70% of 2.5g (1.75g) with the cabin, is examined. The energy needed for this motion will consist of potential, kinetic, and rotational energy and in order to calculate these energies, it is necessary to determine the centre of gravity of the system. This is done by assuming that the rotating part of the robotic arm will be a beam with a length of 4.6 m and with a mass of 6000 kg (half the mass of the total robotic arm). Furthermore the cabin will be a point mass, located at 0.75 m from the end of the robotic arm. With the position of the centre of gravity known, only the angular acceleration of the system is still needed to determine the required energy of the system. Looking at off-the-shelf robotic arms, it can be concluded that an angular acceleration of  $0.5 \text{ rad s}^{-2}$  can be achieved [10]. With this acceleration and a starting position of  $\varphi = -45^\circ$ , the required g-force of 1.8g is reached at a position of  $\varphi = 29^\circ$ . The total energy that must be generated in order to perform this manoeuvre, which includes only the acceleration and not the deceleration of the system, is calculated with Eq. 2.6.

$$E_{\text{potential}} + E_{\text{kinetic,cabin}} + E_{\text{rotational,arm}} + E_{\text{losses}} = E_{\text{generated}} \quad (2.6)$$

The additional energy generated due to energy losses of the system is set to 10% of the total energy generated for the system [11]. For calculating the rotational energy, the assumption is made that the robotic arm can be modelled as a beam. The resulting mass moment of inertia  $I$  for a beam rotating around one of its ends will then be  $\frac{1}{3}ml^2$  and the resulting rotational energy will be  $\frac{1}{2}I\omega^2$ . The potential energy will be calculated with  $mgh$  and the kinetic energy of the cabin is calculated using  $\frac{1}{2}mv^2$  respectively. Finally Eq. 2.6 can be expanded to Eq. 2.7 and the average power needed for this manoeuvre can be calculated by dividing the total energy by the duration of the manoeuvre, resulting in an average power of 18 kW

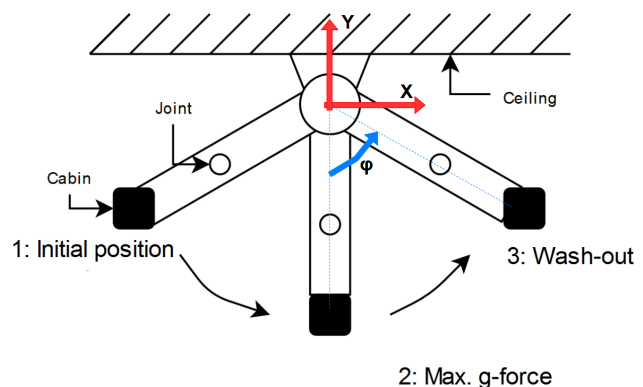


Figure 2.4: Sketch of the slingshot manoeuvre

$$mgh + \frac{1}{2}mv^2 + \frac{1}{2}I\omega^2 + 0.1E_{\text{generated}} = E_{\text{generated}} \quad (2.7)$$

Note that this average power only includes the power needed to accelerate the system; the deceleration will either be done by mechanical or electrical and regenerative braking. In case of mechanical braking, the power needed to activate the brakes will be negligible and the average power of the manoeuvre including the deceleration will therefore be approximately the same as without deceleration. In the case of electric, regenerative braking, the average power of the manoeuvre including the deceleration will be even lower than without deceleration and therefore electric regenerative braking will be the preferred choice.

**Feasibility** Although this concept can likely meet the sustainability requirement and the onset g-forces requirement, there are some drawbacks. First off, when the slingshot manoeuvre is initiated, the pilot temporarily experiences less g-loading rather than more. This ‘false’ cue can be detrimental to the training [2]. Secondly, when the required onset g-forces have been reached, the washout will either be a rapid deceleration or spin out in centrifugal motion. Both will again provide false motion cues to the pilot. Thirdly, a simulator like this has never been built and the effects of mounting the robot arm of this calibre upside down are not known. Also, the feasibility and costs of reinforcing the building structure to be able to carry a 12 tonne robot arm from the ceiling are not known. Therefore, this concept carries a significant design risk. In conclusion, this concept is considered infeasible due to many false cues and a high design risk.

**Verification** First, the gravitational, centripetal, and angular acceleration vectors are checked one by one for different angles  $\phi$  by comparing them with hand calculations. The potential, and rotational energies of the cabin and the robot arm are also checked by deriving them one by one for different angles, velocities, and accelerations and comparing with hand calculations. Both the accelerations and energies are within machine epsilon of the hand calculations so these are considered verified. Finally, the numerical integration scheme is verified by plotting the position, velocity and acceleration through time. These plots all have their expected shape so the numerical integration is considered verified.

## 2.3. Iteration Selection

With the possibilities provided by the four concepts previously discussed, the following table summarises the strengths and weaknesses of each of the iteration, aiding in the final motion cueing system selection.

Table 2.2: Strength and weaknesses of each iteration

Concept	Strengths	Weaknesses
<b>Linear Rail</b>	<ul style="list-style-type: none"> <li>✓ Meets all requirements after revision of on-board power budget</li> <li>✓ Design entirely feasible</li> <li>✓ Works using mostly standardised components</li> <li>✓ Facilitates integration with operator’s logistics</li> </ul>	<ul style="list-style-type: none"> <li>✗ Revision of on-board power budget required</li> <li>✗ Needs a g-seat for sustained loading</li> <li>✗ Cueing latency</li> </ul>
<b>Sustained Circular Rail</b>	<ul style="list-style-type: none"> <li>✓ Meets the sustained g-loads within the required sustainability limit</li> <li>✓ Acceleration to final velocity is trade-off between power input and time required</li> </ul>	<ul style="list-style-type: none"> <li>✗ The jerk required for reliable training is too low</li> <li>✗ High design risk</li> <li>✗ Robotics have to be designed from scratch</li> <li>✗ Carriage and rail systems have to be designed from scratch</li> </ul>
<b>Braking Circular Rail</b>	<ul style="list-style-type: none"> <li>✓ Meets the onset cueing requirements</li> <li>✓ All components are commercial off-the-shelf and pre-certified</li> <li>✓ Can cue an increased range of onset acceleration vectors</li> </ul>	<ul style="list-style-type: none"> <li>✗ Requires repeated braking, thereby wearing out the track</li> <li>✗ Minute vestibular cues will have to be generated using, e.g., a g-seat</li> <li>✗ High design risk due to the uncertain cueing algorithm</li> <li>✗ Cueing latency prior to braking</li> <li>✗ Perceptible centripetal acceleration as a side-effect of (quasi)linear motions</li> </ul>
<b>Ceiling mounted</b>	<ul style="list-style-type: none"> <li>✓ Meets sustainability requirement</li> <li>✓ Meets onset g-force requirement</li> </ul>	<ul style="list-style-type: none"> <li>✗ High design risk</li> <li>✗ High cost uncertainty</li> <li>✗ False cues are very prevalent</li> <li>✗ g-loads not sustained</li> <li>✗ Requires a ceiling mount to be designed</li> </ul>
<b>Floor mounted</b>	<ul style="list-style-type: none"> <li>✓ Minimalist</li> <li>✓ Can reach all g-loads</li> </ul>	<ul style="list-style-type: none"> <li>✗ Dependent on a g-seat</li> <li>✗ Revision onboard power budget required</li> <li>✗ Control over g-loads not as high as other systems</li> </ul>

**Chosen concept** From Tab. 2.2, it was decided to further develop the *Linear Rail* concept. The linear rail is deemed to be entirely feasible at this point, but is not capable of meeting all initial requirements set by the customer. Therefore, a revision of the requirements was made in consultation with the customer, as was shown in Sec. 1.1. It is believed that it is possible to use a large array of standardised components, minimising the amount of design required to integrate all the system elements.

**Rationale for discarded concepts** The sustained circular rail was not chosen due to its high design risk and the redesigns required. The braking circular rail was not chosen due to the issues presented by repeated braking and high design risk presented by the cueing algorithm. The ceiling mounted design is far too exotic; this poses a high design risk alongside a high cost uncertainty. Additionally, the design of the ceiling mount is likely to be expensive. The floor mounted concept was not chosen as it is believed that it lacks control over the g-forces produced compared to the linear rail.

**Off-board station** As will be stated later within the budgets, an off-board section, or station, will be added. This part is meant to deliver an integrated section with a professional instructor and co-pilot for the pilot that is being trained; this satisfies the multi-crew training requirement. The off-board section will feature all the tools present in the cabin, except for the motion system.

## 2.4. Updated Budgets

The second design iteration result in the following updates to the system mass budget shown in Tab. 2.3. The initial budgets determined in [2] were 517 kg, 26 466 kg, 290 kg, 282 kg for the cabin, motion system, IOS and off-board cabin, respectively. Additionally, in order to maintain a clear overview of the power used by the system, the updated power budget as a result of the second iteration can be seen in Tab. 2.4. The initial power budgets determined in [2] were 1773 W, 1270 kW, 65 W and 1773 W for the cabin, motion system, IOS and off-board cabin respectively.

A data rate budget is also set up in this report, shown in Tab. 2.5. The explanation behind the chosen bitrates is explained next: First off, the force feedback components together with the motion system are analysed. Unfortunately, bitrates are hard to find for off-the-shelf components. As a first estimate, each controlled/measured degree of freedom is assumed to have a refresh rate of 1000 Hz. This is a conservative estimate as these normally seem to be in the order of  $\sim 100$  Hz<sup>6</sup>. Furthermore, each time it refreshes, a double precision floating point number is assumed to be sent (64 bits). Any buttons present on the controls are assumed to have a negligible bitrate compared to the main control axes. The stick has three degrees of freedom resulting in a bitrate of  $192 \text{ kbit s}^{-1}$  to the stick. Since both forces and positions are measured, it has a bitrate of  $384 \text{ kbit s}^{-1}$  back to the computer. The pedals have three degrees of freedom (toe rotation on each foot + sliding), resulting again in  $192 \text{ kbit s}^{-1}$  to the pedals and  $384 \text{ kbit s}^{-1}$  back to the computer. Next, the throttle has five degrees of freedom (two thrust levers + trim + flaps + speed brake). Only the positions are measured so it has  $320 \text{ kbit s}^{-1}$  to and from it. The haptic gloves are assumed to have six degrees of freedom per finger (position+orientation). Again, only forces are sent but both position and forces are assumed to be measured. This results in  $3840 \text{ kbit s}^{-1}$  to them and  $7680 \text{ kbit s}^{-1}$  from them. The external motion system has 14 degrees of freedom (six joints + four wheel motors + four wheel brakes). It is assumed only the power is sent to each wheel/joint, but both speed and position are measured. This results in  $896 \text{ kbit s}^{-1}$  to the motion system and  $1792 \text{ kbit s}^{-1}$  from it. Finally, the g-seat has four degrees of freedom (four actuators), where the input power is sent to them and the actuator forces and positions are sent back to the computer. This results in  $256 \text{ kbit s}^{-1}$  to the seat and  $512 \text{ kbit s}^{-1}$  from the seat.

For the emergency system, it is hard to quantify a bit rate since the signal only consists of breaking/completing a circuit. However, if one would be able to press the button 10 times per second, the bitrate would be  $20 \text{ bit s}^{-1}$ . For now, the maximum refresh rate of a computer (which is checking if the button was pressed) is taken;  $200 \text{ kbit s}^{-1}$ <sup>7</sup>. This figure is used for the emergency buttons, the kill switch and the data switch.

Keyboards and computer mice have been around long before high bitrate connections and are therefore assumed to have low data rates. One unreliable source claimed their data rates to be "a few kbits/sec"<sup>8</sup>. For now a conservative estimate of  $20 \text{ kbit s}^{-1}$  for the two combined is used.

The IOS is assumed to contain two high definition screens, each requiring a bitrate of around  $25 \text{ Mbit s}^{-1}$ <sup>9</sup> resulting in a total bitrate of  $50 \text{ Mbit s}^{-1}$ . For the VR a conservative estimate of a set of

<sup>6</sup>WHEEL GUIDE - Force FeedBack Extra Tuning PC Version

[cited 2020-06-22]

<sup>7</sup>At what frequency/rate does the digitalRead function read an input?

[cited 2020-06-19]

<sup>8</sup>What is the transfer rate of a mouse, keyboard, and screen?

[cited 2020-06-19]

<sup>9</sup>HDV Format (ver. 1.0) Main Specifications (Revised)

[cited 2020-06-19]

high-resolution, high-refresh rate VR glasses is used. This is not unreasonable as both aspects have been increasing in recent years and are likely to keep increasing in the future. VR headsets with 8K ( $3840 \times 2160 \times 2$ ) resolution<sup>10</sup> are already available as well as those with a 144 Hz refresh rate<sup>11</sup>. Assuming the bitrate of the  $1080 \times 1440$ , 60 Hz IOS monitor scales proportionally with number of pixels and refresh rate, an 8K, 144 Hz VR headset would require a bitrate of  $640 \text{ Mbit s}^{-1}$ . For the bitrate back to the computer, the same approach as in the control loading- and motion system is used. The VR sensors are assumed to have ten degrees of freedom (six for head orientation and position + four for eye tracking). This results in a bitrate of  $640 \text{ kbit s}^{-1}$  back to the computer. For now, these figures are also used for the data rates of the AR.

The recording system camera is assumed to record  $1920 \times 1080$  video at 60 FPS as a conservative estimate. A surveillance camera with the same resolution, but running at 30 FPS puts out a bitrate of  $4 \text{ Mbit s}^{-1}$ <sup>12</sup>. Assuming doubling the FPS doubles the bitrate, the pilot recording camera puts out  $8 \text{ Mbit s}^{-1}$ .

Next, the audio system carries three separate audio channels to each headset: the communication from the other two people and the cabin sounds. A typical single channel audio bitrate is  $320 \text{ kbit s}^{-1}$ <sup>13</sup>, so the total incoming bitrate is  $960 \text{ kbit s}^{-1}$  and the outputted bitrate is  $320 \text{ kbit s}^{-1}$ .

Finally, the data rate between the main computer and the IOS computer will consist of the view of both pilots (in 1080p), the audio of the two pilots and the plane, the recording of the pilot in training, the control inputs of both pilots and the model parameters. All of these data rates have been sized except for the model parameters. Again the conservative estimate of a 1000 Hz refresh rate is used. The model parameters consist of: the aircraft state, the flight deck state, the cueing state, measures of performance, measures of flight envelope fidelity, and the aircraft operational limits. Since the aircraft model has not been developed yet, giving accurate degrees of freedom on these parameters is currently not possible. As a very rough first estimate each of them is assumed to have ten degrees of freedom, resulting in sixty degrees of freedom. With one 64-bit double sent for each degree of freedom, this results in a bitrate of  $3840 \text{ kbit s}^{-1}$  to the IOS. The IOS will send the voice recording and commands like startup, stop and event queues to the main computer. However, these commands will not be subject to a refresh rate as they are sent just a single time. Furthermore, only the command itself will have to be sent as the event queues themselves will already be programmed on the main computer. Therefore, the bitrates of these commands is assumed to be negligible with respect to the audio sent to the main computer.

---

<sup>10</sup>Pimax Vision 8K

[cited 2020-06-22]

<sup>11</sup>Valve index headset

[cited 2020-06-22]

<sup>12</sup>Simple guide of IP camera bitrate setting

[cited 2020-06-19]

<sup>13</sup>Ultimate Guide To Audio Bitrate & Audio Formats

[cited 2020-06-19]

Table 2.3: Light-Weight Design Mass Table

Category	Sub-Category	Mass
Cabin	1 Structure	235 kg [12]
	1 G-seat	50 kg <sup>14</sup>
	1 Aural System	10 kg <sup>15</sup>
	1 Pilot	100 kg
	1 Visual System	2 kg <sup>16</sup>
	1 Haptic System	80 kg <sup>17 19 21</sup>
	1 Power System	30 kg
	<b>Total Mass</b>	<b>527 kg</b>
Motion System	11 Rail	1025 kg m <sup>-1 4</sup>
	1 Robotic Arm	12500 kg <sup>1</sup>
	13 Energy Chain	5.7 kg m <sup>-1 4</sup>
	1 Carriage	2460 kg <sup>4</sup>
	4 Brake	39 kg <sup>23</sup>
	<b>Total Mass</b>	<b>26166 kg</b>
IOS and Infrastructure	1 Instructor/Operator Station	100 kg
	1 Operator Seat	150 kg
	1 Computer	7 kg
	1 Computer	30 kg
	<b>Total Mass</b>	<b>287 kg</b>
Off-board Cabin	1 Pilot	100 kg
	1 Seat	40 kg
	1 Aural System	10 kg
	1 Visual System	2 kg
	1 Haptic System	30 kg
	1 Power System	30 kg
	<b>Total Mass</b>	<b>212 kg</b>
<b>System Total Mass</b>		<b>27237 kg</b>

Table 2.4: Light-Weight Design Power Table

Category	Sub-Category	Power
Cabin	1 Structure and Shell	20 W <sup>2</sup>
	1 G-seat	3000 W <sup>2</sup>
	1 Aural System	75 W <sup>15</sup>
	1 Visual System	20 W [13]
	1 Haptic System	660 W <sup>17 18 19 21 32</sup>
		<b>Total Power</b>
Motion System	1 Rail	4800 W [2]
	1 Robotic Arm	8000 W <sup>27</sup>
	4 Brake	130 W <sup>23</sup>
		<b>Total Power</b>
Instructor/Operator Station	1 IOS Computer	90 W <sup>29 30</sup>
	2 Monitor	24 W <sup>31</sup>
	1 Aural System	150 W <sup>15</sup>
	1 Main Processing Unit	589 W <sup>31</sup>
	<b>Total Power</b>	<b>877 W</b>
Off-board Cabin	1 Aural System	75 W <sup>15</sup>
	1 Visual System	20 W [13]
	1 Haptic System	660 W
	<b>Total Power</b>	<b>684 W</b>
<b>System Total Power</b>		<b>18747 W</b>

Table 2.5: Light-Weight Design Bitrate Table

Component	Input Bitrate	Output Bitrate
Stick	192 kbit s <sup>-1</sup>	384 kbit s <sup>-1</sup>
Pedals	192 kbit s <sup>-1</sup>	384 kbit s <sup>-1</sup>
Throttle	320 kbit s <sup>-1</sup>	320 kbit s <sup>-1</sup>
Gloves	3840 kbit s <sup>-1</sup>	7680 kbit s <sup>-1</sup>
External motion system	896 kbit s <sup>-1</sup>	1792 kbit s <sup>-1</sup>
G-seat	256 kbit s <sup>-1</sup>	512 kbit s <sup>-1</sup>
Emergency button	-	200 kbit s <sup>-1</sup>
(data) Kill switch	200 kbit s <sup>-1</sup>	-
Keyboard+mouse	-	20 kbit s <sup>-1</sup>
IOS screens	50 Mbit s <sup>-1</sup>	-
VR headset	640 Mbit s <sup>-1</sup>	640 kbit s <sup>-1</sup>
AR headset	640 Mbit s <sup>-1</sup>	640 kbit s <sup>-1</sup>
Recording camera	-	8 Mbit s <sup>-1</sup>
Audio system + microphone	960 kbit s <sup>-1</sup>	320 kbit s <sup>-1</sup>
IOS connection to main computer	46 Mbit s <sup>-1</sup>	320 kbit s <sup>-1</sup>

<sup>14</sup> Simxperience.com: GS-5 G-Seat

[cited 2020-05-12]

<sup>15</sup> Amazon.com: Logitech Z506 Surround Sound Home Theater Speaker System

[cited 2020-06-03]

<sup>16</sup> VentureBeat.com: Panasonic VR glasses hands-on: An intriguing vision in need of a platform

[cited 2020-05-14]

<sup>17</sup> Amazon.de: Hi5 VR Glove Compatible with HTC Vive and Noitom's Project Alice (M)

[cited 2020-05-13]

<sup>18</sup> Fsc.it: B737 TQ Throttle Quadrant Metal Pro Version

[cited 2020-05-14]

<sup>19</sup> Brunner-innovation.swiss: CLS-E MK II RUDDER with Toe Brakes

[cited 2020-05-14]

<sup>20</sup> Brunner-innovation.swiss: CLS-E MK II YOKE

[cited 2020-05-14]

<sup>21</sup> Brunner-innovation.swiss: CLS-E FORCE FEEDBACK JOYSTICK – A320 CAPTAIN INCLUDING GRIP

[cited 2020-05-14]

<sup>22</sup> Dell.com: PowerEdge R740 Rack Server

[cited 2020-05-13]

<sup>23</sup> KEB Automation KG: Magnet Technology, Clutches and Brakes

[cited 2020-05-18]

<sup>24</sup> Ikea: ODGER

[cited 2020-06-03]

<sup>25</sup> Opencockpits.com: B737's Pilot Seat Captain

[cited 2020-05-12]

<sup>26</sup> FSC.it: 737NG Control Loading YOKE Hardware KIT with NO Software

[cited 2020-05-14]

<sup>27</sup> Fanuc: Datasheet M-2000iA-1700L

[cited 2020-06-03]

<sup>28</sup> PSU Calculator Part List

[cited 2020-06-03]

<sup>29</sup> Raspberry Pi Foundation: Raspberry Pi 15.3W USB-C Power Supply

[cited 2020-06-03]

<sup>30</sup> Gigabyte GeForce GTX 1050 Ti OC 4G

[cited 2020-06-03]

<sup>31</sup> Amazon, Inc.: HP 24w Full HD Monitor (1920 x 1080) 23.8 Inch (1 HDMI, 1 VGA) - Black

[cited 2020-05-13]

<sup>32</sup> Vuzix M4000: Technical Specifications

[cited 2020-06-03]

# 3 Financial and Market Analysis

This simulator is designed such that better upset prevention and recovery training can be offered to pilots. In order for this to be done successfully, a proper market analysis needs to be performed on the viability of creating such a simulator and making it marketable. In order to do this, the target market, market size and competition are determined. Following this a SWOT analysis is performed on the concept of this simulator. Next, the costs of building and running the simulator will be estimated. Lastly, an estimate of the return on investment for this project is made.

## 3.1. Target Market

The target market for this project is the pilot training market for upset prevention and recovery for the Airbus A320 family. This market consists of large airliners with a lot of A320s that wish to train their pilots, and training centres who rent the simulators out to smaller airliners. An airliner could buy a simulator for every 2000 pilots they have in terms of available training hours assuming 4 hour training sessions, but it's most likely also financially attractive to buy one even for airlines that employ fewer pilots. The Airbus A320 is currently the largest family of planes flying around the world<sup>33</sup> and is therefore the most appropriate target market for this simulator. Considering that this simulator is relatively simple to adapt to fit a different aircraft family, this target market may expand in the future.

## 3.2. Market Size

In 2019, the total market size for simulators comprised a revenue of 5.7 billion USD at a growth rate of 5.2% annually<sup>34</sup>. As this simulator is not Level D certified, however, it cannot compete on the entirety of this market, and a further analysis is required. An additional problem is the impact of COVID-19: for this project, it is assumed that the market will be back to 2019 figures in 2021, though nothing is certain in this regard, and the lasting cultural impact of the pandemic is yet to be clear and may also have an effect on the aviation industry. For now though, an analysis is provided to detail the possibilities in terms of a UPRT simulator market under this assumption.

In 2017, CAE published an analysis of the state of the aviation industry and their prediction of the ten years after: it is assumed that the world recovers sufficiently from the COVID-19 pandemic such that the predicted numbers for 2027 still hold at that point in time. In that analysis, CAE predicted that the total amount of pilots in service worldwide will be 440,000, while 60% of all aircraft in service will be a narrow-body type jet and as a result 60% of all pilots will be a pilot rated for such a type of aircraft: additionally, they predict that an average of 15,000 newly trained pilots will enter this market segment on a yearly basis<sup>35</sup>. Since 2019, every pilot must perform 4 hours of UPRT in the simulator on a recurrent, yearly basis<sup>36</sup>, and as part of advanced UPRT, each pilot-in-training is required to complete at least 3 flight hours of advanced UPRT by FCL.745.A, which could potentially be performed in the simulator if it is sufficiently representative of the real case, but no specific recommendations are given for basic UPRT<sup>37</sup>. Therefore, it is assumed that basic training flight hours are not a part of the relevant market, though advanced UPRT flight hours are taken into account. Then, the total amount of yearly flight hours in demand comes to roughly 1.1 million.

Assuming that the customer runs their simulator 23 hours a day, 351 days a year and at a 100% efficient allocation of these flight hours, that comes to the equivalent of 131 simulators. If operated by a single instructor for only 8 hours a day, this equates to 376 simulators to supply the worldwide flight hour demand. Hence, it can be assumed that the market comes down to somewhere between 131 and 376 "simulator equivalents" over the average lifespan of such a device, which is taken to be roughly 20 years: "simulator equivalent" is taken to mean the amount of training hours a simulator of this type can provide over its lifetime. In that case, an average of between 7 and 19 simulator equivalents can be expected to be sold over the entirety of the market yearly if the demand is to be met in a sustained manner, assuming perfect allocation of training hours. However, in order to make this a viable market, regulation changes will be required to exclude non-UPRT specific

<sup>33</sup>Airbus: A320 Family - Passenger Aircraft

[cited 2020-06-22]

<sup>34</sup>MarketsandMarkets Research Private Ltd.: Flight Simulator Market by Platform

[cited 2020-06-04]

<sup>35</sup>CAE Inc.: Airline Pilot Demand Outlook

[cited 2020-06-04]

<sup>36</sup>BAA Training: Mandatory training to prevent upsets and recover from unexpected situations

[cited 2020-06-04]

<sup>37</sup>European Union Aviation Safety Agency: Easy Access Rules for Flight Crew Licensing (Part-FCL)

[cited 2020-06-04]

simulators. The regulations and possible regulation changes will be further discussed in Ch. 4. With the knowledge that such simulators will be competing with in-aircraft training, too, one should be careful and assume that the figure for actual simulators should rather be near the low side of this estimate.

Taking into account the customer's requirement of breaking even at 50 devices sold and assuming a market lifetime of the project of 20 years: a market share of 38.2% should then be obtained to guarantee break-even after those 20 years, again, assuming the break-even figure of 50 devices. As this simulator is restricted to use in the A32X family, the 45% market share that Airbus has in narrow-body jets means that 85% of all A32X simulator equivalents sold should be of this type. This is not a favourable outlook since this simulator is a newcomer in a conservative market, but perhaps still possible given the current lack of competitors if a regulation change were to happen. After a discussion with the customer, it was deemed acceptable to have a lower break-even point given an acceptable price for the simulator. This may also allow for a better return on investment and an earlier reaching of the break-even point. The new break-even point is determined in Subsec. 3.5.2 after a cost analysis and is achieved after selling 20 simulators, which is possible in 10 years with a more reasonable market share of 63.5% for the A32X simulators. This market share is calculated with respect to the most conservative estimate of 7 simulator per year demand, and the the actual required market share is thus likely to be lower. Such a construction would allow the project to turn a profit for the second half of its life.

By supporting the project for longer, widening the profit margin or by offering a variant that supports B737 training, it is possible to reach break-even at a lower sales fraction or at an earlier point in time. Do note that the initial demand for simulators like this, after a regulation change, will be a lot higher than 7 allowing any break-even point to be reached faster then predicted (given the same market share)<sup>38</sup>. Additionally, if regulations were to change in favour of this simulator, which is not unlikely given the recent happenings around LOC-I published by IATA in 2019 [4], that would most likely result in an increased amount of required UPRT-hours which would further expand this market. However, if the change in regulations does not occur, obtaining the relatively high market share will be a lot more difficult given the high amount of competition. A lower market share might still be acceptable however, but the break-even point will be reached later, making the project a bit less attractive from an investment point of view.

It can thus be concluded that, while there is absolutely still risk involved, the risk in terms of market size could very well be deemed acceptable for investors, especially given the possibilities in terms of further investment into broadening the available market and the likelihood of further regulation changes with respect to UPRT, alongside the return on investment detailed in Sec. 3.6.

### 3.3. Competition

The current market has many manufacturers which produce simulators certified for UPRT under current regulations. However, these are not UPRT specialised simulators like the one this project is designing. Given a regulation change making the simulator requirements for UPRT more stringent, most of these simulators will not be competing with this simulator. However, this does not mean that these competitors won't create new simulators in order to compete in this new market segment. While this will come at a delay, these companies already have loyal customers and a reputation, making them possible threats. Examples of competitors for regular all-purpose simulators are CAE and L-3 Commercial aviation.<sup>39 40</sup>

The market for UPRT specific simulators is very limited currently. The closest examples would be centrifugal simulators like the Desdemona or the Kraken<sup>41 42</sup>. Very few of these simulators were created however, indicating a mismatch between what the market desires and what these systems provide. This project aims to create a simulator which can provide the high quality UPRT with a simpler simulator at a lower cost to be more attractive.

Lastly, there is the competition due to the possibility of carrying out UPRT in training aircraft. Doing this in a training aircraft may provide a unique and high quality training experience, since it is performed while flying. However, these training aircraft are not of the same type as the aircraft the pilot is training for, hence there will be some discrepancies. The simulator would have an advantage in terms of simulating the correct aircraft. A simulator also is not dependent on weather conditions and can operate much longer every day, allowing for more pilots to be trained. Despite these benefits,

<sup>38</sup>FlightGlobal: Flight Fleet Forecast's single-aisle outlook 2016-2035

[cited 2020-06-04]

<sup>39</sup>L3: L3 RealitySeven Full Flight Simulator (FFS)

[cited 2020-06-22]

<sup>40</sup>CAE: Civil Aviation: Full-Flight Simulators

[cited 2020-06-22]

<sup>41</sup>Desdemona: motion simulation for your proficiency

[cited 2020-06-22]

<sup>42</sup>The Drive: 'Kraken' Is the U.S. Navy's Monster Motion-Based Research Simulator

[cited 2020-06-22]

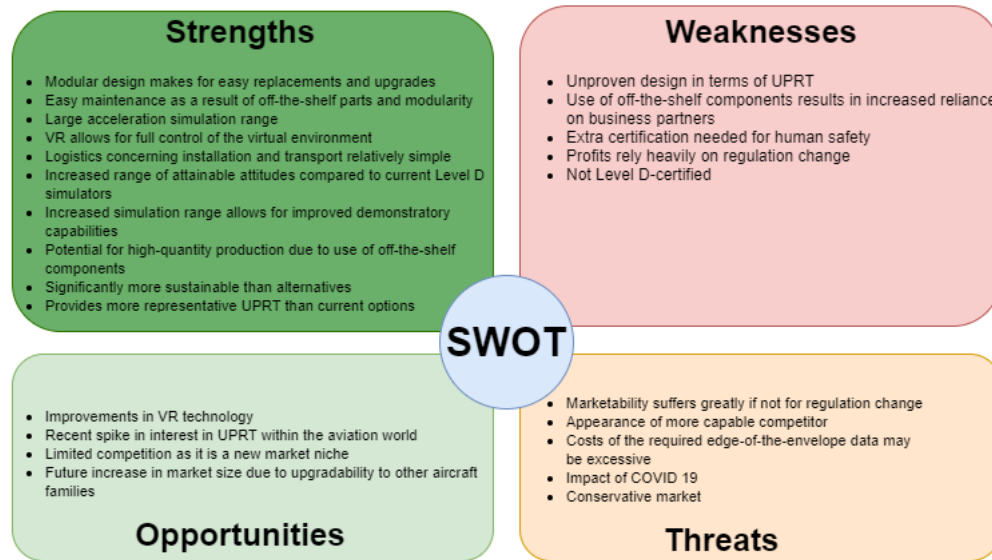


Figure 3.1: SWOT analysis

the simulator should be cheaper per hour of training over its lifespan than a training aircraft to be in the best market position.

### 3.4. SWOT Analysis

To aid in the identification of opportunities and high-risk areas in terms of investment for the design, a Strengths-Weaknesses-Opportunities-Threats (SWOT) analysis was performed. An overview of this analysis is provided in Fig. 3.1, and a more in-depth explanation of each of the bullet points shall be given in this section.

#### 3.4.1. Strengths

Strengths of the simulator are those properties inherent to the device itself that offer it an advantage: identification and awareness of these at an early stage allows for a design in which these strengths are maximally exploited and utilised, which in turn allows for a strong position on the market. Firstly, the modular design of the arm allows for easy switching of components, which also means that replacements (whatever the reason may be) or upgrades are easily installed. Additionally, this combines with the use of off-the-shelf components to make for quick and easy maintenance. The range of acceleration vectors that can be simulated is, due to the increased motion space of the arm, larger than that of current hexapod simulators, which aids in simulation of the recovery portion of UPRT. The use of VR as a visual system allows for full control of the presented (virtual) environment, meaning that visual changes in the cabin do not require an interchange of cabin components and visual changes in the outside environment are as simple as inputting a command into the simulator, as opposed to in-aircraft training where neither of these factors can be influenced to this degree. The modularity of the simulator as well as the lack of large-volume components mean that installation and transport of the simulator is relatively simple logistically (so



Figure 3.2: The delivery of SIMONA's collimating mirror. Image courtesy of ir. Olaf Stroosma.

so

long as the simulator is transported in parts, that is). This is in contrast to the traditional Level D simulator, in which the collimating mirror (to name one example) is large enough to present issues in this regard, making installation and transport a large operation: to illustrate, consider the delivery of the collimating mirror of TU Delft's SIMONA shown in Fig. 3.2.

Additionally, the robotic arm-based simulator provides a far greater range of attainable attitudes than the traditional hexapod simulator. While this is not immediately an advantage (the human body does not perceive attitude, only accelerations), the increased range does mean that a larger amount of manoeuvres can be recreated one-to-one in terms of attitude, reducing the risk of inducing false cues in the wider attitude regime associated with upset recovery training. In terms of prevention, the increased range of situations that can be simulated means that it is very well-suited for demonstration of the concepts associated with upset prevention, being energy management and a better understanding of the fundamentals of aerodynamics, among others<sup>43</sup>, meaning that this simulator would be a valuable tool in the toolbox of any instructor. Apart from this, the use of off-the-shelf components in this design offers a lot of potential for high-quantity production if needed, meaning that the chance of missing out on an opportunity for high-volume sales (as a result of, say, the introduction of new regulations in favour of this design) is lower than it would be in case of full in-house production, where expansion of production would require a hefty investment that takes a long time to set up. Another strength offered shows up in terms of sustainability, where this simulator is more than 80% sustainable in terms of CO<sub>2</sub> emissions compared to the alternative of in-aircraft training using aerobatic aircraft. Lastly, the capabilities of this simulator allow for more representative UPRT than current options: simulators lack the capabilities to go to the extremes of the flight envelope either in terms of model or in terms of motion capabilities, while aircraft training is performed in aerobatic aircraft which behave significantly different from their airliner cousins. Now, there is no such thing as free lunch and all these strengths come at the cost of some weaknesses, however. These shall be discussed next.

### 3.4.2. Weaknesses

There are a few weaknesses which are inherent to the simulator itself. First of all, there are currently no commercially available robot arm simulators for UPRT. While there has been some research done proving its potential, it has yet to be used in the market [9]. Secondly, since a lot of the components can be found on the market, this simulator would be very dependent on its suppliers. If an important component is no longer available on the market, an alternative needs to be found. This also complicates things for customers who might need some replacement parts. Another weakness would be that the demand for this simulator relies heavily on a change in regulations to enforce a special type of simulator for UPRT. If this change in regulations were not to happen, the market size for this simulator would become a lot more limited. The market size is already limited due to this simulator not being level D certified, and therefore not applicable on most of the required training outside of UPRT. Additionally, a simulator needs to be safe, but to prove that it will be safe to put humans at the end of a robot arm may require additional certification compared to regular simulators.

### 3.4.3. Opportunities

Some opportunities of which this simulator may take advantage of are present as well. Recently, there has been a great increase in interest in UPRT within the aviation world; this increased interest already resulted in a change in regulations to make UPRT mandatory<sup>44</sup>, hence it is reasonable to assume more regulation can follow. A simulator focused around UPRT is currently a very niche market, though this market is sure to open up further with regulation changes to make better UPRT mandatory.

The future also holds a lot of opportunities. Due to how most of the cockpit is virtual in its design, and the cabin is very bare boned, it will be easy to reconfigure this simulator to different planes. This allows the target market and market size to increase in the future. Hence, whether it's a brand new aircraft or a different, already existing, one, there is plenty of opportunity to expand the target market size. Besides this, the quality of the simulator may also go up relatively quickly. This is due to the rapid progression in technology for virtual reality, which can be followed by the customer without having to buy a full new simulator each iteration.

<sup>43</sup>The Boeing Company: Aerodynamic Principles of Large-Airplane Upsets

[cited 2020-06-03]

<sup>44</sup>BAA Training: Mandatory training to prevent upsets and recover from unexpected situations

[cited 2020-06-04]

### 3.4.4. Threats

Lastly then, there are some external threats that must be mitigated or at least accounted for. First of these is the fact that, as use of a simulator like this is not required under current regulations, marketability of the simulator suffers a great deal if no regulation changes in its favour occur. This may be mitigated through lobbying but also through advertising of the safety advantages training in a simulator like this will have: if it is clearly shown that the capabilities of this simulator are within the realm of possibilities, regulatory authorities may no longer see a reason not to demand such training. Secondly, there is the very present threat of a competitor appearing: especially if the regulations change in favour of a simulator like this, it is very well possible that some of the larger simulator producers will set their eyes upon an UPRT simulator. Such companies have access to a vastly larger pool of resources than this team, which may mean that they can produce a simulator that beats this one; additionally, as the aviation industry is a very conservative one, customers are likely to stick with companies they previously bought reliable products from, meaning that those same companies entering this market would drain the pool of possible customers. Unfortunately, there is no way to mitigate this threat apart from a large marketing campaign, which would require significant investments. Another threat that should be accounted for is the possibility that the type-specific edge-of-the-envelope data required for the simulator is either very expensive to acquire, or not yet available at all. In the latter case, the acquisition of the necessary non-generic data to make the model representative would require a large investment such that the data can be collected through flight tests. While there is no way to mitigate this per se, this could be turned into a positive investment opportunity if the collected data is then sold to third parties. This does not, unfortunately, reduce the initial investment, however. An additional factor that should not be discounted is the short-term but also lasting impacts of COVID-19: aviation may not recover very well from the pandemic which would mean that the market this device would be entering is a lot smaller than desired. By taking this into account in the broader market analysis and the establishment of the cost, the threat this poses can be mostly done away with, though the uncertainty will still remain. Lastly, the fact that the aviation industry is inherently conservative and non-trusting of outsiders means that entering the market as a new, unproven company is a hard thing to do, even more so in a safety-focused environment such as the simulator part of the industry. By properly supporting the product and design however, it is hoped that the industry can be convinced of the worth of the simulator. By identifying each of these threats at this stage, they can be taken into account and the risk related to them can be minimised.

## 3.5. Cost estimate

To get an idea of the amount of money the simulator shall sell for, a cost budget is estimated. Where possible, this budget is already based on the analysis provided in Ch. 5. The overall cost of the simulator is split up in five categories: parts on-board, parts motion system, IOS & infrastructure, administrative and fixed costs. Parts on-board, motion system and IOS & infrastructure are all costs concerned to the parts as explained earlier within the report for the other budgets. Administrative comprises all costs that are not a part of hardware of the product, though these costs are marginal (determined on a per-product basis) and describe the process and administrative tasks behind the simulator: costs that do not directly relate to the physical parts of the simulator but that are still incurred on a per-simulator basis. These costs includes costs for certification, insurance, labour and vehicle model, but also things like rent or utilities: due to the low amount of simulators produced relative to the amount of space used, these are also assumed to scale linearly, such as to account for any possible upscaling or downscaling of production. Fixed costs describe the cost that are incurred irrespective of the amount of products sold. These will not be on a year-to-year basis and they have to be distributed over the amount of sold articles. These costs are costs such as software updates, development and testing costs. Any costs without reference or with engineering judgement as reasoning are estimates based on discussions within the project group. These discussions are based on assumptions and are therefore bound to be off, but they may provide a decent enough cost estimation. As such, the given numbers should be read as a cost budget rather than an estimate, though it does of course also serve as an estimate of the device cost. Therefore, a margin of 20% is applied to the total. All of these costs are summed up and can be found in Tab. 3.1 with further explanation. In Fig. 3.3 the Cost Breakdown Structure is presented.

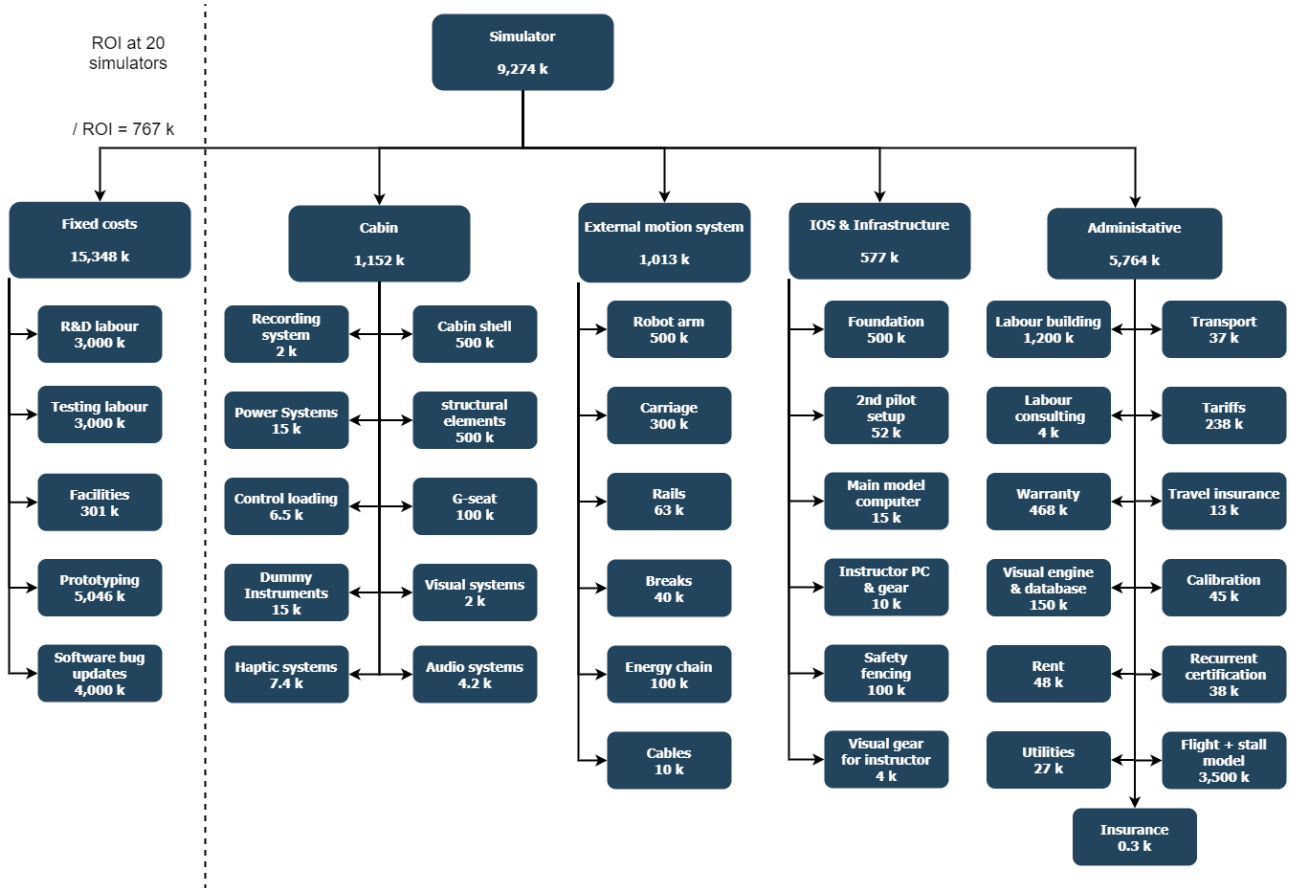


Figure 3.3: Cost Breakdown Structure

### 3.5.1. Cost explanation

Not all costs are based directly off of sources but rather off a calculation based on several assumptions, and these shall therefore be highlighted shortly: additionally, to prevent unnecessary repetition of such lengthy tables, this table presents the most up-to-date estimates based on the results from sizing (described in Ch. 5). It is expected that the project will be supported for a period of 20 years, that the throughput time for each simulator is roughly 25 weeks and that a single production line is capable of producing two simulators a year. The cost of renting a location for production, utilities and insurance are assumed to scale linearly with the amount of simulators built. Due to its proximity to a large international harbour and a large university, Rotterdam is chosen as assumed location for production.

The amount of engineers/employees that is expected to be required to build the simulator is 20, based on an estimate of the average size of small single-product aerospace companies, each accounting for 60 euros an hour in employer costs (salary and non-salary costs such as insurance premiums and taxes) and an additional 30.000 euros each year in licensing fees for the appropriate software to use. For the aeroplane dynamics, an OEM-specific model is considered, which is licensed on a per-simulator basis. For warranty, European law is considered for electronic goods such that a 2 year warranty is required.

### 3.5.2. Break-even point

With the marginal and fixed costs known the break-even point can be determined. The break-even point is the amount of simulators needed to be sold in order to earn back the initial investment (fixed costs). This is therefore in balance with the costs and the price at which the simulator is sold. The original break-even point was set as a requirement to be at a market of 50 devices. However after a market analysis and a discussion with the customer, it became clear that a lower break-even point is appreciated. It seems optimistic to assume a dominant market position given that the market is conservative and our simulator is a newcomer. By calculating the required price of the simulator to reach a given break-even point, it was determined that a reasonable break-even point would be 20 simulators. The required price for such a break-even point for the simulator requires the simulator to only cost 9.27 million euros, or 11.12 million euros assuming the estimated cost to be off by 20%.

Tab. 3.1 presents the cost build up assuming a break-even point of 20 simulators. The total cost

arising from a certain item is shown on the left, and the marginal (per-unit) cost is shown on the right i.e. in the format (total/marginal). As the other costs are purely on a per-device basis, only the marginal costs arising from them are shown. In this manner, the required price for break-even is automatically calculated. After selling 20 units, all invested money has been earned back and from that point on profit will be made.

Table 3.1: Cost budget and estimate

Category	Component	Budget (×1000 €)	Reasoning
		per unit	
<b>Onboard</b>	Cabin shell	500	Engineering judgement
	Structural elements	500	Engineering judgement
	G-seat	100	[14]
	Visual systems	2	Consumer price of 2 VR glasses (1 spare)
	Aural systems	4.2	Consumer price of the complete aural system estimated in Sec. 5.6
	Haptic systems	7.4	Consumer price of haptic gloves and position tracker <sup>5655</sup> including spares for rotation
	Recording system	2	Based of multiple <sup>47</sup>
	Power systems	15	Engineering judgement
	Control loading systems	6.5	determined in Ch. 5.21
	Dummy instruments	15	Based on calculations done in Sec. 5.8
<b>Motion system</b>	Robot arm	500	High-side estimate from industry <sup>48</sup> with additional margin to account for necessary changes
	Carriage	300	Engineering judgement based on price of the arm
	Brakes	40	Engineering judgement
	Energy Chain	100	Engineering judgement
	Rails	63	Train rail material cost <sup>49</sup>
	Cabling	10	200 m at 50 euros per meter
<b>IOS and foundation Infrastructure</b>	Foundation and supporting structure	500	Engineering judgement: varies on a per-customer basis
	Offboard 2nd pilot setup	52.1	Onboard systems without structure, shell and g-seat (for the co-pilot)
	Main model Computer	15	Price of a high-end system including spares
	Instructor Computer and gear	10	Consumer price estimate and spares
	Safety fence	100	Engineering judgement: varies on a per-customer basis
Visual gear (instructor)	4	Based off <sup>50</sup> assuming a spare	
<b>Administrative</b>	Transport	37	Worst-case cost estimate of a worst-case distance of 20.000 km <sup>51</sup>
	Travel tariff	237.9	2.7% of product value based on <sup>52</sup>
	Travel insurance	13.2	0.15% of product value <sup>53</sup>
	Calibration costs	44.6	2 engineers ×21 day trip ×(daily living costs+daily salary) + 2 round trip flight tickets 1 day, 4 times a year for 20 years
	Lifetime recurrent certification costs	38.4	
	Vehicle model, with stall and replication	3500	Based off [14]
	Labour-Building	1200	60 euro per hour ×40 hour work week ×20 engineers ×25 weeks
	Labour-Consulting	4	1 week of €100 an hour
	Warranty	463.7	5% of product value
	Rent	48	Based on a standard factory hall available in a location of interest for half a year
Utilities bill	27.1	Based off average for Dutch industry <sup>53</sup>	
Insurance	0.32	Based off Dutch insurance for companies <sup>54</sup>	
<b>total marginal costs</b>		<b>8504</b>	
		total / per unit	
<b>Fixed costs</b>	Software bug updates	4000 / 200	Based on one FTE software engineer paid 200.000 EUR each year over a period of 20 years (estimated required support lifetime of the device)
	Labour-R&D	3000 / 150	€150 per hour for 10 engineers for 50 weeks of 40 hours per week
	testing phase labour	3000 / 150	€150 per hour for 10 engineers for 50 weeks of 40 hours per week
	testing facilities	301 / 15.1	Based on a standard factory hall available in a location of interest for 2 years
	prototyping	5046 / 252	creating 3 cabins and buying all other components once.
<b>total fixed costs</b>		<b>15347 / 767.4</b>	
<b>Total costs per unit Including a 20% margin</b>		<b>9274 11128</b>	

### 3.5.3. Hourly cost budget

As specified by the customer in requirement UPaRTS-SH-SO-4, the hourly operating costs of the simulator should not exceed 1200 euros excluding the costs for the instructor. To demonstrate that this requirement is met, an estimate is made of the costs incurred because of power usage, maintenance and operating personnel (excluding the instructor), and maintenance material or parts. At an industrial energy price of 9.41 cents per kWh and the power budget as presented in Sec. 5.9, an hourly power price of 1.75 euros is found, which is hardly significant. The hourly employee cost for an engineer that was assumed in the budget (75 euros per hour) is assumed to be representative of the costs that will be made for the mentioned employees: it is then assumed that four full-time equivalent (FTE) actor-pilots and similarly four FTE maintenance engineers are sufficient based on the 23 hour-a-day, 7 days per week operation and two weeks of downtime. This then comes to a total of eight full-time employees paid 150,000 euros a year divided over 50 weeks of 23 hours-a-day operation for the "hourly" price of operation in terms of personnel, which comes to a contribution of 111.80 euros hourly. Assuming the same type of industrial building as taken for the factory hall in the cost estimate is used (at a rent of 95,000 euros yearly) this converts to a cost of roughly 11.91 euros hourly (only counting operational hours). It is assumed that the robotic arm is the most failure-prone component due to the amount of moving parts and joints and the accelerations imposed upon each of them: considering that the average modern industrial robotic arm has a mean-time-between-failure of roughly 50,000 hours [15], this is taken as the lowest-reliability estimate of the entire system: a worst-case estimate using these numbers then means that, on average, all parts will be replaced once over any period of  $\frac{50000}{23 \cdot 7 \cdot 50} = 6.2$  years, which results in an estimated effective part maintenance cost of 56.35 euros hourly. Hence, a total estimated hourly cost of 181.81 euros is established, which is well over six times lower than the cost bound given by the customer in UPaRTS-SH-SO-4: one should be careful to note that this estimate was based on the customer's estimated cost of a centrifugal simulator concept. Hence, for a more suitable comparison: a conventional Level D simulator would require an hourly rate of roughly 400 euros [16], and given the sensitivity of these calculations it can confidently be said that this will not be exceeded by this concept; hence, the (current) lack of Level D-certification can be made up for at least partially by the price of the simulator not just in terms of acquisition, but also in terms of operation costs.

## 3.6. Return on investment

The return on investment (ROI) is calculated using Eq. 3.1 and is a term often used to describe how attractive a investment is. A positive ROI is a good investment and a higher ROI is considered better than a low one.

$$\text{ROI} = \frac{\text{Net return on investment}}{\text{cost of investment}} \quad (3.1)$$

The ROI of this project is relatively easy to calculate since the price is determined based on the return on investment. Currently it is assumed that the return on investment will be reached after 10 years. If the same production rate and price is kept, the ROI will be 1 after 20 years. This ROI is however very sensitive to the profit made from each simulator since this is only 8.3% of the price. If the profit is half a million more the ROI would be 2.3 while half a million less profit would result in a ROI of -0.3. Given that the demand of simulators will be a lot higher in the beginning due to the creation of a new market as discussed in Sec. 3.2, it is reasonable to assume that a higher profit can be achieved or more simulators can be sold.

To conclude, this project will be worthwhile investing into because the return on investment is very likely to be very good.

<sup>45</sup>Onkyo HT-S7805

[cited 2020-08-06]

<sup>46</sup>CaptoGlove the world's first wireless wearable controller for gaming and smart devices

[cited 2020-08-06]

<sup>47</sup>RLC-410

[cited 2020-08-06]

<sup>48</sup>Insights: What is the real cost of an industrial robot arm?

[cited 2020-06-08]

<sup>49</sup>MelbPT: Rail Construction Costs

[cited 2020-06-08]

<sup>50</sup>ANIWAA: X2 thirdeye gen

[cited 2020-06-09]

<sup>51</sup>Alliance Experts: Transportation for international trade

[cited 2020-06-08]

<sup>52</sup>European Customs Portal: HS Code 85012000

[cited 2020-06-08]

<sup>53</sup>ShipHub.co: Container insurance - why is it worth it to insure a container?

[cited 2020-06-08]

<sup>53</sup>TeamDeals: Energie Zakelijk - Gemiddelde energiekosten bedrijfspand berekenen? (English: "Business Energy - Calculate average electricity costs [for your] company building?")

[cited 2020-06-09]

<sup>54</sup>Centraal Beheer: Zakelijke verzekeringen voor ondernemers (English: "Business insurance for entrepreneurs")

[cited 2020-06-09]

<sup>55</sup>unboundvr.nl: HTC Vive tracker (2018)

[cited 2020-06-09]

<sup>56</sup>bestware.com: Manus Prime One

[cited 2020-06-09]

<sup>57</sup>Statista: Prices of electricity for industry in the Netherlands from 2008 to 2019 (in eurocents)

[cited 2020-06-19]

# 4 Training Systems

This chapter covers the training aspects of the system, presenting a training envelope, and illustrating both a pilot and instructor guide for one of the simulated upsets. In Sec. 4.1, an overview on pilot training, in specific UPRT, is given. Firstly, a brief description of the current regulatory framework is given, and then a training gap is identified and solutions to overcome this in the system are suggested. Building on this, Sec. 4.2 includes the training envelope of the system, together with brief descriptions of the covered upsets, which were compiled with the solutions identified previously in mind. Then, in Sec. 4.3, the pilot and instructor training guides are presented for a single upset as a proof of concept. Finally, Sec. 4.4 presents some final considerations and recommendations for the future development of the project.

## 4.1. An overview on pilot training

The aviation industry, and all activities surrounding it, have always been led by safety, it being the number one priority and, ultimately, being the driver for most decisions taken and processes adopted within the industry. Pilot training is at the very core of this goal, and an inalienable process for safe and efficient crewed flight. Defining what pilot training should entail is an extremely broad exercise, as the full extent of the goals to be achieved is very vast and would largely exceed the scope of this report. However, a few high-level requirements that all types of pilot training should meet can be drafted, as synthesised from the lengthy descriptions of [17–19], and will provide useful guidance during the development of training curricula for the system. In general terms, it is desirable that pilot training is **beneficial** for safe flight operations, **efficient** in terms of time required to achieve proficiency, **easily accessible** in order to correctly equip as many pilots as possible, **repeatable** such that positive learning habits can be fostered, and **comprehensive** to ensure pilots are trained for all scenarios that can realistically be encountered in flight. These will be the driving requirements for the proposed training coverage and resulting routines, and their effect will be further explained where pertinent.

The simulator to be designed will, as per the Mission Need Statement of the project, focus on Upset Prevention and Recovery Training (UPRT), and so this will be the focus for the training objectives to be set in this chapter. This section serves as the base work to understand the extent to which UPRT is incorporated in current pilot training, and to identify a training gap that might exist and the system objectives derived from it.

### 4.1.1. Current regulations

Upsets leading to loss of control in-flight (LOC-I events) are amongst the most prominent causes of fatal accidents in commercial aviation. Even though these events are very rare, they have accounted for more fatalities in the past decade than any other incident category [20]. Such upsets are in their vast majority preventable and, when dealt with appropriately, their threat to the safety of a flight can be mostly eliminated. The required training pilots must undergo to possess these skills, however, is quite specific, and was for a long time not included in training curricula of commercial pilots. Regulators have since realised that the potential effect of these in-flight upsets must be addressed, and so today UPRT forms an integral part of commercial pilots' formative and recurrent training.

From extensive research by operators and regulators, it has been established that pilot-induced accidents are the most frequently occurring form of this type of accidents. Within this category, the following causes can be identified: application of improper procedures, poor energy management, improper training, spatial disorientation, and cabin crew distraction. The first three causes can be seen as preventable and not situation-dependent, meaning that with coherent and widespread changes to operating procedures and, to a larger extent, training, these accidents can be avoided. It is then worth to summarise the UPRT in use today, in order to later identify the existing training gaps and define system goals to improve safety with regards to LOC-I.

In general, more recent efforts in terms of UPRT adopt a multifaceted approach to the issue at hand. As more is known about these kinds of incidents and the physical and human factors behind them, emphasis has shifted from active recovery procedures to, first and foremost, detection and prevention. In most UPRT curricula in use currently, the training philosophy is to prioritise *prevention*, then *recognition*, and only then *recovery*, in this order. Prevention encompasses all activities that promote "timely action to avoid progression toward a potential upset" [21]. Recognition

focuses on "timely action to recognise divergence from the intended flight path and interruption of progression toward a potential upset" [21]. Finally, recovery are all the actions taken by the crew with the aim of recovering from an in-progress upset. These three concepts will be present throughout the chapter, and the shift towards the former two concepts will drive the design of training curricula to a great extent. A brief summary of the UPRT-related skills included in different levels of pilot instruction will now be given. All of the information presented is extracted from EASA's Part-FCL [22] (EASA's regulatory document which covers all aspects of pilot training) and in accordance with current regulations.

**PPL/CPL** The first contact pilots will have with formal UPRT is at the very start of their flying career, as they train towards their PPL (Private Pilot License). Due to integrated nature of many pilot training courses currently, the competence blocks concerning UPRT are common for both PPL and CPL (Commercial Pilot License) curricula, which aligns with EASA's concept of different "levels" of UPRT, further discussed later in this subsection. The UPRT skills are transmitted through a theoretical and a practical part, as expected.

For the theoretical part, carried out in ground school, the pilot will have contact with topics such as: *human performance* (understanding the integration of sensory inputs, sources and types of human error, human behaviour and its effect on flying performance), *aircraft knowledge* (understanding the concept of structural envelope and its implications when manoeuvring), and *principles of flight*, which are subdivided into *stall* (covering flow separation, buffet, stall warning systems, and stall recovery) and *spin* (causes, recognition, development, and recovery).

As for the practical component, a number of UPRT related actions are included in the skill test required to obtain a PPL/CPL certification, as well as their periodic renewal. The covered skills are: stall recover with power in clean configuration, approach to stall on a descending turn with 20° bank and in approach configuration, approach to stall in landing configuration, and steep (> 45°) turns, including recognition of and recovery from a spiral dive. These skills are to be performed in the trainer aircraft, as it is expected that the core flying competencies are transferable between aircraft types after sufficient pilot familiarisation.

**ATPL(A)** Moving on to an ATPL(A), this is often the highest flying certification most pilots will achieve in their career, and so it is logical that it includes a broader and more in-depth look at UPRT. Both the theoretical and practical parts are more thorough and demand a higher level of skill than that seen in the PPL/CPL curricula. In addition, the practical skills also include a specification of the type of platform they should be conducted on. These can be a Flight Training Device (FTD, no motion cueing), a Full Flight Simulator (FFS, comparable to a Level D simulator), or the actual aircraft (A).

The topics to be covered with regard to human performance are: *sensory cues* (sensory threshold, sensory adaptation, and habituation), *attention and vigilance* (with a focus on avoiding hypovigilance), *human performance degraders* (stress, fatigue, startle, and surprise), and *automation complacency* (causes, effects, and pitfalls). Concerning aircraft systems, the covered topics are: *flight envelope protection* (system description and types of protection, different control laws and their effect on manoeuvring), and *structural limitations* (G-force envelope, loading and unloading the frame, structural constraints). The most relevant category, principles of flight, covers the following topics: *stall* (stall warning systems, power-off and power-on stalls, climbing and descending stall, super-stall, and stick-pusher systems), *spins* (causes, recognition, development, and recovery, as in the PPL), *buffet* (identification, causes, and appropriate reactions), and *spiral dive and Dutch roll* (start conditions, identification, and avoidance, no practical recovery).

The practical competences required for the ATPL(A) skill test are: tuck under and Mach buffets (to be performed in an FFS only, aircraft not possible), wind shear at take-off and landing (to be performed in an FFS only, aircraft not possible), steep turns (> 45° turns, to be performed in an FFS or aircraft), early stall recognition and counter measures (to be trained up to the activation of stall warning, without entering full stall, performed in either an FFS or aircraft), and recovery from full stall (to be performed in an FFS only, aircraft not possible).

**Type rating** Concerning type ratings, there is currently no UPRT requirement set by Part-FCL that introduces new competencies during training. What is required by type ratings, which is not exclusive to UPRT but to most skills related to manoeuvring the aircraft, is that the pilots delve into the specific characteristics of the aircraft type they wish to become rated to fly, as well as any particular differences with type ratings they might already hold. This would cover, for example, a certain aircraft's tendency to enter a spiral dive when performing sharp turns, as well as specific envelope protection or augmentation systems that might alter the manoeuvring characteristics of the aircraft. Type ratings are mostly focused on system particularities, and so UPRT is not a focus for this kind of certifications.

**Recurrent training and proficiency checks** In order to ensure pilots are current with their flying competencies and cover any new introductions to legislation or training curricula, all rated pilots must undergo recurrent training and/or proficiency checks, from PPL to ATPL(A) with multiple type ratings. As regulatory concern mostly lies with ATPL(A) license holders, the discussing will be limited to the recurrent training requirements imposed to this class of pilots. Different types of recurrent training and proficiency checks exist (base checks, line checks, SEP training, etc.), and their required interval is set by the operator, respecting local legislation. Mostly commonly, such checks must be performed every six months, and focus on scenario based training, where the pilot must apply but theoretical and practical skills. Concerning the practical scenarios required for an ATPL(A) certification, as presented above, none of them are required during proficiency checks, as per Part-FCL. While operators could opt for broader and more complete proficiency checks (and many do), UPRT related skills are not required in proficiency checks according to current legislation.

From the summary above, it can be seen that there is a progression in depth in terms of UPRT as a pilot advances in their qualification path, which EASA has formalised by setting different "levels" of UPRT<sup>58</sup>. Having a good overview on the current level of inclusion of UPRT in pilot education, and keeping in mind the objectives set for pilot training in the beginning of the section, a gap in pilot training can be identified and system objectives drawn.

#### 4.1.2. Identified gap

Before constructing a UPRT programme that fulfils the need of the customer and that separates itself from other UPRT programmes while still maintaining adherence to regulations, it is of importance that a "training gap" is identified. Potentially finding a solution to this gap could lead to new insights that would give this system an edge over other existing systems, both in terms of marketability and system effectiveness.

For UPRT there already exist extensive syllabi and frameworks that adhere to [18, 19] such as the Desdemona syllabus [23]. However, certain performance-impacting factors are still not taken into account, and the employment of widespread UPRT is still not a reality today. Looking at the description of current training done in Subsec. 4.1.1, there are some improvements that can be suggested in order to increase not only the quality but the reach of UPRT, which will effectively comprise the identified gap in this field. This identified gap is summarised in three points: the effect of emotional response, pilot's disorientation, and the continuity of UPRT during a pilot's career. These points will be further discussed below.

**Emotional response and pilot performance** The effect of a pilot's emotional response when confronted with an unexpected upset and its effect on recovery performance is largely recognised by operators and regulators alike. However, proper startle and surprise training in ground-based simulators is not yet achieved in current UPRT programmes [21] and therefore most curricula make use of on-aeroplane training to simulate startle and surprise. This results in a clear gap in FSTD operations, as supported by [21], which defines startle as a key research topic for future UPRT support. Being able to understand the full extent of the effect of startle in an upset situation, incorporating it into FSTD operations in a consistent way, would improve pilots' preparedness to such events in the real aircraft. Startle will be dependent on the results of Sec. 5.5, as it relies heavily on the inclusion of sudden and extreme cueing actions, while surprise is directly related to the aircraft state and should be taken into account in the training curriculum. Hence, the system should attempt to fill this gap by being able to induce, as much as practical, the full physiological effects of startle and surprise encountered when managing an aircraft upset.

**Disorientation** Apart from the emotional response and its effect on pilot performance, other human factors, such as disorientation, can impact flight safety and even lead into an upset. Spatial disorientation (SD) is an "erroneous sense of the aircraft position and motion" [24] by the pilot, leading to pilot-induced accidents in the case of over-correcting control inputs, for example. This effect can be incorporated into the training provided by the system by carefully designing situations that lead to pilot disorientation, mimicking real-life conditions. Practical training with regards to spatial disorientation is not currently regulated by Part-FCL [22], even though some effort has been made to include these skills in training curricula, especially in military contexts where SD is more prevalent. Even then, the extent to which SD can be faithfully simulated in traditional hexapod FSTDs is limited, and there is a current gap in this dimension of human factors that the system can bridge.

**UPRT continuity** As UPRT takes a more central role in pilot training and certification, there is still a clear gap in its continuity throughout a pilot's career. UPRT related skills are developed with other essential manoeuvring skills during a commercial pilot's ATPL(A), but unlike the latter, are

<sup>58</sup>European Union Aviation Safety Agency: Opinion 06/2017

[cited 2020-08-06]

not refreshed and their currency is not verified over the course of the pilot's career. This presents a clear opportunity to improve safety by keeping pilots UPRT current, standardising the coverage of the training, and reaching a much higher number of pilots. To cover this gap, the system should thus be able to support UPRT in a proficiency check environment, which will be further discussed in Subsec. 4.1.3.

**Limitations on FSTD training** To maximise accuracy of UPRT and minimise the risk of negative training, it is essential for the instructors and operators to have knowledge of several training aspects [25] which will be further elaborated on in Sec. 4.2. One of these aspects is that the instructor must have knowledge of the limitations that come with FSTD training. These missing experiences lead to gaps in pilots' proficiency and understanding when confronted with actual upsets. This subsection serves as an overview for instructors and operators covering these limitations.

In essence, the danger of the limitations of FSTD training for UPRT lay in the potential negative transfer of training. One of the main reasons for this is that current simulators are not (yet) capable of generating sustained g-loading which means that dynamic manoeuvring will simply not be simulated correctly [18]. Practising g-awareness in FSTDs could lead to negative training with improper validation. Therefore, extreme care needs to be taken and awareness of this limitation needs to be raised by the instructor to the pilot in the briefing and debriefing to prevent negative transfer of training. Furthermore, negative vestibular cueing can also induce pilots into looking for effects not experienced in the real aircraft, which once again promotes negative transfer of training, and must thus be clearly identified and, if possible, eliminated.

Secondly, each FSTD has been programmed for a finite amount of flight scenarios of which the set encompassing all these scenarios is called the training envelope. Operating the FSTD outside of this envelope may cause it to behave differently from how the aircraft would behave to a pilot's control inputs. This may result in non-accurate forces and rates fed to the pilot by the motion cueing system leading to negative training. To avoid this, a preliminary training envelope will be given in Subsec. 4.2.1.

Finally, as mentioned before, FSTD are not (yet) able to simulate the full physiological effects of startle and surprise which implies that the pilot has a reduced emotional response compared to the real life situation, leading to non-fully representative behaviour to these upsets. Startle is the reaction of an individual to the perception of a certain threat which affects the individual physiologically, cognitively and emotionally. How impactful and severe an individual's reaction to such events will be is difficult to predict and therefore startling effects could potentially lead to catastrophic consequences. Surprise, on the other hand, is an effect which is more drawn out in time, and arises when the pilots are confronted with different stimuli than expected. By [17, 21] it is recommended to include elements of "unexpectedness" in UPRT to train pilots to adjust to surprising phenomena and to deal with a highly charged emotional factor. This has been discussed in Subsec. 4.1.2 and will be a driving factor in the design of the training curricula.

These limitations, while hard to fully overcome, must be thoroughly considered in the design process of the system. As seen in Subsec. 4.1.1, many of the practical competencies included in an ATPL(A) certification are to be performed exclusively in a FFS, without the option of using a real aircraft. This means that, before encountering a certain upset in a real operational situation, pilots will be exposed only to it in a simulated environment. If the simulation is not faithful, these competencies will effectively have very low levels of proficiency and their training is not satisfactory. Overcoming these limitations, even if partially, will result in a much more faithful simulation and, as a result, a more effective training device.

### 4.1.3. System objectives

For every FSTD, the main goal is to provide realistic pilot training, which can be broken down into the 5 high-level requirements that also have been mentioned in the beginning of this section. Pilot training should be **beneficial**, **efficient**, **easily accessible**, **repeatable**, and **comprehensive**. As the system that is taken into consideration is specifically designed for UPRT purposes, this goal can be extended to provide realistic pilot training for upset prevention and recovery while still adhering to current UPRT curricula regulations, and ultimately overcoming some of the gaps identified in Subsec. 4.1.2. Specifically for the UPRT part of training, the pilot is deemed as successfully trained whenever the following definition is applicable as provided in [25]:

A pilot who has successfully completed UPRT will demonstrate knowledge and skill in preventing, recognising and, if necessary, recovering from an upset.

In the ideal case, the FSTD adheres to all the 5 high-level requirements. However, considering the UPRT training regime and the limitations thereof as elaborated on in 4.1.2, it is important to

realise that this makes it more difficult for the system to adhere to all 5 requirements. Therefore, each requirement will be elaborated upon in context of UPRT. Subsequently, the identified gaps will be further analysed and system from them system objectives will be drawn.

**Beneficial** - UPRT in itself is beneficial to the safety of air transport as most accidents are due to LOC-I events. For FSTD training to be effective, its fidelity must be high to ensure that negative training transfer is kept to a minimum or eliminated completely. Accurate simulation paired with thorough and consistent training curricula will result in a system which is beneficial to flight safety.

**Efficient** - The efficiency of the training system is defined as the throughput of pilots of the system. In other words, the number of pilots that can effectively be trained in a specific time interval. For training performed in FSTDs it is known that the ratio between time spent in an actual aircraft and time spent in the simulator relates as 1.5/2 hours [26]. That is, the FSTD is effectively 33% more efficient than the trainer aircraft in terms of useful training time. Furthermore, the efficiency of the FSTD is significantly increased when taking into account the operational time as specified by the requirements (see requirement UPaRTS-SH-SO-1) as this up-time is significantly higher compared to that of a trainer aircraft. More details on the operations and logistics of the training of pilots can be found in Sec. 6.2. However, the current limitations on UPRT in FSTDs, and any potential negative training transfer, make that the effectiveness of the training may be decreased.

**Easily accessible** - With an easily accessible system it is meant that the system allows operators flexibility and ease of integration with current operation. Logically, this is in tie with the pilot throughput of the system as discussed in the previous paragraph, but it is also determined by the availability of the FSTDs that can provide UPRT, the prevalence of instructors, the locations of available FSTDs, and the cost for training in such a system. For the latter, it makes sense that providing UPRT using FSTDs is more advantageous for accessibility as this decreases cost per training significantly, as the use of such devices is reportedly much lower compared to trainer aircraft. The remaining constraints will be elaborated upon in Sec. 6.2.

**Repeatable** - Repeatability of the training provided is essential to recurrent training, one of the identified gaps. It is of importance that all aspects of the training regime are replicated for every UPRT scenario to avoid negative training and inconsistencies in pilot performance. The system is deemed repeatable whenever each aspect within the training regime is reproducible and results in similar performance results of the pilot in training. It is important to note that for UPRT purposes, the identified gap on continuity of UPRT plays an important role here. As has been mentioned before, UPRT is currently not part of the recurrent training curricula which results in discontinuity of UPRT. By implementing UPRT in FSTDs and consequentially introducing UPRT into recurrent training, the knowledge gap would be filled and the system would satisfy the repeatability requirement.

**Comprehensive** - For the system to be comprehensive the system has to be able to cover both regular training and UPRT in both their entirety and with adherence to all regulations corresponding to both training schemes. This would require the system to be Level D certified and in an UPRT sense, the system should be able to cover all upsets that are to be encountered during nominal flight. As has been mentioned before, UPRT in FSTDs is limited to its training envelope if negative training is to be avoided, which will be elaborated on in more detail in Sec. 4.2.1. This poses that the system will be bounded by its training envelope regarding the extent to which it can simulate upsets. Additionally, taking into account that Level D certification is not achievable at the moment for this system, this implies that a fully comprehensive system is not yet reachable at the moment.

Considering these high-level requirements and their associated constraints, a certain "training space" can be sketched and some objectives drawn. This specific UPRT FSTD will have the ultimate goal of filling the gaps as elaborated upon in Subsec. 4.1.2. To improve both the inclusion of pilots' emotional response and the continuity of UPRT throughout their career, while maintaining simulation fidelity and training feasibility, a certain training strategy will be adopted.

It has been discussed that, in order to reach a high level of simulation fidelity, comparable emotional response to that encountered in the real aircraft, in particular startle, must be present. This is, of course, a very challenging feat: pilots are aware they are in an FSTD, and expect to be confronted with certain non-nominal scenarios, such as an engine failure or an in-flight upset. Pure UPRT in an FSTD will never truly achieve the full extent of startle as experienced in reality, and this is a limitation that must be widely recognised by instructors and pilots alike. Some form of emotional response, however, is deemed to be possible, by adding a certain "randomness" factor to the type of upset and the time at which it is encountered. Let us now discuss training continuity for a moment.

Currency is an essential part of flight skills, which is promoted by mandatory recurrent training actions and proficiency checks. UPRT, however, has vastly been left outside of these actions, creating a varying level of skill amongst pilots and to some extent disregarding the importance of upset prevention and recovery skills in everyday flight operations. Adding some form of UPRT com-

ponents into the already existing proficiency checks is the simplest way to ensure these knowledge gaps are overcome and that UPRT becomes more widespread between pilots. In order to make this economically feasible for operators, however, the system to be designed must support both UPRT as well as inside-the-envelope (both nominal and non-nominal) operations, allowing continuity training and checks to be done using a single FSTD. This concept also allows for an improved inclusion of startle in the training. By adding a number of UPRT scenarios to the existent proficiency check skill list, one of these can be experienced at a "random" time during the training session, mimicking the startle effect to some extent. The pilot would expect some sort of UPRT content during the training session, but by removing previous knowledge on the type and moment of the upset, some emotional response can be simulated.

Some mention must be made to the multi-crew environment that is required as per the Part-FCL regulations [22], and must thus be taken into account in the system as well. In the current design iteration, the second pilot is a member of the training staff, and represented to the pilot-in-training in a virtual manner. The interaction between crew members and the communication skills required in this sort of operation, both nominal and non-nominal, are key skills for training, UPRT included [17, 22]. A system objective must then be to accurately include these interaction in all simulated scenarios, conserving the synergies by them created.

There are some limitations to this solution, however. To achieve market feasibility, it's necessary that the system is capable of providing both formative and recurrent training as per the regulations in place, meaning it must fully fulfil the definition of an FFS as per EASA's Part-FCL [22]. In practical terms, this means achieving a Level D certification or similar. At this stage of the project, this will not be the goal, and a Level D certification will not be achieved. The option of supporting training as required in a Level D simulator will be explored, but the focus will remain on the UPRT portion of the training envelope. If the system, as a proof of concept, is feasible, a Level D certification or equivalent can be pursued in the future, which is further discussed in Sec. 4.4 and Ch. 9.

In summary, the system objectives are to bridge the identified gaps in FSTDs, namely the lack of emotional response and continuity in UPRT, while keeping in mind the top level requirements set at the beginning of the chapter. How these objectives translate to a training envelope, and the training scenarios to be included will be elaborated upon in Sec. 4.2.

## 4.2. Training breakdown

Once the system objectives have been set, these can be translated into a training envelope, taking into account any limitations resultant from the expected cueing performance of the system. In Sub-sec. 4.2.1, the training envelope is defined, by listing a number of training scenarios that should be covered by the system and indicating their relevance to the training objectives. Then, in Sub-sec. 4.2.2, a more detailed description of each of these scenarios is given, briefly explaining what they entail in terms of aircraft condition.

### 4.2.1. Training envelope

In this subsection, the extent of the training envelope will be defined by listing a number of training scenarios that the system should be able to accurately simulate. Firstly, the key UPRT scenarios will be identified, to then be complemented by non-UPRT scenarios required for recurrent training and proficiency checks.

**UPRT scenarios** These scenarios have the goal of bridging the identified gap in current UPRT, making accurate simulation of potential LOC-I situations possible in FSTDs. They span different types of commonly encountered upsets, which are chosen to provide a wide variety of required recovery manoeuvres, cueing scenarios, emotional responses and, in general, broad training opportunities. This list of upsets was compiled taking into account the UPRT objectives as described in [17–19, 21, 23], and extensively discussed with the Cueing team in order to ensure the feasibility of the simulation. The final list of UPRT related scenarios covered by the simulator is:

- **Unusual attitude upsets** - extreme pitch ( $< -10^\circ$  and  $> 25^\circ$  of nose angle) and extreme bank ( $> 45^\circ$ ).
- **High altitude wind gust events** - vertical and horizontal wind shear situations of significant magnitude.
- **Wake vortices encounter** - extreme wake scenarios, at both high and low altitudes, in clean, approach, and landing configurations.
- **System failures** - full control surface deflection, automation failures, and thrust asymmetry, at both high and low altitudes.
- **High altitude stall recovery** - clean configuration stall, with approach to stall, full-stall development and recovery.

- **Low altitude stall recovery** - approach and landing configurations stall, with approach to stall, full-stall development and recovery.
- **Energy management upsets** - thrust profile variation in different configurations.
- **Stall recovery with envelope protection:** envelope protection systems demonstration (not to be explored at this stage in the project).

A more thorough description of what is understood by each of these upsets is given in Subsec. 4.2.2.

**Standard scenarios** This list of practical scenarios covers the standard flight events as required for an ATPL(A) skill test and proficiency check as in Part-FCL [22]. In order to make possible the solution discussed in Subsec. 4.1.3, this class of events must be included within the training envelope, allowing the system to simulate the full extent of situations required to eventually obtain a Level D certification (which, as per Subsec. 4.1.3, will not be an objective at this stage in the project, but rather a goal for future development). The event list, as compiled from [22], is as follows:

- **Pre-flight preparations and ground movement** - includes all pre-flight activities, engine start, taxiing, and all pre-departure activities.
- **Airwork in VMC conditions** - includes straight, level, and turning flight at various altitudes and airspeeds, as well as showcase of automation abilities.
- **Instrument flight** - departure IFR, en-route IFR, holding procedures, standard procedures given instrument failure or nav aids malfunction, as well as low visibility operations.
- **Arrival and landings** - landing with varying HLD and wind conditions, going around.
- **Abnormal and emergency procedures** - rejected take-off, engine failure at different stages of flight, fire and smoke events, as well as standard events with asymmetrical thrust.

This list is not exhaustive, and the full extent of requirements may be found in [22]. As said before, these standard flight events will not be the focus of the training at this stage in the project, and so these events will not be elaborated upon or considered further in this report. For the same reason, a detailed description of each of these events is not included, but can be found in [22].

#### 4.2.2. UPRT scenarios description

From Subsec. 4.2.1 the extent of training capability of the system has been defined, and from this different training scenarios have been introduced, both for UPRT as well as SOP scenarios. This subsection will give a description of each of the UPRT scenarios.

**Unusual attitude upsets** Unusual attitude scenarios can be categorised into three different scenarios which are **nose high**, **nose low**, and **high bank-angle**. The aircraft is found to be in a nose high attitude whenever the pitch angle is above  $25^\circ$ . Nose low attitude corresponds to a pitch angle of  $-10^\circ$  or below and high bank-angle corresponds to a bank angle over  $45^\circ$ . The pitch attitude is determined from the PFD or Attitude Indicator.

Nose high upsets can be characterised by a decreasing airspeed, increasing altitude and indication of a climb according to the VSI. The initial conditions for this scenario are an altitude of 1000 to 5000 feet above ground level, mid-range centre of gravity, manoeuvring plus 50 knots airspeed and both autopilot and auto-throttle disengaged. Initial attitude must be at  $40^\circ$ , nose-up pitch, wings level [18].

A nose low upset is characterised by an increasing airspeed, decreasing altitude and indication of a descent according to the VSI. The initial conditions for this scenario are an altitude of 5000 to 10000 feet above ground level, mid-range centre of gravity, flaps up, manoeuvring speed and both autopilot and auto-throttle disengaged. Initial attitude must be level flight [18].

A high-bank angle upset should be performed under either one of the initial conditions of nose high or nose low upset as the high bank-angle upset must be performed during one of these upsets [18].

**High altitude wind gust events** High altitude wind shear upsets are categorised as environmental induced upsets. At high altitudes the upper air currents become significant as the velocities in the jet-stream can be very high. A rapid wind shear can alter the flight path of a high-altitude aircraft and cause substantial and immediate airspeed decrease in both cruise and climb situations leading to clear air turbulence (CAT) [18]. Near the jet stream, CAT is caused by a difference in wind speed and wind shear generated between points. Moderate CAT is defined as having a vertical wind shear equal to or bigger than 5 knots per 1000 feet altitude change and/or an horizontal wind shear equal to or bigger than 20 knots per 150 nautical miles flown. Severe CAT occurs at or above 6 knots per 1000 feet vertical shear and/or at or above 40 knots per 150 nautical miles horizontal shear. The combination of sudden decrease of airspeed and high altitude could result in encountering the

back side of the power curve (where induced drag requires more power to fly at a slower steady-state airspeed than the power required to maintain a faster airspeed on the front side of the power curve)<sup>59</sup>.

**Wake vortices encounter** Wake vortices occur behind a heavy aircraft during take-off and approach configurations, as well as during cruise, leading to wake turbulence if separation is insufficient. The encounter with wake turbulence can cause a prompt roll or pitch moment which can alter the flight path significantly. The wake vortex rolls the aircraft on approach resulting in an over-bank which leads to disengagement of the autopilot and potential rapid loss of altitude and control, leading to a crash.

**System failures** System induced upsets in high and low altitudes are upsets caused by anomalies found in the system which could be either a failure in the flight instruments, the auto-flight systems (automation failure), or the flight controls (control surface deflection, thrust asymmetry etc.).

A failure in the flight instruments is recognised by the pilot if any of the instruments show any discrepancy. An example of this would be that the Pilot Monitoring observes a 280 knots airspeed whereas the Pilot Flying observes a 260 knots airspeed on the ASI. These failures occur infrequently but could result in a surprise event for the pilot.

A failure in the auto-flight system is any failure regarding the autopilot, auto-throttles, and all systems related to performing flight management and guidance. The pilot recognises a failure in the auto-flight system if any of these systems are not working properly or warning messages are displayed. Determining the cause of the anomaly proves difficult as the auto-flight system integrates information from a variety of other plane systems.

Finally, failures in flight control are any anomaly in the system that directly affects the control system. These errors often result in an upset as a function of roll, yaw, and pitch path failures. Examples are flap asymmetry, spoiler problems, control surface deflection, and others. These problems are addressed in the aircraft operations manual and quick reference handbook (QRH). Unlike the other system faults, flight control failures could require immediate pilot action.

**High altitude stall recovery** High altitude level flight with autopilot active. An event is introduced or thrust is reduced to less than adequate for manoeuvring flight. This results in reduced roll stability, increased buffeting and an increased AOA. This scenario is conducted near maximum operating altitude of the specific aircraft and may be complemented by input of crew distractions such as air traffic control (ATC) instructions, weather, and minor malfunctions. Simulator capabilities to induce approach-to-stalls may make use of: airspeed slewing, aircraft weight and CG changes, change of attitude, environmental changes, and system malfunctions. In this scenario, it is important to consider the effect of high altitude on stall recovery as in this scenario it is essential to trade altitude for airspeed for recovery. Whenever the aeroplane is encountering low energy states while flying at high altitudes and it requires a reduction in AOA, this raises the necessity for a substantial loss in altitude. Due to the higher airspeed it is logical that the loss of altitude is higher at high altitudes than at low altitudes. Moreover the role of increasing temperature and turbulence at high altitude is important here [27].

**Low altitude stall recovery** Low altitude stall encompasses both take-off and landing configuration stall. For take-off configuration stall the scenario is initiated by inducing an unexpected impending stall on departure prior to flaps being fully retracted. During departure, thrust is reduced to less than adequate for maintaining airspeed and climb rate. The scenario will be conducted at an altitude that will allow for recovery and may be complemented by the same inputs as elaborated on in the High altitude stall recovery paragraph. Simulator capabilities may be used to induce impending stalls. For landing configuration stall the scenario is initiated at 1000 ft above ground level by reducing thrust to a level inadequate to maintain a safe speed or descent angle, resulting in an AOA increase to maintain glide-path. Also within this scenario an unexpected impending stall is induced but now during approach to landing in landing configuration.

**Energy management upsets** Whenever the aeroplane is in a state in which a sudden change between either potential, chemical or kinetic energy is experienced, upsets can follow from this. Recovery from these type of upsets requires understanding and managing of differences between the three energy types and the relationship between pitch, power, and performance. This ties in with for example the high altitude stall in which was explained that a trade from potential to kinetic energy is necessary to reduce AOA and subsequently recover from stall.

---

<sup>59</sup>SKYbrary: Energy Management During Approach

[cited 2020-06-22]

**Stall recovery with envelope protection (concept only)** - This event focuses on the demonstration of stall warning and envelope protection systems existent in the Airbus A320, as they strongly affect what should be the pilot's response to an in-flight upset such as a stall. The A320, as all other A3XX aircraft, has different flight control laws which activate depending on any system failures that might exist. These are Normal Law, Alternate Law, and Direct Law [28]. At this stage of the project, to consider the most extreme scenario, all events will be done under Direct Law, where the control column deflection has a direct relationship with flight controls deflection, without the vast majority of envelope protection systems. However, in Normal Law, which is in place when no failures are present, very strong envelope protection rules exist, and the pilot is actually unable to stall the aircraft. While this means no stall can be encountered, the aircraft's response to a near-stall event may induce an undesirable situation by itself, and the pilot should be aware and very familiar with its behaviour. Therefore, in a future iteration of the design, this class of events should be explored in order to achieve maximum simulation fidelity.

Given a description of what each of these scenarios entails, an example training guide will be given in Sec. 4.3 for one of the upsets, both for the pilot as for the instructor.

## 4.3. Training guides

To allow for effective, repeatable, and, most importantly, consistent training, it is essential to compile training guides both for the pilot-in-training as for the instructor. These guides are the central tool in the briefing and debriefing stages, and allow all parties to have a clear overview of the sequence of events during an upset and the corrective actions required. For the instructor, it is also important that the guide highlights what the initial conditions for the exercise should be, and what the focal points of the training are for the specific upset.

At this stage of the project, and in consultation with the Aeromechanics Team, it has been decided that only the training guide for a single upset, the high altitude stall recovery, will be included in this report. This fits into the decision of analysing solely this upset from an Aeromechanics perspective, and the rationale behind it is further elaborated upon in Subsec. 5.4.1. Analysing this upset and the results from there derived will serve as a proof of concept for the system, and the remainder of the situations named in Subsec. 4.2.1 should be analysed in a future stage of the project.

Given this, Subsec. 4.3.1 presents the pilot guide for high altitude stall recovery, and Subsec. 4.3.2 presents the equivalent instructor guide.

### 4.3.1. Pilot guide

The presented pilot guide covers the theoretical aspects and recovery actions for a high altitude stall upset. First, a few key concept relating to the high altitude stall situation are presented, and secondly a guide including the recovery actions is presented. In this guide, the pilot-in-training is assumed to be the Pilot Flying (PF), and the Pilot Monitoring (PM) actions will be carried out by the acting second pilot. The guide only covers recovery actions for an in-development upset, and the monitoring actions that cover the prevention part of UPRT should be dealt with in the briefing. This guide is based on recommendations included in [17–19, 23].

**Theoretical background** In any stall scenario, particularly high altitude stalls, the primary mechanism to recover from the stall is to reduce the angle of attack, restoring correct airflow over the wings. This always implies a loss of altitude, which should **not** be minimised, as it is the only way to regain control. In many current training curricula, minimising the loss of altitude is given has a priority, which has been found to introduce negative training. Thrust inputs can aid the recovery, but they are not the primary mechanism through which it is achieved. The elevator is the primary control surface to recover from a stalled condition, and deliberate but smooth "stick-forward" action must be taken to reduce the angle of attack. Once below the critical angle of attack, increasing thrust to maximum available can supplement the recovery. In high altitude, there are a vast number of parameters that can affect the aircraft's performance and the recovery process, such as the ISA temperature deviation, aircraft gross weight, available power, automation status, and any malfunctions that may exist.

**Exercise action points** Upon activation of any stall warning system, or any cues that point to an approach-to-stall at high altitude, the points of action are:

- Identify and call "STALL, TOO SLOW"
- Disengage autopilot (AP1/AP2 off)
- Pitch down smoothly and establish descent, AVOID abrupt control inputs
- Set throttles to TOGA detent
- Once at appropriate speed, set throttles to MCT detent
- Monitor TCAS and scan for traffic conflicts

- Notify ATC
- Determine appropriate new cruising altitude

Once steady level flight is achieved, the upset has been resolved. These actions follow the standardised procedure as given in [17–19, 23], with some additions focusing on the MCC and distraction gaps identified previously.

### 4.3.2. Instructor guide

This instructor guide will cover the main points that are relevant to the instructor when performing the high altitude stall exercise. In general, as given in [25], instructors must have knowledge of the limitations of the FSTD, IOS, LOC-I events, energy management, spatial disorientation, startle and surprise, distraction, recognition and recovery strategies, type-specific characteristics, OEM-specific recommendations, and assessment of pilot performance. This list is not exhaustive, and pertains mostly to the actual training instructors must go through to achieve certification, which is beyond the scope of the project and will not be covered. Below the exercise-related action points for the instructor are presented, divided into the briefing, simulation, and debriefing phases.

**Briefing** During the briefing, the following points should be checked:

- Discuss initial conditions - altitude should be near maximum ceiling for the conditions and gross weight as high as possible.
- Discuss environmental conditions - weather phenomena, day or night, QNH, winds, and OAT.
- Verify the pilot-in-training understands and is aware of the maximum VNAV altitude as given by the MCDU, as well as how to obtain it manually from supporting documentation.
- Review different auto-flight modes, especially vertical speed and other climb modes, and cover their caveats and limitations.
- Review conditions that can lead the aircraft to be in the back of the power curve, where slow-down is inevitable, and the correct recovery procedures.
- Review all stall warning systems present on the aircraft and their functioning.
- Review different scenarios leading to high altitude stalls and upset conditions, as well as the correct recovery procedures from each of these situations.

**Simulation** During the simulation, the action points for the instructor are as follows:

- Set up the initial environmental conditions in the IOS as discussed with the pilot-in-training in the briefing phase.
- Set the aircraft parameters as discussed in the briefing phase, concerning both gross weight and any system failures in place.
- Take a "snap shot" of the current conditions, in order to allow for repetition if desired.
- Give the pilot-in-training standard instructions as ATC (vectors, traffic information) in order to aid acclimatisation.
- Disable the auto-throttle by either requesting the pilot-in-training to disengage it or by simulating its failure.
- Induce the upset by increasing the OAT, simulating flight in warmer conditions with no level change, resulting in decreased thrust.
- Induce pilot distraction by giving ATC instructions, such as vectoring, or simulating a TCAS conflict.
- If unnoticed, point out the decreasing airspeed to the pilot-in-training, and prompt recovery manoeuvres.
- If required, repeat the exercise after reviewing the recovery technique, and explore different combinations of upset inducing factors (decrease in thrust, change to an inappropriate flight level) and potentially system failures (auto-throttle, autopilot, stall warning systems, airspeed indicators, etc.).

Once the practical part of the session is concluded, a debriefing should be held in order to synthesise the key competencies covered, and discuss any particularities of the session or questions the pilot-in-training might have. The items to be covered in the debriefing phase are:

- Gather session data to present to the pilot-in-training, such as exercises performed, trigger conditions, main actions taken.
- Make use of extra data available from the IOS in order to break down the pilot's emotional response, and identify improvement points, by looking at physiological indicators, video feed from the cabin, and eye tracking (further elaborated upon in Sec. 5.7), for example.
- Discuss the attempted exercises with the pilot, identifying the upset triggers, time to acknowledgement, predominant cues, actions taken, and recovery of controlled flight.
- Point out any inconsistencies with the standardised recovery procedures and discuss once again the ideal recovery actions.

- Identify strong and weak points, and make recommendations for further training.
- If needed, discuss any outstanding pilot questions or concerns.
- Provide the pilot (and, if applicable, the operator) with a summary of the training session and document it.

This guide covers the key items to be checked by the instructor in any training session. Further points might be added by operator or regulator requirements, but this guide should provide a clear overview on what the workflow should be and on what is supported by the system. A further overview into long-term operation of the system is given in Sec. 6.2.

## 4.4. Final considerations

Throughout this chapter, a summary of the current regulations on UPRT was given, and from it a gap was identified and system objectives drawn. These system objectives focused on improving the current generation of flight simulators for commercial training by introducing reliable UPRT capabilities, as well as bridging other gaps in terms of the pilot's emotional response when confronted with an in-flight upset. A training envelope was also compiled, giving the operators a general overview on the types of UPRT events that the system is capable of faithfully simulating, as well as non-UPRT scenarios that are required for recurrent training and proficiency checks. At this stage of the design, however, the full capability of the system as described in this chapter will not have been achieved, and so this section will include some reflection on the current shortcomings of the simulator, as well as potential improvements to be made in the future. For the complete breakdown of post-DSE activities, Ch. 9 should be consulted.

In terms of the training envelope, and the list of upsets that should be simulated by the system in order to ensure comprehensive and accurate UPRT to commercial pilots, it should be noted that at this stage, a single situation (high altitude stall) will be developed, serving as a proof of concept. While this might seem incomplete, it serves as a good constraint to size the system in its entirety, which is the extent of the scope of this project. Developing an aeromechanics model capable of faithfully simulating each of the listed upsets, however, would not be possible within the time-frame of the DSE, and must be left for a future iteration of the design. Besides this shortcoming in the current iteration of the design, it is possible that the same level of fidelity will not be achieved for all types of upsets, which could create a disparity in the accuracy of the training. Any decrease in fidelity must be clearly documented and communicated to instructors and operators, who must account for this in order to decrease the chances of negative training being passed onto the pilots. A more detailed discussing on the fidelity of the aeromechanics model is included in Sec. 5.4.

One of the largest drivers in the design process of the training systems was the effect of the pilot's emotional response on performance, in particular the effects of startle, surprise, and distractions. As discussed in Subsec. 4.1.3, the solution chosen to overcome this gap was to include UPRT exercises in the already mandatory proficiency checks for ATPL(A) license holders, ensuring not only the continuity of UPRT, but also aiding the introduction of surprise and startle in the simulation. While this is, from a technical standpoint, feasible, and the system will be prepared for it, the regulatory aspects of this solution present some challenges. As per EASA's regulations [22], the skill test in proficiency checks must be carried out in a certified FSTD, which must fulfil certain requirements pertaining to the fidelity of the simulation and immersiveness of the system. This translated directly to a Level D certification, which systems must achieve to be officially recognised as an FSTD. As stated before, this will not be the case for the current iteration of the design. It was not set as a requirement in order to fully explore the design space that does not conform to Level D conditions, achieving an optimal UPRT-capable system, which is the ultimate goal of this project. However, given the achieved design, pursuing a Level D certification in the future should be further explored, as the changes to the system might be compatible with the level of flexibility the design has currently. In short, considering the current regulations set by EASA for the certification of a Level D simulator, the biggest challenges lie with the restrictiveness of the requirements in terms of allowing novel applications of existing technology. The most relevant example of this is the use of a VR system to simulate the cockpit instead of the conventional 1-to-1 physical replica. As per EASA's requirements, a Level D certified simulator must include an "enclosed full-scale replica of the aeroplane cockpit" [29], which the system does not literally adhere to. However, proving that such a system provides the same or even a higher level of immersion and fidelity, and therefore constitutes acceptable means of compliance, should be feasible given the expected performance levels. A further study covering these regulation in-depth will be recommended as a post-DSE activity, as stated in Ch. 9.

# 5 Subsystem Design

The midterm report [2] established how the product worked at a high level to aid in the concept trade-off. With the concept chosen, these high level workings need re-evaluation to make them concept-specific, and tailored to the final concept of choice. This chapter further develops the workings of this product by re-establishing the system and subsystem level sizings of the second iteration in Ch. 2. The functional analysis and system-level block diagrams made in the midterm report are re-evaluated and reconstructed. Additionally, the sub-systems of the concept are established, including structures, control and stability, robotic motion kinematics, aural cueing, visual cueing, and haptic cueing. Verification and validation are carried out within all these sections, with the system verification and validation carried out lastly.

## 5.1. Functional Analysis Overview

The functional analysis provides insight into the functions of the product, initially detailed in the baseline report [1]. Due to new insights obtained throughout the design phase, additional functions have been added. In this section, the functional flow diagram is given on pages 32–33, and the functional breakdown structure is presented on pages 34–38.

## 5.2. Updated System Interface Diagrams

The interface diagrams describe how the system components interact with each other, with each diagram describing a different aspect. The purpose of each diagram is given below:

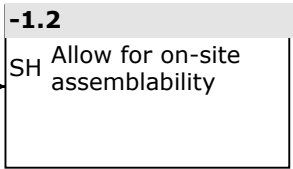
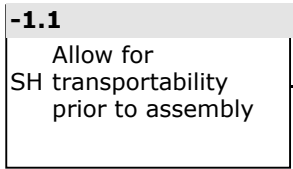
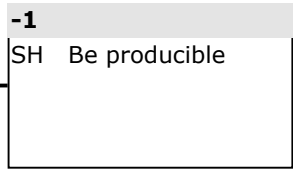
**Hardware Block Diagram** describes the physical connections between components, both in the context of power and information passing, further distinguishing by what type of cable is required. Shown on page 39.

**Software Block Diagram** describes the flow of the over-arching program from startup to shutdown and its information. Given that the software interfaces with the hardware, hardware components providing input/output are also included. Shown on pages 40–41.

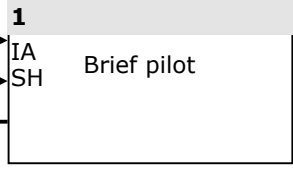
**Electrical Block Diagram** describes the flow of power throughout the system. This is directly related to the hardware block diagram with the power cables. Shown on page 42. Note that when something is expected to have a negligible power consumption (less than 1 W), it is indicated with 0 W.

**Data Handling Block Diagram** describes the flow of information between components, displaying the bitrate for connections. It further provides information regarding computer components as well. Shown on page 43.

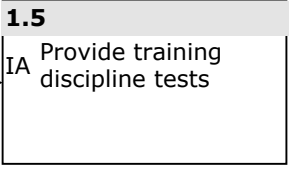
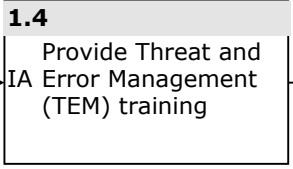
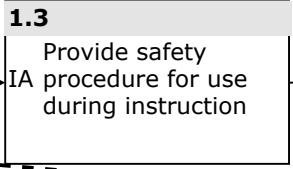
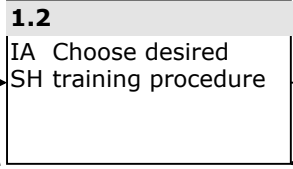
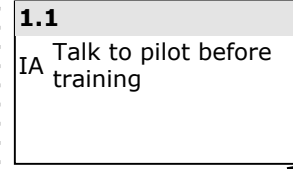
**Communication Flow Diagram** describes the content of information to each hardware component. It is directly related to the software block diagram with the data flow arrows. Shown on page 44.



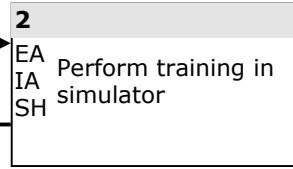
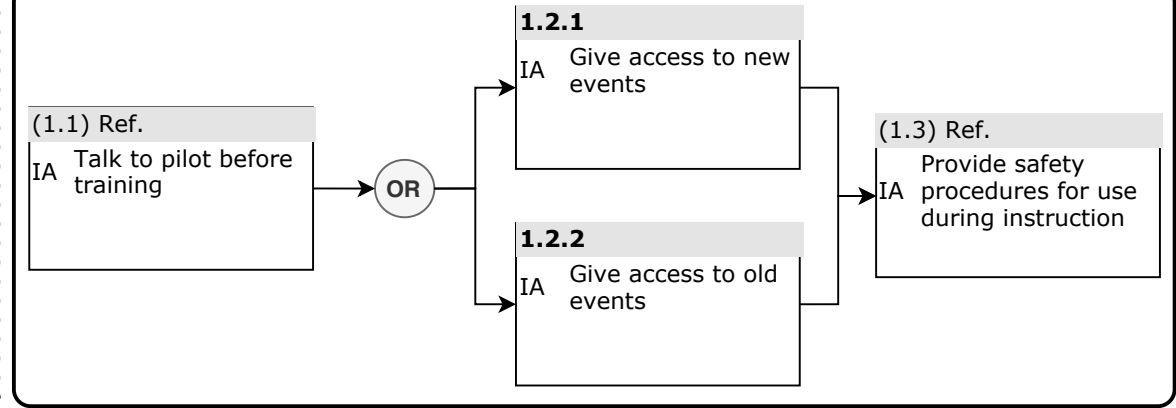
**SECOND LEVEL**



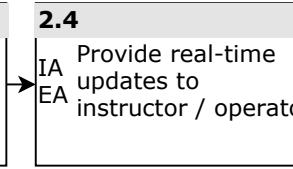
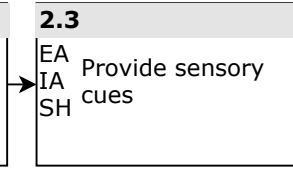
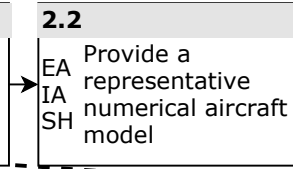
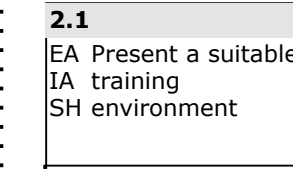
**SECOND LEVEL**



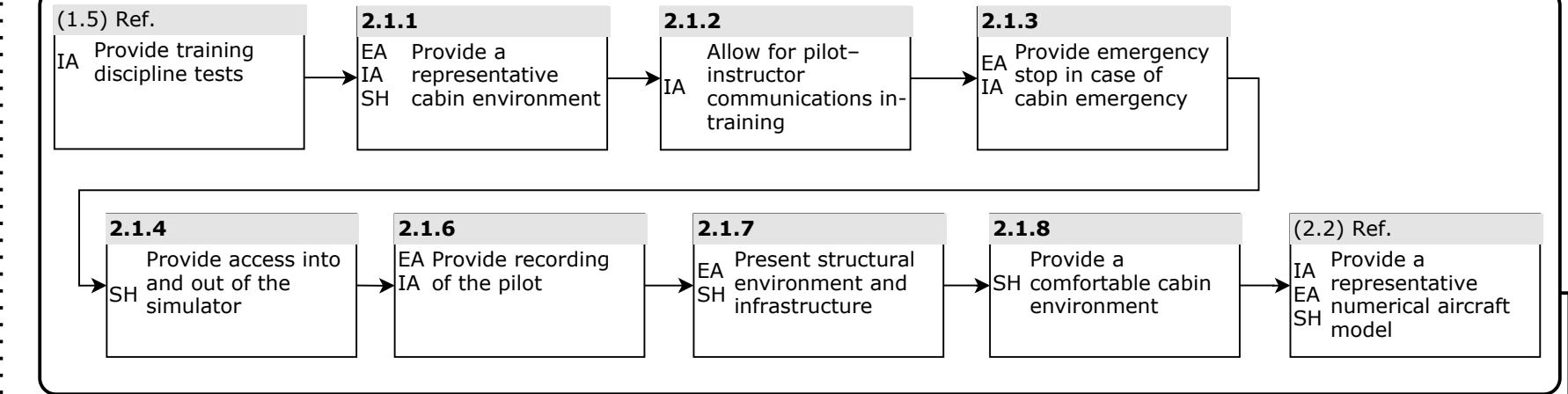
**THIRD LEVEL**



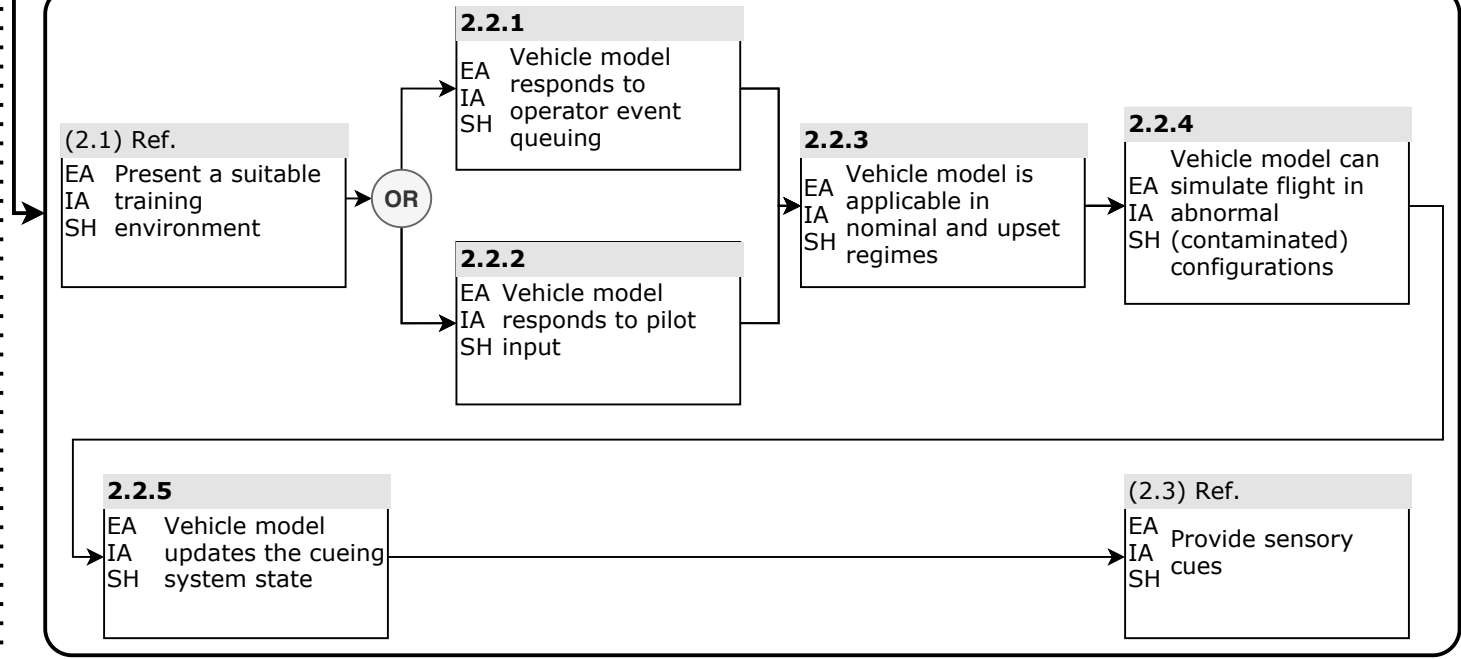
**SECOND LEVEL**



**THIRD LEVEL**



**THIRD LEVEL**

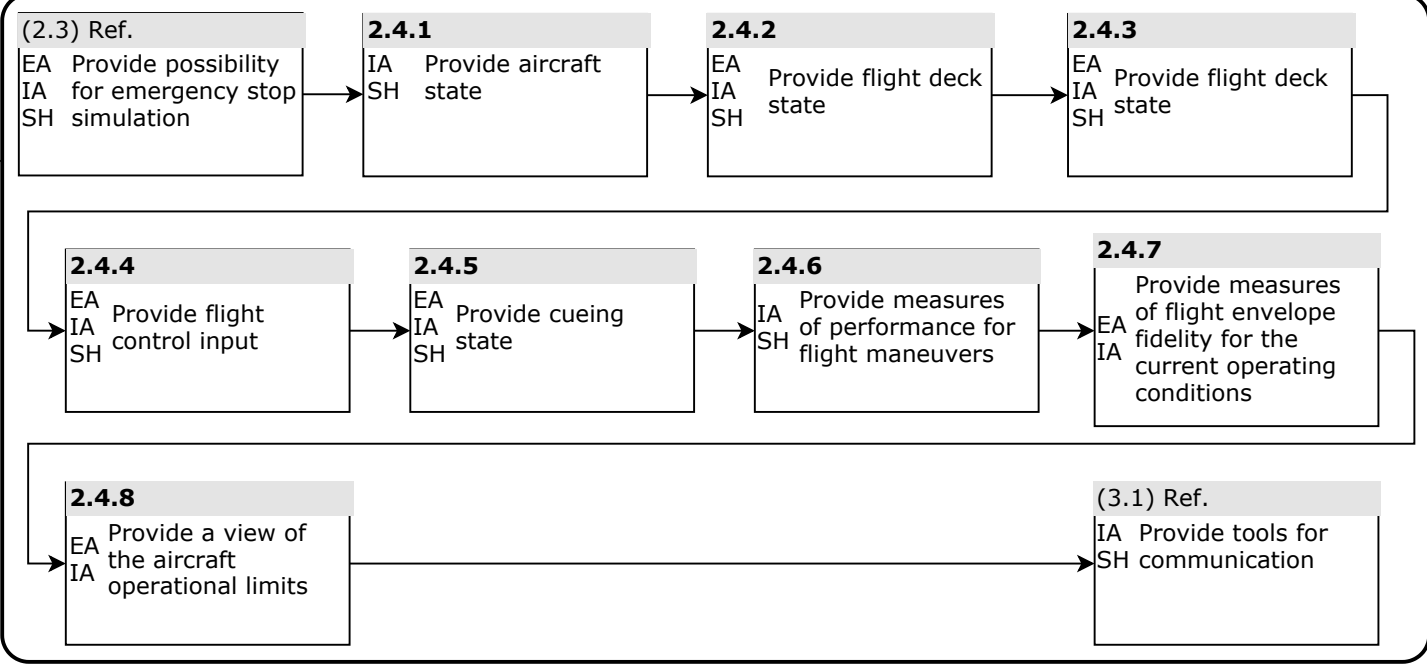


**THIRD LEVEL**

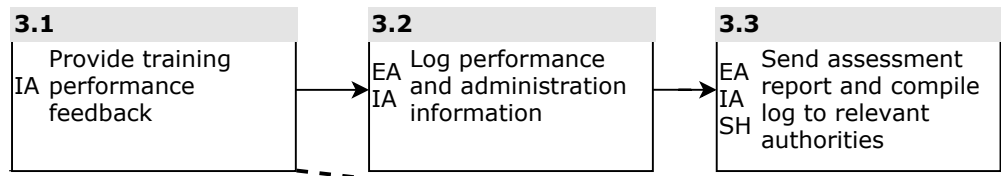




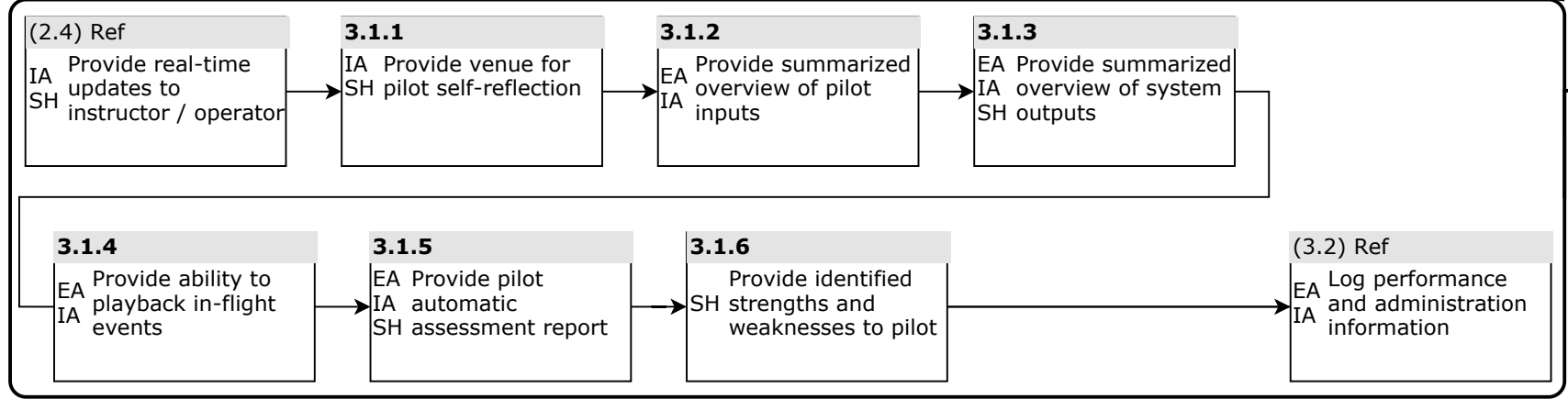
**THIRD LEVEL**



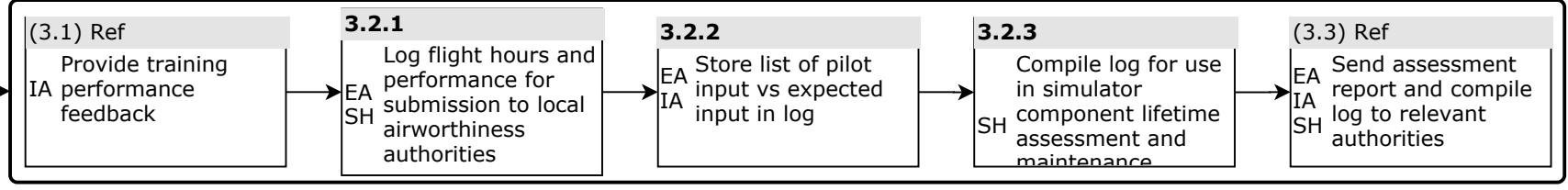
**SECOND LEVEL**



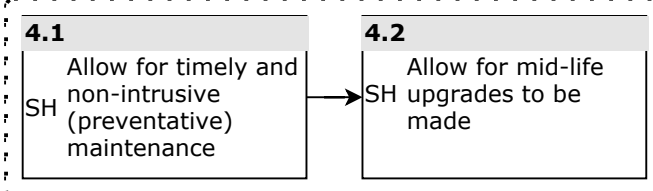
**THIRD LEVEL**



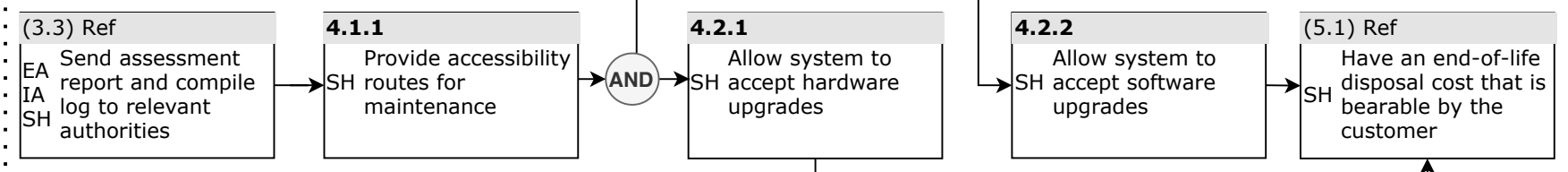
**THIRD LEVEL**



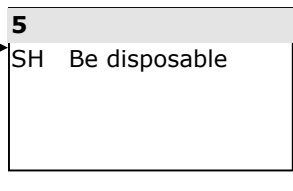
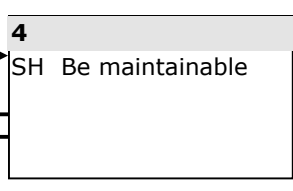
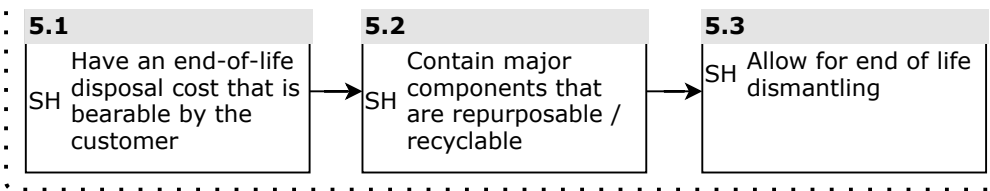
**SECOND LEVEL**

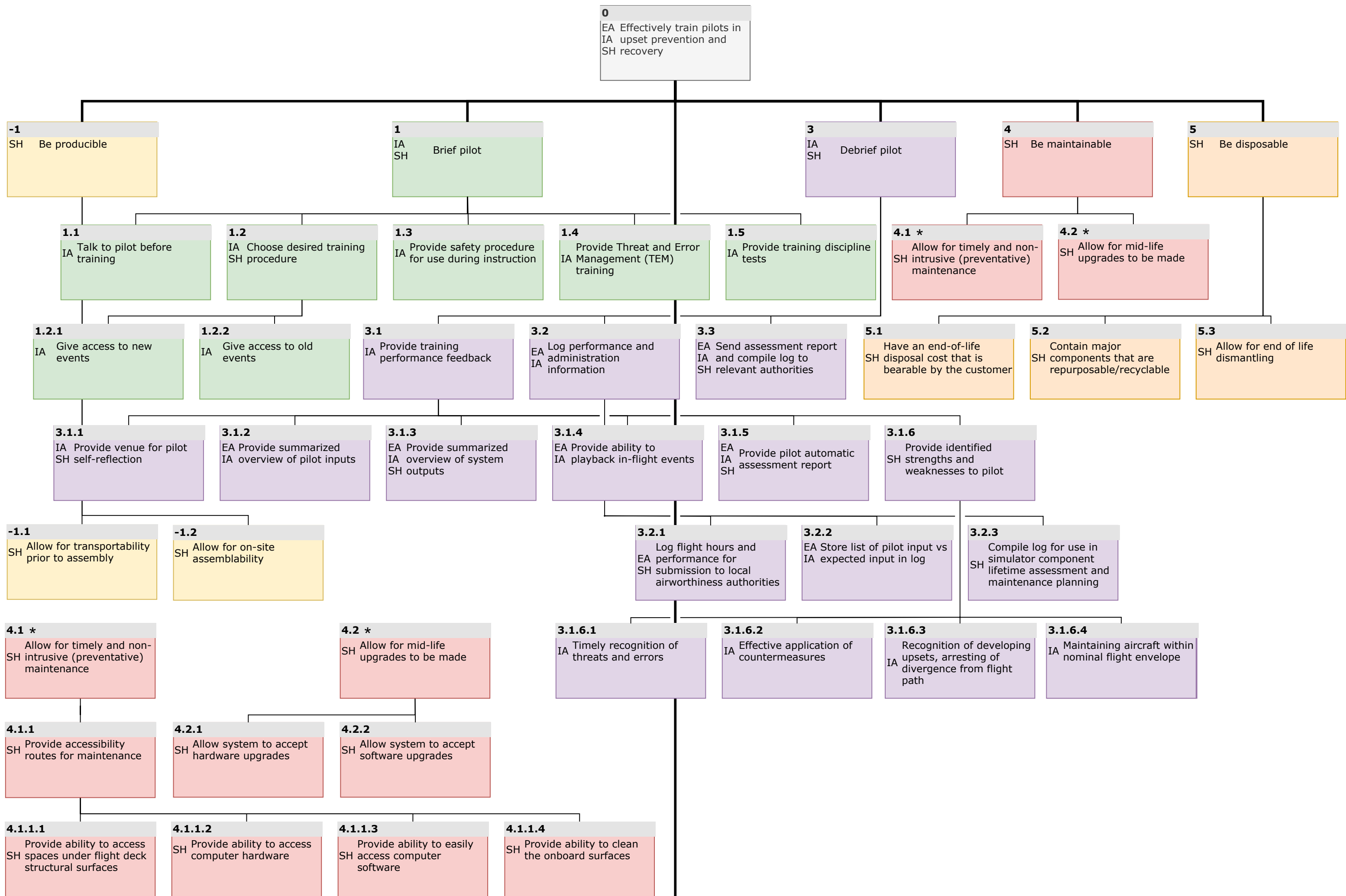


**THIRD LEVEL**



**SECOND LEVEL**





**2**  
EA  
IA  
SH  
Perform training in simulator

**2.1**  
EA  
IA  
SH  
Present a suitable training environment

**2.2**  
EA  
IA  
SH  
Provide a representative numerical aircraft model

**2.3**  
EA  
IA  
SH  
Provide sensory cues

**2.4**  
IA  
EA  
EA to instructor / operator  
Provide real-time updates

**2.1.1**  
EA  
IA  
SH  
Provide a representative cabin environment [H]

**2.1.2**  
IA  
Allow for pilot-instructor communications in-training

**2.1.3**  
EA  
IA  
Provide emergency stop in case of cabin emergency [S]

**2.1.4**  
SH  
Provide access into and out of the simulator [S]

**2.1.6**  
EA  
IA  
Provide recording of the pilot

**2.1.7 \***  
EA  
SH  
Present safe structural environment [S]

**2.1.8**  
EA  
SH  
Provide a comfortable cabin environment [S]

**2.1.1.1**  
SH  
Provide equipment representative to a A320 as needed for training [H]

**2.2.1**  
EA  
IA  
SH  
Vehicle model updates the cueing system state

**2.2.2 \***  
EA  
IA  
SH  
Vehicle model responds to operator event queuing [M]

**2.2.3 \***  
EA  
IA  
SH  
Vehicle model responds to pilot input [M]

**2.2.4 \***  
EA  
IA  
SH  
Vehicle model is applicable in nominal and upset regimes

**2.2.5 \***  
EA  
IA  
SH  
Vehicle model can simulate flight in abnormal configurations (contaminated)

**2.1.8.1**  
EA  
SH  
Provide air conditioning within cabin and IOS station [S]

**2.2.1.1**  
EA  
IA  
SH  
Update all cueing outputs

**2.3.1 \***  
EA  
IA  
SH  
Provide visual cues [V]

**2.3.2 \***  
EA  
IA  
SH  
Provide haptic cues [H]

**2.3.3 \***  
EA  
IA  
SH  
Provide vestibular cues [M]

**2.3.4 \***  
EA  
IA  
SH  
Provide aural cues [A]

**2.4.1**  
IA  
SH  
Provide possibility for emergency stop simulation

**2.4.2 \***  
EA  
IA  
SH  
Provide aircraft state [M]

**2.4.3 \***  
EA  
IA  
SH  
Provide flight deck state

**2.4.4 \***  
EA  
IA  
SH  
Provide flight control input

**2.4.5 \***  
EA  
IA  
SH  
Provide motion cueing state [M]

**2.4.6 \***  
IA  
SH  
Provide measures of performance for flight maneuvers

**2.4.7 \***  
EA  
IA  
Provide measures of flight envelope fidelity for the current operating conditions

**2.4.8 \***  
EA  
IA  
Provide a view of the aircraft operational limits

**2.2.3 \***  
EA  
IA  
SH  
Vehicle model responds to pilot input [M]

**2.2.5 \***  
EA  
IA  
SH  
Vehicle model can simulate flight in abnormal configurations (contaminated)

**2.2.2 \***  
EA  
IA  
SH  
Vehicle model responds to operator event queuing [M]

**2.2.3.1**  
EA  
IA  
SH  
Vehicle model provides force feedback input [M]

**2.2.3.2**  
EA  
IA  
Vehicle model varies the control feedback based on aircraft state

**2.2.3.3**  
EA  
IA  
SH  
Ensure vehicle model is applicable in nominal and upset regime

**2.2.5.1**  
SH  
Simulate loss of control surface effects

**2.2.5.2**  
SH  
Simulate airfoil containment effects

**2.2.2.1**  
SH  
Allow for instructor/operator input [M]

**2.2.2.2**  
EA  
SH  
Allow for non-repeatability in training events

**2.2.2.3**  
SH  
Allow for events to be queued in a non-intrusive manner

**2.2.3.2.1**  
EA  
IA  
Model degradation of control response in pitch, roll, and yaw

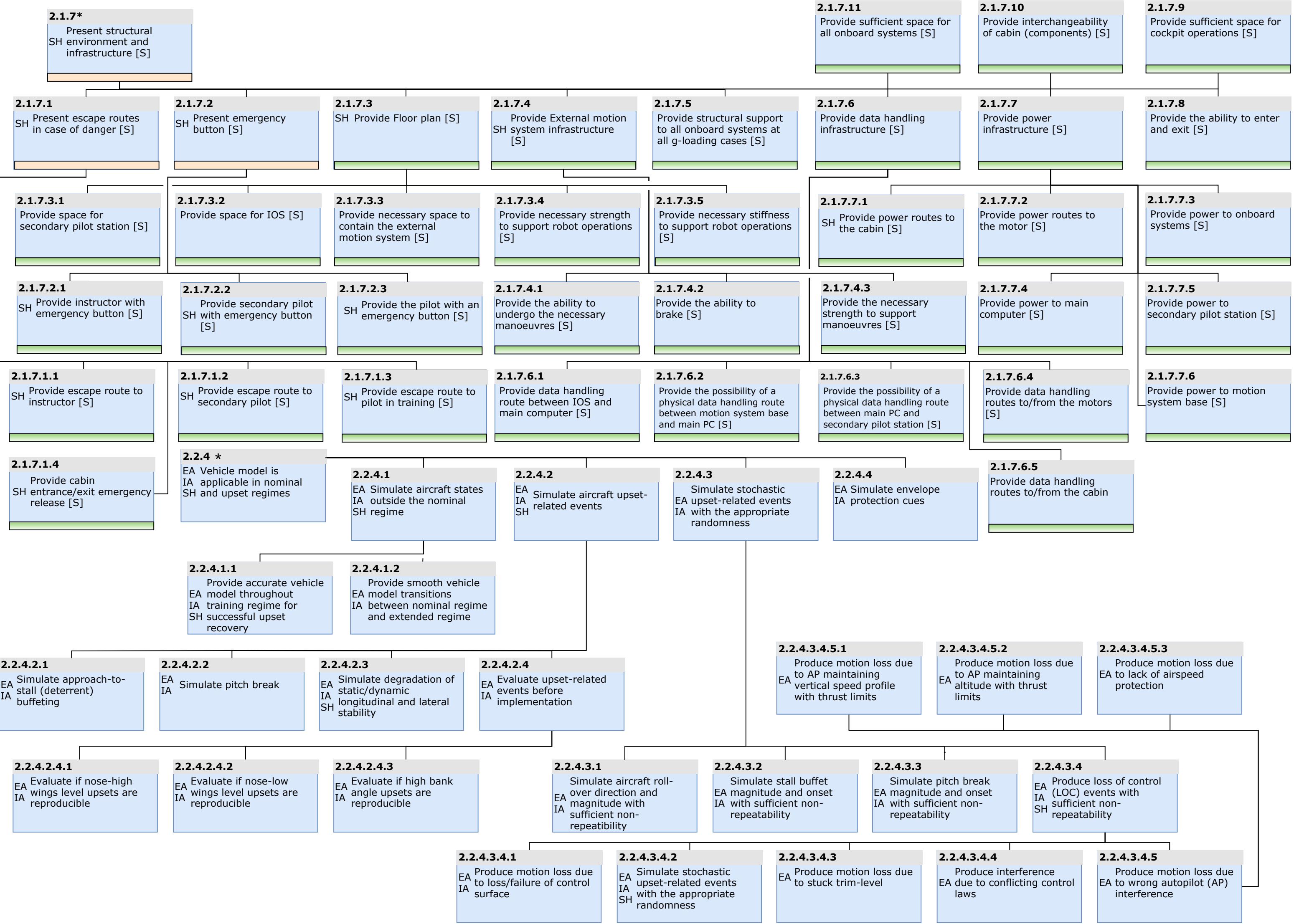
**2.2.3.3.1**  
EA  
Provide a model of uncommanded roll responses that require significant control input

**2.2.5.2.1**  
SH  
Simulate engine and airframe icing

**2.2.2.1.1**  
SH  
Allow for aircraft (sub)system failures to be queued

**2.2.2.1.2**  
SH  
Allow for warnings on the flight deck to be triggered

**2.2.2.1.3**  
SH  
Allow for false motion or force feedback cues to be staged



**2.1.7\***  
Present structural SH environment and infrastructure [S]

**2.1.7.1**  
SH Present escape routes in case of danger [S]

**2.1.7.2**  
SH Present emergency button [S]

**2.1.7.3**  
SH Provide Floor plan [S]

**2.1.7.4**  
SH Provide External motion SH system infrastructure [S]

**2.1.7.5**  
Provide structural support to all onboard systems at all g-loading cases [S]

**2.1.7.11**  
Provide sufficient space for all onboard systems [S]

**2.1.7.10**  
Provide interchangeability of cabin (components) [S]

**2.1.7.9**  
Provide sufficient space for cockpit operations [S]

**2.1.7.3.1**  
Provide space for secondary pilot station [S]

**2.1.7.3.2**  
Provide space for IOS [S]

**2.1.7.3.3**  
Provide necessary space to contain the external motion system [S]

**2.1.7.3.4**  
Provide necessary strength to support robot operations [S]

**2.1.7.3.5**  
Provide necessary stiffness to support robot operations [S]

**2.1.7.7.1**  
SH Provide power routes to the cabin [S]

**2.1.7.7.2**  
Provide power routes to the motor [S]

**2.1.7.7.3**  
Provide power to onboard systems [S]

**2.1.7.2.1**  
SH Provide instructor with emergency button [S]

**2.1.7.2.2**  
SH Provide secondary pilot with emergency button [S]

**2.1.7.2.3**  
SH Provide the pilot with an emergency button [S]

**2.1.7.4.1**  
Provide the ability to undergo the necessary manoeuvres [S]

**2.1.7.4.2**  
Provide the ability to brake [S]

**2.1.7.4.3**  
Provide the necessary strength to support manoeuvres [S]

**2.1.7.7.4**  
Provide power to main computer [S]

**2.1.7.7.5**  
Provide power to secondary pilot station [S]

**2.1.7.1.1**  
SH Provide escape route to instructor [S]

**2.1.7.1.2**  
SH Provide escape route to secondary pilot [S]

**2.1.7.1.3**  
SH Provide escape route to pilot in training [S]

**2.1.7.6.1**  
Provide data handling route between IOS and main computer [S]

**2.1.7.6.2**  
Provide the possibility of a physical data handling route between motion system base and main PC [S]

**2.1.7.6.3**  
Provide the possibility of a physical data handling route between main PC and secondary pilot station [S]

**2.1.7.6.4**  
Provide data handling routes to/from the motors [S]

**2.1.7.7.6**  
Provide power to motion system base [S]

**2.1.7.1.4**  
Provide cabin entrance/exit emergency release [S]

**2.2.4 \***  
EA Vehicle model is IA applicable in nominal SH and upset regimes

**2.2.4.1**  
EA Simulate aircraft states IA outside the nominal SH regime

**2.2.4.2**  
EA Simulate aircraft upset-related events

**2.2.4.3**  
EA Simulate stochastic upset-related events IA with the appropriate randomness

**2.2.4.4**  
EA Simulate envelope IA protection cues

**2.1.7.6.5**  
Provide data handling routes to/from the cabin

**2.2.4.1.1**  
Provide accurate vehicle EA model throughout IA training regime for SH successful upset recovery

**2.2.4.1.2**  
Provide smooth vehicle EA model transitions IA between nominal regime and extended regime

**2.2.4.2.1**  
EA Simulate approach-to-stall (deterrent) buffeting

**2.2.4.2.2**  
EA Simulate pitch break

**2.2.4.2.3**  
EA Simulate degradation of static/dynamic longitudinal and lateral stability

**2.2.4.2.4**  
EA Evaluate upset-related events before implementation

**2.2.4.3.4.5.1**  
EA Produce motion loss due to AP maintaining vertical speed profile with thrust limits

**2.2.4.3.4.5.2**  
EA Produce motion loss due to AP maintaining altitude with thrust limits

**2.2.4.3.4.5.3**  
EA Produce motion loss due to lack of airspeed protection

**2.2.4.2.4.1**  
EA Evaluate if nose-high wings level upsets are reproducible

**2.2.4.2.4.2**  
EA Evaluate if nose-low wings level upsets are reproducible

**2.2.4.2.4.3**  
EA Evaluate if high bank angle upsets are reproducible

**2.2.4.3.1**  
EA Simulate aircraft roll-over direction and magnitude with sufficient non-repeatability

**2.2.4.3.2**  
EA Simulate stall buffet EA magnitude and onset IA with sufficient non-repeatability

**2.2.4.3.3**  
EA Simulate pitch break EA magnitude and onset IA with sufficient non-repeatability

**2.2.4.3.4**  
EA Produce loss of control (LOC) events with sufficient non-repeatability

**2.2.4.3.4.1**  
EA Produce motion loss due to loss/failure of control surface

**2.2.4.3.4.2**  
EA Simulate stochastic upset-related events IA with the appropriate randomness

**2.2.4.3.4.3**  
EA Produce motion loss due to stuck trim-level

**2.2.4.3.4.4**  
EA Produce interference EA due to conflicting control laws

**2.2.4.3.4.5**  
EA Produce motion loss due to wrong autopilot (AP) interference

**2.3.2 \***  
EA  
IA Provide haptic cues [H]  
SH

**2.3.2.1**  
EA Provide force feedback [H]  
IA  
SH

**2.3.2.2**  
EA Provide representative instruments [H]  
IA  
SH

**2.3.2.3**  
EA Provide location data for the pilot's and copilot's hands [H]  
IA  
SH

**2.3.2.1.1**  
EA Provide control vibration feedback [H]

**2.3.2.1.2**  
EA Provide control rotation feedback [H]

**2.3.2.1.3**  
EA Provide engine thrust control feedback [H]

**2.3.1 \***  
EA  
IA Provide visual cues [V]  
SH

**2.3.1.1**  
EA Provide scenery relevant to the scenario [V]  
IA  
SH

**2.3.1.2**  
EA Provide needed instruments [V]  
IA  
SH

**2.3.1.3**  
IA Provide immersion [V]

**2.3.1.4**  
EA Provide sufficient graphical fidelity [V]  
SH

**2.3.1.1.1**  
EA Provide scenery relevant to the aircraft position [V]  
IA  
SH

**2.3.1.1.2**  
EA Provide scenery sky [V]  
IA  
SH

**2.3.1.1.3**  
EA Provide realistic scenery [V]  
IA  
SH

**2.3.1.1.4**  
EA Provide realistic colours [V]  
IA  
SH

**2.3.1.1.5**  
EA Provide spatial (dis)orientation [V]  
IA  
SH

**2.4.4 \***  
EA Provide flight control input [M]  
IA  
SH

**2.4.4.1**  
EA Provide steering input read-out  
IA  
SH

**2.3.4 \***  
EA Provide aural cues [A]  
IA  
SH

**2.3.4.1**  
EA Provide noise isolation [A]

**2.3.4.2**  
EA Be compatible with the visual system [A]

**2.3.4.3**  
EA Fit inside the cabin [A]

**2.3.4.4**  
EA Rise above the acoustic noise level [A]

**2.3.4.5**  
EA Provide Aircraft sounds [A]

**2.3.4.6**  
EA Provide communication channels for pilot [A]

**2.3.4.5.1**  
EA Provide realistic warning sounds [A]

**2.3.4.5.2**  
EA Provide normal and abnormal airframe configuration-related sounds [A]

**2.3.4.5.3**  
EA Provide flight deck sounds under normal and abnormal conditions [A]

**2.3.4.5.4**  
EA Provide engine noise [A]

**2.3.4.5.5**  
EA Provide background noise [A]

**2.4.8 \***  
EA Provide a view of the aircraft operational limits  
IA

**2.3.4.6.1**  
EA Provide communication with instructor/operator [A]

**2.3.4.6.2**  
EA Allow communication with ATC [A]

**2.3.4.6.3**  
EA Provide communication with second pilot [A]

**2.4.8.1**  
EA Provide airspeed limits

**2.4.8.2**  
EA Provide limit load factors

**2.4.8.3**  
EA Provide stall identification angle of attack

**2.4.2 \***  
EA Provide aircraft state [M]  
IA  
SH

**2.4.2.1**  
EA Provide control surface deflection  
IA

**2.4.2.2**  
EA Provide engine thrust  
IA

**2.4.2.3**  
EA Provide aerodynamic state  
IA  
SH

**2.4.2.4**  
EA Provide g-loading [M]  
IA  
SH

**2.4.3 \***  
EA Provide flight deck state  
IA  
SH

**2.4.3.1**  
EA Provide switch positions  
IA  
SH

**2.4.3.2**  
EA Provide autopilot state  
IA

**2.4.3.3**  
EA Provide pilot monitoring  
IA  
SH

**2.4.6 \***  
 IA Provide measures of performance for flight maneuvers  
 SH

**2.4.6.1**  
 EA Provide deviation from nominal training flight path  
 IA

**2.4.6.2**  
 Provide time to SH recovery since entry into upset

**2.4.6.3**  
 EA Provide time-varying g-loading experienced in SH maneuver  
 IA

**2.4.6.4**  
 EA Provide measures for the amount of control applied during an event  
 IA

**2.4.7 \***  
 Provide measures of EA flight envelope fidelity  
 IA for the current operating conditions

**2.4.7.1**  
 EA Provide model validity information for flap settings  
 IA

**2.4.7.2**  
 EA Provide model validity information for angle of attack/sideslip regime  
 IA

**2.4.5 \***  
 EA Provide cueing state [M]  
 IA  
 SH

**2.4.5.1**  
 EA Provide time-history of apparent g-loading and attitude [M]  
 IA  
 SH

**2.4.5.2**  
 EA Provide time-history of SH haptic feedback state

**2.3.3 \***  
 EA Provide vestibular cues  
 IA [M]  
 SH

**2.3.3.1**  
 EA Provide mathematical software model for SH motion system [M]  
 IA

**2.3.3.1.1**  
 Provide data memory and rates behind the signals [M]

**2.3.3.1.2**  
 Provide cueing value for other subsystems [M]

**2.3.3.2**  
 Design mathematics between vehicle model and hardware [M]

**2.3.3.1.4**  
 Provide mathematical integration between all hardware components [M]

**2.3.3.1.3**  
 Provide a method of compliance with the output vehicle model [M]

**2.3.3.1.5**  
 Provide definition for kinematics engine hardware [M]

**2.3.3.2.1**  
 EA Provide translational cues  
 IA [M]  
 SH

**2.3.3.2.2**  
 EA Provide rotational cues  
 IA [M]  
 SH

**2.3.3.2.3**  
 EA Provide sustained cues  
 IA [M]  
 SH

**2.3.3.2.4**  
 EA Provide signaling cues  
 IA [M]  
 SH

**2.3.3.1.5.1**  
 Provide basic code and criteria behind kinematics engine [M]

**2.3.3.1.5.2**  
 Define trajectory possibilities and criteria for kinematics hardware [M]

**2.3.3.2.4.1**  
 EA Provide engine malfunction cues  
 IA  
 SH

**2.3.3.2.4.2**  
 Provide buffet cues EA associated with control surface actuation (manoeuvre buffet)  
 IA

**2.3.3.2.4.3**  
 EA Provide stall-related buffet cues  
 IA  
 SH

**2.3.3.1.5.2.1**  
 Provide definition for cost function [M]

**2.3.3.2.4.3.1**  
 EA Provide thrust effect cues  
 IA  
 SH

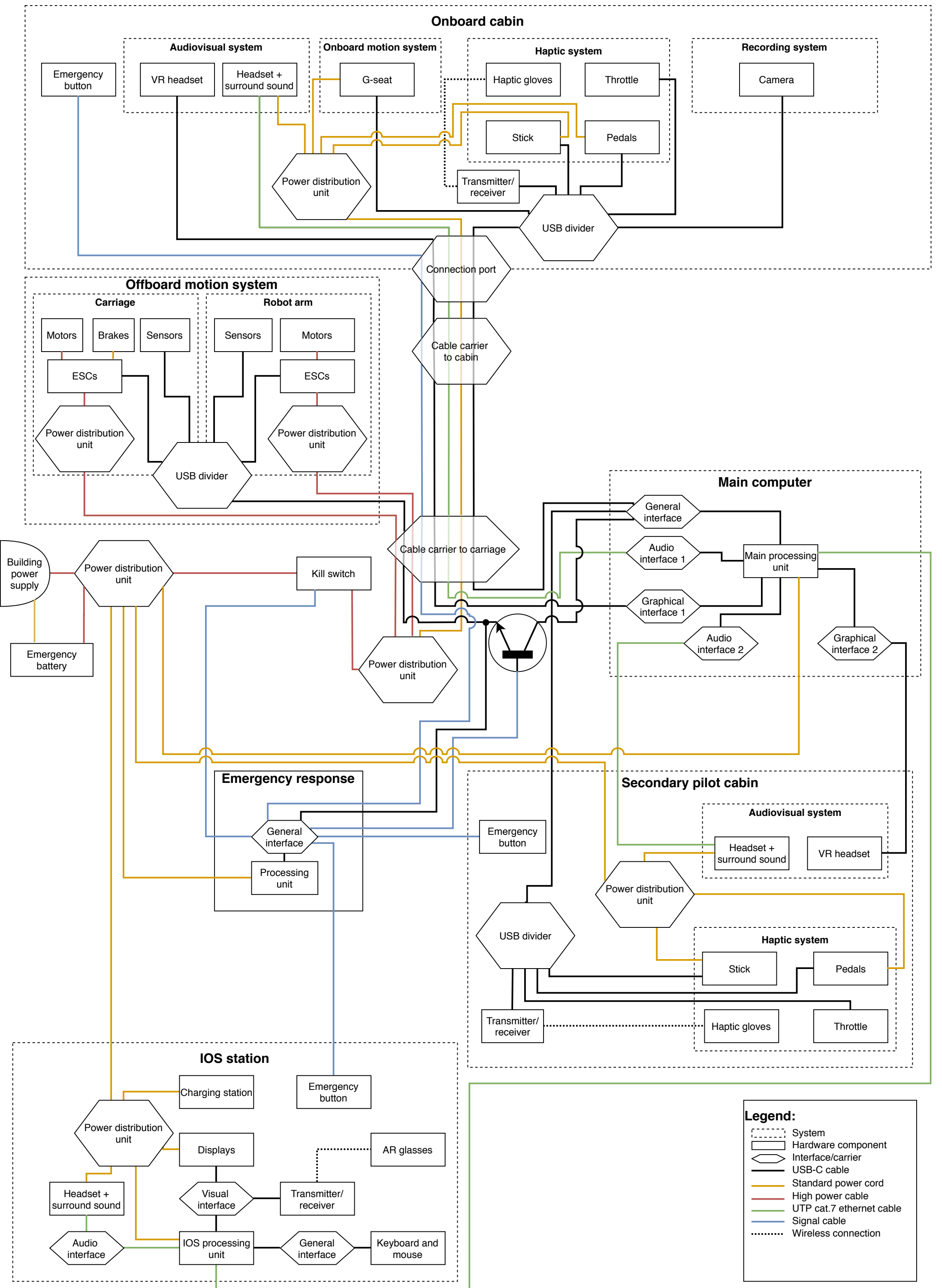
**2.3.3.2.4.3.2**  
 EA Provide motion cues for characteristic buffet

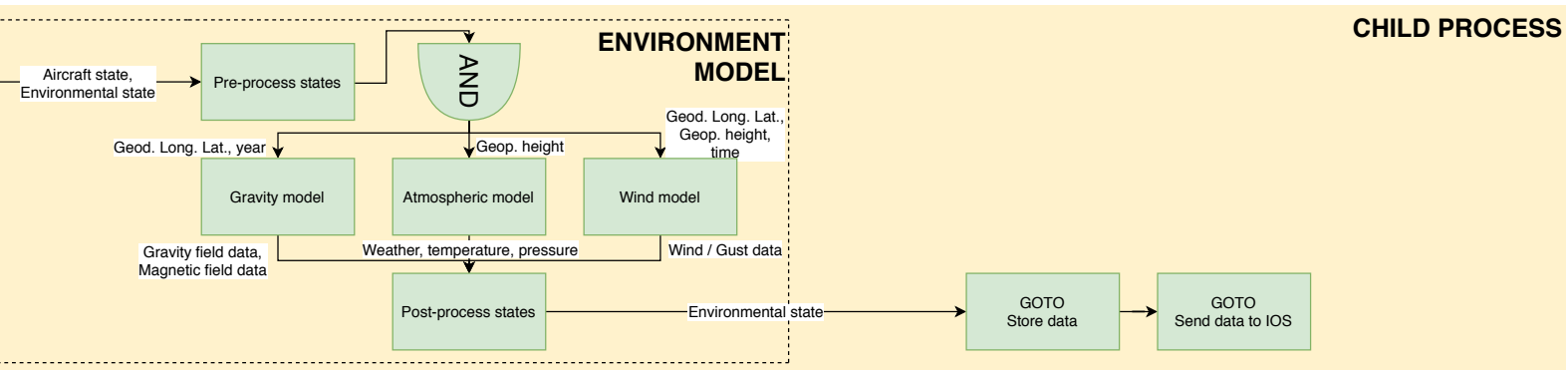
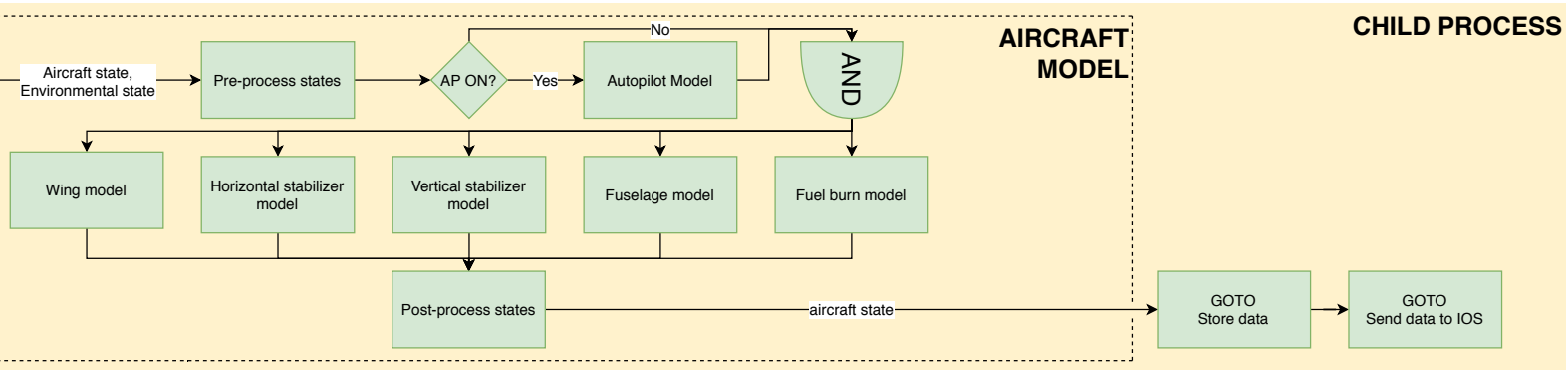
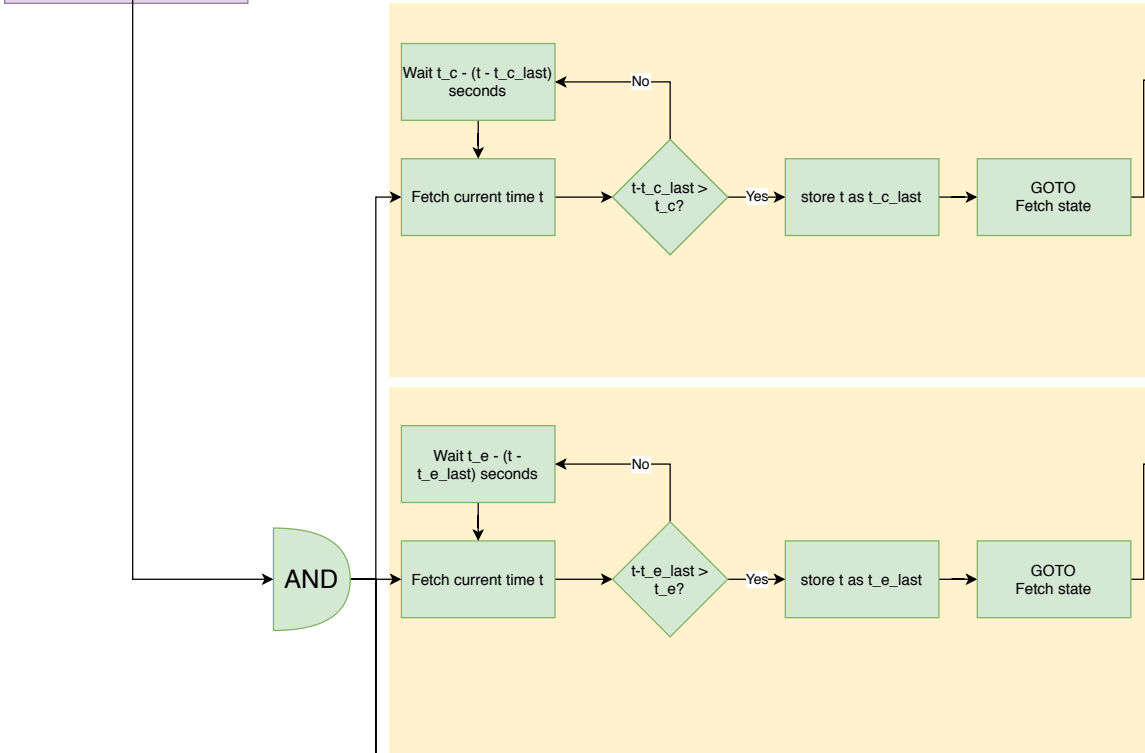
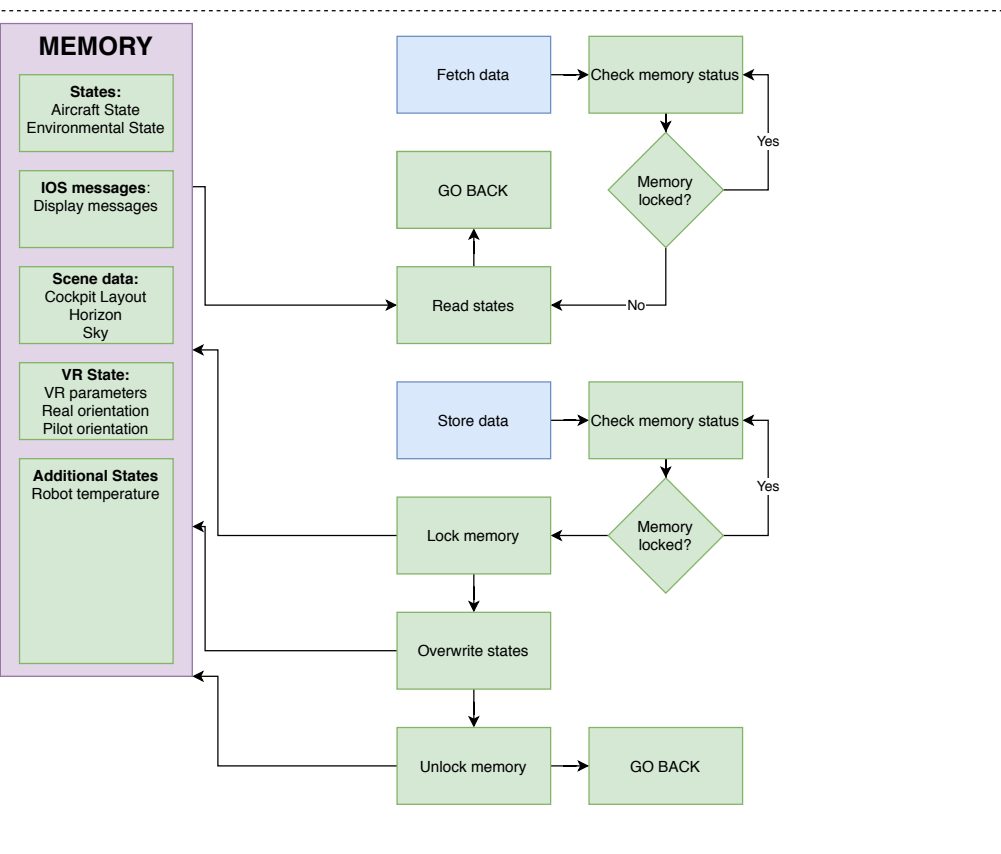
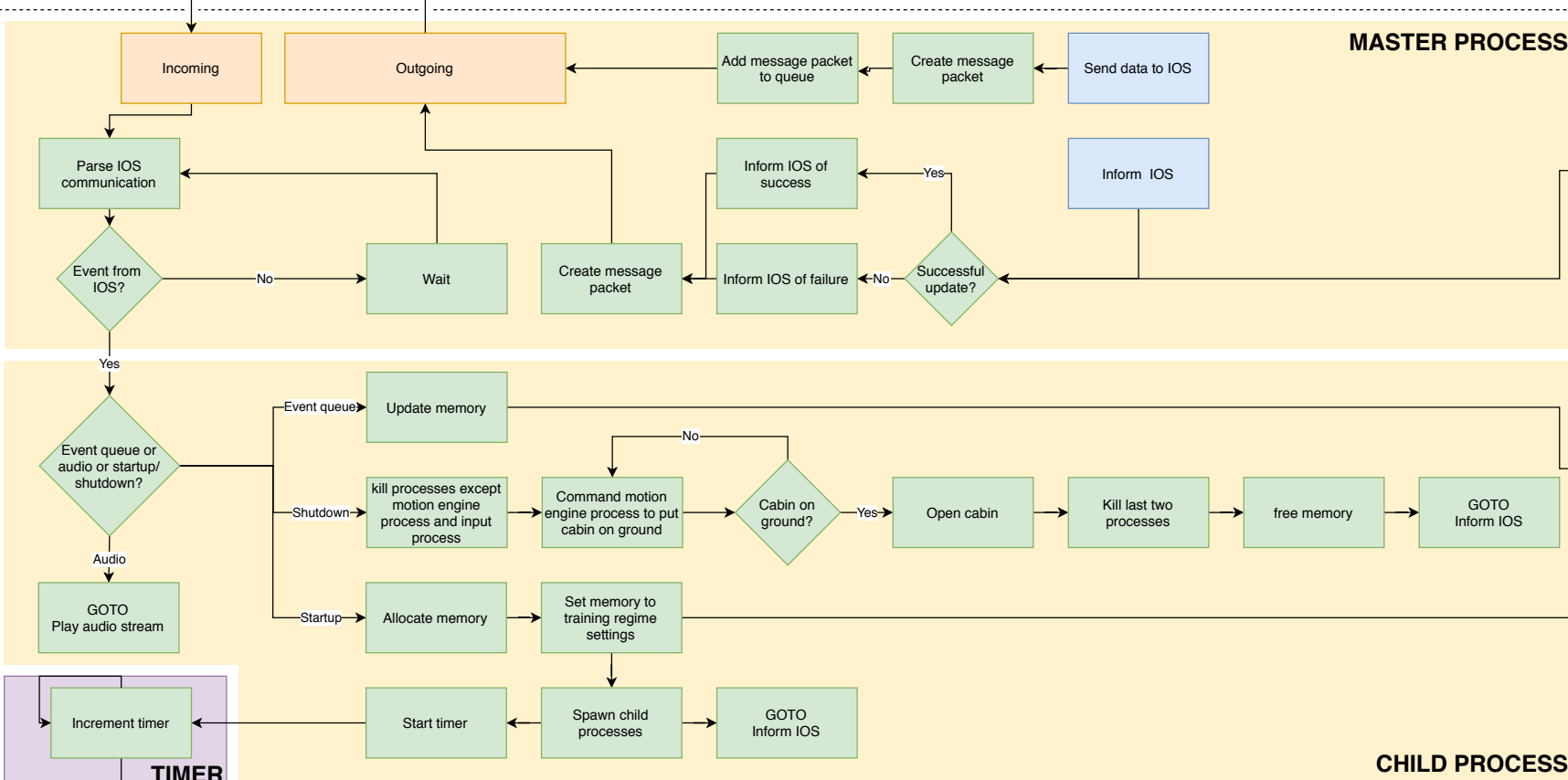
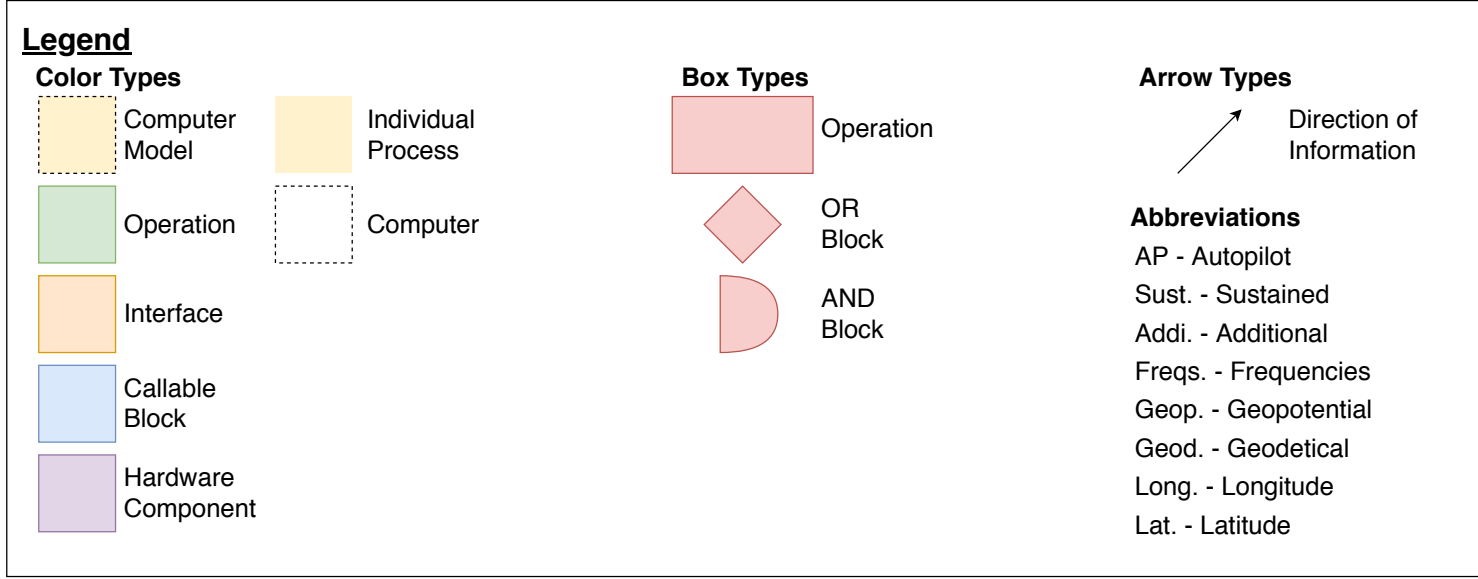
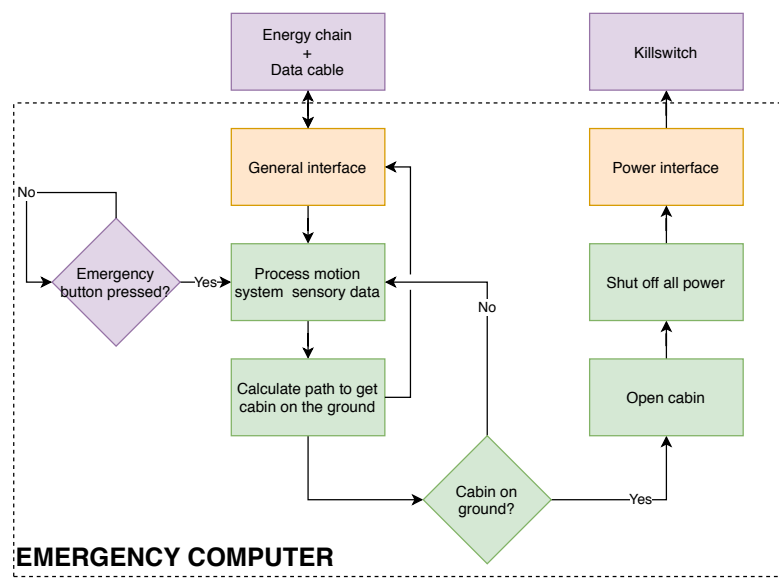
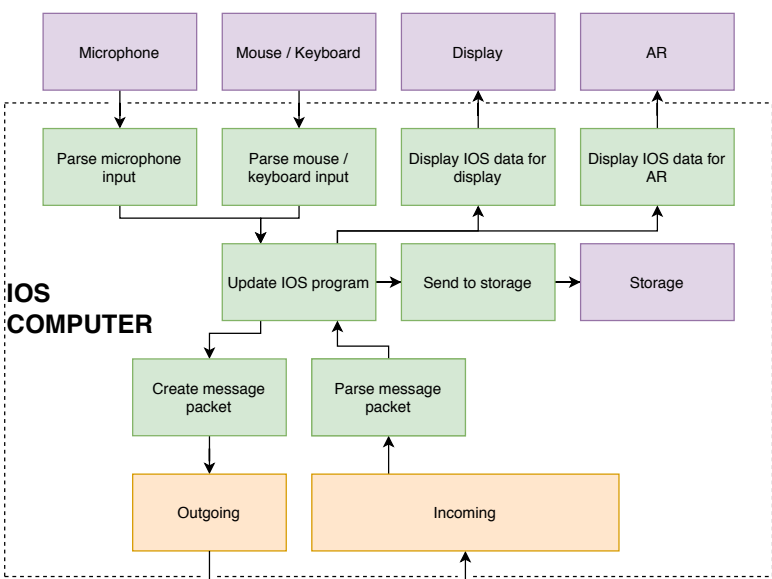
**2.3.3.2.4.3.3**  
 Provide motion cues for approximate atmospheric disturbances  
 EA

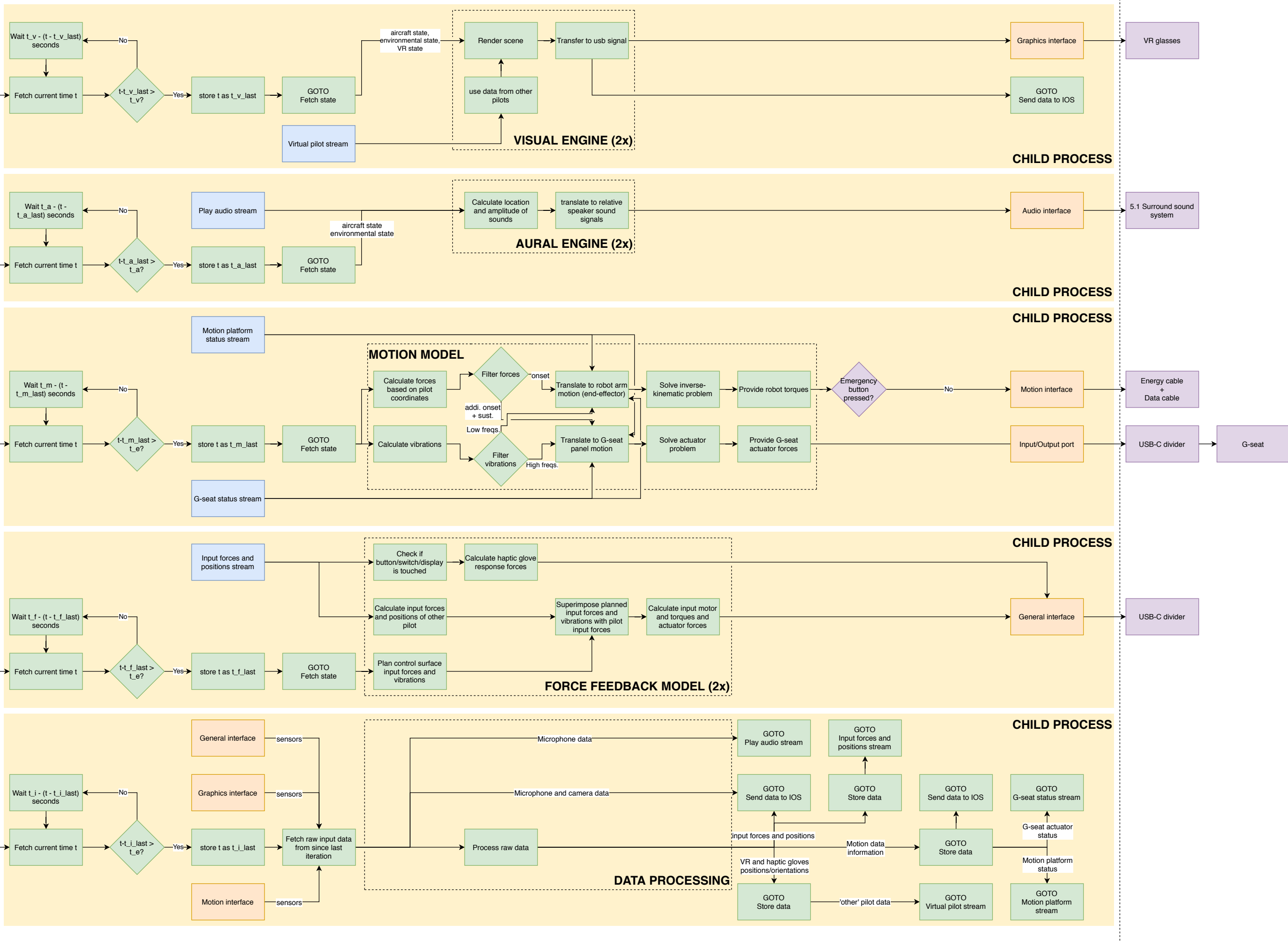
**2.3.3.2.4.3.4**  
 EA Provide approach-to-stall (deterrent) buffet cues  
 IA  
 SH

**2.3.3.2.4.3.5**  
 EA Provide pitch break cues  
 IA  
 SH

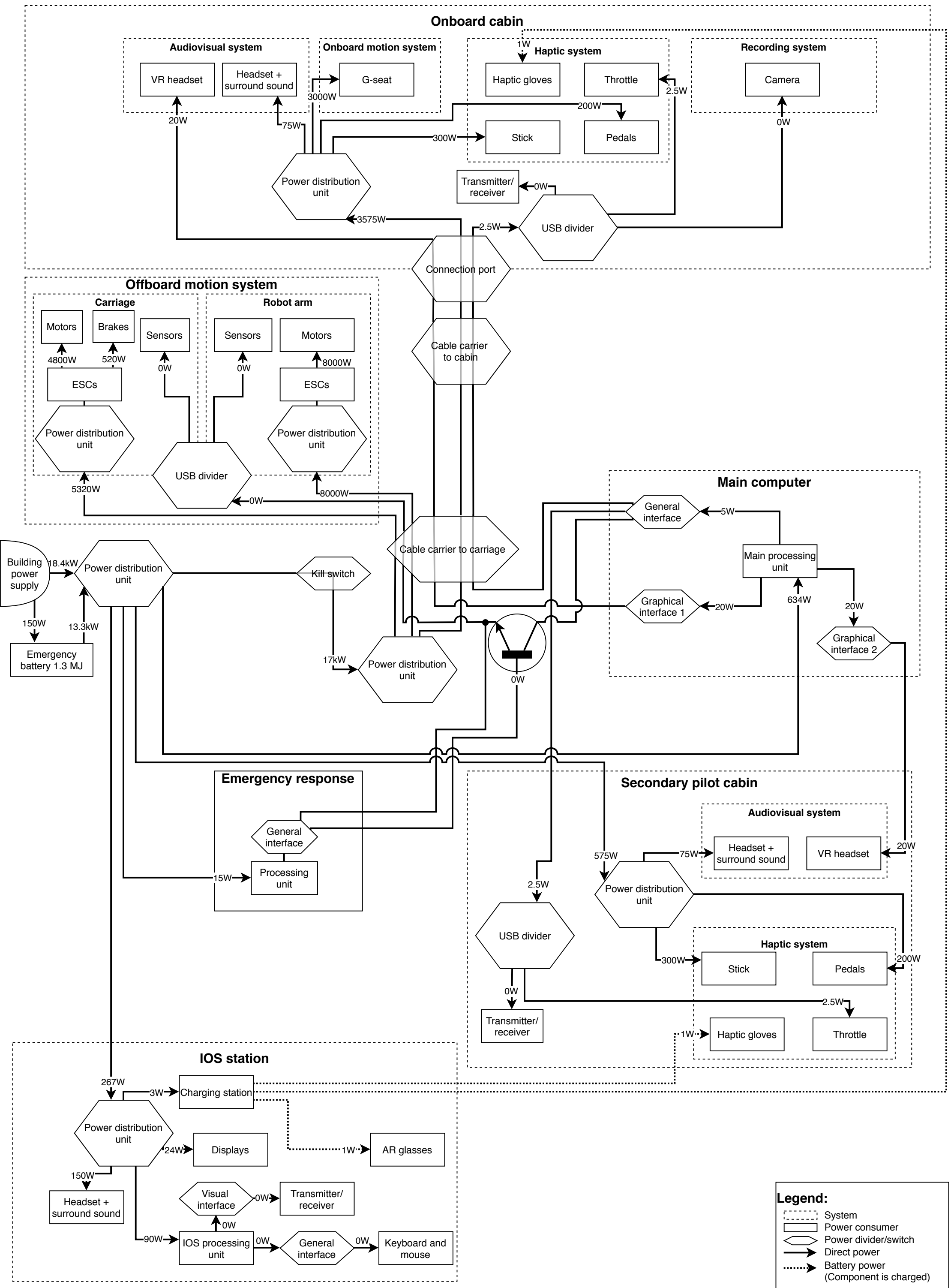
EASA	EA	Structures	[S]
IATA	IA	Haptic	[H]
STAKEHOLDER DEMAND	SH	Visual	[V]
New function wrt Baseline		Aural	[A]
Used function in Final		Robot Motion Kinematics	[M]
New placement wrt Baseline but unused in baseline			



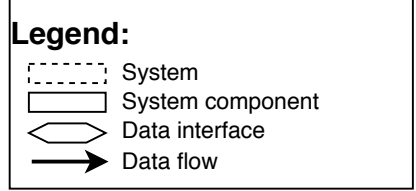
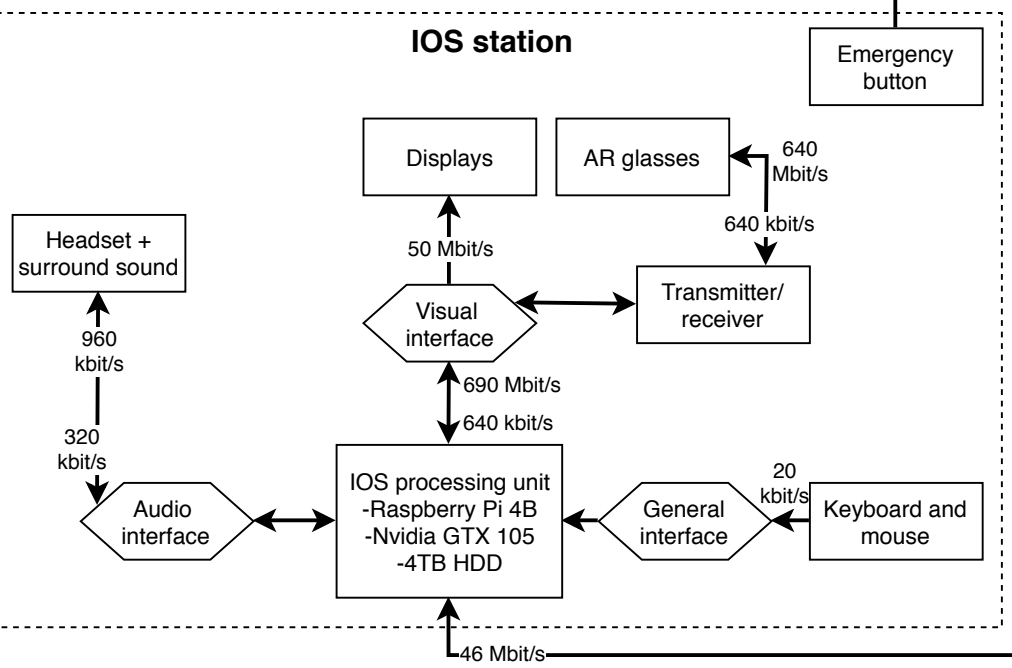
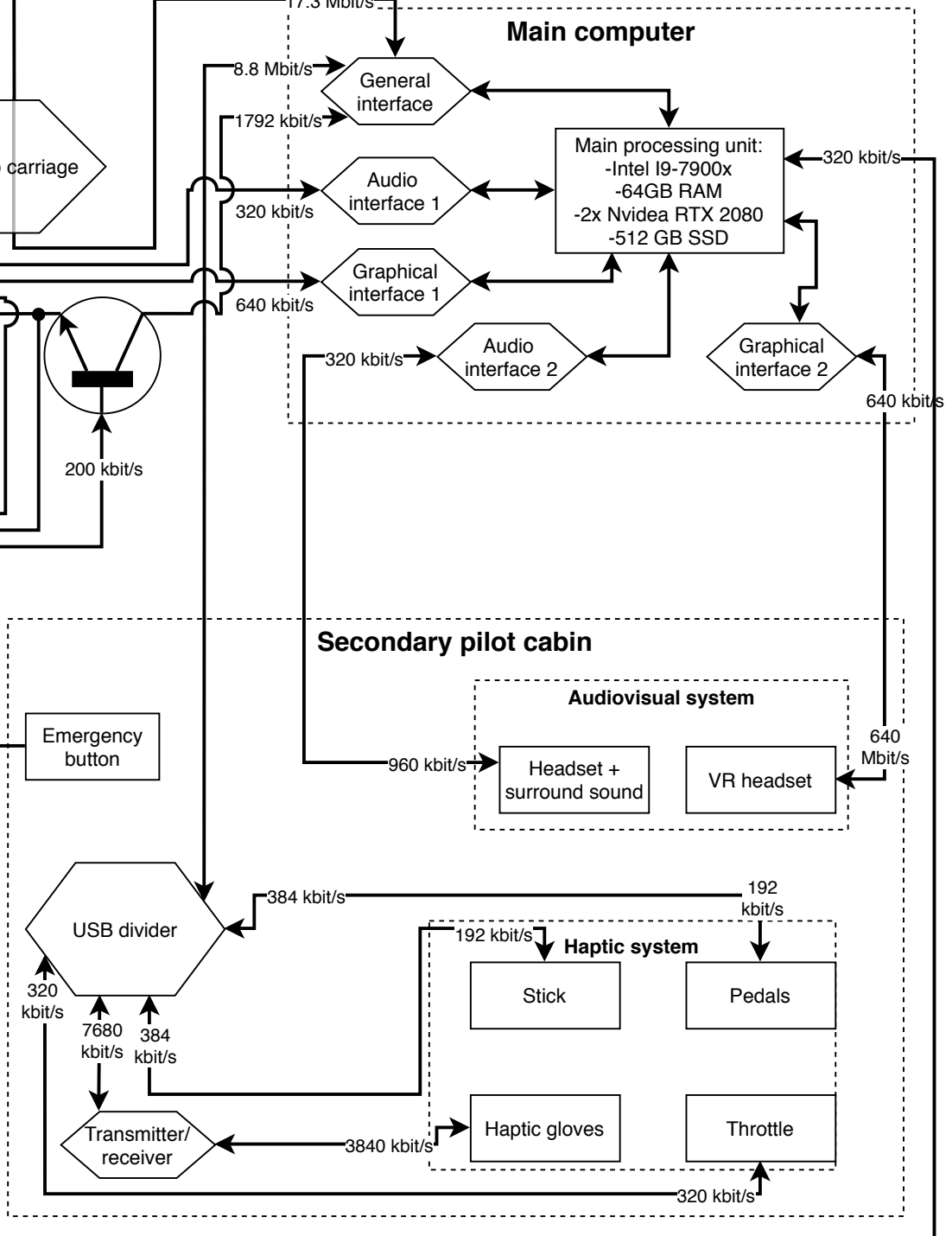
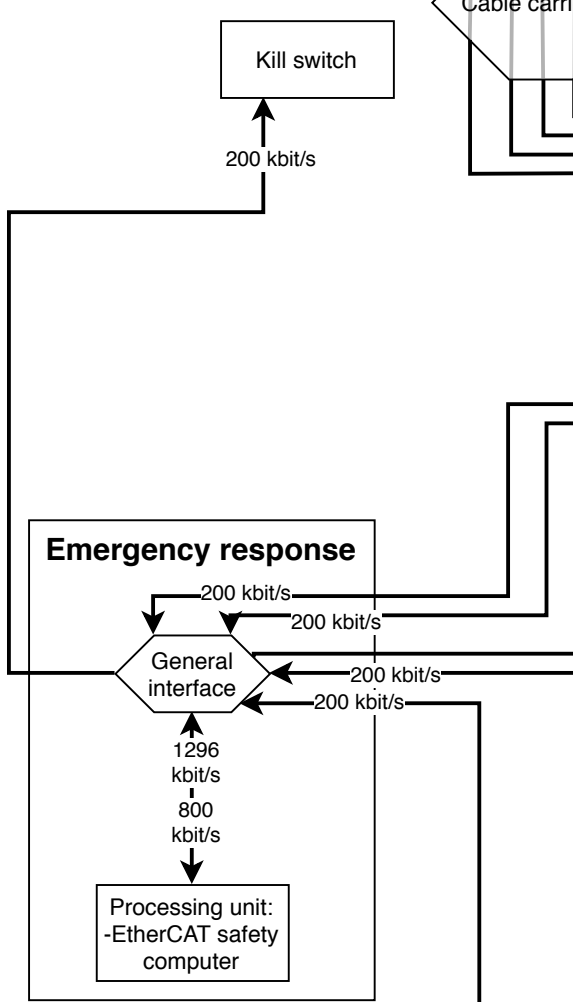
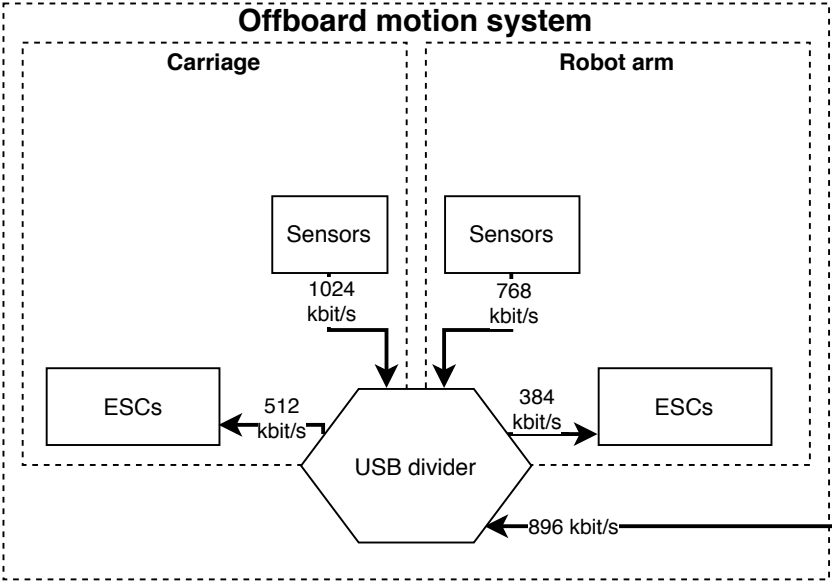
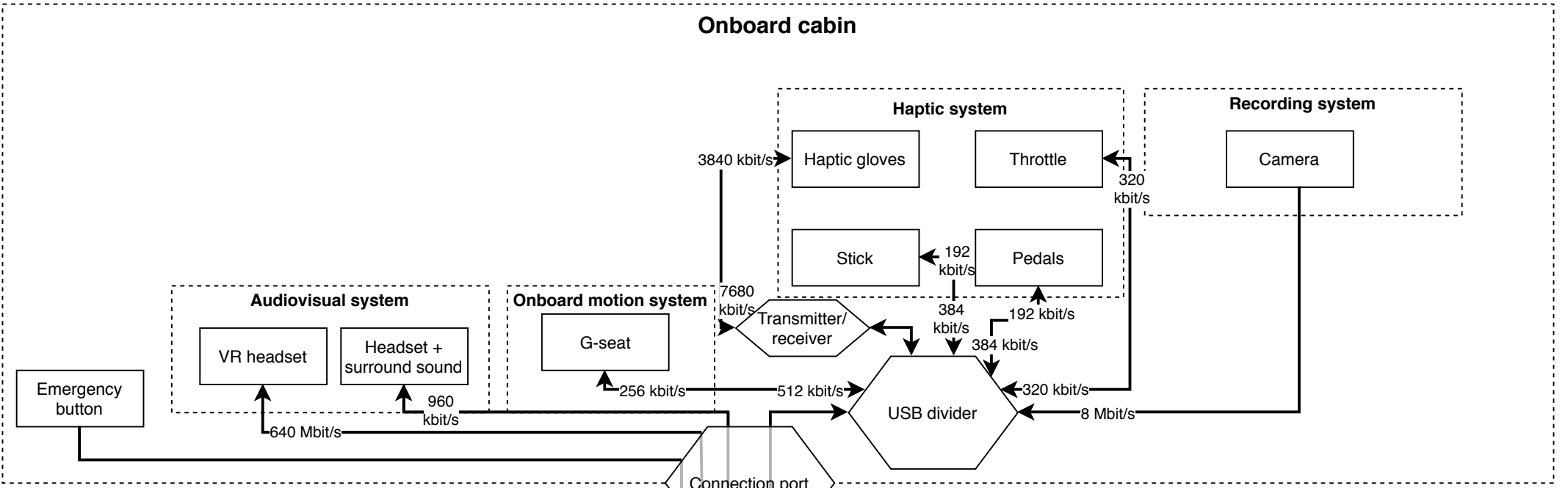




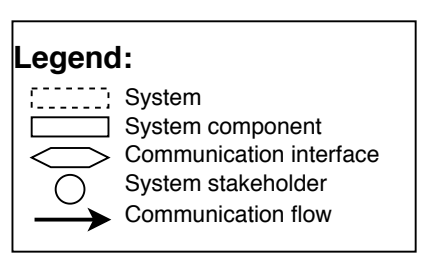
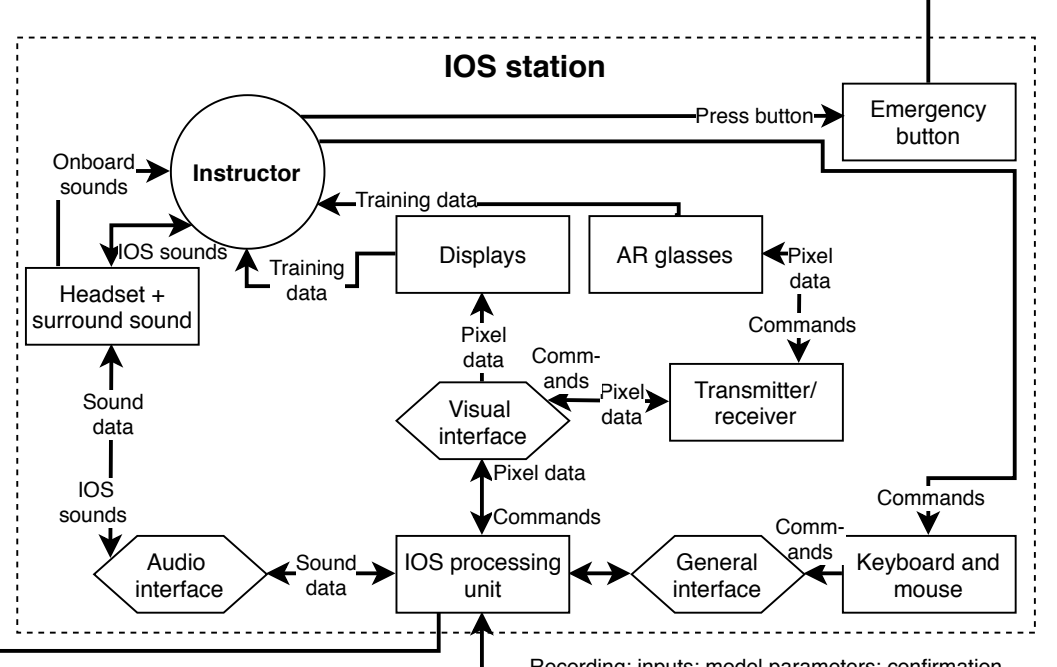
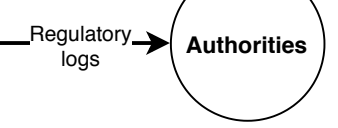
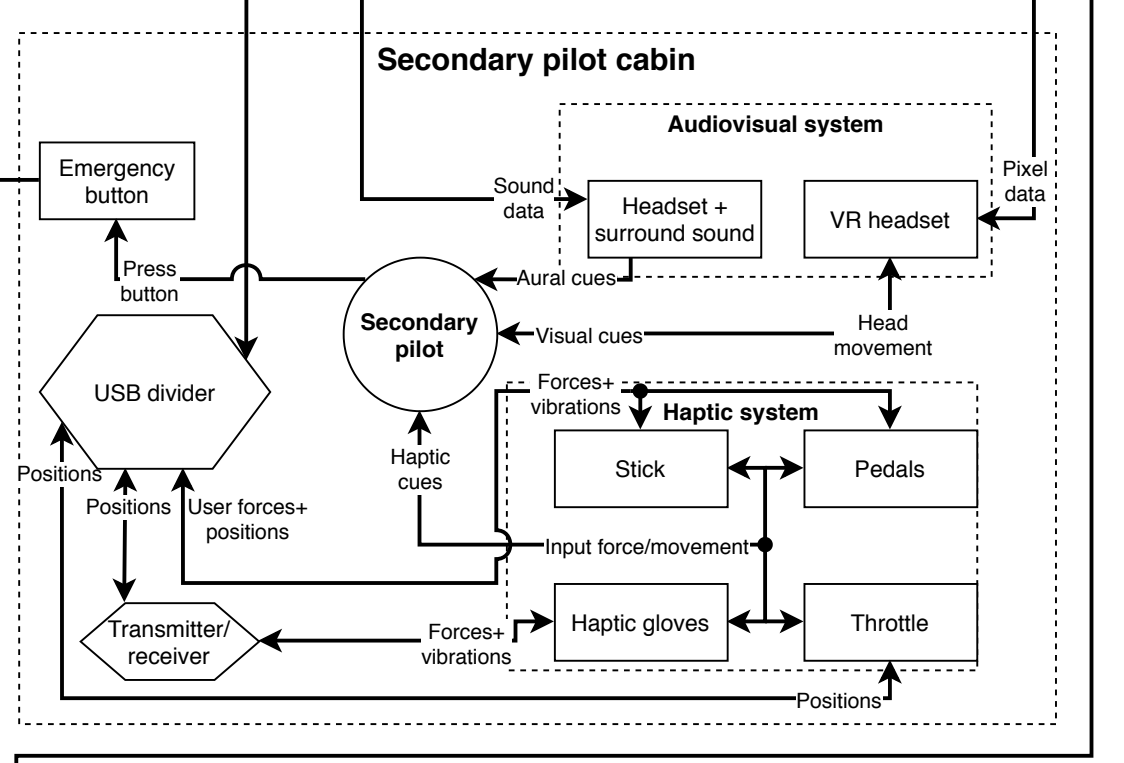
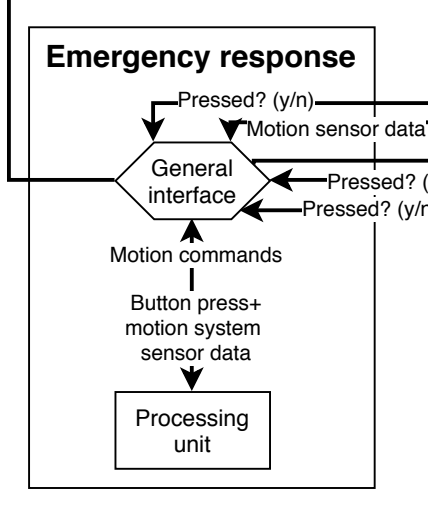
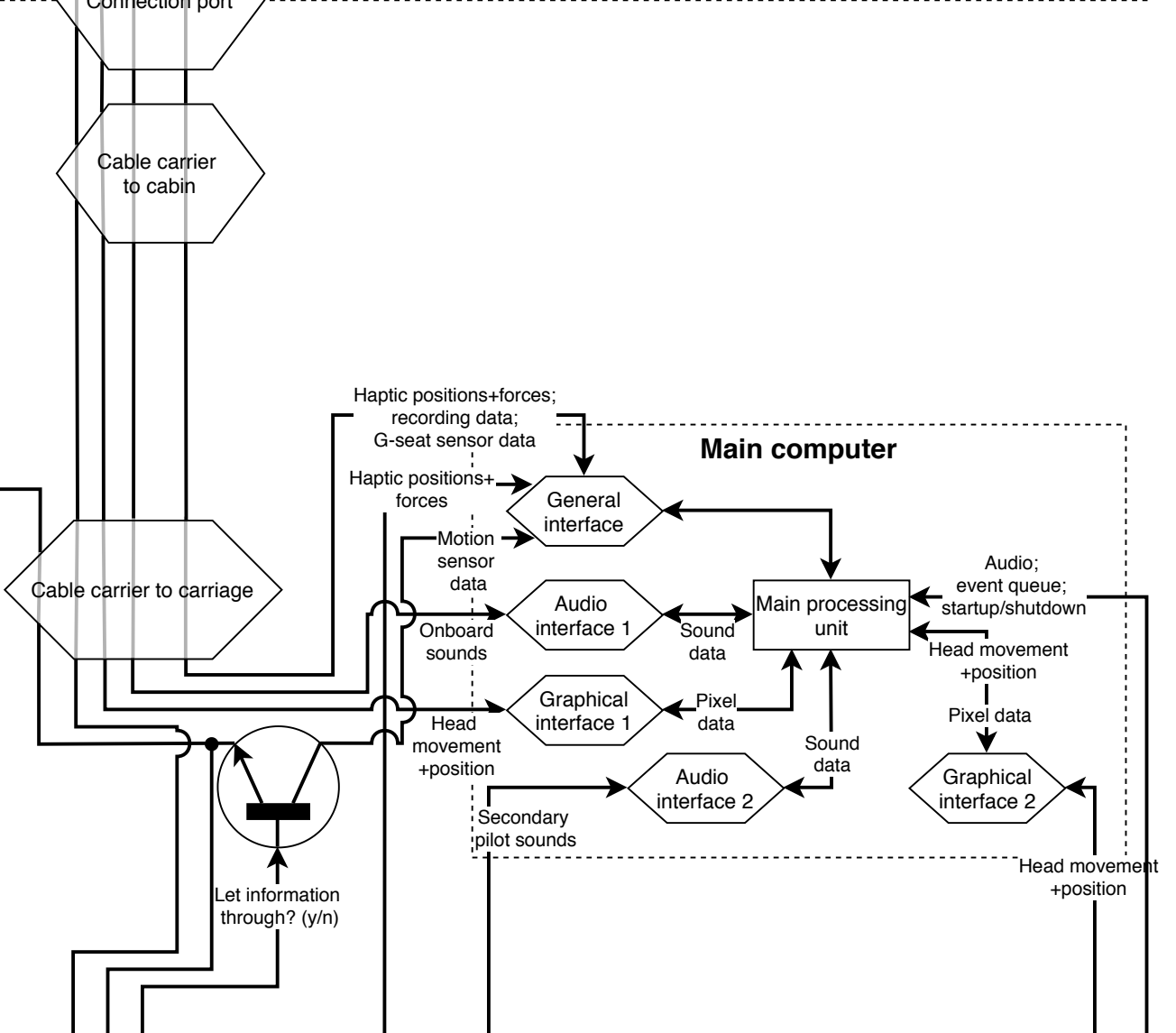
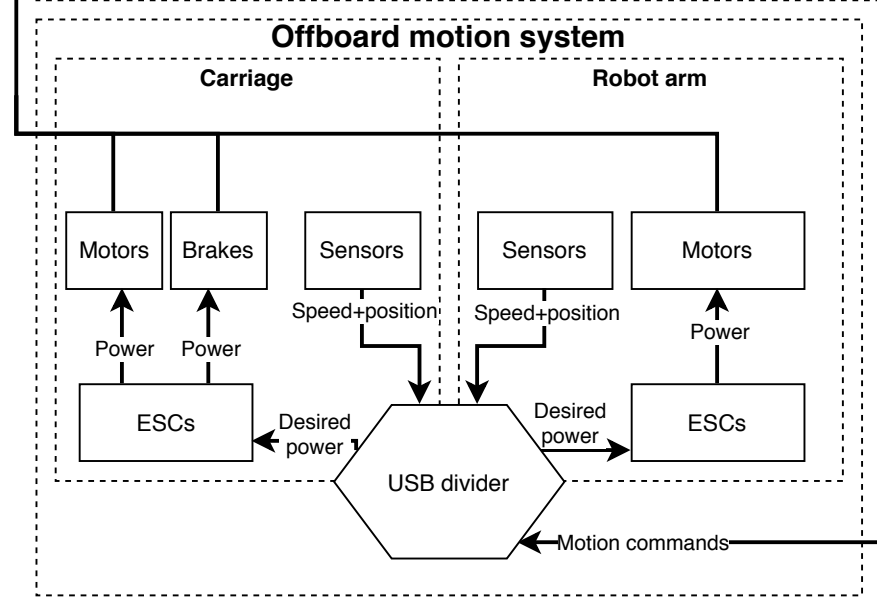
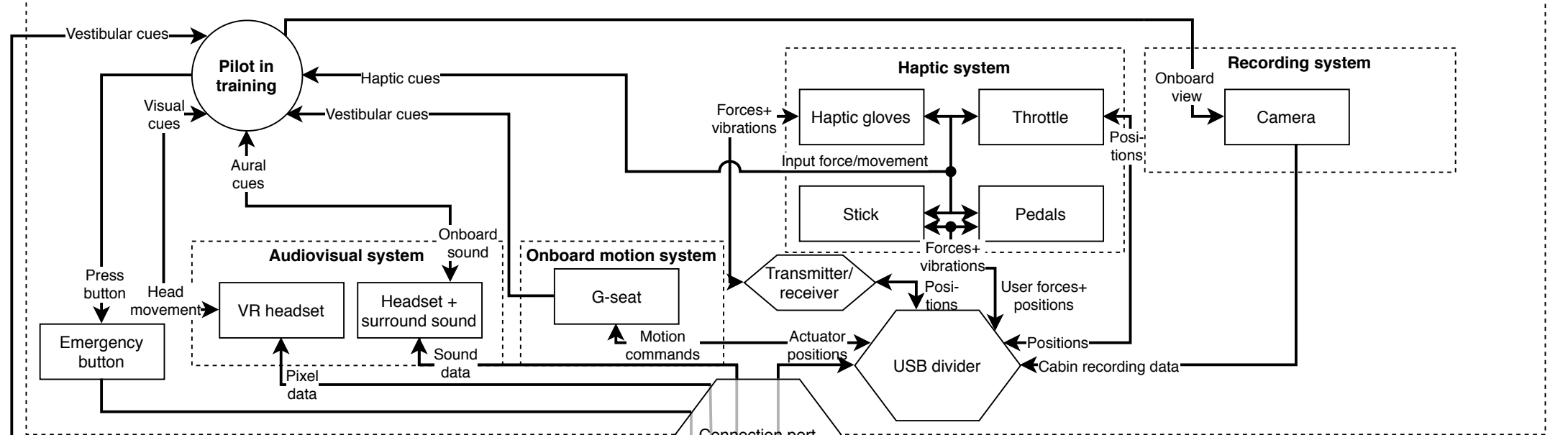
MAIN PROCESSING COMPUTER



# Onboard cabin



# Onboard cabin



## 5.3. Structural Characteristics

The analysis of the structure revolves around five different components: the floor, the rail, the carriage, the robot arm, and the cabin. Due to time constraints, only the floor, the robot arm, and the cabin are analysed. Analysis of the rail and carriage is neglected under the justification that the motion required by the robot arm on these components is within manufacturer specifications<sup>60</sup>. The expected outcome of these analyses is insight into the feasibility of the structural components given the budgets and requirements.

To provide the analyses, this section initially elaborates and expands on the functions requirements of the floor, the robot arm, the cabin, and the maintenance. Then the robot arm forces, the floor loading, the cabin structure, the arm-cabin interface, and the cable management are analysed. Next, the reliability, availability, maintainability, manufacturability, and safety (RAMS) characteristics of the structure are analysed. All calculations and methods are verified and the requirement compliance is checked. Finally, future ideas for validation are proposed.

### 5.3.1. Functional Analysis

To perform adequate structural analysis, a functional analysis was performed. These functions drive the requirements and the design. The functions encompass emergency criteria (2.1.3, 2.1.7.1 & 2.1.7.2), simulator infrastructure (2.1.7.3, 2.1.7.4, 2.1.7.6, 2.1.7.7, 2.1.7.8, 2.1.7.9 & 2.1.7.11), structural security (2.1.7.5), pilot comfort (2.1.4 & 2.1.8) and upgrade-ability (2.1.7.10). Lower level functions can be found on page 34.

### 5.3.2. Requirement Analysis

The design of the simulator structure is based on a set of requirements. These requirements originate from the analysis done in [1] and are expanded upon when necessary. If a quantitative value is yet to be determined for a requirement, <T.B.D.> is used as a placeholder. These requirements require further analysis due to being safety critical or due to a lack of data.

#### Floor requirements

- UPaRTS-SH-SO-5** The simulator facility area shall not exceed  $20 \times 20 \text{ m}^2$  [[1, 3]].
- UPaRTS-SH-SO-19** The simulator floor loading shall not exceed  $11.97 \text{ kN m}^{-2}$  <sup>62</sup> [[1, 3]].
- UPaRTS-REQ-STR-FLR-02** The floor shall withstand the maximum loading condition of the external motion system operations [FBS 2.1.7.3.4].
- UPaRTS-REQ-STR-FLR-03** The floor shall provide an average stiffness of at least 0.297 MPa [FBS 2.1.7.3.5].  
*Based on a 1° maximum deflection given maximum floor loading and a 30 cm thick floor*
- UPaRTS-REQ-STR-FLR-04** The simulator facility area shall grant space for the IOS [FBS 2.1.7.3.2].
- UPaRTS-REQ-STR-FLR-05** The simulator facility area shall grant space for the secondary pilot station [FBS 2.1.7.3.1].

#### External motion system requirements

- UPaRTS-REQ-STR-EMO-01** The external motion system shall provide the necessary strength to support manoeuvres with a safety factor of 2 [FBS 2.1.7.4.3].
- UPaRTS-REQ-STR-EMO-02** The external motion system shall allow for 3.8 kW of power transfer to the cabin [FBS 2.1.7.7.1].  
*Based on the power budget*
- UPaRTS-REQ-STR-EMO-03** The external motion system shall provide a total of 13.3 kW to its motors [FBS 2.1.7.7.2].
- UPaRTS-REQ-STR-EMO-04** The external motion system shall provide a physical connection for data transfer between the cabin and offboard [FBS 2.1.7.6.5].  
*Based on the power budget*
- UPaRTS-REQ-STR-EMO-05** The external motion system shall provide a physical connection for data transfer between the motors and offboard [FBS 2.1.7.6.4].
- UPaRTS-REQ-STR-EMO-06** The external motion system shall be able to brake to standstill within <T.B.D.> s [FBS 2.1.7.4.2].

<sup>60</sup>Productflyer TMF-6

<sup>62</sup>Heavy manufacturing floor loading p.4

[cited 2020-06-29]

[cited 2020-06-18]

**Cabin requirements**

- UPaRTS-REQ-STR-CAB-01** The cabin shall provide enough space to house all onboard systems [FBS 2.1.7.11].
- UPaRTS-REQ-STR-CAB-02** The cabin shall provide structural support to all onboard systems in all g-loading cases with a safety factor of 2 [FBS 2.1.7.5].
- UPaRTS-REQ-STR-CAB-03** The cabin shall provide power to applicable onboard systems [FBS 2.1.7.7.3].
- UPaRTS-REQ-STR-CAB-04** The cabin shall contain an emergency button reachable from the seat for all pilots [FBS 2.1.7.2.2 ].
- UPaRTS-REQ-STR-CAB-05** The cabin shall provide the pilot the ability to enter/exit within <T.B.D.> seconds [FBS 2.1.7.8 ].
- UPaRTS-REQ-STR-CAB-06** The cabin shall contain enough space for the pilot to carry out cockpit operations [FBS 2.1.7.9].
- UPaRTS-REQ-STR-CAB-07** The cabin entrance/exit shall have an emergency release accessible from inside [FBS 2.1.7.1.4].
- UPaRTS-REQ-STR-CAB-08** The connection between the external motion system and cabin shall allow the cabin to be interchanged within 1 hour [FBS 2.1.7.10].  
*based on 23/7 operation*
- UPaRTS-REQ-STR-CAB-09** The cabin shall be assemblable within 3-dimensional Euclidean space [FBS -1.2].
- UPaRTS-REQ-STR-CAB-10** The cabin shall be disposable for less than <T.B.D.> euros. [FBS 5.1].

**Offboard requirements**

- UPaRTS-REQ-STR-OFF-01** The IOS shall contain an emergency button reachable within <T.B.D.> seconds from any where in the IOS [FBS 2.1.7.2.1].
- UPaRTS-REQ-STR-OFF-02** The secondary pilot station shall provide an emergency button reachable from the seat for all pilots [FBS 2.1.7.2.2].
- UPaRTS-REQ-STR-OFF-03** The building shall allow the instructor to evacuate the hall within <T.B.D.> seconds [FBS 2.1.7.1.1].
- UPaRTS-REQ-STR-OFF-04** The building shall allow the secondary pilot to evacuate the hall within <T.B.D.> seconds [FBS 2.1.7.1.2].
- UPaRTS-REQ-STR-OFF-05** The building shall allow the pilot in training to evacuate the hall within <T.B.D.> seconds [FBS 2.1.7.1.3].
- UPaRTS-REQ-STR-OFF-06** The building shall provide a data handling route between the IOS and the main computer [FBS 2.1.7.6.1].
- UPaRTS-REQ-STR-OFF-07** The building shall provide a data handling route between motion system base and main computer [FBS 2.1.7.6.2].
- UPaRTS-REQ-STR-OFF-08** The building shall provide a data handling route between main computer and secondary pilot station [FBS 2.1.7.6.3 ].
- UPaRTS-REQ-STR-OFF-09** The building shall provide power to the main computer [FBS 2.1.7.7.4].
- UPaRTS-REQ-STR-OFF-10** The building shall provide power to secondary pilot station [FBS 2.1.7.7.5].
- UPaRTS-REQ-STR-OFF-11** The building shall provide power to motion system base [FBS 2.1.7.7.6].

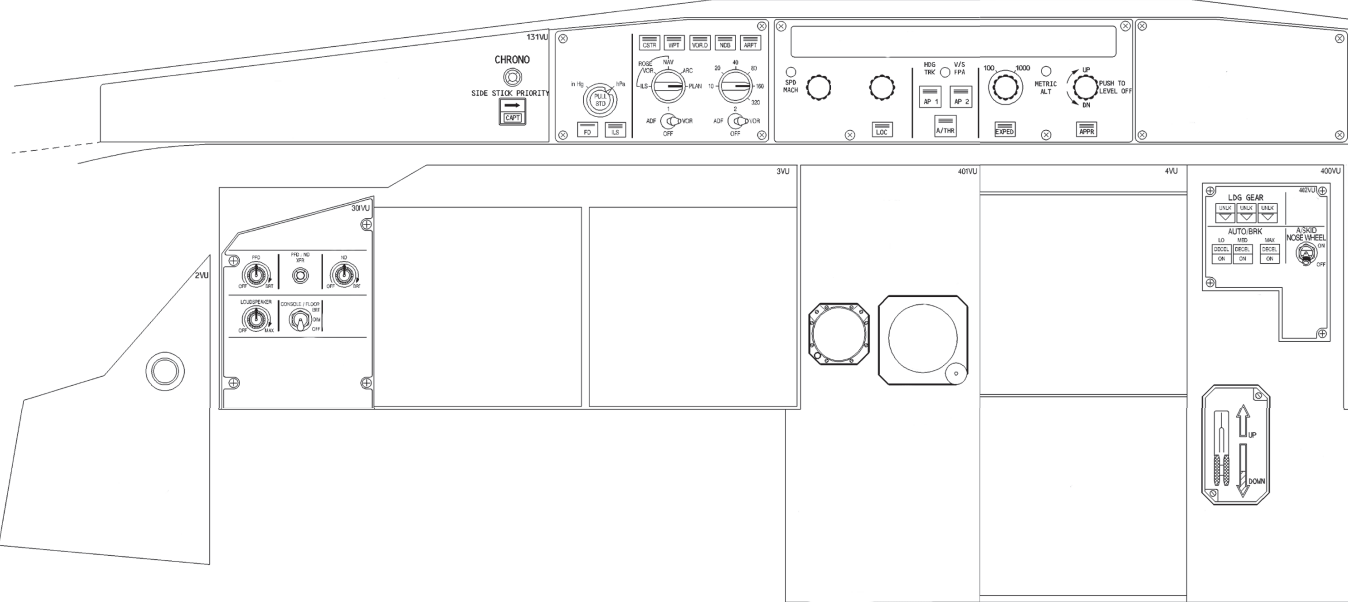
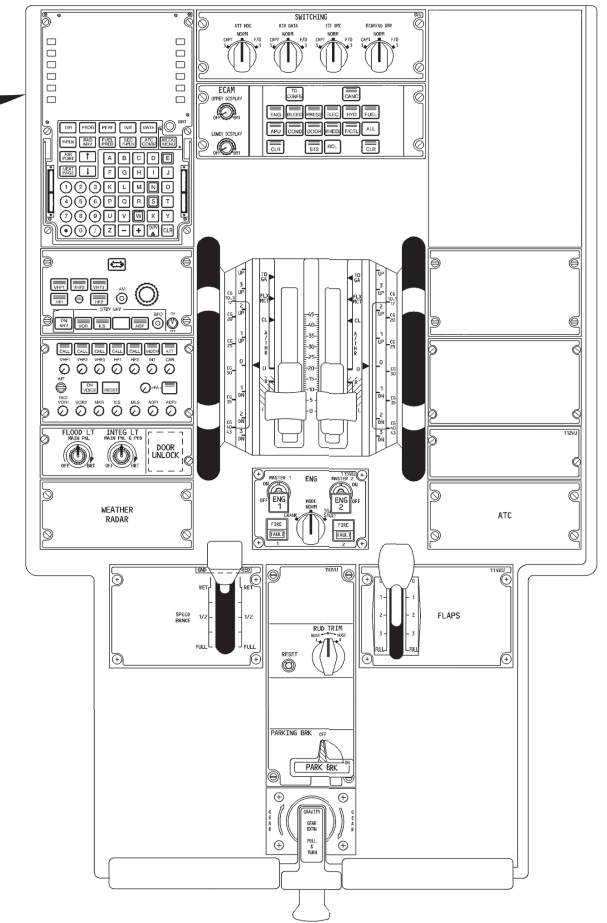
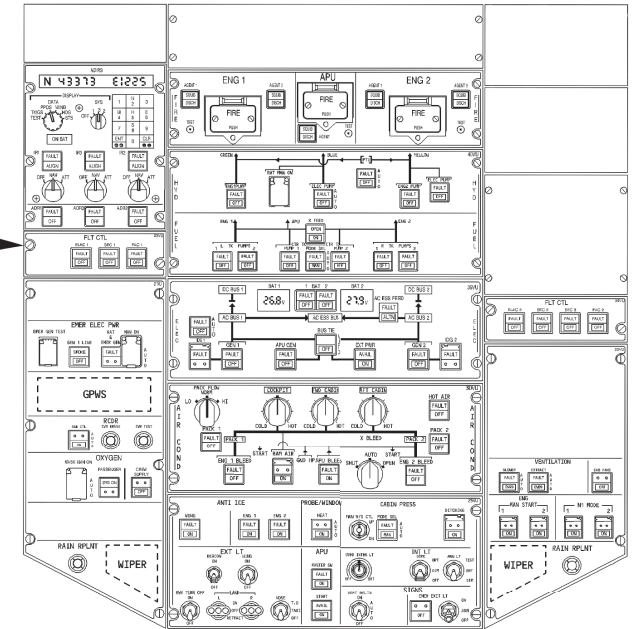
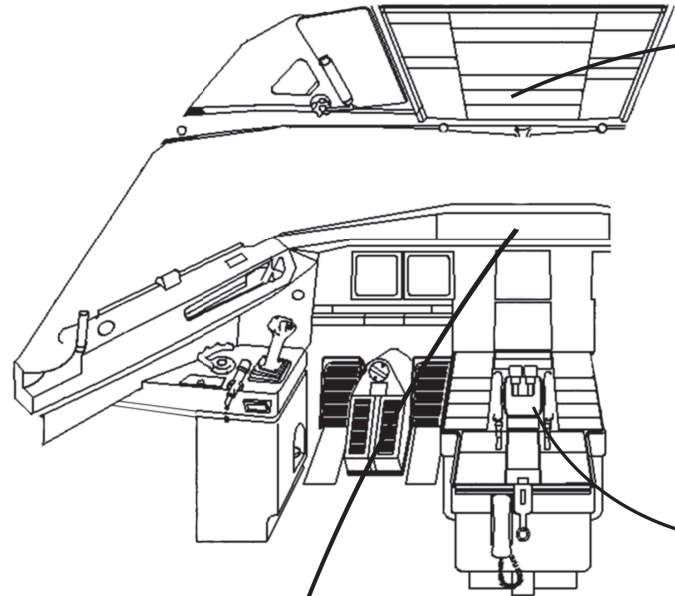
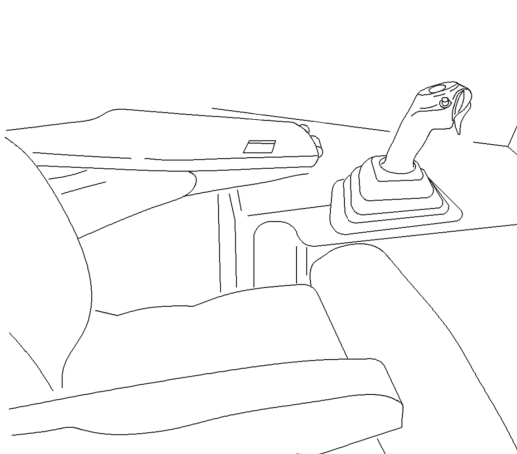
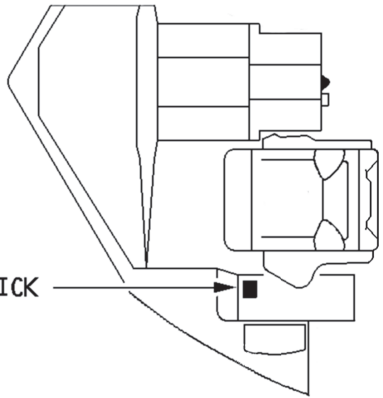
**Maintenance requirements**

- UPaRTS-REQ-STR-MNT-01** The system's maintenance-critical subsystems shall be accessible [UPaRTS-SYS-STR-MNT-1.1 [1]].
- UPaRTS-REQ-STR-MNT-02** The system's computer hardware shall be accessible [UPaRTS-SYS-STR-MNT-1.2 [1]].
- UPaRTS-REQ-STR-MNT-03** The system's computer software shall be accessible [UPaRTS-SYS-STR-MNT-1.3 [1]].
- UPaRTS-REQ-STR-MNT-04** The flight deck shall be resistant to <T.B.D.> list of cleaning solutions [UPaRTS-SYS-STR-MNT-1.4 [1]].
- UPaRTS-REQ-STR-MNT-05** The system shall have the ability to replace fluids if needed within its lifetime [UPaRTS-SYS-STR-MNT-1.5 [1]].
- UPaRTS-REQ-STR-MNT-06** The system shall have the ability to replace parts with a chance of failure higher than <T.B.D.>% during its lifetime[UPaRTS-SYS-STR-MNT-1.6 [1]].

**5.3.3. Updated internal and external configurations**

The midterm report briefly gave sketches regarding the configuration of the robotic arm [2]. This section provides updated sketches for the concept, with the internal configuration on page 47 and the external configuration on page 48.

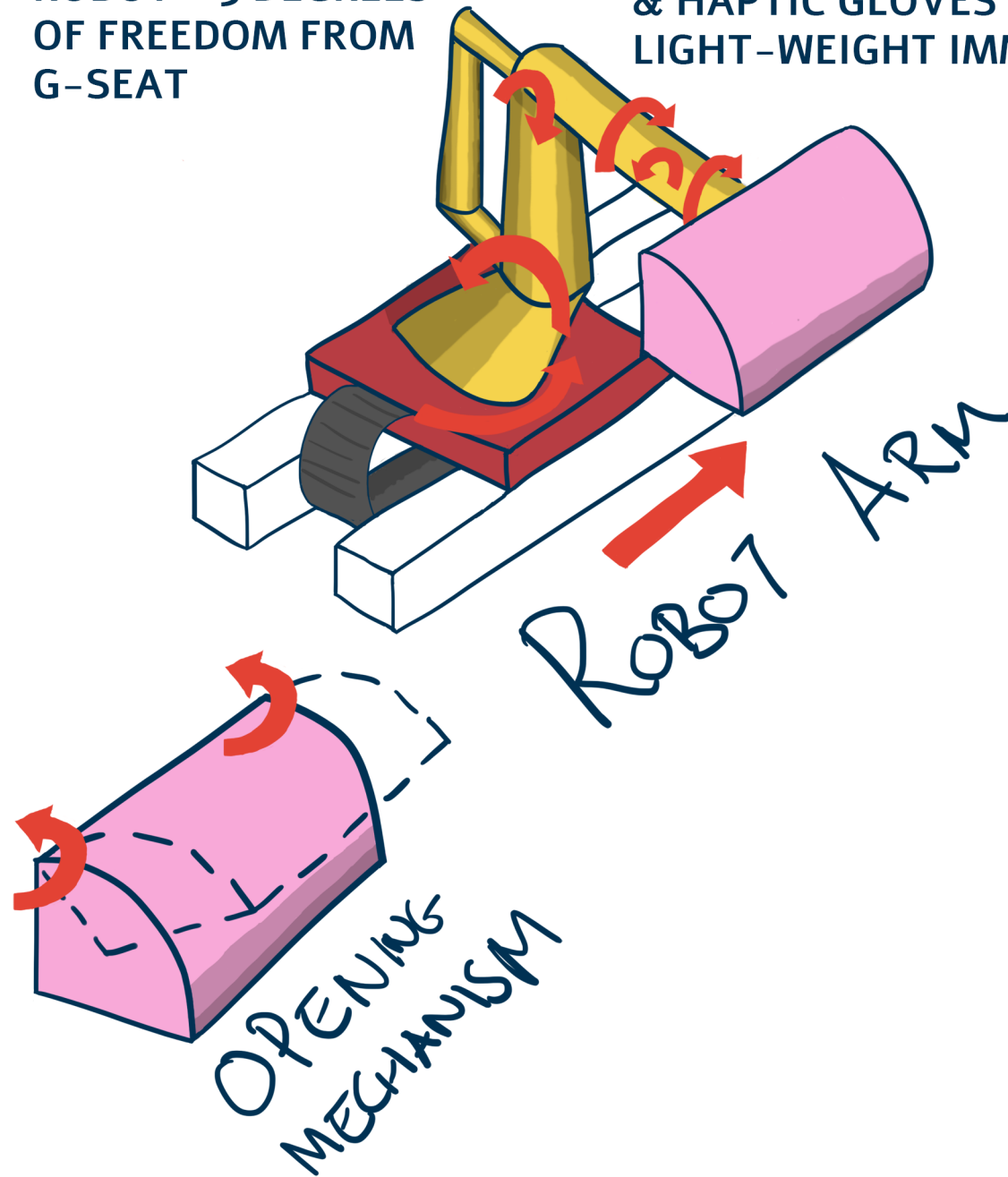
SIDESTICK



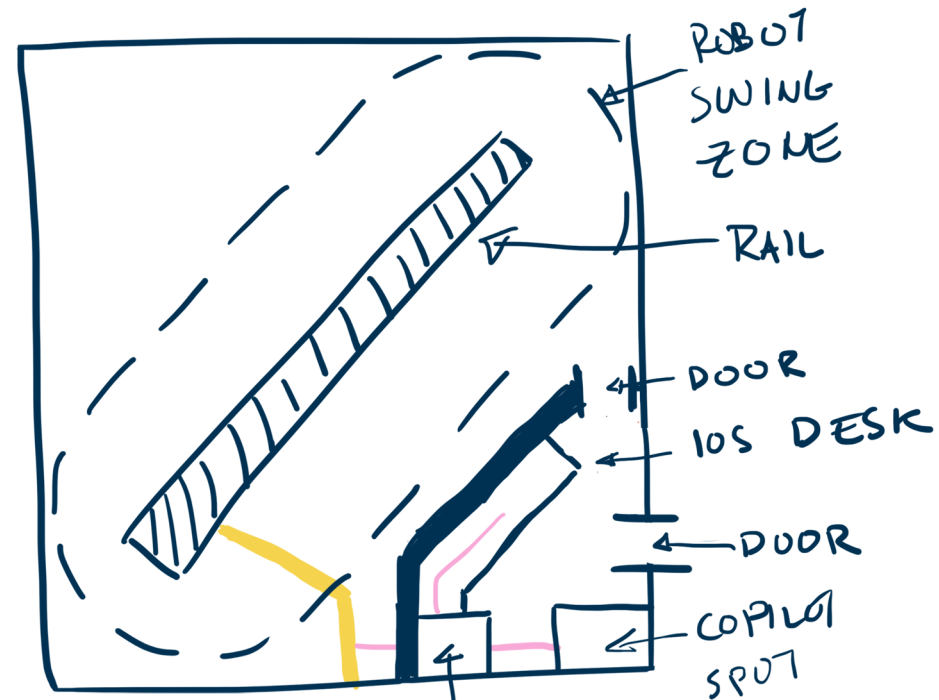
7 DEGREES OF FREEDOM FROM ROBOT + 3 DEGREES OF FREEDOM FROM G-SEAT

ROBOT ARM LIGHT-WEIGHT DESIGN INCLUDES VR-HEADSET & HAPTIC GLOVES FOR LIGHT-WEIGHT IMMERSION

IOS AND SECONDARY PILOT SEPARATED FROM ONBOARD CABIN



# FLOOR PLAN



## LEGEND

- - WALL
- - HIGH POWER LINE
- - LOW POWER LINE

### 5.3.4. Forces imposed by the robot

The primary focus of the structural characteristics of the system is to ensure that the robot arm is capable of the necessary motions. To this extent, the forces caused by a predefined robot configuration are analysed. The results of this analysis are the cabin forces and moments for the design of the cabin, and the base joint forces and moments for the floor analysis.

#### The Denavit-Hartenberg coordinate system

For this problem, the classic Denavit-Hartenberg coordinate system is utilised due to the available literature and its convenience in the upcoming kinematic problem. The following principles are used in this system<sup>63</sup>:

- The  $z_n$ -axis lies through the joint's rotational axis.
- The  $x_n$ -axis lies parallel to the normal  $z_n \times z_{n-1}$ , where  $n$  is the joint looked at. For parallel  $z_n, z_{n-1}$ , the choice of the offset  $d$  along the  $z_{n-1}$  axis to the new coordinate system origin is a free parameter.
- The  $y$ -axis lies perpendicular to the  $z, x$ -axes such that a right handed system is the result.

These principles result in the following constraints:

- The  $x_n$ -axis is perpendicular to both  $z_{n-1}$  and  $z_n$ .
- The  $x_n$ -axis intersects both  $z_{n-1}$  and  $z_n$ .
- the origin of the new coordinate system is located at the intersection of  $x_n$  and  $z_n$ .
- The  $y_n$ -axis completes a right handed frame of reference.

The parameters that drive this coordinate system are given by:

- $r$  – length of the normal between the two axes.
- $d$  – offset along  $z_{n-1}$ -axis to the new origin
- $\theta$  – angle about  $z_{n-1}$  from  $x_{n-1}$  to  $x_n$ . Defined positive using the right hand system.
- $\alpha$  – angle about  $x_n$  from  $z_{n-1}$  to  $z_n$ . Defined positive using the right hand system.

The implementation of these rules to the FANUC M-2000iA/1700L yields a total of six joint frames, one cabin frame, and two intermediate frames, with parameters shown in Table 5.1. Note that the direction of the  $z$  axis is defined based on what is a positive rotation for the FANUC M-2000iA/1700L. The six joint frames and cabin frame are represented in Fig. 5.1, where the black squares represent the joints and the grey lines represent the connections. The intermediate frames (3a and 4a) are needed as a direct frame transformation is not possible between joint 3-4 and joint 5-6 based on the rules given. Joint angles can be introduced by adding them to the  $\theta$  of the respective joint.

Table 5.1: Denavit-Hartenberg parameters for the joint coordinate systems

Coordinate Frame	$r$ [mm]	$d$ [mm]	$\theta$ [rad]	$\alpha$ [rad]
Joint 1→2	500	1300	0	$-\pi/2$
Joint 2→3	300	0	$-\pi/2$	$-\pi$
Joint 3→4a	200	0	0	$-\pi/2$
Int. 4a→4	0	-1850	0	0
Joint 4→5	0	-630	0	$\pi/2$
Int. 5→6a	0	0	0	$-\pi/2$
Joint 6a→6	-600	0	0	0
Cabin	0	0	0	$\pi$

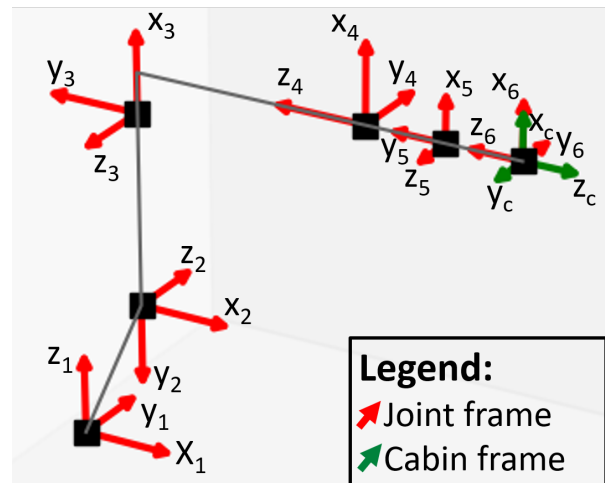


Figure 5.1: Denavit-Hartenberg coordinate frames on the 6 robot arm joints in its neutral position

Using the information from Table 5.1, the transformation matrices from one coordinate system to the next are definable. The following equation describes the transformation matrix  $M$  from one coordinate frame to the next:

$${}^{n-1}M_n = \begin{bmatrix} \cos \theta_n & -\sin \theta_n \cos \alpha_n & \sin \theta_n \sin \alpha_n & r_n \cos \theta_n \\ \sin \theta_n & \cos \theta_n \cos \alpha_n & -\cos \theta_n \sin \alpha_n & r_n \sin \theta_n \\ 0 & \sin \alpha_n & \cos \alpha_n & d_n \\ 0 & 0 & 0 & 1 \end{bmatrix} = \begin{bmatrix} R & T \\ 0 & 0 & 0 & 1 \end{bmatrix} \quad (5.1)$$

<sup>63</sup>tekkotsu.org: Kinematics

[cited 2020-06-18]

To transform back to the previous coordinate system, the inverse of  $M$  is used. Luckily, inverting  $M$  is light on computational resources as:

$$M^{-1} = {}^nM_{n-1} = \left[ \begin{array}{ccc|c} R^T & & & -R^T T \\ \hline 0 & 0 & 0 & 1 \end{array} \right] \quad (5.2)$$

Where the most expensive operation is the transpose as it requires accessing both column and row elements in sequence, removing the benefit of both row and column major ordering.

### Defining inertia

In order to determine the mass moment of inertia around any given joint in their respective reference frame, an Euler tensor is introduced. This Euler tensor is defined in Eq. 5.3 based on [30] p.102. Where the fourth column and row take into account the Steiner terms when transforming the matrix into a different frame of reference.  $x_g$ ,  $y_g$  and  $z_g$  define the distance to the centre of gravity from the origin of the current frame of reference while  $m$  is the mass.

$$J_0 = \begin{bmatrix} J_{xx} & J_{xy} & J_{xz} & x_g m \\ J_{xy} & J_{yy} & J_{yz} & y_g m \\ J_{xz} & J_{yz} & J_{zz} & z_g m \\ x_g m & y_g m & z_g m & m \end{bmatrix} = \begin{bmatrix} \frac{-I_{xx} + I_{yy} + I_{zz}}{2} & -I_{xy} & -I_{xz} & x_g m \\ -I_{xy} & \frac{I_{xx} - I_{yy} + I_{zz}}{2} & -I_{yz} & y_g m \\ -I_{xz} & -I_{yz} & \frac{I_{xx} + I_{yy} - I_{zz}}{2} & z_g m \\ x_g m & y_g m & z_g m & m \end{bmatrix} \quad (5.3)$$

The moments of inertia were simplified to be a point mass for the joints and a solid cylinder for the parts connecting the joints. The sizes of these cylinders were defined according to the specifications of the FANUC M-2000iA/1700L robotic arm. Most of these cylinders were assumed to be a straight connection between the origins of two frames. The cylinder between frame 1 and 2 is assumed to lie in the  $z$ -direction of frame 1, with a height equal to the origin of frame 2. Furthermore, the connection between 3 and 4 lies in the  $z$ -direction of frame 4 with a height equal to the origin of frame 3. The cylinder between joint 6 and the cabin is assumed to have zero height. The main weight of the joints is assumed to be the motor, which is stationary with respect to the frame lying on that joint. Therefore, the joint inertia is expressed in the frame lying on that joint (e.g. inertia of joint 1 is expressed in frame 1). The connection between two joints rotates in the coordinate frame of the 'higher' (further from the base) joint, so the inertia of this connection will also be expressed in this 'higher' frame (e.g. the connection between joint 4 and 5 is expressed in frame 5).

For calculating the moment of inertia of the connections, Eq. 5.4 gives the moment of inertia with respect to the axis which is in line with the cylinder. Eq. 5.5 Gives the moment of inertia for the other two axes, at the end of a cylinder. In these equations  $r$  is the radius,  $l$  is the length and  $m$  is the mass of the cylinder. In Tab. 5.2 the dimensions and locations of the cylinders are presented. The mass of the cylinder was determined by looking at the volume fraction of the cylinder with respect to the total volume off all cylinders together. This volume fraction was then multiplied by the mass of the robot arm without the mass of the joints. The joints were estimated as point masses in their respective locations, noted in Tab. 5.3. The cabin is estimated as a point mass 0.75 m from the end of the robot arm. Its moments of inertia are not taken into account as the Steiner terms are expected to be far larger. Finally, the Euler tensors of the joint and the connection (and the cabin in the last frame) in a certain frame are added up to produce one inertia tensor.

$$I = 1/2mr^2 \quad (5.4)$$

$$I = 1/3ml^2 \quad (5.5)$$

Table 5.2: Robot arm inertia

Segment	$l$ [m]	$r$ [m]	$m$ [kg]	Reference frame	dir.
Cylinder <sub>12</sub>	1.3	0.5	5136	2	-y
Cylinder <sub>23</sub>	1.7	0.3	2418	3	-x
Cylinder <sub>34</sub>	1.85	0.2	1169	4	+z
Cylinder <sub>45</sub>	0.63	0.2	398	5	+y
Cylinder <sub>56</sub>	0.60	0.2	379	6	+z

Table 5.3: Joint mass

Segment	$m$ [kg]
Joint <sub>1</sub>	1000
Joint <sub>2</sub>	800
Joint <sub>3</sub>	500
Joint <sub>4</sub>	300
Joint <sub>5</sub>	200
Joint <sub>6</sub>	200

### Acceleration tensor

The Denavit-Hartenberg velocity tensor is given by Eq. 5.6:

$$W = \left[ \begin{array}{ccc|c} 0 & -\omega_z & \omega_y & v_x \\ \omega_z & 0 & -\omega_x & v_y \\ -\omega_y & \omega_x & 0 & v_z \\ \hline 0 & 0 & 0 & 0 \end{array} \right] \quad (5.6)$$

Where  $\omega_{x/y/z}$  is the angular velocity around the  $x$ -,  $y$ - or  $z$ -axis respectively and  $v_{x/y/z}$  is the linear velocity in  $x$ -,  $y$ - or  $z$ -direction respectively. The velocity tensor of a certain frame is found by initializing a velocity tensor one frame 'lower' (closer to the base) with only an  $\omega_z$ , equal to the angular velocity of the joint associated with this 'lower' frame. This velocity tensor is then transformed to the next frame, where the velocity tensor is desired. This transformation is done using Eq. 5.7 where  $h$  is the 'higher' frame and  $k$  is the 'lower' frame. For example, the velocity matrix of frame 4 is found by initializing the tensor in Eq. 5.6 with  $\omega_z = \omega_3$  and then transforming this to frame 4 using  $W_4 = M_{43}W_3M_{34}$ . Note that this velocity tensor only gives the velocities with respect to the previous joint. Since frame 1 is not rotating, its velocity tensor will only have a  $v_y$  component (due to the carriage).

$$W_{(h)} = M_{h,k}W_{(k)}M_{k,h} \quad (5.7)$$

The derivative of the velocity tensor,  $\dot{W}$ , is defined similar to Eq. 5.6. However, now the angular velocities  $\omega$  are replaced with angular velocities  $\alpha$  and linear velocities  $v$  with linear accelerations  $a$ . These are obtained similar to the velocity tensors; by initialising a tensor with the angular acceleration of the joint associated with the 'lower' frame as  $\alpha_z$  and then transforming to the frame where the derivative velocity tensor is desired. This again results in the derivative velocity tensor only relative to the 'lower' frame. Again, the first frame is not rotating and will therefore not have any angular accelerations. It will have a linear acceleration in the positive  $y$ -direction equal to the acceleration of the carriage and a linear acceleration in the positive  $z$ -direction equal to the acceleration due to gravity. In reality, these accelerations should both be in negative direction. However, this is a hack to correct the force tensors as will be explained in the next section.

Next,  $W$  and  $\dot{W}$  are combined to give a total acceleration tensor  $H$  in local frame  $i$  with respect to the 'lower' frame  $i-1$ :

$$H_{i_{local}} = \dot{W}_i + W_i^2 \quad (5.8)$$

Where the  $W_i^2$  term is calculated by doing matrix-matrix multiplication on the same velocity tensor. This term accounts for the centripetal acceleration due to rotation. Finally, the total acceleration tensor is found for each frame by transforming the total acceleration tensor of frame  $i-1$  to the local frame using Eq. 5.9 and adding it to the local acceleration tensor  $H_{i_{local}}$ . Since the total acceleration tensor of the 'lower' joint is needed each time, this process starts at joint 1. This total acceleration tensor contains the accelerations due to all the 'lower' joints. It should be noted that even centripetal acceleration is correctly calculated for all 'higher' joints.

$$H_i = M_{i,i-1}H_{(i-1)}M_{i-1,i} \quad (5.9)$$

### Calculating forces

The action tensor in a certain frame  $i$ ,  $\Phi_i$ , is calculated using Eq. 5.10. Where  $H_i$  is the total acceleration tensor in the local frame  $i$ , found in the previous section.  $J_i$  is the inertia tensor of the local frame found in the 'Defining inertia' section. Finally,  $\Phi_{i+1}$  is the action tensor one frame 'higher'. Since the action tensor of the higher frame is needed each time, this process starts at the cabin frame as this is the 'highest' frame (so the free end).

This action tensor  $\Phi$  contains forces in  $x$ -,  $y$ - and  $z$ -direction;  $F_{x/y/z}$ , and torques around the  $x$ -,  $y$ - and  $z$ -axis;  $t_{x/y/z}$ . The composition of  $\Phi$  is shown in Eq. 5.11.

$$\Phi_i = H_i J_i - J_i H_i^T + \Phi_{i+1} \quad (5.10)$$

$$\Phi = \left[ \begin{array}{ccc|c} 0 & -t_z & t_y & f_x \\ t_z & 0 & -t_x & f_y \\ -t_y & t_x & 0 & f_z \\ \hline -f_x & -f_y & -f_z & 0 \end{array} \right] \quad (5.11)$$

The forces given by this  $\Phi$  will be on the components in the local- and 'higher' frames. Unfortunately, due to the nature of rotations, the rotation forces on the joint of one frame 'lower' will be in the opposite direction. Meanwhile, the forces due to uniform linear accelerations such as gravity will be in the same direction. As a result, an action tensor is obtained where the forces and moments

represent both reaction forces from the lower joint and forces on the lower joint. As mentioned before, gravitational and carriage accelerations are introduced with opposite signs. This means the resulting  $\Phi$ s will consistently give the reaction forces of the 'lower' joint. Each  $\Phi$  is then multiplied by  $-1$  to obtain the forces on the 'lower' joint.

Iterating the cabin structure weight found in Subsec. 5.3.5 with the kinematics department to find the most critical forces at the joint and at the cabin interface. This iteration process is further described in Subsec. 5.5.2. The critical forces and moments found are shown in Tab. 5.4.

Table 5.4: Most critical forces and moments at the base and the cabin

Frame	Forces/moments [N; N m]					
	$F_x$	$F_y$	$F_z$	$M_x$	$M_y$	$M_z$
Base	4413	18335	-132694	-29711	188860	34320
Cabin	-6498	-1455	1949	1092	-4874	0

### Floor loading

With the forces and moments at the base known, the reaction forces on the carriage wheels can be calculated. The free body diagram of the carriage is shown in Fig. 5.2, where  $w = 1.384$  m and  $l = 2.230$  m<sup>64</sup>. As can be seen, there are three known forces and three known moments, while there are 12 unknown reaction forces. Using deflection equations, this could be solved, but this would require solving an 18-dimensional system of equations. Using the following simplifications, the system can be solved more easily using engineering insights:

- The robot arm forces and moments act exactly in the middle of the carriage.  
*This divides the load evenly over the wheels so this would be done anyway. Mounting the robot arm in the centre with accuracy is doable*
- The carriage base plate has no thickness.  
*Otherwise the wheels will be mounted slightly below the robot arm base, so  $M_y$  and  $M_x$  will be slightly larger at the wheels. However, this distance is in the order of millimetres so this increase in moment is negligible.*
- The base plate and the carriage wheels in x- and z-direction are infinitely stiff.  
*Nonzero deflections would make the upcoming engineering insight invalid. There is already a requirement on stiffness (UPaRTS-REQ-STR-FLR-03), so the deflections will be negligible.*

Solving the aforementioned system of 18 equations to find the 12 unknown reaction forces of interest can now be avoided: Now reaction forces can be calculated for each of the six robot arm forces/moments separately and superimposed later:

$F_z$  Since  $F_z$  is acting exactly in the middle, it will be divided evenly among the reaction forces in z:

$$A_z = B_z = C_z = D_z = -F_z/4.$$

$F_y$  Again,  $F_y$  is acting in the middle and will be divided equally over the reaction forces in y:  $A_y = B_y = C_y = D_y = -F_y/4$

$F_x$  Also  $F_x$  acts in the middle and will be divided equally over the reaction forces in x:  $A_x = B_x = C_x = D_x = -F_x/4$

$M_x$  This will be divided equally over the reaction forces in z. However,  $B_z$  and  $C_z$  will have the opposite sign of  $A_z$  and  $D_z$  so the forces balance out:  $A_z = D_z = -B_z = -C_z = \frac{M_x}{2l}$

$M_y$  Will be done the same as  $M_x$ , where all reaction forces have the same magnitude, but  $A_z$  and  $B_z$  will have the opposite sign of  $C_z$  and  $D_z$  so the forces balance out:  $A_z = B_z = -C_z = -D_z = \frac{M_y}{2w}$

$M_z$  Will technically be influenced by both the reaction forces in y and x. However, the reaction forces in y are due to the brakes while those in x are due to the carriage wheels against the rail. Therefore the reaction forces in x are much stiffer (see the third assumption) and they are assumed to carry the entirety of  $M_z$ . Again,  $D_x$  and  $C_x$  will have the opposite sign of  $A_x$  and  $B_x$  to balance out the forces:  $-A_x = B_x = C_x = -D_x = \frac{M_z}{2l}$

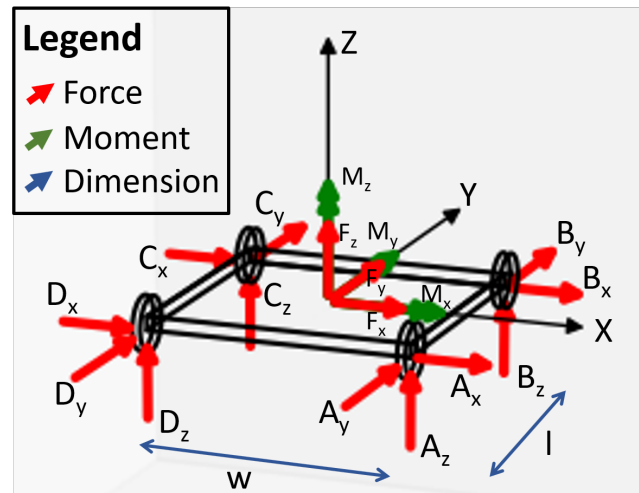


Figure 5.2: Free body diagram of the carriage subjected to the forces and moments of the robot arm base with reaction forces from its wheels

<sup>64</sup>TrackMotion Floor TMF

The final reaction forces are found by superimposing the reaction forces found in the six scenarios above. This process and the final reaction forces can be found in Table 5.5.

Table 5.5: Contributions of the robot arm forces and moments on the carriage wheels reaction forces.

Reaction force	Robot arm force/moment contribution						Total force kN
	$F_x$ 4413 N	$F_y$ 18 335 N	$F_z$ -132 694 N	$M_x$ -29 711 N m	$M_y$ 188 860 N m	$M_z$ 34 320 N m	
$A_x$	-1103	0	0	0	0	-7695	-8.8
$A_y$	0	-4584	0	0	0	0	-4.6
$A_z$	0	0	33174	-6662	68230	0	94.7
$B_x$	-1103	0	0	0	0	7695	6.6
$B_y$	0	-4584	0	0	0	0	-4.6
$B_z$	0	0	33174	6662	68230	0	108.1
$C_x$	-1103	0	0	0	0	7695	6.6
$C_y$	0	-4584	0	0	0	0	-4.6
$C_z$	0	0	33174	6662	-68230	0	-28.4
$D_x$	-1103	0	0	0	0	-7695	-8.8
$D_y$	0	-4584	0	0	0	0	-4.6
$D_z$	0	0	33174	-6662	-68230	0	-41.7

As can be seen in Tab. 5.5, one rail will have 203 kN of wheel forces on it. The other one will have -65.1 kN (so tension) of wheel forces on it. These two rails are assumed to be mounted to a set of sleepers which are mounted to the floor. These sleepers are assumed to be thrice as wide as the width of the carriage. Each rail is assumed to distribute its load equally on both sides, so over a width equal to the carriage width. Furthermore, the point loads of the wheels are assumed to be distributed equally along the rail. The weight of the rail is assumed to be equal to that of the carriage (2460 kg<sup>64</sup>). Taking the rail length as the maximum possible one in the room (10.75 m, see Sec. 2.2.1) gives a floor loading of 7.6 kN m<sup>-1</sup> on one side and -1.5 kN m<sup>-1</sup> on the other side. Both meet the floor loading requirement in terms of magnitude, but the second one is in tension. Generally, floors are worse in tension than compression. If in the future this turns out to be a problem, weight can be added to relieve these loads (although that will also increase the compressive loads).

### 5.3.5. Cabin structure

The cabin is the most significant part of the simulator which requires a custom design. Hence extra attention is paid to the structural layout of the cabin. The stresses are calculated in the main structural elements. The stiffness is assumed to be sufficient due to stiffening elements but will have to be analysed in the near future.

#### Cabin layout and structure

The cabin size was designed based on the A320 cabin, but only taking into account the space the first pilot needs as this is a one person simulator (see page 47). Enough space for the sound system and any possible sensors had to be taken into account as well. For the shape of the cabin, a quarter cylinder was decided upon to keep the design simplistic as is shown on page 48. The attached curved shell will serve as the entrance and exit of the simulator as it can swing open upwards. This includes the sides of the cabin shell, such that the pilot can exit on the side without the need to climb over instruments in front. The panel with the stick will swing out to the side to allow for easy entrance and exit. To ensure that the exit can also be used in case of emergency, the shell is spring loaded to be in the open position. To avoid unwanted accidents, the simulator will have a built in mechanism that prevents the simulator from turning on unless the exit is locked in place. This lock can be overridden manually from within the cockpit.

The shell of the cabin will be made out of carbon fibre to make the cabin as lightweight as possible. Ventilation holes should be taken into account when designing the outer shell of the cabin, to keep the environment inside the cabin comfortable. Preferably these should either be in the back or the bottom of the cabin. If later on it is discovered that the airflow is not sufficient using only ventilation holes, it should be possible to add a fan as well at little power cost.

The main load bearing structure of the cabin will consist of two parallel square aluminium beams running along the whole side of the back and the floor of the cabin. Aluminium was the lightest option considering these beams experience isotropic stresses. The pilot will be seated in a g-seat facing away from the robot arm, which will be mounted directly to these beams at the floor and the back of the cabin. The overhead panel is attached to the curved shell while other components will be indirectly attached via a floor panel. Beam forces are transferred to the robot arm via a connection port, located at the back of the cabin at the same height as the centre of mass.

<sup>64</sup>Tristar VE-5979 - Tafelventilator - Zwart

### Cabin main supporting elements

For the elements supporting the main loads on the cabin, 2 beam elements were considered. These elements are hollow and have a square cross-section of 5×5 cm with a thickness of 5 mm. These beams are located at either side of the cabin, along the back and the bottom. The back of the cabin is connected to the robot arm, this interface is left undefined for now to simplify calculations. The two beam element together carry all the loads resulting from the accelerations of the cabin. Because the beams are on either side of the cabin, their load distribution due to acceleration up or down are assumed to be mirror images, hence only one of the two beams is analysed.

The first step in analysing the beam is to look at the force distribution along the beam. The force distribution is simplified to consist of three different forces as presented in Fig. 5.3. First of all, the mass of the beam elements is calculated based on the density of aluminium and implemented as a distributed force along the horizontal and vertical beam segments in the  $y$ -direction. Next, the mass of the cabin without beams is split up into two loads; there is a distributed load in the  $y$ -direction. This load is implemented along both the vertical and horizontal beam segment, but is offset in the  $z$ -direction to act in the centre of the cabin. And there is also an induced moment around the  $z$ -axis due to the offset of the centre of gravity of the cabin without shell to the centre of gravity of the supporting beam elements. This moment is introduced as a distributed moment load along the entire beam structure. While these loads are not a completely accurate representation of the cabin, it's considered to be a conservative approximation.

In order to obtain the force distribution along the beam, the forces in the horizontal segment are calculated first. In Eqs. (5.12–5.14), the shear force in  $y$ , moment about  $z$  and moment about  $x$  are presented respectively for the horizontal beam segment. Considering the forces assumed for the cabin, there are no forces in the  $x$  or  $z$  direction, nor is there a moment about the  $y$ -axis.

$$V_y = \int_x^L -(q_{y-cab} + q_{y-beam}) dx \quad (5.12)$$

$$M_z = \int_x^L \xi_z dx + \int_x^L -(q_{y-cab} + q_{y-beam}) x dx \quad (5.13)$$

$$M_x = \int_x^L -q_{y-cab} \frac{W}{2} dx \quad (5.14)$$

Where  $L$  and  $W$  are dimensions of the cabin as presented in Fig. 5.3.  $q_{y-cab}$  is the distributed load of the cabin mass without the beams, calculated using  $m_{cab}gn/(H + L)$  where  $m_{cab}$  is the mass of the cabin without beams and  $n$  is the load factor applied in  $g$ -forces.  $q_{y-beam}$  is the distributed load due to the mass of the beam ( $m_{beam}$ ) which is calculated using the same equation with only the mass being different,  $\xi_z$  is the distributed moment due to the cabin.

Along the vertical beam segment, reaction forces were added to simulate the connection to the robot arm. These reaction forces were sized such that the sum of the forces and moments equate to zero at the top of the beam. The moments acting on the horizontal beam are transferred to the vertical beam without change, while the shear force is transferred to act as a normal force in  $y$ .

$$N_y = \int_y^H -(q_{y-cab} + q_{y-beam}) dy + V_{y-root} - F_{Ry} \quad (5.15)$$

$$M_z = \int_y^H \xi_z dy + M_{z-root} + M_{Rz} \quad (5.16)$$

$$M_x = \int_y^H -q_{y-cab} \frac{W}{2} dy + M_{x-root} + M_{Rx} \quad (5.17)$$

Where  $V_{y-root}$ ,  $M_{z-root}$  and  $M_{x-root}$  are the shear and moment forces calculated for the horizontal beam segment at the location where the horizontal and vertical beam members meet.  $F_{Ry}$ ,  $M_{Rz}$  and  $M_{Rx}$  are the reaction force in  $y$  and reaction moments around  $z$  and  $x$  due to the connection with the robot arm. For the forces in the beam below the connections, these equations can still be used with the reaction forces set to zero.

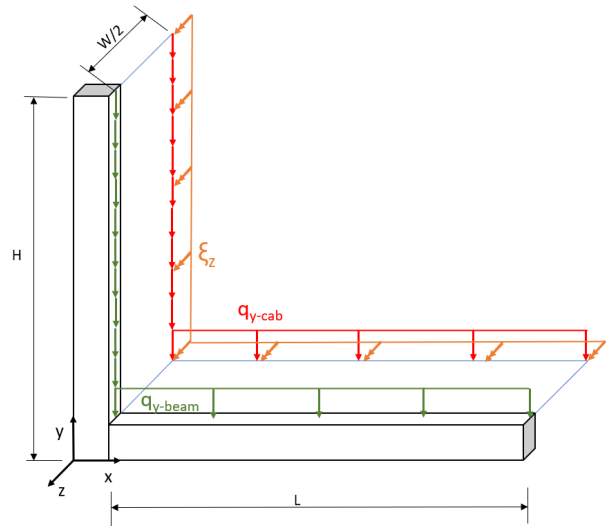


Figure 5.3: Forces on the supporting beam

The stress within the system can now be determined based on the forces and moments applied at any one location. Considering a square thin walled cross-section, the area moment of inertia about the z-axis can be determined through Eq. 5.18 where  $W_{cr}$  is the width of the square and  $t$  the thickness of the wall. The normal and shear stress for the horizontal beam segment are presented in Eq. 5.19 and Eq. 5.20. Here,  $Q$  represents the first moment of area ( $\int ydA$ ),  $M_x$  represents the moment around the x-axis and  $A_0$  represents the enclosed area. This equation uses the thin-walled assumption for the shear stress

$$I_{zz} = \frac{1}{12} (W_{cr}^4 - (W_{cr} - t)^4) \quad (5.18) \quad \sigma_x = \frac{M_z y}{I_{zz}} \quad (5.19)$$

$$\tau_{yz} = \frac{V_y Q}{I_{zz}} + \frac{M_x}{2tA_0} \quad (5.20) \quad \sigma_y = \frac{M_z x}{I_{zz}} + \frac{M_x z}{I_{xx}} + \frac{N_y}{A} \quad (5.21)$$

For the vertical beam segment, there is no shear stress and the normal stress can be calculated with Eq. 5.21, where  $A$  is the cross-sectional area of the material (not enclosed).  $I_{xx}$  is equal to  $I_{zz}$  and is the same as in the calculations for the horizontal beam. Finally, to determine the maximum stress present within the beam, the Von Mises stress is calculated using Eq. 5.22. Do note that most numbers to be filled in are equal to zero given our simplified force model, greatly simplifying the equation.

$$\sigma_{VMS} = \sqrt{\frac{1}{2} ((\sigma_{xx} - \sigma_{yy})^2 + (\sigma_{yy} - \sigma_{zz})^2 + (\sigma_{zz} - \sigma_{xx})^2) + 3(\tau_{xy}^2 + \tau_{yz}^2 + \tau_{xz}^2)} \quad (5.22)$$

Tab. 5.6 presents the variables used in the equations and the resulting loads and Von Mises stress. Fig. 5.5 and Fig. 5.6 display the Von Mises stresses distributed over the sides of the beam structure, with the naming and coordinate system for the figure shown in Fig. 5.4.

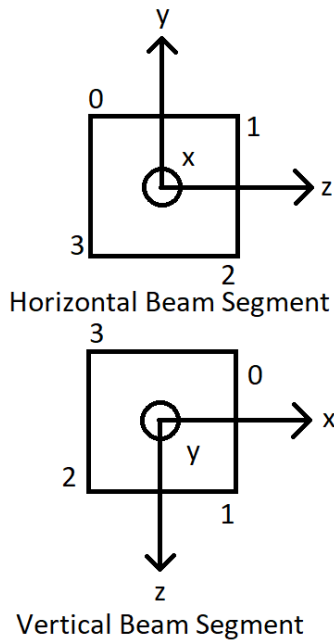


Table 5.6: Cabin structure variables and results

parameter	Value	unit
length beam ( $L$ )	1.74	m
height beam ( $H$ )	1.5	m
width beam ( $W_{cr}$ )	60	mm
thickness beam ( $t$ )	3	mm
Width cabin ( $W$ )	1.6	m
mass beams ( $m_{beam}$ )	13.0	kg
mass cabin ( $m_{cab}$ )	418	kg
load factor ( $n$ )	1.3	g
$I_{zz}$	$9.208 \times 10^{-7}$	$m^4$
$q_{y-cab}$	1221.5	$N m^{-1}$
$q_{y-beam}$	64.9	$N m^{-1}$
$\xi_z$	518	$N m m^{-1}$
Maximum von Mises stress	150	MPa

Figure 5.4: Plate cross-sectional coordinate systems and numbering representing the plate naming for Fig. 5.5 and Fig. 5.6

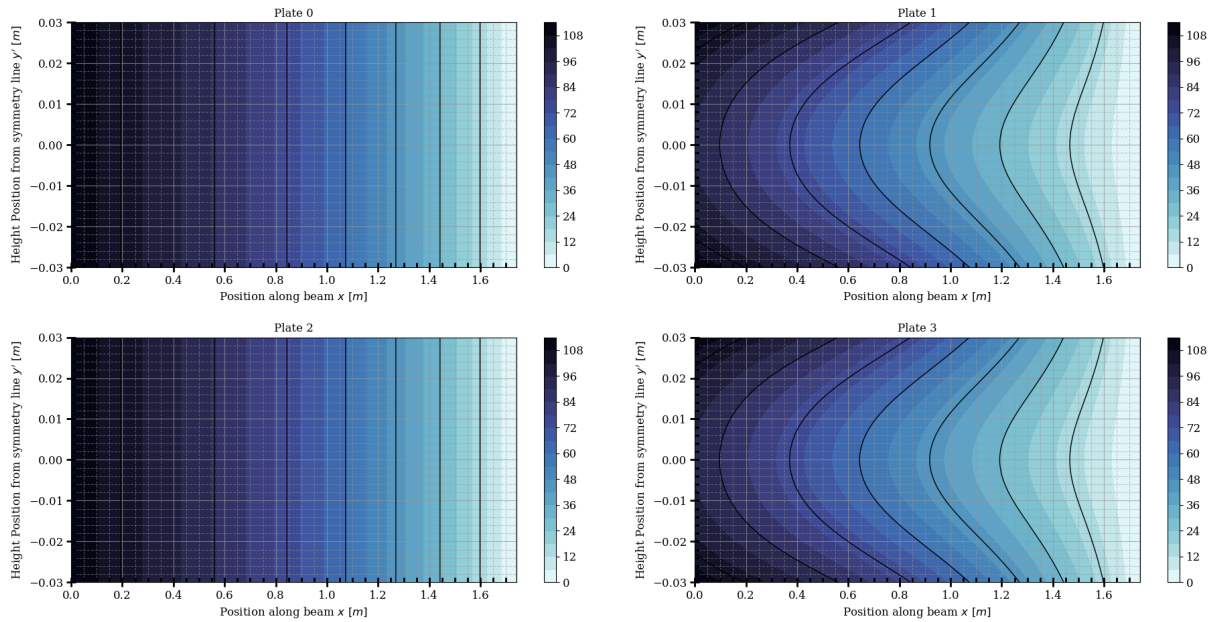


Figure 5.5: Von Mises stress of the four sides of the horizontal beam segment. The color bar is expressed in MPa

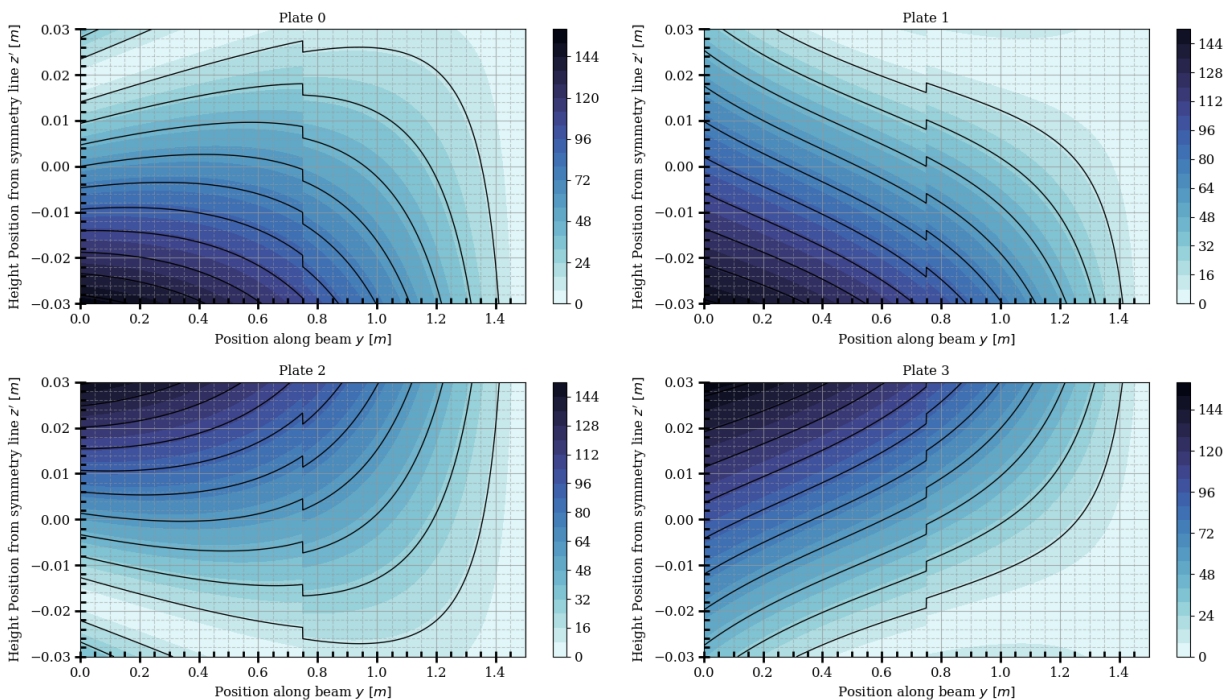


Figure 5.6: Von Mises stress of the four sides of the vertical beam segment. The color bar is expressed in MPa

### Cabin-arm interface

The manufacturer has supplied a front view of the end effector of the robot arm, shown in Fig. 5.7 (including the cabin coordinate frame). As can be seen, the end effector comes with  $30 \times 16\text{mm}$  diameter holes for bolts. Such a bolted connection is excellent in terms of interchangeability of the cabin. However, forces will flow to and from the cabin via these bolts meaning a stress analysis has to be done. For this analysis, the stress in the bolts due to the three forces and three moments is calculated. These bolts are assumed to only carry stress in  $z$ -direction ( $\sigma_z$ ), shear stress in the  $xz$ -plane and shear stress in the  $yz$ -plane. Furthermore, to ease moment calculations it is initially assumed the bolts carry compression, but when all stresses in  $z$ -direction have been superimposed, any negative stresses (compression) are set to zero. In reality, these compressive stresses will be carried by the two plates housing the bolts pressing against each other. Since these plates have a far larger area and will be made of a similar material as the bolts, they should easily be able to carry

these compressive forces.

The forces analysed are those the cabin puts on the end effector (e.g. in the robot arm's rest position, there will be a negative  $x$ -force due to gravity acting on the cabin in negative  $x$ -direction). First, a positive force in  $z$ -direction ( $F_z$ ) would mean the bolts are in tension, so a positive  $\sigma_z$  on all bolts. This  $\sigma_z$  is found by dividing  $F_z$  by the combined cross-sectional area of the bolts. Forces in positive  $x$ - and  $y$ -direction ( $F_x$  and  $F_y$ , respectively) are also found by dividing the respective force by the combined cross-sectional area of the bolts. However, now the shear stresses ( $\tau_{xz}$  and  $\tau_{yz}$  respectively) are found.

Next, the moments around the  $x$ - and  $y$ -axes ( $M_x$  and  $M_y$ , respectively) are analysed. For these calculations, the total moment of inertia needs to be known. Since the radius of the circle on which the bolts are located is much greater than the radius of the individual bolts, only their Steiner terms are considered in this calculation. A positive  $M_x$  will result in tension for bolts with a positive  $y$ -coordinate, meaning the classical equation for bending stress can be used:  $\sigma_z = \frac{M_x y}{I_{xx}}$ . A positive  $M_y$  will result in compression for bolts with a positive  $x$ -coordinate, meaning a minus sign has to be added to the classical equation for bending stress:  $\sigma_z = -\frac{M_y x}{I_{xx}}$ .

Finally, a moment around the  $z$ -axis is analysed. For the polar moment of inertia  $J$ , again only Steiner terms are taken into account. A positive  $M_z$  will cause a shear force perpendicular to the line connecting the bolt to the origin of the cabin coordinate system as shown in Fig. 5.7. This force will be in counterclockwise direction (e.g. the left most bolt in Fig. 5.7 will have a shear force in negative  $x$ -direction). To generalize this for every bolt, the angle  $\theta$  is introduced, see Fig. 5.7. A  $\theta$  of  $0^\circ$  means a shear force in negative  $x$ -direction, so  $\tau_{xz}$  due to  $M_z$  should be multiplied by  $-\cos \theta$ . A  $\theta$  of  $90^\circ$  means a shear force in positive  $y$ -direction, so  $\tau_{yz}$  due to  $M_z$  should be multiplied by  $\sin \theta$ . This results in the following two equations for the shear stresses due to  $M_z$  in the  $xz$ - and  $yz$ -planes respectively:  $\tau_{xz} = -\cos \theta \frac{M_z r}{J}$ ;  $\tau_{yz} = \sin \theta \frac{M_z r}{J}$ , where  $r$  is the radius of the circle containing the bolts.

Superimposing these stresses due to the forces and moments on the end effector, three final stresses are found:  $\sigma_{x,total}$ ,  $\tau_{xz,total}$  and  $\tau_{yz,total}$ . Next, the Von Mises stress can be calculated for each bolt using Eq. 5.22. Using the maximum cabin stresses found in Tab. 5.4, the maximum Von Mises stress is found to be 7.89 MPa, located in the highest bolt (largest  $x$ ). Standard light-weight aluminium bolts have a yield strength of 276 MPa<sup>65</sup> so the bolts are easily able to carry the cabin forces and moments. Bolts can even be left out while still meeting the safety factor of two, but since these bolts comprise only a small part of the cabin weight, 30 bolts are assumed for now.

### Cabin structure mass estimation

In order to determine the possible accelerations and the loads induced, a mass estimation was done. The resulting mass estimate is presented here. Small changes of the mass of the cabin turned out to have relatively little impact on the entire system due to the much larger mass of the robot arm. The resulting mass estimation is presented below.

The curved shell is estimated as a quarter ellipse along the width of the cabin. The area of this shell can be calculated using Eq. 5.23. The sides of the cabin have an area of  $A_{side} = \frac{1}{4} \pi H L$  based on the same quarter ellipse shape. The bottom and back side of the cabin have an area simply calculated by  $A_{bot} = L W$  and  $A_{back} = H W$  respectively. With  $L = 1.74$  m,  $H = 1.5$  m and  $W = 1.6$  m, the total area of the outer cabin skin is 13.36 m<sup>2</sup>.

Assuming a carbon fibre outer skin, the mass density is about 1600 kg m<sup>-3</sup>. Due to a lack of time for proper analysis, an engineering judgment assumption was made for a reasonable thickness of the carbon fibre. This assumption was based on experience with working with carbon fibre in the past and resulted in a 1 mm thickness. A factor 2 was implemented for the mass for the addition of

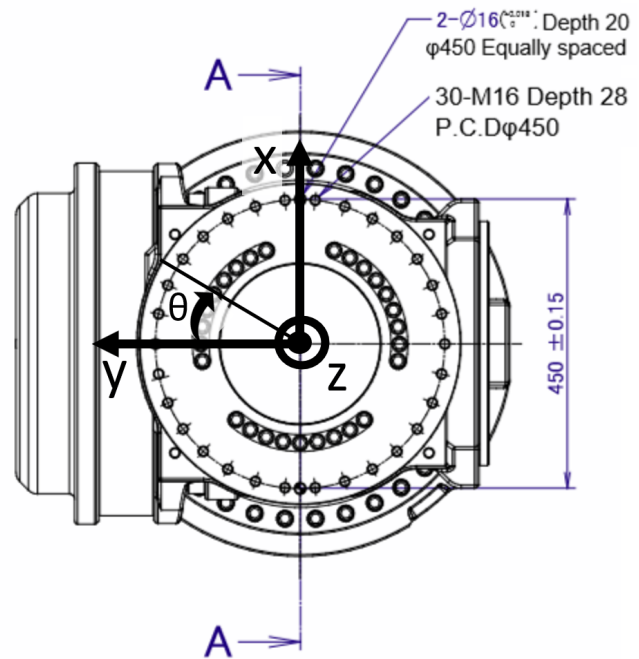


Figure 5.7: Robot arm end effector front view with cabin coordinate frame overlaid

<sup>65</sup>Lightweight Fasteners

stiffeners. this resulted in a mass estimate of 43 kg for the outer skin with stiffeners.

$$A_{shell} = W \cdot \int_0^{\frac{\pi}{2}} \sqrt{H^2 \cos^2 \theta + L^2 \sin^2 \theta} d\theta \quad (5.23)$$

The interface between the cabin is currently very uncertain. Hence, a conservative mass estimation is made that this interface which connects the robot arm with the main supporting structure is as heavy as the main supporting structure, with a mass of 13 kg. The total mass estimation of the structural elements of the cabin is 69.9 kg.

### 5.3.6. Cable handling for cabin

For the system to function properly, it is important to ensure that tangling of cables and interference with the machine is minimised. Moreover, it must be ensured that the power and data can be transferred seamlessly without causing any problematic situations such that the system adheres to requirement UPaRTS-FUN-STR-CAB-03. From the diagrams presented on pages 40-41, 42, 39, and the power budget it can be observed that the power throughput for the cable carrier to the carriage and the cabin is very high as all cables will go through this cable carrier. This subsection will elaborate upon the feasibility of this interface design. In Sec. 5.3.6 the power through the carrier to the cabin will be elaborated upon in terms of cable specifications as well as the data rates through the cables.

**Cabling** The building power supply provides the total power necessary for the functioning of the onboard, offboard, and IOS systems. The power supply and cabling from the power supply to the carriage is done in a similar fashion as with the DLR simulator as can be seen from <sup>66</sup>, as the DLR simulator is similar to the system in consideration and since the DLR simulator is a proven concept. The earth cable and the power and signal cable are connected from the building power supply to the carriage through an energy chain which moves along with the robot arm along the railtrack. The energy chain that is chosen for this design is the Igus E4.1L <sup>67</sup> as this allows for high force loading, easy accessibility as the crossbar is accessible from both sides, and a 30% lower weight and 80% faster installation compared to comparable series. The earth cable connection is needed to avoid electrical shocks within the system. Moreover, As the FANUC M-2000iA/1700L is a 6 DOF robot arm and the cables have to connect the robot arm to the cabin and carriage through cable carriers, it is necessary to use a cable carrier that supports this. The Igus triflex R e-chain<sup>68</sup> is an energy chain that is specifically designed to support 6 DOF robotic arms in their power supply.

Since the robot arm is capable of 6 DOF, for cable management purposes it will be divided into three separate sections: the segments between the sixth and third axes, the third and second axes, and the second and first axes. According to <sup>69</sup>, this is the proper way of cable management to avoid entanglement and consequentially achieve longer lasting cables. For each separate section a minimal cable carrier, a junction box, and strain relief with loops is required. The cable carriers protect the cables from abrasion, the strain relief eliminates stresses on the cables and consists of tie wraps and clamps, and the junction box protects the electrical connectors which join the cables. It is important to note that when adding the strain relief solutions, the cables are positioned in their neutral axis without touching the inner or outer radius of the cable management system as this ensures that the cable is not already in strain in its neutral position. For the first section (sixth to third axis) the sixth axis, which is the moving end, strain relief cables should be present as the stresses will be high here due to movement. The cables will be protected by the Igus triflex R cable carriers here providing 3-axis support: these come equipped with additional strain relief options and also ease the addition and removal of cables as these can be interchanged without needing to dismantle the system. Then at the third axis, a junction box is placed. For the second section (third to second axis) a similar setup is used with the strain relief cables placed on the third axis. This is also done for the last section (second to first axis) but now the strain relief cables are placed on the second axis. Separating the cable carriers into three different, shorter sections prevents the cables from entangling and proper cable carrier design pays off in the long run as it reduces downtime and maintenance costs compared to "easier" solutions such as duct tape or tie wraps. Additionally, the use of shielded cables should be avoided as such cables are more prone to failure due to torsion as this could easily compromise the cable jacket.

<sup>66</sup>DLR Robot Motion Simulator - Flight

<sup>67</sup>Igus E4.1L energy chain

<sup>68</sup>Igus Triflex R e-chain

<sup>69</sup>Tech briefs cable management

<sup>70</sup>Tips for cable management with Igus triflex R

[cited 2020-06-18]

[cited 2020-06-18]

[cited 2020-06-18]

[cited 2020-06-18]

[cited 2020-06-18]

There are also three general rules of thumb to be followed for the use of the Igus triflex R as specified on the manufacturer's website<sup>70</sup>. The first one states that the total hose and cable diameter must not exceed 60% of the carrier's diameter. The Igus triflex R carrier has a fillable inner diameter of 46.8mm. The second rule states that at least 10% clearance needs to be left between any two cables or hoses. Finally, the last rule states that cables and hoses need to move freely inside the carrier.

On page 39, from the hardware diagram showing the connections between the hardware systems, it can be seen that 8 cables are running through the carrier of which 2 are high power cables, 3 USB-C cables, 1 signal cable, 1 ethernet cable for audio, and 1 standard power cable. Taking into account the standard dimensions of USB-C cables and the ethernet cable (8mm) there is approximately 25mm left for the 2 high power cables and the signal cable which is sufficient space to fit the cables. This implies that the USB-C cables and the ethernet cable may fit into one carrier according to the first rule and thus an extra carrier needs to be utilised to carry the two high power cables. This way all three rules can be adhered to for the cables in both carriers.

From [31] the interfaces for wiring are obtained from which it can be observed that for the power cable type A05B-1336-H201 (15m) (AC200-250V) is recommended and for the signal cables type A05B-1336-H501 (15m) is recommended by the supplier. The power cable that goes through the carrier will provide power to the cabin which consists of the audio system (75W), the G-seat (3kW), the yoke and its control loading system (660W), and the VR headset (20W) which together require a total power supply of 3.76kW of the 17kW that flows through the carrier. From the e-chain, a high power cable is connected to a power distribution unit from which 4 standard power cables of aforementioned type flow to the separate systems. Considering that standard power cables can carry up to 4kW (16A, 250V), this proves that using a standard power cable to carry the required 3.78kW for the cabin is sufficient and hence requires no use of a high power cable to carry the power from the carrier to the power distributor in the cabin and thus the A05B-2450-J365 cable will be used for this. The remainder of the power going through the carrier is transferred to the offboard motion system through two high power cables to the offboard motion system.

The connections to the cabin that utilise USB-C, signal or AUX cables provide the required data transfer from and to the cabin. Within the cabin several systems require data to be transferred continuously without hiccups or low transfer rates. For most of the data transfer USB-C cables are utilised except for the audio system which require an ethernet cable. USB-C cables have a maximum data transfer rate of 10Gb<sup>71</sup> per second which implies that the data that flows from and to the systems can be transferred at a sufficiently fast rate as can be seen from 2.5.

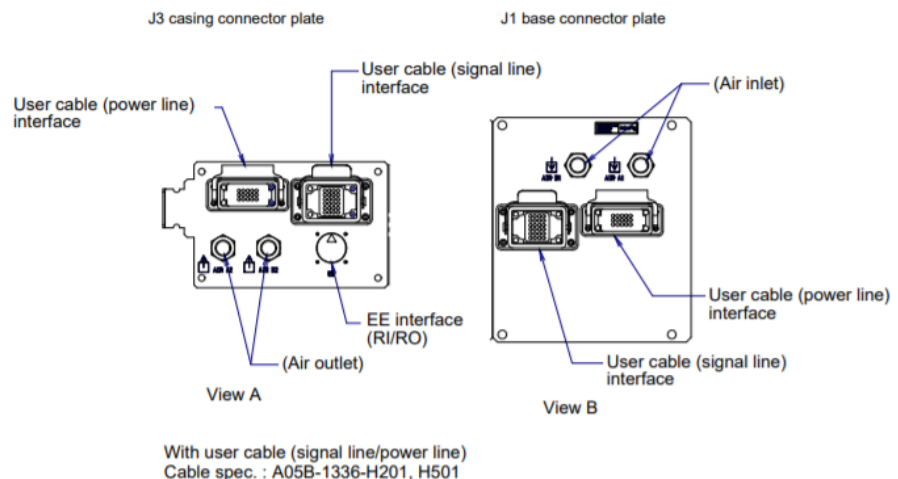


Figure 5.8: Power interface of FANUC M-2000iA/1700L for power and signal cables

### 5.3.7. RAMS Characteristics

The previous two sections described the sizing aspects of the robot arm and the cabin. This section covers the operational aspects of the robot arm and the cabin, by describing qualitatively the reliability of the components used, and the availability, maintainability, manufacturability, and safety of the system.

**Reliability** Reliability relates to how likely components are to fail. The reliability of the simulator structure is off course of the highest priority. The structure is absolutely not allowed to fail since it represents a severe safety hazard.

To avoid failure, a few important steps are taken. First off all, a safety factor of 2 was used when designing the custom structural parts of the simulator. Secondly, any off the shelf components were also chosen with a safety factor in mind, regardless of whether the manufacturer already used a safety factor. Lastly, frequent inspection should be able to detect any sustained damages in time.

<sup>71</sup>USB-C data transfer rate

**Availability and Maintainability** Availability relates to the time required to perform maintenance and inspections, whereas maintainability relates to the effort required to perform maintenance and inspections. Since these two are so interrelated, they are combined into one section.

The operator manual of the FANUC robot arm [31, p. 125] prescribes daily checks of the arm, including a test run. These activities are estimated to take slightly less than an hour. In addition, the rail system should also be tested and inspected, although this will take far less time than the robot arm. Finally, the buttons, controls and the g-seat in the cabin should also be quickly tested daily, which is estimated to take a few minutes. In the end, the daily inspection will take around an hour but can be performed by a single experienced person.

The same operator manual [31, p. 216-218] prescribes monthly checks mainly consisting of checking for damage and re-tightening bolts. The carriage, the rail and the cabin structure should also be inspected for damage once a month and their bolts should be tightened as well. Since the structure is relatively bare-bones, these actions can be performed during the hour long daily checks by another person (although they will be smeared over multiple daily checkups). During further design, structural components should be designed such that if cracks become visible one day after inspection, they have not grown critical before the next inspection.

Yearly checks requiring the replacement of components are also prescribed. These cannot fit within the daily check and therefore one week per year will be scheduled for these. Any unexpected repairs/replacements are expected to not take more than an additional week per year.

**Manufacturability** The manufacturability of the simulator concerns the ease of manufacturing the components. The simulator has two distinctly different types of parts in terms of manufacturability: off the shelf and custom manufactured.

The use of off the shelf components has a few advantages. These components do not require personalised infrastructure to be built. For this simulator, most systems like the robot arm, rail and VR goggles are bought off the shelf. Considering the low quantity of simulators to be produced, it is economically more attractive to buy these components. An additional advantage is that these companies have already established themselves in the market, giving the costumers of the simulator more confidence in the product while reducing risks. A downside would be that the costumer would be dependent on other companies for spare parts during the lifetime of the simulator. Stocking up many reserve components may thus be required to reduce this risk.

The cabin is the main part which needs to be custom made. As discussed before in Subsec. 5.3.5, the main structural component of the cabin is a frame made of aluminium. considering the connections with the rest of the cabin and structural components, a few required production techniques were determined. These include welding, drilling, sheet bending and sheet cutting. The tools and skills required are considered readily available and cheap enough to do in house. For a composite skin, a custom design will need to be sent to a different company which specialises in this production technique. This is not done in house because the costs of the needed tooling are very high and skilled and experienced workforce is required.

To avoid issues due to components made from different materials touching each other and causing corrosion, some preventive steps may need to be taken. This could be a careful choice of which materials may be in contact, or perhaps require a special coating to be applied. Further research into this topic is considered a post DSE activity.

**Safety** Structural safety concerns the measures taken to limit the risk of bodily harm as a direct or indirect result of the system. These measures are as follows:

Structural loads are designed to remain below 50% of the materials ultimate load. This ensures even after a large number of stress cycles and unexpected load concentrations, the structure is still able to carry the loads.

Daily test runs and monthly damage inspections ensure that if a structural component still sustains damage, this damage is discovered before it becomes dangerous.

If a structural component inevitably gets dislodged, there is a physical barrier in the form of a wall with a window between the IOS and the motion system.

The pilot is strapped into his seat with a 5 point seat belt, meaning they will stay in their seat under all g-conditions. They will be able to detach their seatbelt in case of an emergency, but they will be instructed not to do so during regular operations.

The pilot, the secondary pilot and the instructor all have an emergency button in their vicinity. These buttons are connected to an independent computer capable of taking over control of the motion system and safely bringing it to the ground. The code on this computer will be verified even more thoroughly than the main computer.

The cabin door is spring loaded and locked. The simulator cannot start unless the door is locked, but once it is unlocked it automatically opens. Inside the cabin, there is an emergency release but

the pilot is instructed to only use this in case of emergency.

The door between the IOS and the simulator is automatically locked from the outside during operation. This way, no one can accidentally wander in, but the pilot can still get out in case of emergency. If someone were to accidentally be in the room during operation, the floor area where the robot arm is able to reach is marked.

In case the main power cuts out, the main power distribution unit will switch to a battery and supply power only to the emergency computer and external motion system for 100 seconds to safely bring the cabin to the ground.

### 5.3.8. Verification

To ensure the program was written correctly, verification was performed during the entire process of writing the code. The verification of the robot arm code is split up into verification of: The transformation matrices, the inertia transformations, the acceleration and velocity transformations and the resulting force- and moment matrices. Then, the cabin-arm interface- and the cabin structure codes are verified. If something is said to be verified, this means the outputs were within machine epsilon of the hand calculations.

**Transformation matrices** A total of 12 transformation matrices were defined; two between each of the seven frames. Each transformation matrix is verified by multiplying it with a vector  $[x, y, z, 1]^T$ , where  $x$ ,  $y$  and  $z$  are nonzero coordinates in the frame being transformed to another frame. The resulting vector should give the same point but in the coordinates of the new frame. This is done for every transformation matrix with different rotation angles  $\theta$  of each respective joint. All transformation matrices are verified.

**Inertia tensor** A function was created to go from the  $3 \times 3$  inertia tensor to the  $3 \times 3$  Euler tensor. This function is verified by inputting multiple nonzero example matrices, calculating the resulting  $J$  matrix by hand and comparing with the function output. Next, a function was also created to go from the classical  $3 \times 3$   $J$  matrix to the  $4 \times 4$  Denavit-Hartenberg matrix. This function was checked in the same way as the function described above, and it was also verified.

The implementation of the total inertia matrix in a certain frame is verified by giving the components in that frame different nonzero masses. The resulting total inertia matrix is then compared with hand calculations and in the end all inertia matrices and transformations are verified.

**Acceleration matrices** First, the local velocity tensors are verified by inputting a nonzero angular velocity into the joint corresponding to the 'lower' frame (closer to the base). The angular velocity in the local frame should be the same, but around the axis aligned with the  $z$ -axis of the 'lower' frame (it can also be a combination of axes in the local frame). Additionally, a linear velocity should be introduced equal to the angular velocity times the offset of the local frame with respect to the  $z$ -axis of the 'lower' frame. The angle  $\theta$  of the 'lower' frame is also varied, this should change the orientation of the local frame to the 'lower' frame and the resulting velocity tensor should change accordingly. These calculations are performed for all frames (except frame one, which has no 'lower' frame and should have only the linear velocity of the carriage). In the end, all acceleration matrices are verified.

Next, the local derivative velocity tensors are verified similar to the local velocity tensors. This time, the angular acceleration around the  $z$ -axis of the 'lower' frame is varied. Again, the local angular acceleration should be the same and in the same direction as the 'lower'  $z$ -axis. Also a linear acceleration equal to the angular acceleration times the offset with respect to the 'lower' frames  $z$ -axis should be present. This verification is performed for multiple angles  $\theta$  of the 'lower' joint. Again, the local derivative velocity tensors are all verified.

With these two matrices verified, the total acceleration tensors are verified. Initially all angular velocities and accelerations are set to zero. Then one by one they are set to a nonzero, nonone (not equal to one) value. The centripetal acceleration of a certain frame should be equal to the angular velocity squared times the distance between that frame and the  $z$ -axis of the frame corresponding to the joint with the nonzero, nonone angular velocity. The direction of this centripetal acceleration should be from the local origin to the 'lower' frames'  $z$ -axis. Of course, only the frames after a joint with an angular velocity will have centripetal acceleration due to this angular velocity. The same verification is performed for the angular accelerations, but now the acceleration caused by this angular acceleration should be equal to just the angular acceleration times the distance between that frame and the  $z$ -axis of the frame corresponding to the joint with the nonzero nonone angular acceleration. This acceleration should now be perpendicular to the line connecting this  $z$ -axis to the local frame in the direction of the angular acceleration. Furthermore, an angular acceleration should also be present with the same magnitude and in the same direction as the nonzero, nonone angular acceleration. This is tested for different joint angles  $\theta$  between the local frame and the joint with the nonzero, nonone angular velocity/acceleration. Furthermore, a combination of angular velocities

and accelerations is checked, the resulting acceleration tensors should simply be the individual acceleration tensors added up. In the end, all acceleration tensors are verified.

For the above calculations, the gravitational- and carriage accelerations were kept at zero. Making these nonzero should introduce them as linear accelerations in the positive y- and negative z-direction of frame 1 respectively.

When all accelerations and velocities are zero, all acceleration matrices should also be zero and this is in fact the case for all seven of them.

As one final check, the velocity of the carriage can be specified, but should not effect the acceleration matrices. Setting the carriage velocity to great values ( $>1\,000\,000\text{ m s}^{-1}$ ) indeed does not affect the acceleration matrices.

**Action matrix** Again, all weights, velocities and accelerations are set to zero. For linear accelerations (due to gravitational/carriage acceleration or an angular velocity) Newton's second law  $F = ma$  applies. These are set to nonzero, nonone values and one by one, each component is given a nonzero mass. This should result in the  $F = ma$  forces through the 'lower' joints, as well as moments proportional to the offset from the line of action of this force. This is tested for all angular velocities and the two linear accelerations at different angles theta. All action matrices are verified.

Angular accelerations will induce a force equal to the angular mass moment of inertia times the angular acceleration times the centre of mass offset from the z-axis of the frame corresponding to the joint being angularly accelerated. The angular acceleration of every joint is tested by setting the mass of a component above that joint to a nonzero value for different angles  $\theta$ . These are all verified.

When all masses and/or accelerations and velocities are zero, the action matrix should also be zero. This is indeed the case for every action matrix.

**Cabin-arm interface** A quick tool is made to show a desired bolt property as a number on the location of that bolt. Forces and moments are introduced one-by-one and the resulting stresses are checked with hand calculations.

First, the total area and total moment of inertia calculations are checked. This is done by reducing the number of bolts to four and manually calculating their area. This area times four is indeed the total area that is outputted. The total moments of inertia should consist of only two bolts with nonzero Steiner terms, which is verified to be the case.

Only a  $F_x$  results in only a  $\tau_{xz}$  which is the same for each bolt and the expected value from the formula. The same is true for only a  $F_y$ , this time with only a  $\tau_{yz}$  and also for  $F_z$ , only with a  $\sigma_z$ .

Next, the moments are checked; a positive  $M_x$  results in only a  $\sigma_z$  with tension for bolts on the left and compression for bolts on the right, as expected. Furthermore, the stress of the outermost bolts corresponds to that expected from the formula. The same is true for  $M_y$ , this time with lower bolts in tension and the upper bolts in compression.

A positive  $M_z$  results in no  $\sigma_z$ , but nonzero  $\tau_{xz}$  and  $\tau_{yz}$  as expected. The highest values of  $|\tau_{xz}|$  are on the left and right, with the left one being negative, as expected. These values also correspond to what is expected from the formula. The same is true for  $\tau_{yz}$ , with the bottom bolts being negative as expected.

Finally, the Von Mises stress is verified. First off, bolts in pure compression should have zero Von Mises stress, this is verified to be the case. Next a few combinations of forces and moments are compared with hand calculations of the Von Mises stress equations. These are all verified. Also, when only  $F_x$ ,  $F_y$  and/or  $F_z$  are present, all bolts should have the same Von Mises stress, which is indeed the case. As a final sanity check, no Von Mises stress should ever be negative, which is the case. With that, this code is considered to be verified.

**Cabin main supporting elements** The cabin structure is calculated using the equations presented in Sec. 5.3.5 using a Python script. In order to verify this code, a few steps are taken:

First off all, the force and moments along the beam segments are plotted in Fig. 5.9. These plots are analysed to see if they had the right sign with respect to the axis system used in fig. 5.3. Also the shape of the lines are determined to be correct. For example, the moment around z increases exponentially along the length of the horizontal beam. Both the horizontal and vertical beam also have no forces at their respective ends, which is correct since they were modelled as free ends. Lastly, in the corner where the horizontal beam transitions into the vertical one, the forces and moments are the same on both beams, which is correct.

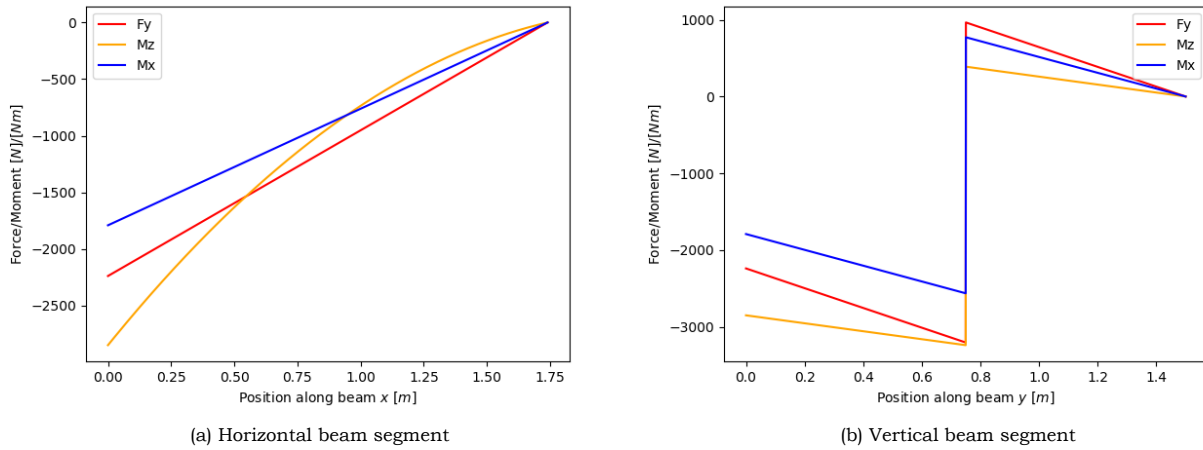


Figure 5.9: Force and moment distribution on the support beam

After the force distribution is determined to be correct, the internal stresses are calculated. The results are visualised in figures similar to Fig. 5.5 and Fig. 5.6, where instead of the von Mises stress, the normal- or shear stress are plotted. Doing so for individual load cases allows for checking if the sign of each stress is correct.

In addition to interpreting the figures, also some hand calculations are performed. These calculations are performed at three distinct locations: halfway along either beam segment and in the corner between the beam segments. These calculations confirm that the forces and stresses displayed by the figures are correct.

### Requirement compliance

Table 5.7: Structural requirements compliance

Identifier	Compliance	Rationale
UPaRTS-REQ-STR-FLR-02	Verifiable	Maximum tensile load survivability verifiable by analysis. Maximum compressive load is indeed below maximum floor loading.
UPaRTS-REQ-STR-FLR-03	Verifiable	Verifiable by analysis when the exact floor material is chosen.
UPaRTS-REQ-STR-FLR-04	Verifiable	Verifiable by demonstration when the IOS is fully sized by fitting the IOS in its designated space with the secondary pilot station.
UPaRTS-REQ-STR-FLR-05	Verifiable	Verifiable by demonstration when the secondary pilot station is fully sized by fitting the secondary pilot station in its designated space with the IOS.
UPaRTS-REQ-STR-EMO-01	Verified	Verified by inspection of design decision: Current robot arm is able to carry a payload more than twice the cabin weight.
UPaRTS-REQ-STR-EMO-02	Verified	Verified by analysis in Sec. 5.3.6; standard power cables are sufficient.
UPaRTS-REQ-STR-EMO-03	Verified	Verified by analysis in Sec. 5.3.6; two high power cables through e-chain and cable carriers.
UPaRTS-REQ-STR-EMO-04	Verified	Verified by analysis Sec. 5.3.6; USB-C connections on both ends through cable carriers and e-chain.
UPaRTS-REQ-STR-EMO-05	Verified	Verified by analysis in Sec. 5.3.6; USB-C connections on both ends through cable carriers and e-chain.
UPaRTS-REQ-STR-EMO-06	Verifiable	Verifiable by analysis using max. momentum and brake forces. The <T.B.D.> is found by safety analysis.
UPaRTS-REQ-STR-CAB-01	Verifiable	Verifiable by demonstration using a CAD model or a prototype.
UPaRTS-REQ-STR-CAB-02	Verifiable	Verifiable by demonstration in the form of prototype stress test.
UPaRTS-REQ-STR-CAB-03	Verifiable	Verifiable by demonstration within a CAD model.
UPaRTS-REQ-STR-CAB-04	Verifiable	Verifiable by inspection; confirm reach for shortest arm length allowed for pilots.
UPaRTS-REQ-STR-CAB-05	Verifiable	Verifiable by demonstration once prototype is built. The <T.B.D.> is found by safety analysis.

Identifier	Compliance	Rationale
UPaRTS-REQ-STR-CAB-06	Verifiable	Verifiable using demonstration with real pilot in prototype.
UPaRTS-REQ-STR-CAB-07	Verified	Verified since it is implemented in the design; functionality verifiable by demonstration.
UPaRTS-REQ-STR-CAB-08	Verifiable	Verifiable by demonstration; current connection allows for it.
UPaRTS-REQ-STR-CAB-09	Verifiable	Verifiable by analysis using a CAD model or demonstration during assembly of the prototype.
UPaRTS-REQ-STR-CAB-10	Verifiable	Verifiable by analysis of current disposal prices. The <T.B.D.> can be filled in based on a more detailed market analysis.
UPaRTS-REQ-STR-OFF-01	Verifiable	Verifiable by demonstration in the prototype. The <T.B.D.> is found by safety analysis.
UPaRTS-REQ-STR-OFF-02	Verifiable	Verifiable by inspection; confirm reach for shortest arm length allowed for pilots once button is placed.
UPaRTS-REQ-STR-OFF-03	Verifiable	Verifiable by demonstration in prototype. The <T.B.D.> is found by safety analysis.
UPaRTS-REQ-STR-OFF-04	Verifiable	Verifiable by demonstration in prototype. The <T.B.D.> is found by safety analysis.
UPaRTS-REQ-STR-OFF-05	Verifiable	Verifiable by demonstration in prototype. The <T.B.D.> is found by safety analysis.
UPaRTS-REQ-STR-OFF-06	Verified	Verified since it is implemented in the design; both are in the same room and data rates are attainable.
UPaRTS-REQ-STR-OFF-07	Verified	Verified since it is implemented in the design; wires can be transported on the floor.
UPaRTS-REQ-STR-OFF-08	Verified	Verified since it is implemented in the design.
UPaRTS-REQ-STR-OFF-09	Verified	Verified since it is implemented in the design; normal building power connection is sufficient.
UPaRTS-REQ-STR-OFF-10	Verified	Verified since it is implemented in the design; normal building power connection is sufficient.
UPaRTS-REQ-STR-OFF-11	Verifiable	Verifiable by analysis looking into how to get this power to a building.
UPaRTS-REQ-STR-MNT-01	Verified	Verified by manufacturer for robot arm and carriage[31]. Verified by analysis of current structural cabin layout, see Sec. 5.3.5.
UPaRTS-REQ-STR-MNT-02	Verified	Verified by analysis; computer is placed in the open in the IOS.
UPaRTS-REQ-STR-MNT-03	Verified	Verified by analysis; computer has constant connection to IOS computer and monitor can be directly connected.
UPaRTS-REQ-STR-MNT-04	Verifiable	Verifiable by analysis of materials and the updated <T.B.D.>. The <T.B.D.> is found by analysing required cleaning solutions.
UPaRTS-REQ-STR-MNT-05	Verified	Verified by manufacturer[31], only robot arm and carriage use fluids.
UPaRTS-REQ-STR-MNT-06	Verifiable	Verified by analysis using CAD model. Chance of failure found using analysis of stress cycles and crack growth. The <T.B.D.> is found by analysing when replaceability is cheaper than failure risk.

### 5.3.9. Validation

Due to a lack of data and time, the current models cannot be validated for now. Hence, in this section some advice for future validation tests will be given.

The model for the cabin structure can be validated using existing validated FEM software. As a first test, the magnitude of the maximum Von Mises stress should be compared. Contrary to the simplified model, the FEM code will model stress concentrations, therefore the maximum Von Mises is expected to be higher at points like the intersection between the beam along the back and the beam along the floor. These higher stresses will not invalidate the model, however, as during detailed design reinforcements will be added here, getting rid again of these stress concentrations. Therefore, the maximum Von Mises stress at locations along the beam without stress concentrations should also be compared. Since conservative estimates were used for the distributed loads, higher Von Mises stresses at these locations for the FEM model will mean the simplified model is not valid. If the Von Mises stresses of the FEM model of these points are found to be less than half those of

the simplified model, the assumptions are considered far too conservative and the model will also not be considered valid.

The model for the forces on the robot arm can be validated using a validated model for a different robot arm. Such a comparison will require the model developed in this project to be altered to fit the other validation robot model. Such changes include creating new transformation matrices to fit the size and joint configuration of the other robot. As long as these transformation matrices are defined in exactly the same way as they currently are, this comparison should suffice to validate the code. The forces along the beam are expected to be similar in both the project model and the validated code, with some differences due to a less accurate representation for the robot arm shape and mass distribution. This difference should be conservative, hence the forces calculated with the project code should be higher than the validation code for any critical scenario. If this is not the case, the model is not valid.

Another extreme would be if the model used is too conservative. If this is the case, This might affect other parts of the model to a large extent. For example, if due to the lack of a counterweight, the moments on the floor are much higher than they should be, extreme measures might unnecessarily be taken to mitigate this. The model is considered to be too conservative if the largest carriage wheel force is overestimated by more than 50 %. A more accurate model should be developed in order to be considered valid.

### 5.3.10. Sensitivity analysis

Many inputs in this section were estimated based on engineering judgement. The effects of changing these estimations will be discussed next: Changing the mass distribution of the robot arm will not affect the forces on the cabin, only the floor loading. When weight is distributed equally over the joints, the floor loading becomes  $13 \text{ kN m}^{-1}$ . Though slightly above the maximum floor loading, this mass distribution is very conservative; the real mass distribution will likely have more mass towards the base, so it is unlikely the floor loading is exceeded due to a different mass distribution.

For the structure of the cabin, a maximum acceleration of 1.3 g was used based on the kinematics of the robot arm. If an acceleration of 1.75 g is used, such that the g-seat is not needed to reach the requirement, the mass of the main structural components increases by 4.3 kg, by increasing the beam width to 70 mm to keep the same safety factor.

Increasing the acceleration would also increase the forces and moments on the bolts between the robot arm and the cabin. However, these would increase linearly and the yield stress of the bolts is currently almost 35 times the bolt stress, so even if the accelerations double, the bolts will still hold easily.

The carriage loads were assumed to be equally distributed over the entire rail over a width twice that of the carriage. The floor loading scales inversely with both, so if the load was either distributed over half the rail, or only one carriage width, the floor loading would double. Therefore the floor loading is sensitive and a detailed analysis should be done as soon as possible.

If the cabin mass doubles, the cabin structure needs to be reconsidered. Using beams with a width of 80 mm and a thickness of 4 mm will suffice and only increase the mass by 20 kg (77%). The bolts will still hold easily. The floor loading increases to  $8.5 \text{ kN m}^{-1}$  (13%), so these elements are not that sensitive. However, the robot arm is only able to carry 571 kg at 1.75 g with a safety factor of 2. These numbers are already quite high and the mass is not expected to reach this.

The cables to the carriage are already capable of transporting additional power and the cable carrier itself also still has room for additional cables. If the on-board power increases to above 4 kW, the current cabin power cable needs to be upgraded. However, as it is the only cable in the second carrier to the cabin, this can easily be facilitated. If data cables also need to be added, a third cable carrier might be needed to the cabin, but this should not be a problem.

## 5.4. Aeromechanics

The first purpose of this section is to determine the motion cueing requirements from aeromechanic considerations, which will play a central role in later stages of the design. In order to derive these requirements, preliminary figures have been derived through simulation of different upsets extracted from the training curriculum (Subsec. 4.2.1). These numbers provide a framework that will allow the aircraft's motion to be mapped to the flight simulator's motion, guaranteeing safety and training performance. Secondly, the feasibility of developing or obtaining the numerical aircraft model is discussed in Subsec. 5.4.3 and the compliance matrix for the aeromechanics requirements from [1] is presented for completeness.

### 5.4.1. Upsets framework definition

As a starting point the training systems (Ch. 4) were consulted to orient the upset analysis towards cases that are relevant for the training curriculum. Subsec. 4.2.1 lays out a number of upsets which should be part of the training curriculum. Based on these upsets and the available literature on upset data, it was decided to analyse the following cases:

**System failure cases:** Based on the damage cases due to the following damage cases in the NASA Generic Transport Model (GTM): rudder off, vertical tail off, left outboard flap off, left wingtip off, left elevator off, left stabilizer off [32].

**Approach to stall:** Based on a study on UPRT training in flight simulators [33].

**High altitude stall:** Based on crash data of the Airbus A330-203 accident (2009-06-01) [34].

**Recovery from stall:** Based on a study on stall recovery experiments [35].

**System failure cases** The NASA Armstrong Research Center Generic Transport Model (GTM) is used to analyse upsets related to system failure cases. This model was developed using numerical simulations, wind tunnel data, and flight data of a 5.5% scale model of the B757-like aircraft [32, 36]. As the B757 is comparable to the Boeing 737 NG, this model is deemed qualitatively representative in this case. The predefined damage cases of the model are all starting with a 45° bank angle turn at an altitude of 800 ft. Since these damage cases will lead to severe upsets, the simulations will contribute in determining the required limits of the simulator. The data that will be extracted from the simulations for determining these limits is listed below:

- Maximum normal acceleration
- Maximum jerk
- Maximum pitch, roll and yaw rate
- Maximum pitch, roll and yaw acceleration
- Pitch, roll and yaw frequency response

**NASA GTM limitations** Despite the results that can be obtained from the GTM, the model does have a number of limitations. Since the wind tunnel data was acquired at low Reynolds numbers and since the flight data is acquired from a scaled-down aircraft, upsets at high speeds and altitude, such as those a Boeing 737 or Airbus A320 would experience, cannot be simulated. The GTM model does not converge for high speeds (owing to the lack of data in those regimes), hence the simulated responses serve more as guidance and need to be validated to guarantee their use in defining motion cueing requirements is warranted.

**Approach to stall** In order to refine the accuracy and range of the motion cueing requirements, data on the approach to stall is also analysed [33]. The relevance and importance of an approach to stall scenario to train for upset prevention is described in Subsec. 4.2.2.

**High altitude stall** In order to perform the preliminary design of the motion system, one training scenario has been singled out. As explained in Subsec. 4.2.2, the high altitude stall scenario [35] is a relevant and promising training scenario at this stage of the design. It has the advantage that there is more confidence in the validity of the data compared to the simulated responses of the NASA GTM model [32]. This is because accurate flight crash data of the Airbus A330-203 on 2009-06-01 is openly available [34]. The Airbus A330-203 is not the only commercial airliner that crashed due to high altitude stall; Icelandair and West Caribbean Airways also crashed in this way [35]. These aircraft got into a high altitude stall because the autopilot was set up to hold the altitude and the cruise thrust until an angle of attack of 25° is reached. The aircraft, already being at the altitude ceiling, while trying to maintain altitude with cruise thrust caused the aircraft to decelerate until it reached a fully developed stall attitude. Exceeding the 25° angle of attack limit in Airbus aircraft turns off the autopilot which causes a general pitch down tendency and the pitch control becomes very sensitive since the aircraft is exposed to less aerodynamic damping at high altitudes [35]. The data that will be used from the crash data to help size the motion system is listed below:

- Maximum and minimum normal acceleration
- Maximum lateral acceleration
- Onset buffet frequency and amplitude
- For future design it is deemed that the ground speed, calibrated airspeed, flight path angle, pitch angle, angle of attack, heading angle, roll angle, altitude, stick position, pedal position and engine throttle can be useful. These were also extracted from the FDR data.

**Recovery from stall** For completeness and to give an initial impression of the performance expected during the recovery of a stall, data on stall recovery is analysed. As upset recovery is a large part of UPRT, one has to make sure the motion cueing system can simulate the entire recovery phase. In terms of cueing requirements, it is interesting to know the time it takes for recovery and the experienced g-loading during recovery, in part to judge the requisite sustained cueing requirements [35]. The data for stall recovery is obtained from [35], which is a NASA study on a stall recovery guidance system. In their experiment, 40 experienced pilots recovered from an high altitude stall in a vertical motion simulator. For this simulator, an aircraft model similar to the Boeing 757 is used in combination with an extensive aerodynamic database [35]. It is assumed that this model is representative enough to give insight into recovery from stalls of large passenger aircraft.

### 5.4.2. Upset analysis

This subsection presents the results of the four main cases presented in Subsec. 5.4.1.

**System failure cases results** In order to analyse the relevant simulation data of the damage cases, first a number of variables are exported as .csv files from the NASA GTM model (in Matlab) such that these can be further analysed in Python. The exported variables are: timestamp, total acceleration, accelerations along body reference axes  $x$ ,  $y$  and  $z$ , and angular rates for roll, pitch and yaw. The maximum g-loading and angular rates could be plotted as a function of time rather straightforwardly from the .csv files. For the time derivatives of the motion (i.e., jerk and angular accelerations) the Numpy function `gradient` is used to compute the time derivative. For the frequency analysis first the discrete Fourier transform of the pitch, roll and yaw rates was plotted using the SciPy functions `fftpack.fft` and `fftpack.fftfreq`. As the data for the angular rates was not centred around zero, the Fourier transform focused too much on the offset with respect to zero rather than on the periodic components. To resolve this, a first degree polynomial regression of the data was generated with the Numpy function `poly1d` and subtracted from the data such that the angular rates were centred around zero. Now, in order to validate the Fourier transform, a sine function was fitted using the data using  $L^2$  norm minimisation (sum of squares of the error). The amplitude and phase of this sine function were changed such that the error at time zero was minimised. The frequency of the sine function was then compared to the dominant frequency of the Fourier transform. Note that in contrast to reality, the damage to the aircraft in the GTM simulation occurs instantaneously. This results in unrepresentative data for the first moments of the upset and therefore the data belonging to these moments has been omitted; this was achieved by instantiating the data from the earliest of the second zero-intercepts of the angular rates. The results of the simulation of the upsets caused by the six different damage cases can be seen in Tab. 5.8.

Table 5.8: Results of GTM damage case simulations [32]

	Rudder	Vertical tail	Left outboard flap	Left wingtip	Left elevator	Left stabiliser
Max normal acc.	1.4 g	3.8 g	2.0 g	2.3 g	1.4 g	1.4 g
Max jerk	$2.4 \text{ m s}^{-3}$	$131.8 \text{ m s}^{-3}$	$21.3 \text{ m s}^{-3}$	$8.6 \text{ m s}^{-3}$	$6.4 \text{ m s}^{-3}$	$27.2 \text{ m s}^{-3}$
Max pitch rate	$7.9^\circ \text{ s}^{-1}$	$69.7^\circ \text{ s}^{-1}$	$28.3^\circ \text{ s}^{-1}$	$30.3^\circ \text{ s}^{-1}$	$7.9^\circ \text{ s}^{-1}$	$10.3^\circ \text{ s}^{-1}$
Max. pitch acc.	$1.3^\circ \text{ s}^{-2}$	$585.6^\circ \text{ s}^{-2}$	$14.5^\circ \text{ s}^{-2}$	$17.1^\circ \text{ s}^{-2}$	$8.7^\circ \text{ s}^{-2}$	$20.7^\circ \text{ s}^{-2}$
Pitch frequency	1.6 Hz	0.5 Hz	0.2 Hz	0.3 Hz	1.6 Hz	0.9 Hz
Max roll rate	$5.4^\circ \text{ s}^{-1}$	$499.1^\circ \text{ s}^{-1}$	$116.9^\circ \text{ s}^{-1}$	$128.6^\circ \text{ s}^{-1}$	$15.4^\circ \text{ s}^{-1}$	$24.6^\circ \text{ s}^{-1}$
Max. roll acc.	$7.3^\circ \text{ s}^{-2}$	$1837.9^\circ \text{ s}^{-2}$	$15.6^\circ \text{ s}^{-2}$	$710.6^\circ \text{ s}^{-2}$	$2.1^\circ \text{ s}^{-2}$	$5.0^\circ \text{ s}^{-2}$
Roll frequency	1.0 Hz	0.3 Hz	0.4 Hz	0.4 Hz	1.1 Hz	0.4 Hz
Max yaw rate	$8.2^\circ \text{ s}^{-1}$	$257.7^\circ \text{ s}^{-1}$	$22.4^\circ \text{ s}^{-1}$	$26.0^\circ \text{ s}^{-1}$	$7.9^\circ \text{ s}^{-1}$	$10.0^\circ \text{ s}^{-1}$
Max. yaw acc.	$2.6^\circ \text{ s}^{-2}$	$627.8^\circ \text{ s}^{-2}$	$22.0^\circ \text{ s}^{-2}$	$34.3^\circ \text{ s}^{-2}$	$5.8^\circ \text{ s}^{-2}$	$2.5^\circ \text{ s}^{-2}$
Yaw frequency	1.6 Hz	0.2 Hz	0.3 Hz	0.4 Hz	1.2 Hz	0.2 Hz

The values shown in red in Tab. 5.8 are considered as not valid and are therefore not used. Starting with the first damage case, rudder off, it can be seen that the pitch frequency is considered as not valid. This is due to the pitch rate being too aperiodic. The second damage case simulates a vertical tail off upset. Although it is proven that it is possible to safely land a B-52 aircraft without vertical tail<sup>72</sup>, this damage case is very rarely seen and still considered as fatal and therefore there is no

need for this damaged case to be trained and the data will not be used. Additionally, the simulation results of damage case 2 are unrepresentative because this upset event significantly exceeds the present motion cueing requirements. The third damage case, which simulates a left outboard flap off, contains some useful values. Although, the roll rate simulated is more than three times larger than the maximum roll rate that can be induced by the pilot with an Airbus A320 in clean configuration and direct law and therefore the simulated roll rate is assumed as not valid [28]. Furthermore, the roll rate is also too aperiodic to determine the frequency response. The pitch and yaw rate are also assumed as not valid. Since there is no documentation of pitch rate limits of an Airbus A320, the maximum achievable pitch rate is for now determined by crash reports which results in a pitch rate of approximately  $10^\circ \text{s}^{-1}$  [37]. This maximum pitch rate is about half the maximum roll rate of an Airbus A320. Looking at the difference in moment of inertia for the two axes of rotation ( $I_{yy}$  2–5 times greater than  $I_{xx}$ ), this ratio is reasonable [38, 39]. If the same reasoning is applied for the yaw rate, an even lower maximum achievable yaw rate is the result ( $I_{zz}$  is greater than  $I_{yy}$ ). However, the maximum achievable yaw rate will also be set on  $10^\circ \text{s}^{-1}$  for now. The other values for this damage case are still considered as valid, because the rates and accelerations are simulated independently at the centre of gravity of the aircraft. Damage case 4 simulates a left wingtip off. The roll, pitch and yaw rate, the roll acceleration and the roll frequency of this case are assumed not valid for the same reason as damage case 3. The data from the left elevator off case, damage case 5, is within the limits of an Airbus A320 and is therefore assumed as valid. For the last damage case, the left stabiliser off, only the yaw frequency is assumed as not valid because of its aperiodicity. The resulting constraints that are derived from this data are highlighted in Tab. 5.8.

**Stall approach analysis** Approach to stall is characterised by stall buffeting. These vibrations are due to flow separation which occurs as the aircraft enters into a stall. It is important to properly cue these vibrations as they serve as an indication for the pilot that the aircraft will stall [33]. According to the FAA Advisory Circular, the initial stall buffet is as subtle as  $\pm 0.05G$  for commercial transport aircraft [33]. Hence if one hopes to accurately cue stall buffets, high frequency vibrations of  $0.1G$  should be cued to the pilot. This requirement might be lowered even more since depending on the type of aircraft buffet vibrations of  $\pm 0.05G$  can occur when already stalling, as opposed to the approach to stall. Because of that and the fact that humans can perceive vibrations of lower amplitude, the ICATEE recommends that stall buffets are cued with an accuracy of  $\pm 0.025G$  [33].

**High altitude stall crash data** As mentioned in the previous section, data from the flight data recorder (FDR) of an Airbus A330-203 involved in the Air France 447 was used to provide a means of validating the general magnitudes and time-dependencies for use in the remainder of this report. To extract this data, a custom script was devised capable of converting scalable vector graphic (SVG) polylines into raw plotted data. The advantage of this approach is that data could be extracted at the original sampling frequency at quite a high precision, since all spatial information of the labels and lines could be extracted from the SVG definitions. The details of this process, which involved non-orthogonal transformations and linear scaling procedures, are omitted here in the interest of brevity. This process, however, was validated by plotting the altitude data side to side with the original altitude data from BEA, which appeared to closely match.

To provide a measure of precision, one should consider that each float value used in the screen coordinate definition<sup>73</sup>, as well as the values given in the transformation matrices, were recorded with a precision in the order of  $10^{-3}$  or better. In general, the spatial separation between 15-second time increments is 17 user units, while the horizontal axis featured a y-label separation of 9.3 user units. Combining this with numerical precision previously stated, a precision of around 1% of the physical value per user unit is attained. As an example, for the altitude data, this would give a maximum precision of 60 feet.

In addition to the theoretical numerical precision of this data, the logging (or plotting) frequency can also be ascertained. For the normal accelerations, a logging frequency of 8 Hz was found, while the lateral and longitudinal accelerations were logged at 4 Hz. All other values were logged at sub-1 Hz frequencies, making them ill-suited for a Fourier analysis. To provide more backing for the validity of the Fourier analysis presented in the previous section, it must be noted that the dominant frequency of 3 Hz is below the Nyquist frequency of the normal acceleration time series (4 Hz), thus attesting the validity of the analysis that lead up to this. One must not be misled by the higher frequency range plotted in Fig. 5.12, since this is an artefact of over-discretisation (i.e., discretisation of interpolated values as well as logged values) of an analogue (printed) time series that was sampled from a digital time series with a lower logging frequency.

<sup>72</sup>youtube.com: B-52 Emergency Landing - Flying Without A Tail Fin - 1964 Air Force Education Film [cited 2020-06-09]

<sup>73</sup>W3C: Scalable Vector Graphics (SVG) 2 – Coordinate Systems, Transformations and Units

[cited 2020-06-10]

From the crash data, one can see that the maximum normal acceleration is 1.6 g and the minimum normal acceleration is 0.7 g. As for the lateral accelerations, these have been recorded at  $\pm 0.2$  g. As mentioned before in Subsec. 5.4.1, since the high altitude stall is the main upset case considered, it is believed that for future detailed design it is worth having detailed data about the entire attitude of the aircraft during such an upset.

An additional source of the flight data from the FDR of the Air France 447 (AF447) crash was studied to infer the qualities of onset buffet. This particular data set was studied to extract vibrational cueing requirements as experienced throughout a fully developed high altitude stall caused by instrument failure. The data in question have been extracted from the official investigation of the French Bureau d'Enquêtes et d'Analyses (BEA), in particular from the flight data records provided in Annexe 3<sup>74</sup>.

In addition to this source, data from an investigation report on the same crash, in the possession of Shem Malmquist, co-author of the "Angle of Attack" book on the same crash, was consulted<sup>75</sup>. From this source, the vertical and lateral accelerations experienced by the pilot have been extracted. The pilot seat accelerations have been extracted by means of an automatic digitisation software<sup>76</sup>, yielding the following response (Fig. 5.10):

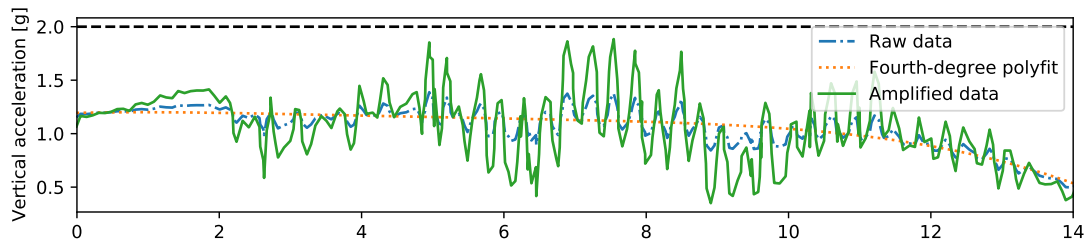


Figure 5.10: Air France 447 vertical buffet data

As can be seen, the data required some additional amplification to match the original pilot seat vibrational data, which was too noisy to be extracted. As a result, data from Air Data Inertial Reference Unit (ADIRU) 3 was extracted instead; this sensor is located 2 metres aft of the pilot seat (Fig. 5.11):

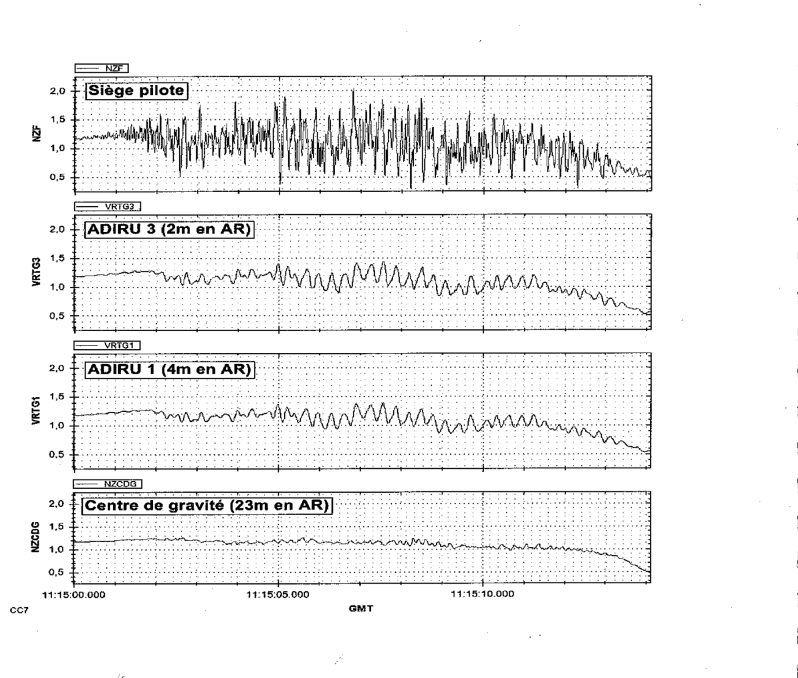


Figure 5.11: Air France 447 ADIRU vertical acceleration measurements<sup>75</sup>

To achieve a higher degree of congruence between the ADIRU 3 measurements and the pilot seat accelerations, the data was centred by subtracting a fourth-degree polynomial, scaling the difference

<sup>74</sup>Bureau d'Enquêtes et d'Analyses: Accident to the Airbus A330-203 registered F-GZCP and operated by Air France occurred on 06/01/2009 in the Atlantic ocean [cited 2020-06-09]  
<sup>75</sup>Shem Malmquist: High Altitude Stalls – how well do you understand them? [cited 2020-06-09]  
<sup>76</sup>Ankit Rohatgi: WebPlotDigitizer [cited 2020-06-10]

by a factor of two, and finally adding back the polynomial fit. To provide an idea of the goodness of fit, the mean value of the difference between the raw data and this fourth-degree polynomial is  $O(10^{-16})$ , i.e. negligible. Then, the maximum difference from the mean (i.e., the amplitude), was found to be 0.51 g. Finally, a Fourier transform of the amplified signal provides insight into the frequency composition of the vibrations (Fig. 5.12):

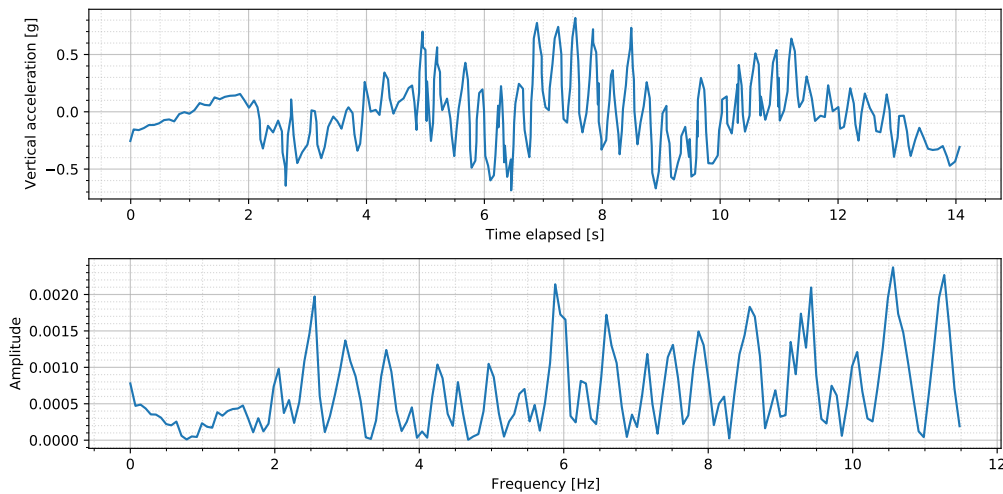


Figure 5.12: Air France 447 vertical buffet Fourier analysis

From this figure, the dominant low-frequency mode is found to be 3 Hz; higher frequency buffet occurs roughly at integer multiples of this value. Resulting from this analysis are a required  $\pm 0.5$  g amplitude vibration at a frequency of 3 Hz.

**Recovery from stall analysis** This subsection presents the g-loading and recovery time expected for recovery from a high altitude stall of a large commercial aircraft. Fig. 5.13 shows the change in load factor over time for all the runs of the NASA stall guidance recovery experiment [35] (Chapter 7, Figure 15). The most interesting lines are the grey ones, as these depict the pilot's unguided response, such as would be experienced in a training scenario. The red dotted line shows the load factor limits and the blue and purple lines represent the response of two different guidance systems. Note that the original NASA figure [35] has been modified to indicate the maximum and minimum g-loading and the duration of the stall recovery. The pilot experienced a maximum g-force of 1.9 g and a minimum of 0.2 g. It is hard to tell from Fig. 5.13 how sustained the g-loading cues would have to be. The initial nose down manoeuvre can probably be cued as an onset g-force since it spikes down over a short period of time. The latter phase (10 to 30 seconds) is a more gradual increase towards the maximum g-loading. This contrast indicates that the onset and sustained g-forces might have to be cued by separate motion systems, in this case the robotic arm would generate the high onset cues, whereas the g-seat would cue the sustained loading. Furthermore, it is assumed that the stall recovery is completely over after 170 s since the load factor remains fairly close to 1 from that point on. The implications of such a long recovery need to be taken into account when cueing. Accelerating along the linear rail is not feasible because of its short length, the latter part of the recovery will have to rely more on the robotic arm itself.

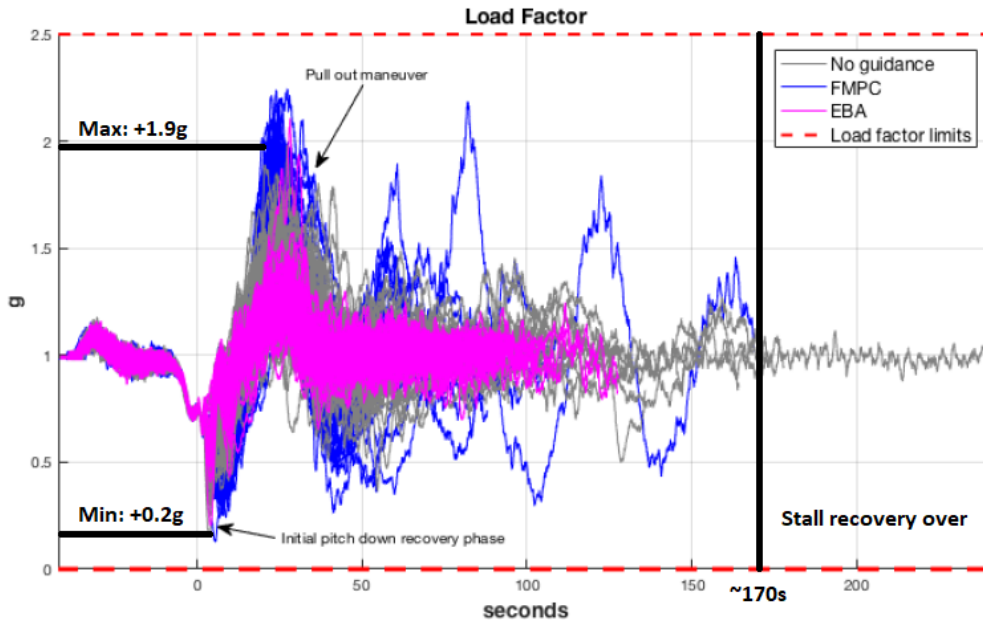


Figure 5.13: G-loading for all runs of the Nasa stall guidance recovery experiment [35]

### 5.4.3. Numerical model analysis

The upset events that pilots often find themselves in are dynamically highly non-linear. Consequentially, an accurate model of the extended envelope is required for a successful simulation of the event. To consider the feasibility problems that come with extended envelope flight simulation models, it is important to study existing approaches to extended envelope modelling. Doing so will serve to show that it is possible to generate accurate flight dynamics within the constraints imposed on this project, while still maintaining a required level of fidelity and similitude of the actual aircraft.

First, the aforementioned GTM, and a polynomial reduction of this model are discussed. Then, considerations for phenomena such as pitch break and stall buffet, as well as roll over are expanded upon. On top of that, ways of determining how aerodynamic derivatives are affected by high stall behaviour are presented. Finally, a concise discussion on the process of adapting existing general extended envelope aerodynamic models to type-specific models is presented.

**The Generic Transport Model** As mentioned previously, the GTM is an extended envelope flight dynamics model of a 5.5%-scale model of a Boeing 757-like transport aircraft [35]. This flight dynamics model is composed of both a nonlinear part and a linearised polynomial model [35]. To consider why this particular model was chosen, consider the following quote from [40]:

Generally, existing full-scale transport non-linear simulations are proprietary simulations that have been developed by the manufacturer of the aircraft being simulated and therefore are only available for use by means of licensed-rights and non-disclosure agreements.

From this, it is quite obvious that research models are the only models that may be openly analysed as part of this preliminary effort. Later stages of the design may see the team committing to a commercial (manufacturer licensed) flight dynamics model.

Prior to considering the polynomial version of the GTM model, it is of importance to consider the general nonlinear version. According to [41], the nonlinear GTM model has the form of:

$$C_i = \Gamma(\alpha_i, \beta_i, \xi_i, \eta_i, \zeta_i, \hat{p}_i, \hat{q}_i, \hat{r}_i) + \epsilon_i, \quad (5.24)$$

where  $\Gamma(\cdot)$  is some unknown nonlinear mapping that takes the angle of attack  $\alpha_i$ , side-slip angle  $\beta_i$ , surface deflections  $\xi_i, \eta_i, \zeta_i$ , and normalised body rates  $(\hat{p}_i, \hat{q}_i, \hat{r}_i)$ , and  $C_i$  is a vector of aerodynamic coefficients  $(C_{X,i}, C_{Y,i}, C_{Z,i}, C_{L,i}, C_{m,i}, C_{n,i})$ ;  $\epsilon_i$  is the (unknown) modelling error. The subscript  $i \in [1, k]$  corresponds to each experimental measurement of the aerodynamic coefficients given a combination of the arguments of  $\Gamma(\cdot)$ ; the interstitial parameters are given through some form of interpolation.

In [41, p. 65], a compelling argument is made that a polynomial fit is not capable of reasonably capturing the nonlinearities encountered in the above model. Notwithstanding this fact, the GTM model is capable of producing a linear-in-the-variables polynomial approximation [40]. To provide a representation of what such a polynomial model may look like, consider the following simplified

dynamics utilised by [35] to provide a model for the stall warning and upset recovery guidance systems developed in their work:

$$C_D(\alpha) = C_{D_0} + C_{D_\alpha} \alpha + C_{D_{\alpha^2}} \alpha^2 + C_{D_{\delta_{sp}}} \delta_{sp} + C_{D_{\delta_{fl}}} \delta_{fl} + C_{D_{\delta_{lg}}} \delta_{lg} + C_{D_{\alpha\delta_{fl}}} \alpha \delta_{fl}; \quad (5.25)$$

$$C_L(\alpha) = C_{L_0} + C_{L_\alpha} \alpha + C_{L_{\delta_{sp}}} \delta_{sp} + C_{L_{\delta_{fl}}} \delta_{fl} + C_{L_{\delta_{lg}}} \delta_{lg}, \quad (5.26)$$

where  $\delta_{sp}$ ,  $\delta_{fl}$ ,  $\delta_{lg}$  refer to the spoiler deflection, flap deflection, and landing gear setting, respectively. The pitch moment is then defined as:

$$C_m = C_0 + C_{m_{\delta_e}} \delta_e + C_{m_{\delta_e^2}} \delta_e^2 + C_{m_T} \frac{T}{\bar{q} d_{eng}^2} \quad (5.27)$$

$$C_0(\alpha, q, i_h, \delta_{sp}, \delta_{fl}, \delta_{lg}) = C_{m_0} + C_{m_\alpha} \alpha + C_{m_{\alpha^2}} \alpha^2 + C_{m_q} \frac{q \bar{c}}{V} + C_{m_{i_h}} i_h + C_{m_{\delta_{sp}}} \delta_{sp} + C_{m_{\delta_{fl}}} \delta_{fl} + C_{m_{\delta_{lg}}} \delta_{lg}, \quad (5.28)$$

where  $i_h$  is the stabiliser position,  $\bar{c}$  is the mean aerodynamic chord,  $d_{eng}$  is the engine diameter, and  $\bar{q}$  is the dynamic pressure. Using these equations, a representative model of the vehicle can be attained, as was done in [35].

**Improvements for extended envelope models** The GTM model in its polynomial form comes with a number of shortcomings. According to [41], the aerodynamic coefficients are not amenable to polynomial fitting in the case of a flight envelope that includes the post-stall regime. Therefore, he proposes a piecewise model identification scheme, whereby the pre- and post-stall regimes are modelled separately as polynomials. Beyond these analytical means, model fidelity can be ascertained by purchasing proprietary flight data and comparing with other research models. In addition, pilot testing will be a core element of ensuring model quality; indeed, the EASA FSTD standards recommend this as exemplified by the “as demonstrated by a suitable pilot”-clauses in the UPRT annexes [29].

The above improvements have been shown to work in the literature [41], and can therefore also be applied in a commercial setting, as warranted by airworthiness authority standards.

**Aerodynamic derivatives** In order to have a high model fidelity for stall behaviour, one has to know how the aerodynamic derivatives change. This is important as the feel of the instrument changes for the pilot when the aircraft is stalling. There are multiple ways of acquiring data on such aerodynamic derivatives. Flight test data can be used, but that might be very expensive and hard to gather. Another possibility is to predict the new aerodynamic derivatives through CFD [42]. As mentioned before the only really reliable means would be licensed commercial stall models from the manufacturers, do note though that smaller and cheaper stall extensions also exist<sup>77</sup>.

#### 5.4.4. Motion system requirements

The goal of the previous subsection was to come up with preliminary sizing requirements for the motion cueing system. These requirements and their respective rationale are presented below.

- UPaRTS-CUE-VES-2** The system shall be able to mimic in-aircraft vibrations with a maximum frequency of 3 Hz and a maximum amplitude of 0.5 g. [Subsec. 5.4.2 - High altitude stall analysis]
- UPaRTS-CUE-VES-3** The system shall be able to mimic an in-aircraft maximum g-force of 1.75g. [UPaRTS-SH-SO-22]
- UPaRTS-CUE-VES-4** The system shall be able to mimic an in-aircraft minimum g-force of 0.2 g. [Subsec. 5.4.2 - Recovery from stall analysis]
- UPaRTS-CUE-VES-5** The system shall be able to mimic a minimum in-aircraft  $\Delta$  g-force of 0.025 g. [Subsec. 5.4.2 - Stall approach analysis]
- UPaRTS-CUE-VES-6** The system shall be able to mimic a maximum in-aircraft roll rate of at least  $25^\circ \text{s}^{-1}$ . [Subsec. 5.4.2 - System failure cases results]
- UPaRTS-CUE-VES-7** The system shall be able to mimic a maximum in-aircraft pitch rate of at least  $10^\circ \text{s}^{-1}$ . [Subsec. 5.4.2 - System failure cases results]
- UPaRTS-CUE-VES-8** The system shall be able to mimic a maximum in-aircraft yaw rate of at least  $10^\circ \text{s}^{-1}$ . [Subsec. 5.4.2 - System failure cases results]
- UPaRTS-CUE-VES-9** The system shall be able to mimic a maximum in-aircraft roll acceleration of at least  $16^\circ \text{s}^{-2}$ . [Subsec. 5.4.2 - System failure cases results]
- UPaRTS-CUE-VES-10** The system shall be able to mimic a maximum in-aircraft pitch acceleration of at least  $21^\circ \text{s}^{-2}$ . [Subsec. 5.4.2 - System failure cases results]

<sup>77</sup>Stallbox

**UPaRTS-CUE-VES-11** The system shall be able to mimic a in-aircraft yaw acceleration of at least  $35^\circ \text{s}^{-2}$ . [Subsec. 5.4.2 - System failure cases results]

**UPaRTS-CUE-VES-12** The system shall be able to mimic in-aircraft jerk of at least  $28 \text{ m s}^{-3}$ . [Subsec. 5.4.2 - System failure cases results]

### 5.4.5. Verification

In this section, both analysis verification and requirement compliance verification will be carried out.

**Analysis verification** Prior to verifying compliance with the requirements, it is of importance to verify the analysis presented above. To this end, a number of checks are presented, chiefly related to the Fourier analysis, the damped sine fitting routines, and the zero-intersection algorithm.

For the Fourier analysis, Python's SciPy's `fftpack` was utilised. To show that these functions generate predictable results, a period test function of the following form was devised:

$$f(t) = 2 \sin(20 \cdot 2\pi t) + \sin(50 \cdot 2\pi t) + 0.5 \sin(80 \cdot 2\pi t)$$

It is expected that this function will yield a Fourier transform with descending peaks at 20, 50, and 80 Hz. Indeed, this is the case (Fig. 5.14):

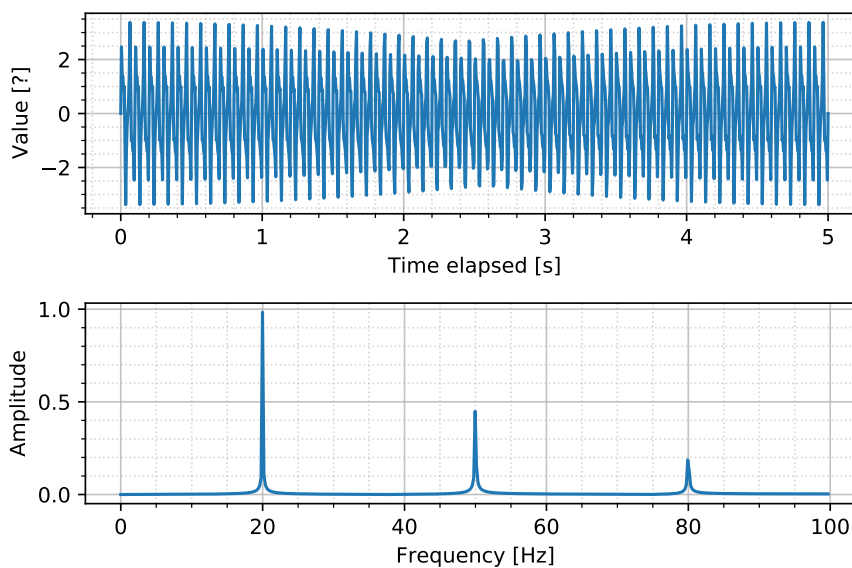


Figure 5.14: Fast Fourier transform verification using a period test function

Moving on to the damped sine fitting routines, a damped sine wave test function was designed:

$$g(t) = \exp(-\lambda t)A \sin(2\pi f t + \phi), \quad (5.29)$$

where the damping coefficient  $\lambda$  was chosen as 0.5, the amplitude  $A$  was set at 1, the frequency  $f = 2 \text{ Hz}$ , and the phase shift  $\phi = \pi/4 \text{ rad}$ . Then, all variations of both the damped and undamped sign fitting routines were tested (Fig. 5.15):

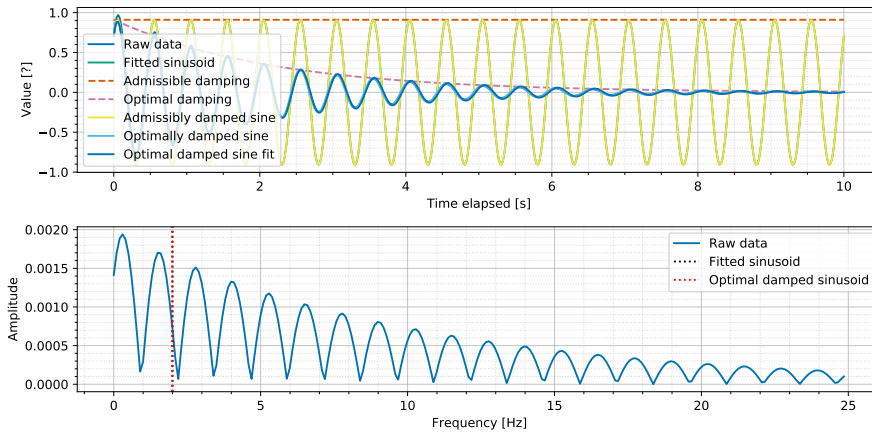


Figure 5.15: Damped sine fitting routine verification using a damped periodic test function

In addition to this figure, several numerical results are produced, which give a quantitative assessment as to the validity of the results in Fig. 5.15. The verbose output of this function yields a fitted amplitude of 0.91, a frequency of 1.99 Hz, a damping factor of 0.45, and a phase shift of 0.89 rad. All these variables are within 15% of the actual value, which can further be refined at the exchange of performance.

Finally, the zero-finding routines must be considered. These routines were used to skip certain ill-behaved parts of signals, i.e. ones that contained artefacts of artificial initial value clamping in the NASA GTM code. These routines find the  $i$ 'th occurrence of a zero intersect given an array of values. To test this functionality, a test function of the form  $h(t) = \sin(2\pi t)$ , where  $t \in [0, 5]$  and was discretised as 500 points. Then polling each intersect, the following result is found (Fig. 5.16):

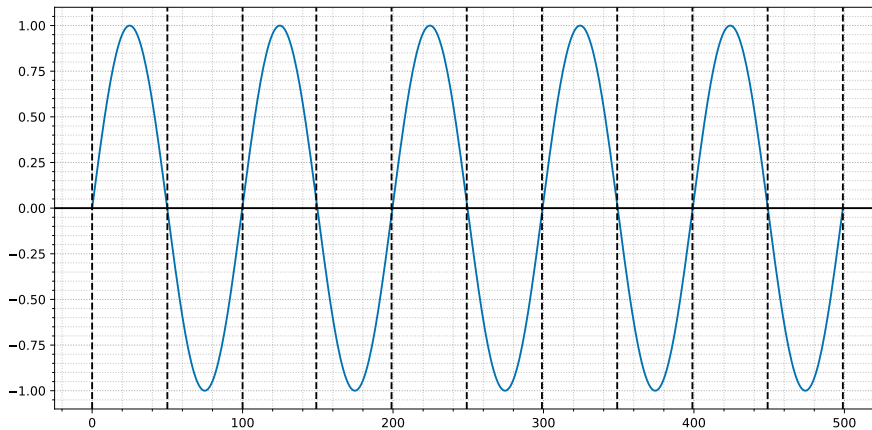


Figure 5.16: Zero-intersect finding function verification using a periodic test function

Note that each value was found within one index of the true index (this is a function of the numerical tolerance), thus verifying that this algorithm works as expected.

**Requirement compliance verification**

The compliance of the aeromechanics requirements derived in [1] is presented in Tab. 5.9. Note that due to the lack of a developed or purchased numerical vehicle model these requirements are not yet verifiable but will be when the numerical model is defined.

Table 5.9: Aeromechanics requirements compliance

Identifier	Requirement	Compliance	Rationale
UPaRTS-SYS-AM-MOD-1	The numerical aircraft model shall include roll angles greater than 120 deg	Verifiable	This can be ascertained by studying the base models for the extended envelope.
UPaRTS-SYS-AM-MOD-2	The numerical aircraft model shall include pitch angles greater than 45 deg	Verifiable	This can be ascertained by studying the base models for the extended envelope. In addition the stall model will dictate the maximum angle of attack.

Identifier	Requirement	Compliance	Rationale
UPaRTS-SYS-AM-MOD-3	The numerical aircraft model shall be applicable in an extended training regime as evaluated by a suitable pilot	Verifiable	This can be ascertained by studying the base model.
UPaRTS-SYS-AM-MOD-4	The numerical aircraft model shall respond to instructor/operator event queues	Verifiable	The numerical model will, by design, allow for external inputs, including IOS event queuing.
UPaRTS-SYS-AM-MOD-5	The numerical aircraft model shall allow for remote instructor/operator control input	Verifiable	The numerical model will, by design, allow for external inputs, including IOS event queuing.
UPaRTS-SYS-AM-MOD-6	The numerical aircraft model shall allow for non-repeatability in queued events	Verifiable	This will be accounted for in the numerical model through stochastic parameters.
UPaRTS-SYS-AM-MOD-7	The numerical aircraft model shall allow for non-intrusive event queuing	Verifiable	This will have to be verified through pilot testing with the event cueing system.
UPaRTS-SYS-AM-MOD-8	The numerical aircraft model shall allow for aircraft (sub)system failures to be queued	Verifiable	The numerical model will have a number of failure modes that it can simulate.
UPaRTS-SYS-AM-MOD-9	The numerical aircraft model shall allow for flight deck warnings to be triggered	Verifiable	The numerical model will allow for all flight deck instruments to be controlled.
UPaRTS-SYS-AM-MOD-10	The numerical aircraft model shall allow for false motion cues to be staged	Verifiable	This will be possible by feeding in motion errors to the simulation model.
UPaRTS-SYS-AM-MOD-11	The numerical aircraft model shall be capable of simulating flight in abnormal configurations	Verifiable	The numerical model will allow for a range of aircraft configurations to be simulated.
UPaRTS-SYS-AM-MOD-12	The extended training regime shall include the entire aircraft operating regime required to successfully recover from an upset	Verifiable	The numerical model will support an extended envelope, up to the states required in recovering the aircraft from an upset.
UPaRTS-SYS-AM-MOD-13	The numerical aircraft model shall respond to pilot control input	Verifiable	The numerical model will process pilot input.
UPaRTS-SYS-AM-MOD-14	The numerical aircraft model shall provide the full aircraft state	Verifiable	The numerical model will produce the full aircraft state, which can also be accessed by the IOS.
UPaRTS-SYS-AM-MOD-15	The numerical aircraft model shall provide the full flight deck state	Verifiable	The numerical model will produce the full flight deck state, which can also be accessed by the IOS.
UPaRTS-SYS-AM-MOD-16	The numerical aircraft model shall provide the autopilot state	Verifiable	The numerical model will produce the full autopilot state, which can also be accessed by the IOS.
UPaRTS-SYS-AM-MOD-17	The numerical aircraft model shall provide for pilot input monitoring	Verifiable	The pilot input state will be passed on to the IOS by design.
UPaRTS-SYS-AM-MOD-18	The numerical aircraft model shall not contain any unphysical jumps when transitioning from the nominal regime to the extended regime as evaluated by a suitable pilot	Verifiable	This will be verified through testing as well as analysis of the equations of motion.
UPaRTS-SYS-AM-MOD-19	The numerical aircraft model shall simulate characteristic buffet	Verifiable	This will be part of the numerical model's design.
UPaRTS-SYS-AM-MOD-21	The numerical aircraft model shall allow for force feedback cues to be staged	Verifiable	The numerical model will interface with the motion control system to stage feedback cues, including force feedback.
UPaRTS-SYS-AM-MOD-22	The numerical aircraft model shall provide the flight envelope of the current configuration	Verifiable	The numerical model will inform the IOS station of the current aircraft state, as well as the quality of the underlying models.
UPaRTS-SYS-AM-IFC-1	The numerical aircraft model shall provide the flight control input state	Verifiable	The pilot input state will be passed on to the IOS by design.
UPaRTS-SYS-AM-IFC-2	The numerical aircraft model shall provide the cueing system state	Verifiable	The numerical model will be capable of requesting the cueing system state from the motion cueing system.
UPaRTS-SYS-AM-IFC-3	The numerical aircraft model shall provide input to the cueing system	Verifiable	The numerical model will be capable of submitting motion cueing requests to the motion cueing system.
UPaRTS-SYS-AM-IFC-4	The numerical aircraft model shall provide input to the motion system	Verifiable	The numerical model will be capable of submitting motion cueing requests to the motion cueing system.
UPaRTS-SYS-AM-IFC-5	The numerical aircraft model shall provide input to the haptic feedback system	Verifiable	The numerical model will be capable of submitting haptic cueing requests to the haptic feedback system.

Identifier	Requirement	Compliance	Rationale
UPaRTS-SYS-AM-IFC-6	The numerical aircraft model shall provide input to visual system	Verifiable	The numerical model will be capable of submitting visual cueing requests to the visual system.
UPaRTS-SYS-AM-IFC-7	The numerical aircraft model shall provide input to the audio system	Verifiable	The numerical model will be capable of submitting aural cueing requests to the aural system.
UPaRTS-SYS-AM-IFC-8	The numerical aircraft model shall provide data to the instructor and operator station	Verifiable	The numerical model will interface with the IOS.
UPaRTS-SYS-AM-UPS-1	The numerical aircraft model shall simulate upset-related events	Verifiable	The numerical model is designed to allow for upset events to be simulated.
UPaRTS-SYS-AM-UPS-2	The numerical aircraft model shall simulate upset-related events with non-repeatability during a single pilot training program	Verifiable	The numerical model will include stochastic elements that prevent repetitive training in case this is not desired.
UPaRTS-SYS-AM-UPS-3	The numerical aircraft model shall simulate envelope protection cues as applicable to the aircraft	Verifiable	The numerical aircraft model will include a simulation of the autopilot.
UPaRTS-SYS-AM-UPS-4	The upset regime of the numerical aircraft model shall simulate approach-to-stall (deterrent) buffeting	Verifiable	The numerical aircraft model will include a stall buffet model.
UPaRTS-SYS-AM-UPS-5	The upset regime of the numerical aircraft model shall simulate pitch break	Verifiable	The numerical aircraft model will include a pitch break model.
UPaRTS-SYS-AM-UPS-6	The upset regime of the numerical aircraft model shall simulate degradation of static/dynamic longitudinal and lateral stability	Verifiable	The numerical aircraft model will include a dynamic model in all support flight regimes.
UPaRTS-SYS-AM-UPS-7	The upset regime of the numerical aircraft model shall only simulate upset-related events when their fidelity is guaranteed by a suitable pilot	Verifiable	In production, the numerical model can be limited to only allow for cues that are verified by a suitable pilot.
UPaRTS-SYS-AM-FBK-1	The numerical aircraft model shall provide measures of performance for flight maneuvers as performed by the pilot	Verifiable	The numerical model will keep track of pilot performance using predefined measures that are logged.
UPaRTS-SYS-AM-FBK-2	The numerical aircraft model shall provide measures of the envelope fidelity for the present operating conditions	Verifiable	The numerical model will report its current state to the IOS, including the fidelity of the current model envelope.
UPaRTS-SYS-AM-FBK-3	The numerical aircraft model shall provide the aircraft operational limits for the present operating conditions	Verifiable	The numerical model will provide the current aircraft state to the IOS, which will report whether or not the aircraft is within the manufacturer's design limits.

### 5.4.6. Validation

In order for the aeromechanics aspect of the analysis to be properly validated, two aspects must be focused on in particular: representative handling of the simulator in upset regimes, and quantitative validation of the numerical model in the normal flight envelope.

In upset regimes, regulations recommend that the upset regime be approved of by a suitable pilot [29]. The general approach would be to develop an in-house upset flight model based on past academic research, that reflects the qualitative handling capabilities of the Airbus A320. This model can then be tested by pilots that have extensive experience, or experience with upsets in this aircraft. From these test campaigns, of which there will be multiple, the model can be refined based on feedback, which is collected using tested methods as the Cooper-Harper rating scale [43]. This will provide a concise and directed overview of the aspects of the numerical model that need to be reconsidered.

For the normal flight envelope, since it not the first priority to reach Level D certification, a wide array of representative models become available for testing. These models include Airbus-licensed flight simulation software, as well as research flight dynamics codes, which can be drawn upon to compare aircraft handling properties in nominal flight. Since commercial licensed flight dynamics models can be prohibitively expensive, and are likely lacking in the number of parameters than can be varied, it is expected that the numerical will be developed in-house. If the budget allows for it, additional flight test data can be purchase from the airframe manufacturer to further enhance the

<sup>78</sup> Airbus SE: Airport and Maintenance Planning

[cited 2020-06-19]

capabilities and validity of the in-house model.

## 5.5. Robotic Motion Kinematics

In this section, the specifics surrounding robotic motion kinematics are discussed. This includes an analysis of the motion capabilities of the robot arm and the g-seat, as well as a detailed development of a potential motion planning algorithm that fits the needs of UPRT vestibular cueing. To this end, the theoretical preliminaries are presented, leading to the development of a set of feasible motion trajectories, and finally an optimisation problem that will yield a desired motion path.

Throughout this discussion, several notes regarding implementations caveats and gotchas are interspersed, strengthening the feasibility of the ideas presented.

### 5.5.1. Functional analysis

The main functions that the Robot Motion Kinematics should adhere to are listed below. These functions are based on the inputs/outputs in the control software (2.2.2, 2.4.2, 2.4.3, 2.4.4, 2.4.5) and describe the vestibular motion of the motion cueing (2.3.3). The vestibular cueing points are presented in a software fashion (2.3.3.1) and in a hardware fashion (2.3.3.2). Lower level functions can be found in page 34.

### 5.5.2. Requirement analysis

The requirements presented in this section are based of the requirements presented in [1] Besides, although not written in this particular requirement analysis section, the additional requirements that are created in Sec. 5.4.4 are also being tackled in this section and will be discussed in depth later.

<b>UPaRTS-SH-SO-16</b>	The simulator shall be able to provide the pilot with visual, audible, vestibular and haptic cues.
<b>UPaRTS-SH-SO-21</b>	The simulator shall provide onset g-forces at 70% of the real aircraft.
<b>UPaRTS-SYS-05</b>	The system shall capture aircraft properties within an extended training envelope.
<b>UPaRTS-SYS-17</b>	The training shall be representative of the simulated manoeuvres as determined by a suitable pilot
<b>UPaRTS-CUE-VES-1</b>	The system shall provide accurate vestibular cues as judged by a suitable pilot.
<b>UPaRTS-CUE-VES-1.1</b>	The vestibular system shall provide repeatable motion cues in six degrees of freedom.
<b>UPaRTS-CUE-VES-1.2</b>	The vestibular system shall provide cues on the attitude of the aircraft model.
<b>UPaRTS-CUE-VES-1.3</b>	The vestibular system shall provide vibration cues.
<b>UPaRTS-CUE-VES-1.4</b>	The vestibular system shall be able to reach at least 70% of the g-force a real aircraft reaches during upset prevention and recovery training in each of the six degrees of freedom.

### 5.5.3. Robot arm capabilities analysis

Prior to considering the details surrounding robot arm kinematics and the motion planning algorithm, it is of importance to determine what the maximum performance levels of the robot arm (including the linear unit) are. This concerns both the maximum linear and angular accelerations, but also the worst-case (i.e., maximum) reaction forces and torques.

As described in Sec. 5.3, a means of computing the kinematic and inertial characteristics of the robot arm structures has been derived. What is left to be deduced, then, are the maximum angular rates and angular accelerations of the joints, as per the manufacturer's specifications. While the maximum joint velocities are given in [31], the maximum angular acceleration is a function of the inertia of the structure, as determined by the payload. In addition, the provided manufacturer specifications do not give an angular acceleration per se, but do provide a measure for the deceleration time required in controlled braking. These braking times are only given for joint 1, 2, and 3, requiring that the remaining accelerations are deduced by some other means. In this report, it was chosen to consider the minimum acceleration found in joints 1–3 for use in determining the cueing performance, and the maximum acceleration for use in determining the structural requirements.

In addition to the foregoing, it should be noted that the braking times are given for maximum load operations; in the present analysis, this would not be the actual load case. Therefore, the obtained acceleration is scaled by the ratio of the 1700 kg inertia (of each joint) and the (preliminary) 500 kg inertia of the cabin. This analysis yields the following results (Tab. 5.10):

Joint #	Max. ang. vel.	Max. ang. acc.	Inertially scaled max. ang. acc. [scale]
1	0.349 rad s <sup>-1</sup>	0.228 rad s <sup>-2</sup>	0.335 rad s <sup>-2</sup> [1.468]
2	0.244 rad s <sup>-1</sup>	0.167 rad s <sup>-2</sup>	0.270 rad s <sup>-2</sup> [1.615]
3	0.244 rad s <sup>-1</sup>	0.167 rad s <sup>-2</sup>	0.312 rad s <sup>-2</sup> [1.872]
4	0.314 rad s <sup>-1</sup>	0.166–0.228 rad s <sup>-2</sup>	0.359–0.491 rad s <sup>-2</sup> [2.156]
5	0.314 rad s <sup>-1</sup>	0.166–0.228 rad s <sup>-2</sup>	0.503–0.669 rad s <sup>-2</sup> [3.022]
6	0.698 rad s <sup>-1</sup>	0.166–0.228 rad s <sup>-2</sup>	0.593–0.812 rad s <sup>-2</sup> [3.562]

Table 5.10: FANUC M-2000iA/1700L motion constraints

With these numbers known, it suffices to compute the critical state; this turns out to be quite cumbersome. As a matter of fact, the only sensible way is to compute all sign combinations (-1, 0, +1) for the accelerations and velocities of each joint, as well the linear rail state. This is done by virtue of a Cartesian product with 8 repeats, yielding 6561 combinations. These combinations are made for a given joint deflection state. Then, for each combination, it must be checked if this yields a maximum parameter norm (maximum torque, force, linear acceleration, or angular acceleration), the state of which is then stored.

In addition to the ‘optimal’ states, a given kinematic state must be supplied to the algorithm. Checking for a particular state by varying all state parameters was found to be far too computationally intensive, therefore justifying the present procedure of iterating through all feasible joint 2 and 3 states (10 discretisation steps); all other joints were left at 0. This yielded deflections  $\theta_2 = 0.814$  rad and  $\theta_3 = 0.611$  rad.

With this procedure and state, a cueing performance of at most 1.28 g was found. In addition to this, the worst-case torque and forces have been found, which were relayed back to the structures team for a design iteration (see Sec. 5.3). This iteration yielded a new cabin mass of 431 kg, which gave new inertia ratios for each joint. A revised analysis resulted in a maximum cueing acceleration of 1.29 g, thus attesting to the relative insensitivity of the code, as expected given the inertial properties of the robot arm under consideration.

#### 5.5.4. Sustained motion cueing seat analysis

The sustained motion cueing seat (also known as g-seat) will fulfil an essential role within the vestibular cueing of the simulator. The g-seat uses padding that extends. This padding will influence how the person sits in the seat. By changing the attitude of the human skeleton, the flesh area changes and the muscle tonality changes, through which certain accelerational forces can be mimicked. As one might have noticed, this is not done by providing acceleration forces on the pilot, but by changing the position of the human body and the pressure on the human body [44].

The design of this product is quite exclusive; leading companies in this industry such as SimXperience, Cranfield Aerospace and Acme worldwide are quite protective of their numbers<sup>79 80 14</sup>. The two companies whose numbers are available for analysis are MOOG and Stirling dynamics<sup>2 81</sup>. Although Stirling dynamics has more information about g-loading on their g-seat, it was decided to go with the MOOG design as one of the most important modes the g-seat should produce, the vibrational mode, is covered by MOOG. Besides, it is believed that the limits of the g-seat of the MOOG system are greater and will fulfil the purpose of this simulator better. The g-seat product provides unfamiliar classical mechanics and therefore makes this product difficult to analyse. Going into the depths of the human body as well as trying to obtain company-specific data/help without buying or showing interest in buying, is beyond the scope of this project. Therefore, certain assumptions for the g-seat for analysis have to be made:

- 1 The minimal operating power of the g-seat is equal to 500 W.(Engineering judgement)
- 2 All power is equally distributed over all pads(Engineering judgement)
- 3 The minimum force capacity as stated in MOOG is equal to the force exerted on the human body. (MOOG Data-sheet interpretation)
- 4 Power scales linearly with distance. In other words, the force during the extension is considered to be constant. (MOOG Data-sheet interpretation)
- 5 The vibrational mode is considered to be sinusoidal. (Engineering judgement)
- 6 The accelerative force in surge is determined by the cushion but has to be reached by help of the surge back padding. (Engineering judgement)

<sup>79</sup>Cranfield Aerospace Solutions: G-cueing & simulation

<sup>80</sup>Acme Worldwide Enterprises inc.: Dynamic Motion Seats

<sup>81</sup>Stirling Dynamics: Motion Cueing System

[cited 2020-06-11]

[cited 2020-06-11]

[cited 2020-06-11]

7 The power consumption of 3 kW is considered for all modes used simultaneously. (MOOG Data-sheet interpretation)

**Sustained motion cueing seat power determination** The data sheet provided by MOOG provides only addresses the continuous power consumption, here stated as in assumption seven. Therefore, 500 kW of minimal operating power is assumed as stated in assumption 1. To determine the distribution between all different modes, the following equations were used, who are based on the general power equation relations between energy, time and force.

$$\tau_{g-seat} = \frac{\sum(F_{g-seat}x_{g-seat})}{P_{max} - P_{nom}} \tag{5.30}$$

$$P_{mode} = \frac{F_{g-seat}x_{g-seat}}{\tau_{g-seat}} \tag{5.31}$$

**Vibration** The g-seat as provided by MOOG presents certain vertical displacements with velocities and accelerations. The up-and-down motion provided by this g-seat is assumed to be a periodic motion. Solving for this specific case with an amplitude equal to the displacement and a velocity equal to 0.065 m s<sup>-1</sup>, both as found in <sup>2</sup> will lead to the following periodic equation for the displacement:

$$x_{vert} = 0.003 \cos(2\pi(3.448t)) \tag{5.32}$$

What can be concluded from this analysis, is that the maximum possible frequency of the system is equal to 3.45 Hz, while the maximum acceleration is equal to 1.44 g.

**Summary of sustained motion cueing seat performance** The calculation for the three modes (surge, sway and height) are based on Newton’s second law using the forces in <sup>2</sup>. Tab. 5.11 will show a complete summary of the g-seat.

Table 5.11: Vibrational response of the g-seat

Buffet	Value
Frequency	0.7136 Hz
g-max	1.152 g
Power	2.854 W

Table 5.12: Accelerations and power of the G-seat during operation

Direction	Acceleration	Power Consumption
Sway	0.7136 g	172.06 W
Surge	1.152 g	722.06 W
Height	2.854 g	1433.84 W

### 5.5.5. Planning regime

The planning regime describes the general workings of the control calculations. The whole goal behind the control-orientated part of the simulator is to have a single input from the IOS determine the motion of upset within the simulator and have a control-orientated model serve to fix the upset (human is in the loop). However, due to the complexity and out of scope nature for a control-oriented system, the design of a controller will not be tackled. Rather, this section tackles all parts needed (calculations and information flow) to be able to create a controller in the future.

**Causality Diagram** The causality diagram describes the general flow of control information. It features three distinct inputs: the human input into the IOS (the software input for the whole system), the pilot input for the vehicle model and the Data input for the Optimisation Problem. Aside from, the diagram features two distinct outputs, the state of the robot arm and the state of the g-seat. The general Causality diagram can be found in Fig. 5.17. One of the functions of the simulator is that event queuing should be doable for an instructor, whereby a straightforward input should be translated to one of the upsets that will be fed through the vehicle model. The vehicle model, as also discussed in Sec. 3, is based on the vehicle model from the OEM’s, this is due to the fact that the aircraft (aerodynamic) parameters are copyrighted and can not be used without consent of the OEM. Therefore, due to the standardised manner of the vehicle model, the assumption is made that the output of the vehicle model is equal to the three modes of translation and the three modes of rotation. One of the results of the vehicle model should than be translated to the mechanics of the robot arm and will be solved in the "Optimisation Problem" block.

The "Optimisation Problem" block takes the desired Vehicle model output and transforms it into the desired motion for the robot arm and g-seat. This is translated as inputs  $\bar{u}(t)$  and  $\bar{y}(t)$  for the g-seat and robot arm. The block "Inertia of Robot Arm" and "g-seat" describes the dynamics behind the movement and transforms the inputs to current motions. This block can be derived from manipulating the Lagrange equation for a non-holonomic system. The result of this equation, will be an equation concerning the inertia of the whole system. The Lagrange equation that has to be solved for the non-holonomic case is equal to:

$$\frac{d}{dt} \left( \frac{\delta L}{\delta \dot{q}_k} \right) - \frac{\delta L}{\delta q_k} - \mu \alpha_k = Q_k \quad (5.33)$$

Here the term  $\mu \alpha_k$  is stated that is used for non-holonomic cases. This will add an extra unknown and contains unknown, difficult to determine, constraints. It is decided not to solve Eq. 5.33 for the robotic arm kinematics. This section will only look at determining the future motion of the robot arm.

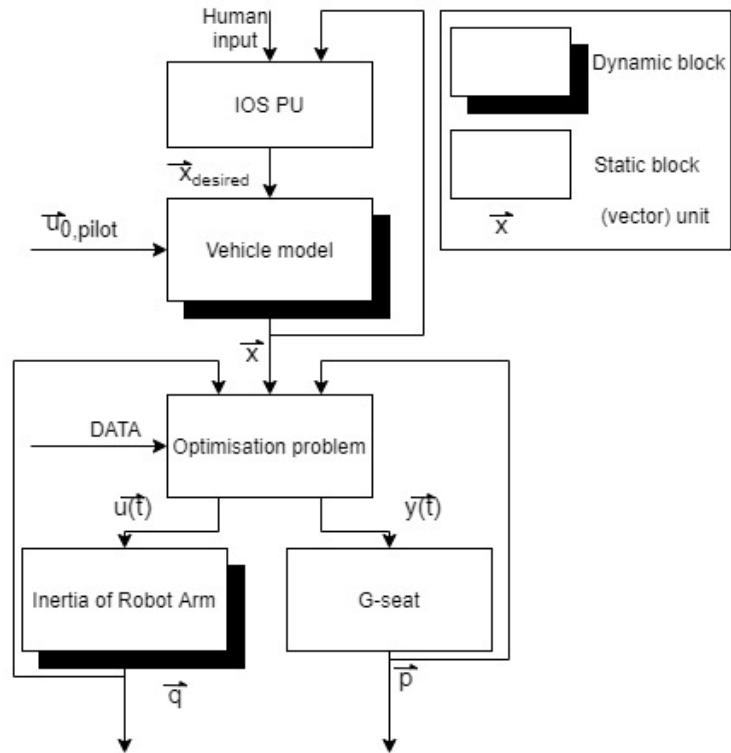


Figure 5.17: Causality diagram describing the interface for path planning

This section will only look at determining the future motion of the robot arm.

### 5.5.6. On the necessity of motion cueing algorithm analysis

While the motion capabilities have previously been determined, it is not clear how these are to be combined to produce realistic and timely motion cues, while utilising the full system capabilities and ensuring the algorithm is feasible within the constraints. Since past (research) algorithms have not been focused on planning for quick-response high-bandwidth motion as is the case in UPRT [45], it becomes necessary to thoroughly consider the architecture on which such an algorithm would be based. If this were not done, it is likely that it turns out preconceptions on the capabilities of current hardware and dynamics algorithms were false after all, thereby invalidating a significant part of the design process. This in turn would cause big performance drops, and leaving requirements unmet.

To exemplify this risk, a number of past projects can be mentioned. One of these is the Federal Aviation Administration's Advanced Automation System, which attempted to automate air traffic control, but underestimated the complexity of ATC and the difficulty of parallelising critical processes [46]. Indeed, for this project it is very easy to underestimate the complexity of motion planning, which differs greatly from the largely explored problem of *path planning* [47]. To add to this, it is necessary to make all processes safety-oriented, which requires forethought at the earliest stages of the design to see if proposed hardware implementations will have a suitably performant and safe software counterpart. If this is not the case, a major revision must take place before continuing the design process, which is to be avoided in this part of the project. Therefore, a thorough examination of the algorithmic and implementational aspects of a motion cueing algorithm are explored in due detail in the following sections.

### 5.5.7. Motion planning algorithm preliminaries

Prior to developing the motion planning algorithm, a number of definitions must be agreed upon to ease the discussion. In particular, a number of (real) variable spaces concerning the various aspects of the robot arm state are developed, as well as the general mappings between these spaces as defined later.

Since optimising a nonlinear system such as the robot arm poses a number of practical issues (local minima, computational cost associated with cost function evaluations, etc.), other venues for optimisation must be explored. This is especially motivated by the fact that true motion planning of the end effector (EE) state (including its higher order derivatives) is neigh unattainable, whereas efforts have almost exclusively been focused on path planning (the instantaneous EE state) [30].

Past efforts in motion planning have proven to be very involved, even for a low-degree-of-freedom systems [48], and often require multiple iterations for higher-degree-of-freedom systems, as is the case for recursive inverse kinematics algorithms that incorporate constraint and collision checking [47].

To this end, it was decided to focus instead on methods of discrete optimisation, as exemplified by the celebrated fields of dynamic programming and other forms of combinatorial optimisation. One of the driving factors in this choice, is the fact that iterative methods that require a non-determinate number of trials can be executed *offline*, thereby providing pre-computed results to the discrete algorithm used in implementation. This notion of offline pre-processing, or ‘memoisation,’ has seen widespread use in industry in the form of lookup tables for real-time systems and code optimisation at compile time<sup>82</sup>, further strengthening the case for discrete optimisation.

Now, it remains to set out an overarching methodology that leverages the apparent advantages of discrete optimisation. A key problem that arises when using the robot arm, is the computation of the joint parameters given a desired joint state—this problem is known as the inverse kinematics (IK) problem [30]. Many of the current implementations of algorithms that solve this problem require multiple iterations, as they perform additional feasibility checks regarding the joint constraints and rigid-body collision—this makes for implementations that have a non-determinate execution time, and are therefore not suited for real-time use [47]. Therefore, it is reasoned that computing feasible IK solutions *offline*, and implementing a lookup table with the pertinent results, would be the best way to proceed. In this manner, only reachable points are stored, and the only computational burden lies in accessing these values.

**Mapping feasible IK solutions.** Having discussed the utility of inverse kinematics solutions, it is now possible to show how these solutions will be generated and used. Do note, however, that a discussion on algorithmic implementations of IK algorithms lies beyond the scope of this project, and extensive coverage of the topics may readily be found in literature (see, e.g., [47]). As an example of a popular IK algorithm, the reader may refer to the rapidly-exploring random tree (RRT) algorithm; this method is used in the implementations shown in this report.

To efficiently tabulate the IK solutions, a discrete 3D Cartesian grid in the (inertial) world coordinate system is generated. These points in  $\mathbb{R}^3$  serve to describe the position of the EE (in this case, the cabin) in inertial space. The fact that adjacent points have the same distance as part of this implementation admits a number of favourable optimisations to be made, as will be discussed later.

This discrete Cartesian grid in  $\mathbb{R}^3$  serves its purpose in describing the position of the EE, but fails to convey any information on the orientation. To this end, a space in  $\mathbb{R}^2$  is required to store the azimuth and elevation angle of the EE.

Since the definition of the feasible IK state space is not known *a priori*, a conservative space of EE states must be checked to extract a discrete representation of the feasible IK space—naturally, it is required that the IK state space is a subset of this space.

Let  $\mathcal{T}_{\text{position}} \subset \mathbb{R}^3$  be the test space of positions (in inertial space), and  $\mathcal{T}_{\text{orientation}} \subset \mathbb{R}^4$  be the test space of orientations that subsumes the feasible IK state space. The orientation is purposefully defined using four Euclidean coordinates, to prevent gimbal lock; particular implementation of this description would be quaternions or Euler vectors, among others.

Additionally, let  $\mathcal{T} = \mathcal{T}_{\text{position}} \oplus \mathcal{T}_{\text{orientation}} \in \mathbb{R}^7$  be defined as the ‘test space’, which is constructed by a direct summation of the position and orientation test spaces (i.e.,  $\mathcal{T} \subset \mathbb{R}^6$ ). Note that  $\mathcal{T}$  is strictly a subset of  $\mathbb{R}^6$  due to the fact that only non-holonomic systems are considered. Elements of  $\mathcal{T}$  are  $(x, y, z, a, b, c, d)$ .

To aid in the forthcoming discussion, let  $\mathcal{T}'_{\text{orientation}} \in \mathbb{R}^3$  be the orientation test space described by Euler (or Tait–Bryan) angles (pitch, yaw, and roll). This leads to the definition of  $\mathcal{T} = \mathcal{T}_{\text{position}} \oplus \mathcal{T}'_{\text{orientation}} \in \mathbb{R}^6$ . The elements of  $\mathcal{T}'$  will then be  $(x, y, z, \phi, \theta, \psi)$ . In general, any space with a prime (‘’) will be understood to refer to the 6-dimensional version of the redundant 7-dimensional state description.

Now, let  $\mathcal{K} \subseteq \mathcal{T} \subset \mathbb{R}^5$  be the space of kinematically feasible EE states (i.e., the feasible IK state space); this space is composed of a position (3-tuple) and an orientation (2-tuple), as is the case for the test space. An IK solver serves to discern which elements of  $\mathcal{T}$  belong in  $\mathcal{K}$ :

$$\mathcal{K} \equiv \{t \in \mathcal{T} : \text{IK}_{\text{feasible}}(t) = t\}, \quad (5.34)$$

where  $\text{IK}_{\text{feasible}}(t)$  yields  $t$  if  $t \in \mathcal{K}$ , else it returns the best approximation of  $t$  in  $\mathcal{K}$ .

In addition to providing information on the kinematic feasibility of a given EE state, the IK solver provides a solution in the form of an  $n$ -tuple containing the joint parameters. Since for this to reliably succeed, the system degrees of freedom must correspond to the rigid-body’s degree of freedom. For

<sup>82</sup>Paul McNamee: Automated Memoization in C++

[cited 2020-06-18]

this reason, only the robotic arm's revolute joints are considered, adding up to a total 6-degrees-of-freedom (i.e.,  $n = 6$ ). The remaining degree-of-freedom, i.e. the linear unit, will be considered separately in the optimisation algorithm.

The six-degrees-of-freedom are defined by joint parameters  $q_i$ ,  $i = 1 \dots 6$ . These parameters are combined to form a 6-tuple  $q$ , which resides in the space of feasible joint parameters  $\mathcal{Q} \subset \mathbb{R}^6$ ; henceforth, this space will be referred to as the 'joint space'.

As alluded to previously, the IK solver produces an IK solution, i.e. the joint state  $q$  corresponding to a given feasible EE state. This is described by the following bijective map:

$$\text{IK}_{\text{solution}}: \mathcal{K} \rightarrow \mathcal{Q}. \quad (5.35)$$

**IK solution lookup** Given the previous definitions, a framework for mapping a given kinematically feasible EE state to a joint state has been devised. Since exactly 6-degrees-of-freedom are considered, this mapping is found to be one-to-one and onto (i.e., it is bijective). Therefore, from a given joint state, the corresponding EE state can also be found, provided that both are computed either online or offline.

In the current case, a discretisation in both the position and the orientation is proposed, yielding a test space that can easily be stored in memory. To show this, consider the following pseudocode for a lookup (Algo. 1):

---

**Algorithm 1** Joint state lookup algorithm

---

```

1:  $k \leftarrow \{x, y, z, \phi, \theta, \psi\} \in \mathcal{K}'$  // Queried lookup state
2:  $k_o := \{x_o, y_o, z_o, \phi_o, \theta_o, \psi_o\}$  // Lookup database origin definition
3:  $\Delta k := \{\Delta x, \Delta y, \Delta z, \Delta \phi, \Delta \theta, \Delta \psi\}$  // Lookup step size definition
4:  $\text{DB}_{\mathcal{K}', \mathcal{Q}}$  // Lookup data structure

5: function GetIdx( $i$ )
6:    $i \leftarrow i \bmod 6$  // Ensures index validity
7:   return  $\lfloor (k[i] - k_o[i]) / \Delta k[i] \rfloor$ 
8: end function

9: return  $\text{DB}_{\mathcal{K}', \mathcal{Q}}[\text{GetIdx}(0)][\text{GetIdx}(1)][\text{GetIdx}(2)][\text{GetIdx}(3)][\text{GetIdx}(4)][\text{GetIdx}(5)]$ 

```

---

Here,  $\lfloor \cdot \rfloor$  represents the 'floor'-function, which rounds down to closest integer. The data structure ( $\text{DB}_{\mathcal{K}', \mathcal{Q}}$ ) is defined to include entries with fixed discretisation steps in each of the five axes, starting at some origin  $k_o$ . In this algorithm it is of importance that the array read access operator (" $[ ]$ ") does not throw exceptions when the index is out of range; instead, it should return `null`. This could potentially be checked before accessing the array, since the dimensions of the array are known at compile time. If an entry of the database is invalid (due to it being infeasible), that particular lookup should also return `null`.

**Adjacent node trajectory generation** Having defined a database  $\text{DB}_{\mathcal{K}', \mathcal{Q}}$ , it is possible to consider each element in this database to be a 'node'. If  $\mathcal{T}$  is defined in a 6-dimensional Cartesian grid in task space (as is the case in Algo. 1), then the following observations can be made.

Each node will have at most six neighbours in (positional) space, i.e. two on each axis. However, each node may possess a multitude of different (recorded) orientations. These orientations can be expressed as an additional Cartesian grid in  $\mathbb{R}^4$ , where the coordinates are the four orientation-description scalars,  $(a, b, c, d) \in \mathcal{T}_{\text{orientation}}$ . Let the number of discrete points in each of these axes be given as  $(n_a, n_b, n_c, n_d)$ , respectively. Then, for each node in space, there will be  $n_a \cdot n_b \cdot n_c \cdot n_d$  orientations that are to be stored. As a numerical example of this, consider  $n_a = n_b = n_c = n_d = 4$ ; with this configuration, the resulting number of orientations for a single spatial location is  $4^4 = 256$ . To visualise the distribution of these orientations, consider the following orientation vectors that have been generated with the same parameters, and visualised by multiplying the resulting rotation matrix by a unit vector in  $x$ -direction (Fig. 5.18).

Given this result, it is found that the total number of neighbour states to be  $N_{\text{neighbours}} = 6n_a n_b n_c n_d$ ; for  $n_a = n_b = n_c = n_d = 4$ , this number equals 1536 entries. Note that in this discussion, the alternative rotational states of the current spatial node are not stored, as it is clear to see that such a manoeuvre, i.e. one that keeps the cabin near-stationary, will not produce sufficient acceleration to be of real use. An alternative, but equivalent, storage solution (that will be invoked later), is to store the orientation in terms of Euler angles; this will yield  $N'_{\text{neighbours}} = 6n_\phi n_\theta n_\psi$ .

Note that the numbers mentioned above are all worst-case scenarios, and some candidate states will be invalidated *a priori* by considering the feasibility of the joint motion needed to move between the given node–neighbour pair. This will especially be the case near the boundaries of  $\mathcal{K}$ . One further criterion for determining the feasibility of node–neighbour pairs could be the maximum possible acceleration magnitude along the trajectory, or the minimum time of motion. These criteria would serve to further economise on the memory requirements for the node database.

Consider the function  $\text{NN}(q) = \{q\}_{\text{NN}}, q \in \mathcal{Q}$ , which returns the set of nearest neighbours to node  $q$ . As discussed previously,  $\{q\}_{\text{NN}}$  has a cardinality of at most  $N_{\text{neighbours}} = 6n_a n_b n_c n_d$ . Based on the joint constraints (deflection, velocity, and acceleration bounds), the fastest possible motion between the base node and each of its neighbours can be computed; the feasibility of this motion (i.e., the feasibility of each instantaneous state along the trajectory), can be ascertained *a priori*, and for the fastest possible trajectory, the maximum acceleration (magnitude and direction) experienced at the EE can be tabulated. A key advantage here, is that a would-be coupled inverse dynamics–forward dynamics problem can now be solved at a much lower cost, since the only required operation would be a number of linear interpolations between the two joint states, given the criterion of near-minimum manoeuvring time.

### 5.5.8. Feasible motion trajectory definition

The above discussion is best illustrated by means of an example. Consider initial state  $q^{(0)} \in \mathcal{Q}$  and final state  $q^{(1)} \in \mathcal{Q}$ , which are neighbours in the sense that  $q^{(1)} \in \text{NN}(q^{(0)})$  (the inverse does not have to hold *per se*). In the case of this example, the motion trajectory is computed such that the system is at rest at the initial state and the final state. Consider the triangular function  $\Lambda(t)$ :

$$\Lambda(t) \equiv \begin{cases} 1 - |t| & , |t| < 1; \\ 0 & , \text{else} \end{cases} \quad (5.36)$$

To produce an acceleration profile that moves the system and ends with zero velocity, two of these triangular functions must be combined to have an integrated area of zero. This function must also be scaled in its maximum acceleration ( $A$ ) and the total time for which it is nonzero ( $T$ ). Given these requirements, the following modified triangular function is obtained:

$$\Lambda^*(t, A, T) \equiv A\Lambda(4t/T - 1) - A\Lambda(4t/T - 3). \quad (5.37)$$

As an illustration of this function, see the following figure for the function  $\Lambda^*(t, 2, 3)$  (Fig. 5.19):

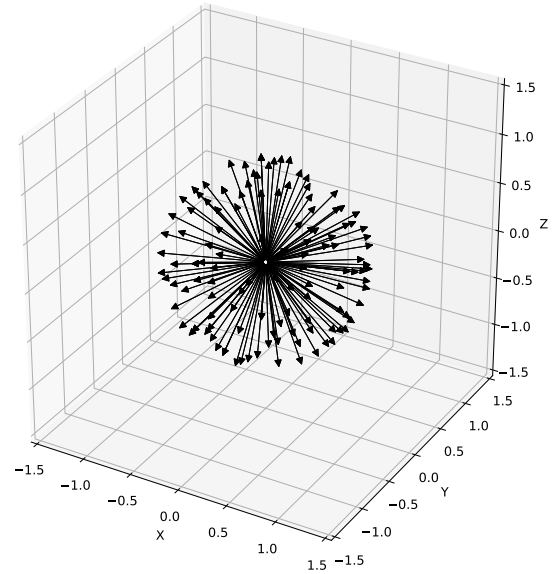
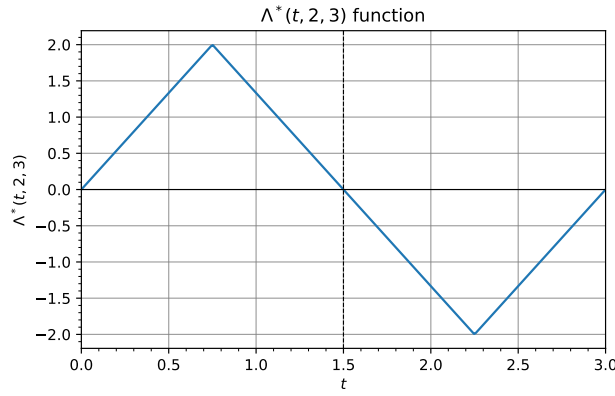


Figure 5.18: Orientations for uniformly distributed discretised Euler vectors with  $n_a = n_b = n_c = n_d = 4$

Figure 5.19: Plot of  $\Lambda^*(t, 2, 3)$  for  $t \in [0, 3]$ 

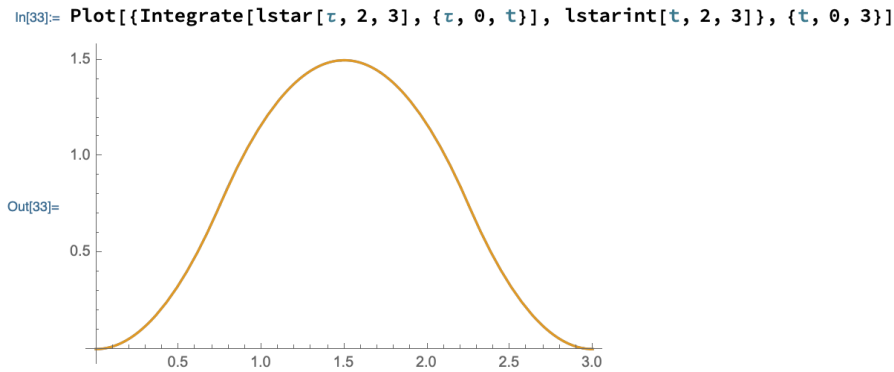
To compute the remaining variables of interest, i.e. the velocity and deflection profiles, it is necessary to integrate the above  $\Lambda^*$  function. It is apparent that this function is doubly symmetric about  $t = T/2$ ; therefore,  $\Lambda^*$  need only be integrated up to time  $t = T/2$ , as the remainder of the function is simply its mirror image. Let the integral of  $\Lambda^*$  be denoted as  $\Lambda_{\text{int}}^*$ . The following can be shown:

$$\begin{aligned} \Lambda_{\text{int}}^*(t, A, T) &= A \int_0^t \left[ \Lambda\left(\frac{4\tau}{T} - 1\right) - \Lambda\left(\frac{4\tau}{T} - 3\right) \right] d\tau \\ &= \Lambda_{\text{int},1/2}^*(t, A, T) \mathbb{1}(T/2 - t) + \Lambda_{\text{int},1/2}^*(T - t, A, T) [\mathbb{1}(T - t) - \mathbb{1}(T/2 - t)], \end{aligned} \quad (5.38)$$

where  $\mathbb{1}(t)$  denotes the Heaviside (unit) step function; for the purposes of this report, the Heaviside step function is taken to be right-continuous, i.e.,  $\mathbb{1}(0) \equiv 1$ . Furthermore,  $\Lambda_{\text{int},1/2}^*$  is defined as:

$$\begin{aligned} \Lambda_{\text{int},1/2}^* &\equiv A \int_0^t \Lambda\left(\frac{4\tau}{T} - 1\right) d\tau \\ &= A \left[ \int_0^t \frac{4\tau}{T} d\tau \right] \mathbb{1}(T/4 - t) + A \left[ \int_0^{T/4} \frac{4\tau}{T} d\tau + \int_{T/4}^t \left(1 - \frac{4}{T}(t - T/4)\right) d\tau \right] [\mathbb{1}(T/2 - t) - \mathbb{1}(T/4 - t)] \\ &= \frac{2At^2}{T} \mathbb{1}(T/4 - t) + A \left[ \frac{T}{8} + 2t - \frac{2t^2}{T} - \frac{3T}{8} \right] [\mathbb{1}(T/2 - t) - \mathbb{1}(T/4 - t)]. \end{aligned} \quad (5.39)$$

To verify the correctness of this result, a symbolically evaluated solution for the integral of  $\Lambda^*(t, A, T)$  was constructed in Wolfram Mathematica 12 (which incidentally does not yield a closed-form solution, and is evaluated numerically internally), and was plotted alongside the analytically derived solution (based on  $\Lambda_{\text{int},1/2}^*$ ). The result of this analysis provides solid evidence that the derived result is indeed the integral of  $\Lambda^*$  (Fig. 5.20):

Figure 5.20: Analytical and symbolic evaluation of  $\int_0^t \Lambda^*(\tau, 2, 3) d\tau$  for  $t \in [0, 3]$ 

As can be deduced from the preceding discussion, the  $\Lambda_{\text{int}}^*$  function denotes the velocity profile, which starts and ends at rest, as per the above specifications. Of importance is the maximum

velocity attained, which is constrained by the hardware. By evaluating  $\Lambda_{\text{int},1/2}^*(T/2, A, T)$ , this value is readily found. In this process, note the fact that  $t = T/2$  coincides with the x-intercept of  $\Lambda^*$ , and is the only abscissa with a negative derivative (cf. Fig. 5.19), therefore being the global maximum. Evaluating this expression, it is found that the maximum is  $\max_{t \in [0, T]} \Lambda_{\text{int}}^*(t, A, T) = \frac{AT}{4}$ . This is also verified by Fig. 5.20, since the maximum in that case evaluates to  $2 \times 3/4 = 1.5$ .

Finally, to compute the position, a similar reasoning will be applied to alleviate the analytic effort. Looking back at Fig. 5.20, it is found that the function is symmetric about  $t = T/2$ ; therefore, it suffices to compute the integral up to  $t = T/2$ , which will be denoted by  $\Lambda_{\text{int},1/2}^{*,2}(t, A, T)$ . Then, the double integral of  $\Lambda^*$  will be:

$$\Lambda_{\text{int}}^{*,2}(t, A, T) = \Lambda_{\text{int},1/2}^{*,2}(t, A, T) + \left(2\Lambda_{\text{int},1/2}^{*,2}(T/2, A, T) - \Lambda_{\text{int},1/2}^{*,2}(T - t, A, T)\right) \mathbb{1}(t - T/2), \quad (5.40)$$

where the  $2\Lambda_{\text{int},1/2}^{*,2}(T/2, A, T)$  originates by necessity from the fact that the initial value of the second half of the function must be restored and the function that follows is negative. Here,  $\Lambda_{\text{int},1/2}^{*,2}$  is defined as:

$$\begin{aligned} \Lambda_{\text{int},1/2}^{*,2}(t, A, T) &\equiv \int_0^t \left[ \frac{2A\tau^2}{T} \mathbb{1}(T/4 - \tau) + A \left[ -\frac{2\tau^2}{T} + 2\tau - \frac{T}{4} \right] [\mathbb{1}(T/2 - \tau) - \mathbb{1}(T/4 - \tau)] \right] d\tau \\ &= \frac{2At^3}{3T} \mathbb{1}(T/4 - t) + A \left\{ \frac{2(T/4)^3}{3T} + \int_{T/2}^t \left[ -\frac{2t^2}{T} + 2t - \frac{T}{4} \right] d\tau \right\} [\mathbb{1}(T/2 - t) - \mathbb{1}(T/4 - t)] \quad (5.41) \\ &= \frac{2At^3}{3T} \mathbb{1}(T/4 - t) + A \left[ -\frac{2t^3}{3T} + t^2 - \frac{Tt}{4} + 2\frac{T^2}{96} \right] [\mathbb{1}(T/2 - t) - \mathbb{1}(T/4 - t)]. \end{aligned}$$

Given this equation, it is then possible to rewrite Eq. 5.40 as:

$$\Lambda_{\text{int}}^{*,2}(t, A, T) = \Lambda_{\text{int},1/2}^{*,2}(t, A, T) + \left( \frac{AT^2}{8} - \Lambda_{\text{int},1/2}^{*,2}(T - t, A, T) \right) \mathbb{1}(t - T/2). \quad (5.42)$$

To verify this result, turning back to the symbolic analysis in Wolfram Mathematica, the following congruence is found after performing numerical integration on  $\Lambda_{\text{int}}^*$  (Fig. 5.21):

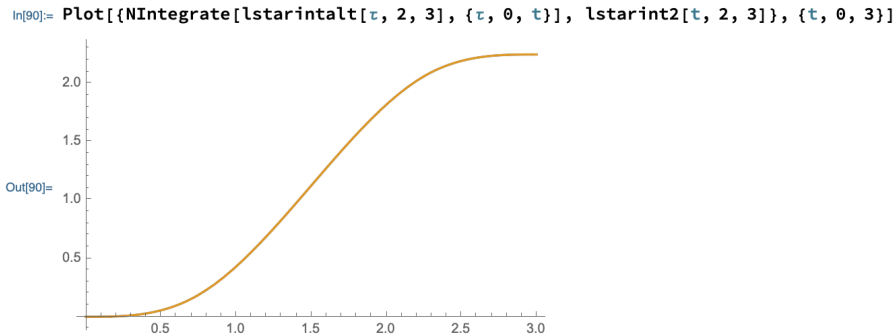


Figure 5.21: Analytical and numerical evaluation of  $\int_0^t \Lambda_{\text{int}}^*(\tau, 2, 3) d\tau$  for  $t \in [0, 3]$

As before, it is desired to find a closed-form solution for the final deflection given the variables that define the original acceleration profile  $(A, T)$ . With Eq. (5.42) this is in fact possible, yielding a maximum deflection of  $\max_{t \in [0, T]} \Lambda_{\text{int}}^{*,2}(t, A, T) = \frac{AT^2}{8}$  at  $t = T$ . To verify this result, referring back to Fig. 5.21 reveals that the final deflection should be  $2(3^2)/8 = 2.25$ , which it in fact is.

### 5.5.9. Feasible motion trajectory generation

Having defined what constitutes (a possible) feasible trajectory, it is now possible to generate such ‘optimal’ trajectories in the presence of (hardware) constraints. In the following, ‘optimal’ is understood to mean ‘least time’, while respecting the hardware constraints.

The aforementioned hardware constraints take the form of a system of constant non-strict inequalities, and are applied to all six robot joint states. Take  $q_i = \{q_i, \dot{q}_i, \ddot{q}_i\} \in \mathbb{R}^3$  to be the joint state of the  $i$ 'th joint for  $i \in [1, 6]$ . Then, the joint constraints manifest themselves as:

$$\begin{aligned} q_{\min,i} &\leq q_i \leq q_{\max,i}, \\ \dot{q}_{\min,i} &\leq \dot{q}_i \leq \dot{q}_{\max,i}, \\ \ddot{q}_{\min,i} &\leq \ddot{q}_i \leq \ddot{q}_{\max,i}. \end{aligned} \quad (5.43)$$

To solve for the optimal trajectory (i.e., acceleration profile) parameters given the constraints of system (5.43), it is of importance to restate the solutions for the maximum deflection acceleration and velocity found previously. The deflection found in Eq. 5.42 is in fact a change in the joint angle, and can therefore be denoted as  $\Delta q_i^{(0,1)} = q_i^{(1)} - q_i^{(0)}$  for  $i \in [1, 6]$ , where superscript '(0)' and '(1)' denote the initial and final joint state, respectively. It is now straightforward to obtain the following system of equations:

$$\frac{A_i T_i^2}{8} = \Delta q_i^{(0,1)}, \quad (5.44a)$$

$$\dot{q}_{\min,i} \leq \frac{A_i T_i}{4} \leq \dot{q}_{\max,i}, \quad (5.44b)$$

$$\ddot{q}_{\min,i} \leq A_i \leq \ddot{q}_{\max,i}. \quad (5.44c)$$

Following some elementary manipulation, the following equations may be retrieved:

$$\frac{\dot{q}_{\min,i}}{2\Delta q_i^{(0,1)}} \leq T_i \leq \frac{\dot{q}_{\max,i}}{2\Delta q_i^{(0,1)}}, \quad (5.45a)$$

$$\frac{\ddot{q}_{\min,i}}{8\Delta q_i^{(0,1)}} \leq \frac{1}{T_i^2} \leq \frac{\ddot{q}_{\max,i}}{8\Delta q_i^{(0,1)}}, \quad (5.45b)$$

$$A_i = \frac{8\Delta q_i^{(0,1)}}{T_i^2}. \quad (5.45c)$$

From these equations, it is apparent that the smallest time acceleration will be obtained at the upper bound of Eq. 5.45b, i.e.  $T_{i,\min} = \sqrt{\frac{8\Delta q_i^{(0,1)}}{\ddot{q}_{\max,i}}}$  for a positive deflection  $\Delta q_i^{(0,1)}$ , and  $T_{i,\min} = \sqrt{\frac{\ddot{q}_{\min,i}}{8\Delta q_i^{(0,1)}}}$  for a negative deflection.

A final step in this process is to ascertain if the second inequality of Eq. 5.45a is honoured; if so, the trajectory is feasible and the two neighbours are indeed connected, if not, then the to-be neighbour will be discarded.

Now, given that each joint has a feasible trajectory, all that is left is to compute the maximum time required to execute the manoeuvre among all six joints. Given this time, the required maximum acceleration for each joint is then again computed. This yields the final minimum time trajectory, which can be used to generate the maximum acceleration perceptible in the cabin by means of a forward dynamics simulation.

**Analysis of the feasible trajectory generation routine** Given the previous results on the computation of a feasible trajectory between neighbouring nodes, it is now possible to analyse the computational complexity of these operations.

For two neighbouring nodes, trajectory existence is checked in one multiplication and two inequality operations (Eq. 5.43). If a trajectory is found to exist, the computation of its parameters  $(T_i, A_i)$  takes an additional six multiplications and one inequality to find the sign of  $\Delta q_i^{(0,1)}$ . Finally, to recompute  $A_i$  based on a prescribed  $T_i$ , another three multiplications are required. In the worst case for a given feasible trajectory, a total of 11 multiplications and three inequality evaluations are needed; additionally, the maximum value of the manoeuvre time must be extracted among six values, which has complexity  $\mathcal{O}(6 + k)$  in the case of counting sort.

Then, for all 34 neighbouring nodes, a total of 374 multiplication operations are required, in addition to 102 inequality evaluations. With this light of a computational burden, these computations could conceivably be executed online.

**Considerations for the seventh degree-of-freedom** In the foregoing, the analysis was based purely on the assumption of a 6-DOF system, on account of the fact that such a system is kinematically determinate; this allowed for unique IK solutions to be generated given a desired (and feasible) EE state, thereby making for a straightforward scheme for generating feasible IK states. In practice, however, the system is outfitted with a linear unit, which permits an additional (translational) degree-of-freedom. To account for the potential contribution of this additional DOF, its impact on the dynamics of the system must be analysed.

In the following, it is assumed that the linear unit only adds a linear acceleration component to the motion of the robot arm, whereas in reality Coriolis and centrifugal forces must be accounted for. This is acceptable for small manoeuvres, such as those found in the present analysis [30].

Let  $q_0$  be the joint state of the linear unit, which is constrained in the same manner as the other  $q_i$ 's (cf. Eq. 5.43). It is assumed that the linear unit will serve only to add to the overall magnitude

of the originally generated 6-DOF manoeuvre, thereby constraining the direction of the linear unit's movement; the linear unit will only be commanded (if possible) to move in the principal direction of the maximum acceleration as projected on the rail ( $y$ ) axis. To determine this direction, take  $\hat{a} \in \mathbb{R}^3$  to be the unit maximum linear acceleration vector in (inertial) world coordinates, and the rail to be aligned with  $\hat{e}_2 = [0 \ 1 \ 0]^T$ . Then, the principle direction of the acceleration is found as the vector projection of  $\hat{a}$  onto  $\hat{e}_2$ :

$$\hat{a}_{\parallel\hat{e}_2} = (\hat{a} \cdot \hat{e}_2)\hat{e}_2, \quad (5.46)$$

from which one can readily find that the sign of the dot product indicates the direction of the desired linear acceleration, i.e.  $\text{sgn}(\hat{a} \cdot \hat{e}_2)$ , where 'sgn' is the signum function.

With the sign of the desired linear acceleration found, what is left to be done is to find the desired contribution of the linear unit. Let  $a_{\text{des}}$  be the desired EE acceleration, and define  $a_{6\text{-DOF}}$  as the acceleration imparted on the EE by the 6-DOF motion solution. Then, there are two avenues that may be followed: the first would be to match the magnitude of the acceleration projected along the rail by means of the linear unit's contribution, while the other would be to match the acceleration magnitude regardless of direction. It is deemed that the former is the more reasonable option, since inducing accelerations that are improperly oriented was reasoned to negatively impact motion fidelity, as opposed to simply having a smaller magnitude acceleration.

Following this last option, it is simply required that the linear unit produces an acceleration of magnitude  $(a_{\text{des}} - a_{6\text{-DOF}}) \cdot \hat{e}_2$ , as foreshadowed in Eq. 5.46. The final motion acceleration will then be:

$$a_{7\text{-DOF}} = a_{6\text{-DOF}} + a_{\text{LU}} = a_{6\text{-DOF}}(a_{\text{des}} - a_{6\text{-DOF}}) \cdot \hat{e}_2, \quad (5.47)$$

where LU is short for 'linear unit.' From Eq. 5.47, the final 7-DOF motion that will be experienced on the cabin can be found.

Up to this point, the current state of the linear unit has not been considered; it may very well be that the linear unit is close to one of its edges, thus inhibiting it from producing motion in a given direction. While in operation, it could in some cases be sensible to reorient the cabin so as to direct it to the rail direction with the greatest remaining track length, this is not deemed feasible in situations demanding short response times. Instead, the system will require some mechanism that tends to command the linear unit to move back to its centre position, such that it has the greatest range of possible motions. This manoeuvre must be performed tacitly during 'motion downtime,' such that originally uncommanded or unwarranted accelerations are kept to a minimum.

### 5.5.10. Optimisation routines

This section will expand on the optimisation problem as presented in Sec. 5.5.5. The primary use of the optimisation problem is to convert the desired vehicle state to an equivalent simulator state, as constrained by operational limits. First, functional mapping will be tackled where all the principles of the process will be detailed, followed by a procedure for determining what the correct future motion is. Thereafter, a candidate cost function that would yield the desired results is presented. Finally, integration with the g-seat will be discussed.

**Functional mapping** As presented in Sec. 5.5.5, the vehicle model provides a desired state in  $\mathbb{R}^6$ , namely three translational vehicle accelerations and three angular accelerations. As previously mentioned, time-optimal trajectories between neighbouring states are computed *offline*, and are drawn upon during motion planning. This data is presented as a vector in  $\mathbb{R}^{17}$ , containing 6 joint states at the final neighbour, a measure of manipulability, and the time-optimal joint acceleration profile and acceleration experienced on the EE (see Tab. 5.13). The desired vehicle state will be compared to the closest possible acceleration producible by each node, combined with the measure of manipulability, setting the stage for a discrete optimisation to take place. In fact, a cost function will provide a mapping from this extended database space ( $\mathbb{R}^{17}$ ) and the desired acceleration ( $\mathbb{R}^6$ ) to  $\mathbb{R}^1$ , which is then minimised to obtain the optimal trajectory.

As a result of this optimisation, the optimal next state is selected. This state will form a balance between manipulability (or dexterity) and cueing performance, and relates solely to the robot arm and linear rail. The deficit of this motion cue in relation to the desired vehicle acceleration will be then made up for by the g-seat. This selection will then be compared and integrated with the previous state of the robot arm and g-seat and will send out inputs for both the g-seat and the robot arm as  $\rightarrow y(t)$  and  $\rightarrow u(t)$  respectively. This process can be seen in Fig. 5.22. Please note that for the vibrational mode of the vehicle model direct feed through to the command determination block is provided as it is believed that the g-seat will carry all of the vibrational modes as presented through the vehicle model.

**Optimisation rationale** One of the problems concerning motion planning for the robot, is that the robot is constrained in its motions as it has kinematic, spatial and hardware constraint it must adhere to.

Give these constraints, it is of importance to keep the EE in a state that is as controllable as possible, such that the greatest range of motions may be produced. This notion of ‘motion freedom,’ or *dexterity*, plays a central role in both manipulator design and real-time control [49].

To present a number of dexterity measures, one must first be familiar with the forward dynamics problem. Let  $q \in \mathbb{R}^n$  (in this case  $n = 6$ ) be the joint state, and  $x \in \mathbb{R}^m$  (in this case  $m = 5$ ) be the manipulator state in task space. The forward dynamics problem (FDP) can then be expressed as:

$$x = \text{FDP}(q). \quad (5.48)$$

Taking the time derivative of this equation, one obtains:

$$\dot{x} = J(q)\dot{q}, \quad (5.49)$$

where  $J \in \mathbb{R}^{m \times n}$  is known as the *Jacobian matrix*, with its elements being defined as  $J_{ij} \equiv \partial x_i / \partial q_j$ . Eq. 5.49 is also known as the *instantaneous kinematics* equation, since  $J$  is applicable only for a given instant in time, unless the system is fully at rest and stable.

According to [49], the measure of manipulability is defined as:

$$w \equiv \sqrt{\det(JJ^T)}. \quad (5.50)$$

In addition,  $w$  can be defined in terms of  $J$ 's singular values as:

$$w = \prod_{i=1}^m \sigma_i, \quad (5.51)$$

where  $\sigma_i$  are the singular values of  $J$ . To relate manipulability  $w$  back to a physical definition, it has been shown that  $w$  is proportional to the volume of the feasible space of  $\dot{x}$  given that  $\|\dot{q}\| \leq 1$ , with the volume of this feasible space, which is an ellipsoid with dimensions  $\sigma_i$ , being given as [49]:

$$V_e = \{\pi^{m/2} / \Gamma[(m/2) + 1]\}w, \quad (5.52)$$

Note that the reachable volume  $V_e \propto w$ , meaning that a greater value of  $w$  is directly proportional to a greater set of reachable states. One of the key advantages of such a measure of manipulability is therefore that it manifests itself as a scalar value that is solely configuration-dependent, and can therefore be computed *a priori*.

The higher the value of  $w$  for the point in question, the more controllable the system is found to be. To implement this value in a cost function, one must therefore take the inverse of this value as one of its terms.

For optimisation, another value that should be taken into account is the manoeuvring time; if this time is too significant it can be detrimental to simulator performance.

When taking into account the desired vehicle trajectory, the dexterity and the manoeuvring time, one can make a compelling cost function that should be able to correctly future plan robot motion.

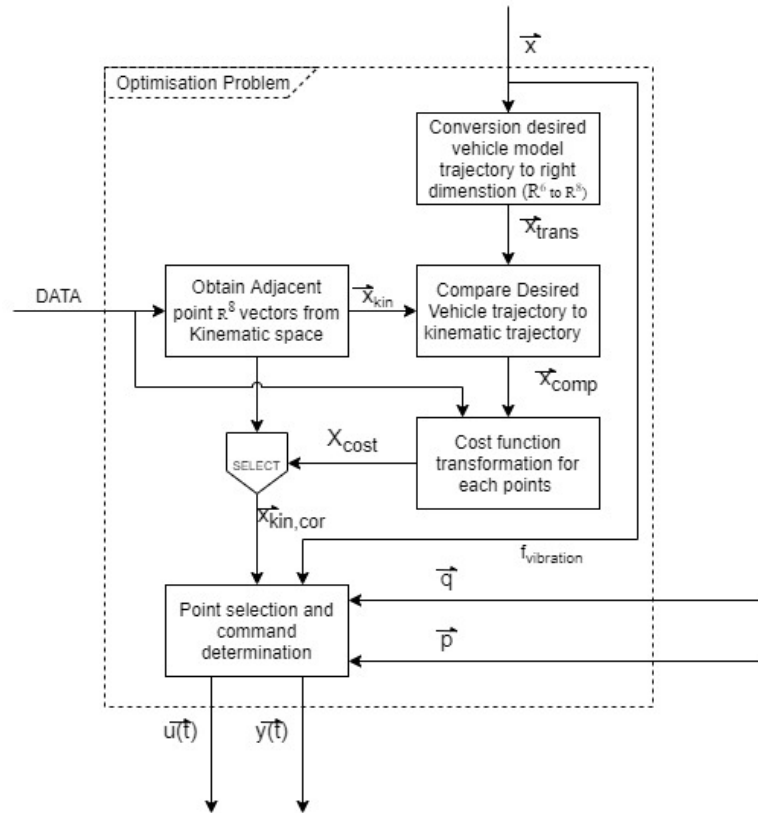


Figure 5.22: Enhancement of the Optimisation block as presented in the Causality Diagram

### Implications on memory management

The foregoing discussion has given some insight into the requisite quantities for use in the planning algorithm, although the feasibility of a real-time variant of the same algorithm was not discussed. To address this, an analysis of the memory requirements is presented here.

First, it is of importance to consider, for a given node–neighbour pair, how many variables need to be stored. In this consideration, one must take account of the fact that some quantities are independent of their neighbours, and may therefore be stored once. The required quantities are tabulated in Tab. 5.13:

Table 5.13: Number of elements to be stored in the kinematic motion database

Quantity	Number	Constant?
Joint states	6	✓
Manipulability	1	✓
Minimum-time acc. profile	6 joint acc., 1 min. time	✗
Maximum lin. acc. vector	3	✗
Maximum ang. acc. vector	3	✗
Total	20	7 const., 13 var.

From Tab. 5.13, it can be seen that each node–neighbour pair will have 13 variable quantities, while each node will have an additional 7 constants to store. Let all dimensions be discretised uniformly in each dimension, with each dimension having  $n_i$  points, where  $i \in \{x, y, z, \phi, \theta, \psi\}$ ; for convenience, each of the elements in this set will be referred to by its (0-based) index  $i \in \{0, 1, 2, 3, 4, 5\}$ .

Now, each point in the test space will have to store at most  $N_{\text{const}} = 7 \prod_{i=0}^5 n_i$  constant values. The neighbour-dependent variables pose a more compelling storage problem. Before consider the upper bound of states to be stored, consider that the minimum-time acceleration profile between two nodes has exactly the same form, regardless of the direction of motion; the only difference is the sign of  $A_i$ . Further expanding on this advantageous property, one could choose to store the sign of each acceleration as a (signed) bit, making it possible to multiply the acceleration magnitude. Here, instead, it is reasoned that it would be in one’s advantage to incorporate a different mechanism: the sign could be flipped based on the relative position of the two nodes in the database. As an example, provisions could be made to store the acceleration profile in such a way that no multiplication is needed if the destination node index is greater than the home node index, and the sign must be flipped in the case that the converse is true. The same holds for the maximum acceleration vector, thanks to the symmetric nature of the acceleration profile (see Fig. 5.19). This tacit mechanism allows for a great amount of storage optimisation, as seen below.

To compute the number node–neighbour pairs, it is important to recall the fact that motion profiles for different orientation states starting from the same node position are not stored; this has far-reaching consequences on the amount of storage required as will be demonstrated shortly. As shown previously, each node will have at most  $N'_{\text{neighbours}} = 6n_\phi n_\theta n_\psi$  neighbours. From the foregoing discussion, it is known that there is a possibility to store a node–neighbour pair once, yielding the following maximum number of unique (undirected) node–neighbour pairs:

$$N'_{\text{neighbour pairs}} = [6(N_{\text{spatial nodes}} N'_{\text{neighbours}})/2], \quad (5.53)$$

where  $N_{\text{spatial nodes}} = n_x n_y n_z$  is the number of spatial nodes, the preceding 6 denotes the fact that each spatial node is connect to at most 6 other spatial nodes, and the division by two ensures that the node–neighbour pairs are undirected.

To put the aforementioned reasoning into perspective, consider the case of  $n_x = n_y = n_z = 50$  and  $n_\phi = n_\theta = n_\psi = 4$ . This will yield a storage budget of  $((50^3) \cdot (4^3)) \cdot 7 + [6 \cdot (50^3) \cdot (4^3)/2] \cdot 10 = 2.96 \times 10^8$  numbers. Considering that these numbers are stored as (8 byte) double precision floating point numbers, the total storage requirement would be 2.368 gigabytes; this amount is very much storable in random-access memory.

Finally, to compute the central processing unit caching requirements, one can consider the storage of the all neighbour node data. If this data requirement exceeds the L1 cache of the CPU, a noticeable performance drop will ensue as it must load data from slower memory sources instead. For the above example, this would yield  $(4^3) \cdot 7 + [(4^3)/2] \cdot 10 = 480$  numbers, i.e. 3.84 kilobytes; this number is no match for the storage capabilities of modern L1 cache, which can handle upwards of 32 kilobytes<sup>83</sup>.

<sup>83</sup>Data retrieved from an actual Intel(R) Core(TM) i5-8257U CPU @ 1.40GHz.

Given this analysis, it is possible to say with due confidence that this particular implementation will be viable on existing hardware, and that performance will not be affected negatively on account of caching issues.

**Cost function** As told in the previous section, a value for the measure of performance is needed to perform an optimisation; this is done by means of a cost function. The main purpose of this function is to convert all of the values of interest as presented in Sec. 5.5.10 to a one-dimensional value using which the loss of performance can be determined; the lower this value, the higher the performance. The structure of the function follows as:

$$J = \mu_1 x_{\text{diff}} + \mu_2 \frac{1}{w} + \mu_3 T \quad (5.54)$$

The cost function is a mapping  $J : (\mathbb{R}^{17}, \mathbb{R}^6) \mapsto \mathbb{R}^1$ , as mentioned previously. It represents the three measures of performance as explained in Sec. 5.5.10. The difference between the attainable trajectory and the desired trajectory is represented as  $x_{\text{diff}}$ , and is given as the  $L^2$ -norm of the difference between the two acceleration vectors. As stated earlier, the inverted value for the manipulability should be taken into account, which yields a scalar value. The last value in question is the manoeuvring time. This value is the time needed to travel from one point to another, which is also scalar.

Not all of these three categories are equally important, and changing their relative importance will have a bearing on the ultimate simulator performance. For this reason, these three elements shall be scaled relative to each other. Therefore, in Eq. 5.54,  $\mu_1, \mu_2, \mu_3$  should be determined. These are determined on a heuristic basis, by performing multiple tests until the best compromise between training continuity and training precision is found. Note that these values will not lead to infeasible trajectories, as this is impossible per the discussion in Sec. 5.5.9.

**Sustained motion cueing seat integration** The robot arm has limited capabilities for g-loading. To cope with these limitations, a g-seat is introduced. During the movement planning of the robot arm, the g-seat is not taken into account until the last moment. In Fig. 5.22 this can be visualised in the "Point selection and command determination" block, as here the old state of the g-seat and robot arm will determine and flow to the new state of the robot arm and g-seat. During the whole desired movement and cost function process, the next state to be visited was determined. This point carries a certain acceleration on the cabin as well as a motion direction. However, as stated earlier, this will not meet the required values. To compensate for that, the g-seat will add to the motion. Note that the g-seat will simply *complement* the robot arm, since the actual motion cues will be preferred over the sensation generated by the g-seat. There is, however, one exception to this notion, which is the vibrational mode of the simulation. The robot arm itself cannot create the required modes of vibration, only the g-seat. So, as can be seen in Fig. 5.22, there is direct feed-through of the vibrational mode from the vehicle model to the "point selection and command determination" block where this value is scaled to the available and required motion of the g-seat.

### 5.5.11. Verification

Based on the previous section, the requirements as stated in Sec. 5.5.2 and Sec. 5.4.4 can be analysed by means of a requirement compliance matrix. Based on the research performed during this section also a rationale can be determined.

Note that the analysis given above was verified during the derivation, as shown by proofs in the text; therefore, further verification is not warranted. Instead, efforts are directed to requirement compliance verification and concept validation procedures.

Table 5.14: Motion system requirements compliance

Identifier	Compliance	Rationale
UPaRTS-SH-SO-16-VES	Verifiable	Verifiable by demonstration as the whole design of cueing is based around the point that the pilot receives it
UPaRTS-SH-SO-22-VES	Verified	Verified by demonstration since the robot arm can generate cues up to 1.3g, while the g-seat complements this with a minimum additional onset cue upwards of 0.7g (see Subsecs. 5.5.2, 5.5.3).
UPaRTS-SYS-05-VES	Verifiable	Verifiable by testing if all extended envelope states are known and the robot arm can handle all
UPaRTS-SYS-17-VES	Verifiable	Verifiable by demonstration, to be performed in a later stage of the design

Identifier	Compliance	Rationale
UPaRTS-CUE-VES-1	Verifiable	Verifiable by demonstration, to be judged by a suitable pilot once a prototype is constructed.
UPaRTS-CUE-VES-1.1	Not Verified	Not verified, but verifiable by analysis of the motion repeatability as provided in the manufacturer's specifications for the robot arm, linear unit, and g-seat.
UPaRTS-CUE-VES-1.2	Verified	Verified by demonstration, since the motion system is designed to provide attitude cues.
UPaRTS-CUE-VES-1.3	Verified	Verified by demonstration, since the motion system is designed to provide vibrational cues.
UPaRTS-CUE-VES-2	Verified	Verified by analysis, since the g-seat is capable of producing vibrations with frequencies up to 3.45 Hz (see Subsec. 5.5.3).
UPaRTS-CUE-VES-3	Verified	Verified by analysis, since the robot arm can generate cues up to 1.3g, while the g-seat complements this with a minimum additional onset cue upwards of 0.7g (see Subsecs. 5.5.2, 5.5.3).
UPaRTS-CUE-VES-4	Verified	Verified by analysis, since both the robot arm and g-seat possess enough motion control to produce cues lower than this (see Subsecs. 5.5.2, 5.5.3).
UPaRTS-CUE-VES-5	Verifiable	Verifiable by analysis, since this requires more in-depth analysis and access to detailed technical information to see if this accuracy is attainable.
UPaRTS-CUE-VES-6	Verified	Verified by analysis, since the robot arm is capable of generating roll rotations of up to $40^\circ \text{s}^{-1}$ on the J6 axis (see Subsec. 5.5.2).
UPaRTS-CUE-VES-7	Verified	Verified by analysis, since the robot arm is capable of generating pitch rotations of up to $20^\circ \text{s}^{-1}$ on the J5 axis (see Subsec. 5.5.2).
UPaRTS-CUE-VES-8	Verified	Verified by analysis, since the robot arm is capable of generating yaw rotations of up to $20^\circ \text{s}^{-1}$ on the J4/J5 axis (see Subsec. 5.5.2).
UPaRTS-CUE-VES-9	Verified	Verified by analysis, since the system is capable of producing a roll acceleration in excess of $34^\circ \text{s}^{-2}$ on the J6 axis (see Subsec. 5.5.2).
UPaRTS-CUE-VES-10	Verified	Verified by analysis, since the system is capable of producing a pitch acceleration in excess of $26^\circ \text{s}^{-2}$ on the J5 axis (see Subsec. 5.5.2).
UPaRTS-CUE-VES-11	Verified	Verified by analysis. For this requirement, the acceleration is to be considered. Assuming the pilot to be seated 18 metres <sup>78</sup> away from the CG, the required g-loading would be 1.12g. As mentioned previously, this can be attained by the motion platform.
UPaRTS-CUE-VES-12	Verifiable	Verifiable by analysis. This will be verified once detailed servo specification are available from the robot arm manufacturer.

### 5.5.12. Validation

Having considered requirement verification, it is now possible to consider what steps must be taken for a thorough concept validation. Owing to the fact that much of the information pertaining to robotic arms is proprietary, this information is not accessible at this stage in the project. While some research models exist for lower-grade robotic arms, such as the FANUC M900ib-700<sup>84</sup>, advances can be made in this direction by fully carrying out the analysis presented on this robot arm. Indeed, this is possible by using such robot analysis toolkits as the ROS MoveIt Motion Planning Framework<sup>85</sup>, and has been attempted. However, to be able to provide even a minor proof-of-concept, ample computational resources must be available; this is not the case for the present project.

To ROS MoveIt framework provides an interface that can readily be programmed to compute custom IK solutions, as shown in Fig. 5.23:

<sup>84</sup>G.A. van der Hoorn et al. ROS-Industrial package: `fanuc_m900ib_support`

[cited 2020-06-22]

<sup>85</sup>ROS MoveIt

[cited 2020-06-22]

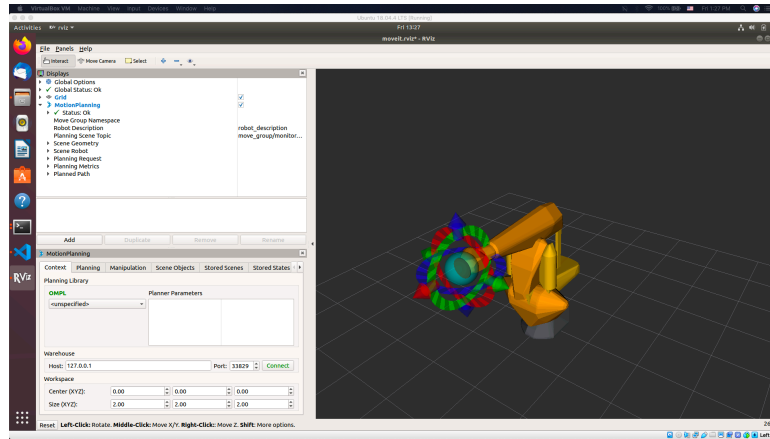


Figure 5.23: ROS MoveIt RViz interface with FANUC M900ib robotic arm

In validating the algorithm, an adequate test space must be constructed, for which each state is checked for feasibility using the `RobotModel` and `RobotState` classes provided by MoveIt in C++<sup>86</sup>. Then, the feasible motion space can be computed, including the corresponding joint states. These states can then be interpolated to compute the least-time motion and acceleration profiles between nodes, which will yield the requisite motion cueing information. Finally, the algorithm can on this database to plan ahead for a given desired motion trajectory.

In validating the model, a key point of attention is runtime and reaction time. It is desired that there is minimum lag between the point in time when a cueing command is issued, and when it is executed. This can be ascertained by running the code many times and retrieving measures on the worst-case execution time; this will give way for code refactoring as required by the cueing frequency. In addition, the quality of the outputted motion with reference to the commanded motion cues can be compared, thereby validating the quality of motion.

All of these tasks can be done in simulation prior to prototype testing, but require a validated physical model of the target robotic arm, which can be constructed in consultation with the manufacturer. Indeed, it is a known fact that FANUC is open to collaborate with customer on cutting-edge technologies<sup>87</sup>, making this a viable endeavour.

### 5.5.13. Sensitivity analysis

To fully grasp the effects of the analysis provided above, it is of importance to consider the sensitivity of the results to changes in the design parameters. If the vestibular cueing performance requirement were to be made less stringent, the result would be that the linear rail could be omitted, since proper washout can be achieved with the static robotic arm alone.

Overall, a reconsideration of safety margins and a greater insight into manufacturer's specifications would allow the design to use a lighter and more nimble robotic arm, which would translate in enhanced motion cueing capabilities. Note that this will not have an effect on the algorithm design, since this was made to work with any combination of robotic arm parameters. As a consequence, however, less reliance on the secondary cueing capabilities (linear rail and g-seat) may result, which would potentially make these elements obsolete.

In general, regardless of changes in cueing requirements or hardware, the motion cueing algorithm was designed to be robust enough to be able to function in any feasible situation; the only difference would be a change in overall performance. As far as computational efficiency goes, this is not compromised as a result of hardware changes. Hence, it is safe to say that the analysis above is insensitive to any feasible design changes.

## 5.6. Aural Cueing

Aural cueing is an essential part of providing the pilot with an accurate presentation of the aircraft's behaviour. Furthermore, it also allows communication between the pilot and the instructor/operator, the ATC and the other cockpit crew. This section starts with an expansion of the functional analysis performed in [1]. Next, this functional analysis is translated into aural subsystem requirements. Finally, the preliminary design of the subsystem is presented, verified and validated.

<sup>86</sup>MoveIt! Motion Planning Framework documentation: Robot Model and Robot State

[cited 2020-06-22]

<sup>87</sup>FANUC Corporation: Research & Development

[cited 2020-06-22]

### 5.6.1. Functional Analysis

The functions of the aural system that were determined in [1] are still considered as relevant for the preliminary design phase and can be seen on page 34 (FBS 2.3.4). However, this analysis must, due to the design choices made in [2] and Ch. 2, be expanded to finalise the requirements list for the preliminary design phase. A design choice that influences the aural system is the off-board positioning of the second pilot, which requires communication over a much longer distance (page 34 FBS 2.3.4.6). Furthermore, the aural system should be compatible with the visual system chosen in Sec. 5.7 (page 34 FBS 2.3.4.2). Also, since the motion system consists of a noise-producing robotic arm and rail system, the aural system should still be clearly audible by the pilot during training (page 34 FBS 2.3.4.4).

### 5.6.2. Requirement Analysis

Most of the requirements are directly translated from the functions determined in the previous subsection. However, some requirements are related to the established budgets, the risk assessment, the sustainability analysis or the other preliminary subsystem designs. Requirement UPaRTS-CUE-AUR-1.5 is changed into the more comprehensive requirement UPaRTS-CUE-AUR-2. The complete list of requirements for the aural system can be seen below:

<b>UPaRTS-SH-SO-01-AUR</b>	The aural system shall function continuously throughout the day with at most an hour of downtime. [50, §2.2, Req. 2.3]
<b>UPaRTS-SH-SO-18-AUR</b>	The aural system shall provide the instructor and pilot a platform such that briefing can take place before, during and after the training.
<b>UPaRTS-RSK-SYS-1-AUR</b>	The aural system shall use, where applicable, components that are standardised and used in other applications. [UPaRTS-SH-SO-10]
<b>UPaRTS-SYS-TRN-REC-1.3</b>	The aural system shall be able to provide the pilot voice after training. [UPaRTS-SYS-TRN-IO-1.3, RDT 1.4.3.1, FBS 2.1.6, FBS 3.1.2, IATA GMBP-UPRT 6.7.3]
<b>UPaRTS-SYS-TRN-SAF-1</b>	The operator shall have access to a communication line with the pilot at all times and vice versa. [UPaRTS-SH-SO-12, FBS 2.1.2, RDT 1.4.2.1, IATA GMBP-UPRT 13.3.2]
<b>UPaRTS-CUE-AUR-1</b>	The aural system shall provide realistic aural cues as judged by a suitable pilot. [UPaRTS-SH-SO-16, UPaRTS-SYS-14, FBS 2.3.4, RDT 1.2.4, AMC1 FSTD(A).300.b.4.v]
<b>UPaRTS-CUE-AUR-1.1</b>	The aural system shall provide warning sounds on the flight deck. [FBS 2.3.4.1.1, RDT 1.2.4.1.1, AMC1 FSTD(A).300.b.4.v.A]
<b>UPaRTS-CUE-AUR-1.1.1</b>	The aural system shall provide warning sounds rising above the cabin noise threshold with at least 15dB. [[51]]
<b>UPaRTS-CUE-AUR-1.2</b>	The aural system shall provide LOC/failure sounds. [FBS 2.3.4.1.2, RDT 1.2.4.1.2, AMC1 FSTD(A).300.b.4.v.A]
<b>UPaRTS-CUE-AUR-1.3</b>	The aural system shall provide engine noise. [FBS 2.3.4.2, RDT 1.2.4.2, AMC1 FSTD(A).300.b.4.v.B]
<b>UPaRTS-CUE-AUR-1.4</b>	The aural system shall provide background noise, including airframe noise. [FBS 2.3.4.4 RDT 1.2.4.3, AMC1 FSTD(A).300.b.4.v.F]
<b>UPaRTS-CUE-AUR-1.5</b>	The pilot shall be able to receive communication from the trainer/operator. [UPaRTS-SYS-6, FBS 2.3.4.4, RDT 1.2.4.4, AMC12 FSTD(A).300.c.1]
<b>UPaRTS-CUE-AUR-1.6</b>	The aural system shall provide correctly perceived audio source location during head movement of the pilot. [Subsec 2.1,[2]]
<b>UPaRTS-CUE-AUR-2</b>	The aural system shall allow communication between the pilot and the trainer/operator. [UPaRTS-SYS-6, UPaRTS-SYS-TRN-SAF-1, FBS 2.3.4.4, RDT 1.2.4.4, AMC12 FSTD(A).300.c.1]
<b>UPaRTS-CUE-AUR-3</b>	The aural system shall allow communication between the pilot and the ATC. [UPaRTS-SYS-6, FBS 2.3.4.5, AMC12 FSTD(A).300.c.1]
<b>UPaRTS-CUE-AUR-4</b>	The aural system shall allow communication between the pilot and the off-board pilot. [UPaRTS-SH-SO-15, UPaTS-FUN-CUE-AUR-1, [2]]
<b>UPaRTS-CUE-AUR-5</b>	The aural system shall be compatible with <TBD> VR glasses. [Sec. 5.7]
<b>UPaRTS-CUE-AUR-6</b>	The aural on-board system shall not use more power than is feasible to supply. [UPaRTS-SH-SO-08, Sec. 2.4]
<b>UPaRTS-CUE-AUR-7</b>	The aural on-board system shall not weight more than 10 kg . [UPaRTS-SH-SO-11, Sec. 2.4]

**UPaRTS-CUE-AUR-8**

The aural system shall not exceed average sound pressure level of 85dB when the pilot is trained for a duration of maximum 2 hours. [UPaRTS-RSK-SAF-3, <sup>88</sup>]

**5.6.3. Sizing**

The sizing of the aural system will be done with a close relation to the requirements listed in the previous section. From the aural system requirements, two main objectives can be derived. The first objective is providing the pilot with flight sounds, which will be done with a speaker system in the cabin. The second objective is providing a communication line between the instructor/ATC, the pilot and the second pilot, for this, the pilot will wear a headset.

**Noise and Sound Pressure Levels**

In order to determine the required sound pressure level (SPL) of the aural system, the noise levels experienced by the pilot must be determined first. This noise will include among other noise, noise induced by the building, noise produced outside the building, noise produced by the computers (fans), noise from the air-conditioning, noise by riding the rail system and the noise of the motion of the robotic arm. Since not yet all the components of the system (simulator, IOS, building) are known, the assumption is made that the noise experienced in the cabin will be equal to noise comparable to a large office, noise induced by the robotic arm and noise induced by the rail system. The noise level of a large office will be 50 dB<sup>91</sup>. The noise produced by the robotic arm will be 72.8 dB, measured for maximum load and speed, according to ISO11201 (EN31201)<sup>89</sup>. The rail system will produce a maximum noise level of 75 dB<sup>90</sup>. Finally, with the assumption that the cabin will isolate the pilot with a value of 20 dB, which is less isolation than a single windowpane would achieve (assuming leakage due to the ventilation holes), the noise level in the cabin due to the environment can be calculated with Eq. 5.55<sup>92</sup>.

$$L_{\text{cabin,environment}} = 10 \log \left( 10^{\frac{L_{\text{building}}}{10}} + 10^{\frac{L_{\text{roboticarm}}}{10}} + 10^{\frac{L_{\text{rail}}}{10}} \right) - I_{\text{cabin}} = 57 \text{ dB} \quad (5.55)$$

The required SPL for the flight sounds (excluding warning sounds) can be determined next. In order to clearly hear these sounds, the sound level must be at least 15 dB higher than the environmental noise level experienced in the cabin<sup>93</sup>. The required SPL is calculated with Eq. 5.56.

$$L_{\text{flightsounds}} = L_{\text{cabin,environment}} + 15 \text{ dB} = 72 \text{ dB} \quad (5.56)$$

The warning sounds will be considered as the limiting case for the aural system. In order to determine the required SPL for the warning sounds, the noise level due to the environment and the flight sounds must be considered first with Eq. 5.57.

$$L_{\text{cabin,flight}} = 10 \log \left( 10^{\frac{L_{\text{cabin,environment}}}{10}} + 10^{\frac{L_{\text{flightsounds}}}{10}} \right) = 72 \text{ dB} \quad (5.57)$$

The SPL of the warning sounds must also be at least 15 dB higher than the sound level experienced in the cabin during training in the simulator. Finally, the required SPL of the warning sounds, and so the aural system, can be determined with Eq. 5.58.

$$L_{\text{warning}} = L_{\text{cabin,flight}} + 15 \text{ dB} = 87 \text{ dB} \quad (5.58)$$

This SPL is easily reached by available headsets on the market today, as these headsets are able to reach an SPL of 110 dB<sup>94</sup>. However, the headset will not be used for representing the warning sounds; this will be done by the speaker set. The SPL that is produced by the different speaker sets available on the market is often provided on the website or datasheet. However, since there is no industry standard in measuring SPL, comparing speaker sets of different manufacturers should be kept to a minimum. For now, the provided SPL will only be used to determine whether the speaker set will reach the required SPL. In addition, better cabin isolation is highly recommended for future iterations, as this will reduce the noise levels experienced in the cabin and so also the number of false cues experienced by the pilot. Note that this may require omission of the current ventilation holes which will result in the need of an actual onboard air-conditioning, which of course, must fit within the mass and power budgets. This will also contribute, besides the better isolation, to an

<sup>88</sup>cdc.gov: What Noises Cause Hearing Loss?

[cited 2020-06-21]

even more realistic aural experience, since this air-conditioning is also present in cockpits of real aircraft.

### Audio Transmission and Connections

As mentioned earlier in this section, the aural subsystem will consist of multiple components and audio channels, distributed over the different sections of the simulator with several meters between them. All these components must be connected, which will be done with either a wired or a wireless connection, the wired connections can be analogue or digital.

The analogue connections are based on the principle of transmitting electric signals and transmit audio with good quality and with no noticeable latency. These connections can be balanced or unbalanced. Unbalanced connections consist of a signal wire and a ground wire, this ground wire easily picks up other (power) signals which will interfere with the original audio signal. Therefore unbalanced connections are not suitable for use over long distances. Balanced connections consist of two signal wires, which transmit the signal with the opposite sign, and a ground wire. The noise picked up by the wires is cancelled out due to the reversed polarity of the signals and is therefore suited for use over distances that can go beyond 50 m. However, only one audio channel can be transmitted per cable, so multiple cables for going into the cabin is required for this solution.

Wired, digital audio transmission can be done by optical, USB, HDMI, coaxial or Ethernet connections. All these connections are able to transmit multiple high-quality audio channels without any noticeable latency and interference by other signals. However, there is a limit in the distance where these connections can transmit the signal. For optical, HDMI and coaxial cables the signal will be lost over a distance of about 10 m, for USB this distance will even be around 5 m<sup>95</sup>. This problem can be prevented by introducing several signal extenders, but each extender individually will need a power supply, which will lead to a cumbersome system. On the other hand, Ethernet connections are able to transmit audio signals over distances up to 100 m without the use of extenders<sup>96</sup>. This type of connection will, therefore, be very suitable for use in the aural subsystem for this simulator.

Finally, there is also an option to use wireless audio transmission. Relevant wireless solutions are Bluetooth or WiFi. Both these options will provide high-quality multi-channel audio transmission. However, the reach of both these options will be questionable and very dependent on the situation and will, therefore, introduce a high design risk<sup>98</sup>. Furthermore, the signals transmitted by Bluetooth can easily be interfered by other signals like WiFi. Also, WiFi systems that are available on the market today, are still not stable for 100% of the time. In addition, both options will introduce much more latency than wired connections<sup>99</sup>. Therefore, it can be concluded that the most suitable audio transmission option for the simulator will be wired, digital audio transmission by Ethernet connections.

This digital audio transmission by Ethernet connections is called Audio over Ethernet, and is provided by several systems. The system that is considered as the de facto standard is Dante (Digital Audio Network Through Ethernet) by Audinate<sup>97</sup>. This system is supported by a broad range of audio interface manufacturers and is very easy to set up and use. This system also allows the aural system to be extendable and upgradeable. For these reasons, Dante will be the best option for audio transmission.

### Layout and Components

In this section, the layout and components of the preliminary aural system are described. The off-the-shelf components chosen in this design stage are used to give a detailed estimation of the cost, weight and power of the system and is open to change in a later design stage. The Dante aural system will be connected by Ethernet cables, Audinate recommends the use of either CAT5E or CAT6 cables<sup>100</sup>. The cables coming from the different components of the aural system must be connected with an Ethernet switch. This Ethernet switch requires Power over Ethernet, which will be explained later in this section, and must have enough ports to connect all components of the aural system. A switch that satisfies these requirements is the Netgear ProSafe GS108PE and is used in the preliminary design of the aural system<sup>103</sup>. This Ethernet switch can be best positioned

<sup>89</sup>robot-store.co.uk: FANUC M-2000iA Operator Manual

[cited 2020-06-11]

<sup>90</sup>gudel.picturepark.com: TMF-6

[cited 2020-06-11]

<sup>91</sup>chcheating.org: Common environmental noise levels

[cited 2020-06-11]

<sup>92</sup>Soundproofwindows.com: What STC Ratings do Windows Have?

[cited 2020-06-11]

<sup>93</sup>www.icben.org: Optimal installation of audible warning systems in the noisy workplace

[cited 2020-06-11]

<sup>94</sup>audiorecovery.com: HEADPHONES AND YOUR RISK OF HEARING LOSS

[cited 2020-06-11]

<sup>95</sup>showmecables.com: Cable Distance Limits - Audio/Video

[cited 2020-06-12]

<sup>96</sup>showmecables.com: Cable Distance Limits - Data

[cited 2020-06-12]

<sup>97</sup>Audinate.com

[cited 2020-06-12]

<sup>98</sup>audiogurus.com: Bluetooth Audio

[cited 2020-06-12]

<sup>99</sup>aptx.com: Qualcomm® aptX™ Low Latency

[cited 2020-06-12]

off-board since the main processing unit is also located off-board, this will lead to only one Ethernet cable going up to the cabin.

**IOS** The aural system will be controllable from the IOS with the help of a combination of Audinate software installed on the IOS computer. The Dante Virtual Soundcard software is a virtual audio interface that enables connection with the Dante network. Furthermore, this software allows the system to record each audio channel connected to the Dante network. The Dante Controller software is used by the instructor to easily manage where the audio channels need to go. In addition to the software, hardware audio components are also needed in the IOS. In order to record the instructor's voice, the AKG DST 99 S microphone is used<sup>108</sup>. This microphone uses phantom power (very low amounts of power), which will be provided by the Neutrik NA2-IO-DLINE audio interface<sup>104</sup>. This audio interface connects the microphone to the Dante network and receives its power through the Ethernet cable from the Ethernet switch. The audio interface will also be connected with XLR cables to Adam A5X active monitor speakers to provide the instructor with the flight crew voice and flight sounds if desired<sup>31</sup>. Active monitor speakers have built-in amplifiers and are therefore flexible in setup. This model monitor speakers can be turned on at the front side and can be placed close to the walls due to the front-sided bass ports.

**(Off-board) Cabin** The components of the aural system located in the cabin will be identical to the components located in the off-board cabin. The Audio-Technica ATH-G1 headset is used for recording the pilot's voice and for playing the instructor's/ATC's voice<sup>106</sup>. This headset can be worn over the VR glasses determined in Sec. 5.7. This headset is also included with volume control on the cord, making an extra headphone controller unnecessary. This headset will be connected to the Dante network and provided with phantom power with the help of the analogue input and output of the Neutrik NA2-IO-DPRO audio interface<sup>105</sup>. This audio interface also includes a digital output, which is used to connect the speaker system to the Dante network. The Logitech Z906 5.1 surround sound speaker system is used for the preliminary design because it is able to reach an SPL of 110 dB and allows the audio to be sourced from 5 different locations<sup>110</sup>. The power used by the speaker system will be dependent on the output volume and will not be equal to the value listed by the manufacturer. The Logitech Z906 5.1 speaker set has a listed power of 500 W, however, the assumption can be made that the maximum of 500 W will not be reached during operation and therefore the estimated power for the speaker system is assumed to be at most 150 W. In a later design stage of the aural system, the use of a semi customised (built-in) speaker set is recommended to be able to source the audio from more than 5 locations and create a 3D instead of 2D audio experience.

**Main Computer** The system main computer will output the flight sounds in the digital audio format. To send these sounds to the Dante network and therefore the flight crew, either a build-in Dante interface or an external Dante interface is required. With the assumption that the system main computer can output these sounds via USB, the comparatively cheaper external Dante Avio USB interface is chosen<sup>109</sup>.

A complete overview of the aural system components can be seen in Tab. 5.15. The required onboard power will be 150 W and the total onboard mass of the system will be 9.8kg. The total costs of the aural system is estimated at approximately 4200 EUR. Note that some of the components can be replaced by cheaper ones, however, if the speaker set used in the cabin is replaced by a semi custom, built-in speaker set, this will most likely be more expensive.

Table 5.15: Aural System Components

Model	Type	Location	Weight	Power	Cost
<b>2x Neutrik NA2-IO-DPRO</b> <sup>105</sup>	Interface	Cabin, Off-board cabin	0.5 kg	Power over Ether- net	798 EUR
<b>2x Audio-Technica ATH-G1</b> <sup>106</sup>	Headset	Cabin, Off-board Cabin	0.3 kg	Phantom Power	189 EUR
<b>2x Logitech Z906</b> <sup>110</sup>	5.1 Speakerset	Cabin, Off-board Cabin	9 kg	150 W	399 EUR
<b>Onboard Aural System Total</b>			9.8 kg	150 W	1386 EUR
<b>Dante Controller</b> <sup>101</sup>	Control Software	IOS Computer	-	-	0 EUR
<b>Dante Virtual Soundcard</b> <sup>102</sup>	Interface Software	IOS Computer	-	-	27 EUR
<b>2x Adam A5X</b> <sup>107</sup>	Monitor Speakers	IOS	6.4 kg	130 W	362 EUR
<b>Neutrik NA2-IO-DLINE</b> <sup>104</sup>	Interface	IOS	0.4 kg	Power over Ether- net	269 EUR

Model	Type	Location	Weight	Power	Cost
<b>AKG DST 99 S</b> <sup>108</sup>	Microphone	IOS	0.8 kg	Phantom Power	139 EUR
<b>Dante AVIO USB</b> <sup>109</sup>	Interface	Main Processor	0.2 kg	Power over Ethernet	129 EUR
<b>Netgear ProSafe GS108PE</b> <sup>103</sup>	Ethernet switch	TBD	0.5 kg	53 W	86 EUR
<b>5x UTP Cat5e 20M</b> <sup>111</sup>	Ethernet Cable	-	1 kg	-	10 EUR
<b>Aural System Total</b>			1 kg	463 W	4196 EUR

### 5.6.4. RAMS

As it is very important that the flight crew and the instructor can communicate throughout the entire training, the aural system should be reliable. It is virtually impossible to quantify how reliable a Dante system is, but if all components of the system are assessed separately, the software running on the IOS computer will likely be the limiting factor. Fortunately, all routes and settings are stored on the hardware interfaces, which allows the aural system to work even when the IOS computer or software crashes. This feature also contributes to the availability of the system, the system does not need to be set up again when starting up the simulator. Even when the power cuts off suddenly, the system will work immediately as before. The components used in the aural system will need very little maintenance and can easily be replaced when defect. The Ethernet cable connecting the cabin with the system will most likely wear out first due to the continuous movement. If an Ethernet slip ring is needed, it will also experience wear. However, due to the limited rotations and speed of the simulator, a long lifetime of the slip ring is expected. The aural system will mainly consist of off-the-shelf components, probably only the speaker system will be semi customised for the final design. Therefore, there is no need to worry about manufacturing the system. In terms of safety, only the produced sound pressure levels can lead to hearing loss. This problem can be eliminated by correctly managing the sound level limits.

### 5.6.5. Verification

Since only straightforward, simple mathematical analyses are performed in this section, the verification of these calculations is done by performing the calculations by hand. In addition, the weights and costs of each individual component sourced from the footnotes have been checked through multiple sources. Finally, in Tab. 5.16, the requirement verification provided with rationale can be seen for the requirements mentioned in Subsec. 5.6.2. Some of the requirements could already be verified, the other requirements will be verifiable in a later stage of the design.

Table 5.16: Aural requirements compliance

Identifier	Compliance	Rationale
<b>UPaRTS-SH-SO-01-AUR</b>	Verifiable	Verifiable by demonstration when operational prototype is developed
<b>UPaRTS-SH-SO-18-AUR</b>	Verified	Verified by analysis of design decisions: Provided by the pilot's headset, the IOS microphone and speakers and the Dante network.
<b>UPaRTS-RSK-SYS-1-AUR</b>	Verified	Verified by analysis of design decisions: Almost all components of the aural system are standardised and used in other applications
<b>UPaRTS-SYS-TRN-REC-1.3</b>	Verified	Verified by analysis of design decisions: Dante Virtual Soundcard allows recording of each channel connected to the network
<b>UPaRTS-SYS-TRN-SAF-1</b>	Verified	Verified by analysis of design decisions: Provided by the pilot's headset, the IOS microphone and speakers and the Dante network
<b>UPaRTS-CUE-AUR-1</b>	Verifiable	Verifiable by test when operational prototype is developed

<sup>100</sup>Audinate.com: Networks and Switches

[cited 2020-06-12]

<sup>101</sup>Audinate.com: Dante Controller

[cited 2020-06-12]

<sup>102</sup>Audinate.com: Dante Virtual Soundcard

[cited 2020-06-12]

<sup>103</sup>Coolblue.nl: Netgear ProSafe GS108PE

[cited 2020-06-12]

<sup>104</sup>thomann.de: Neutrik NA2-IO-DLINE

[cited 2020-06-12]

<sup>105</sup>thomann.de: Neutrik NA2-IO-DPRO

[cited 2020-06-12]

<sup>106</sup>amazon.nl: Audio-Technica ATH-G1 Premium gaming-headset

[cited 2020-06-12]

<sup>107</sup>thomann.de: Adam A5X

[cited 2020-06-12]

<sup>108</sup>thomann.de: AKG DST 99S

[cited 2020-06-12]

<sup>109</sup>thomann.de: Dante Avio USB

[cited 2020-06-12]

<sup>110</sup>logitech.com: Z906

[cited 2020-06-12]

<sup>111</sup>Allekabels.nl: U/UTP-kabel CAT 5e - 20 meter

[cited 2020-06-12]

Identifier	Compliance	Rationale
UPaRTS-CUE-AUR-1.1	Verifiable	Verifiable by demonstration when operational prototype is developed
UPaRTS-CUE-AUR-1.1.1	Verifiable	Verifiable by demonstration when operational prototype is developed
UPaRTS-CUE-AUR-1.2	Verifiable	Verifiable by demonstration when operational prototype is developed
UPaRTS-CUE-AUR-1.3	Verifiable	Verifiable by demonstration when operational prototype is developed
UPaRTS-CUE-AUR-1.4	Verifiable	Verifiable by demonstration when operational prototype is developed
UPaRTS-CUE-AUR-1.5	Changed	Included in UPaRTS-CUE-AUR-2
UPaRTS-CUE-AUR-1.6	Verified	Verified by analysis of design decisions: Fixed speaker system used in the cabin
UPaRTS-CUE-AUR-2	Verified	Verified by analysis of design decisions: Provided by the pilot's headset, the IOS microphone and speakers and the Dante network
UPaRTS-CUE-AUR-3	Verified	Verified by analysis of design decisions: Provided by the pilot's headset, the IOS microphone and speakers and the Dante network
UPaRTS-CUE-AUR-4	Verified	Verified by analysis of design decisions: Provided by the pilot's headset, the off-board pilot's headset and the Dante network
UPaRTS-CUE-AUR-5	Verifiable	Verifiable by analysis when final VR glasses are chosen
UPaRTS-CUE-AUR-6	Verifiable	Verified by analysis of design decisions: On-board system total power will never exceed the maximum value of 4kW as determined in Subsec. 5.3.6
UPaRTS-CUE-AUR-7	Verified	Verified by analysis of design decisions: On-board system total mass of 9.8kg
UPaRTS-CUE-AUR-8	Verifiable	Verifiable by demonstration when operational prototype is developed

### 5.6.6. Validation

In order to validate the speaker set power usage assumption, a small measurement is taken. An estimation of the average power usage when playing flight and warning sounds at a sound pressure level of 87dB at a distance of 1m from the speakers is determined with a power usage monitor and a decibel monitor. This resulted in power usage of less than 20 W, while the used monitor speaker has a RMS of 150 W. This can not be translated to the Logitech Z906 5.1 speaker set, which has an RMS of 500 W, however, it is in line with the assumption that the maximum of 500 W will indeed not be reached during operation and shows that the budgeted power of 150 W is still conservative.

The use of Dante audio systems in applications similar to FSTDs is not yet reported as proven, however, the SIMONA simulator of the TU Delft is currently in the process of switching to a system based on Dante[52]. Furthermore, the use of Dante audio systems is already shown as proven in many other, larger and more complicated systems like recording studios, stadiums, universities and conference centres<sup>112</sup>.

### 5.6.7. Sensitivity Analysis

The aural system is reliant on several subsystems, among others the main processor and the visual system. If changes are applied to these subsystems, the aural system will most likely also be subjected to changes. Fortunately, the aural system is very easy to adjust and single components can be changed or replaced while the overall system can remain the same. As a result of this, only small changes to the mass, power and cost will occur during later design stages and a total redesign of the aural system will not be necessary.

## 5.7. Visual Cueing

To provide the pilot with the sense that he or she is truly flying an aircraft, one of the essential senses to fool is vision. By choosing VR as the solution to the problem of simulating visuals, this introduces the additional hurdle of having to simulate not just the environment but also the inside of the cabin, alongside several other challenges. This chapter describes the process of sizing the visual system of the simulator to tackle these problems in an effective and satisfactory manner.

<sup>112</sup>audinate.com: What is Dante?

[cited 2020-06-14]

### 5.7.1. Functional Analysis

The main functions that the visual cueing system should provide are listed below [1]. The functions related to what the visual cues should show the pilot are rather straightforward (2.3.1, 2.3.1.1, 2.3.1.1.2, 2.3.1.2) as these depend on the outputs of the simulation model. Another part of the visual cueing functions, are the ones connected to immersiveness (2.3.1.1.3-5, 2.3.1.3-4) as this will directly translate into training quality. Lower levels of these functions are described in page 34.

### 5.7.2. Requirement Analysis

In order to fulfil these functions a set of requirements was derived. These are listed below. Note that the rationales refer to [1].

- UPaRTS-SYS-CUE-VIS-1** The system shall provide realistic visual cues equivalent to an EASA Level D flight simulator, as judged by a suitable pilot. [[50, Section 2.2, Req. 1.2], UPaRTS-SH-SO-16, FBS 2.3.1, RDT 1.2.1, AMC1 FSTD(A).300.b.3.4]
- UPaRTS-SYS-CUE-VIS-1.1** The system shall provide realistic visual representations of scenery as judged by a suitable pilot. [FBS 2.3.1.1, RDT 1.2.1.1, AMC1 FSTD(A).300.b.3.4]
- UPaRTS-SYS-CUE-VIS-1.2** The system shall provide realistic visual representations of instruments relevant during the training exercise as judged by a suitable pilot. [UPaRTS-SYS-14, FBS 2.3.1.2, FBS 2.3.1.3, RDT 1.2.1.2, AMC1 FSTD(A).300.b.3.4]
- UPaRTS-SYS-CUE-VIS-1.3** The system shall provide realistic visual representations of controls relevant during the training exercise as judged by a suitable pilot. [UPaRTS-SYS-14, FBS 2.3.1.2, FBS 2.3.1.3, RDT 1.2.1.3, AMC1 FSTD(A).300.b.3.4]
- UPaRTS-SYS-CUE-VIS-1.4** The system shall provide realistic visual representations of runway attributes as judged by a suitable pilot. [FBS 2.3.1.1, FBS 2.3.1.3, RDT 1.2.1.4, AMC1 FSTD(A).300.b.3.4]
- UPaRTS-SYS-CUE-VIS-1.5** The system shall provide sufficient graphical fidelity as judged by a suitable pilot. [FBS 2.3.1.4, RDT 1.2.1.5, AMC1 FSTD(A).300.b.3.4]
- UPaRTS-SYS-16-VIS** The system shall not cause more motion sickness than an equivalent upset in a real aircraft. [Social Sustainability ([1] Ch. 4)]
- UPaRTS-RSK-SAF-3-VIS** The system shall not induce adverse health effects due to prolonged use. [[1] Subsec. 3.3)]
- UPaRTS-RSK-SAF-3.1-VIS** The system shall keep unintentional nauseating effects to a minimum. [[1] Subsec. 3.3)]

Most of these requirements can directly be linked to the functions above (see rationale at the end of each requirement). Requirement UPaRTS-SYS-16, however, stems from social sustainability rather than system functions. One of the main challenges is to avoid motion sickness which can be caused by a slight offset between the different cues. The risk of motion sickness is also reflected in the risk requirements UPaRTS-RSK-SAF-3 and UPaRTS-RSK-SAF-3.1. Furthermore, the term adverse health effects is used in UPaRTS-RSK-SAF-3 to also cover the possibility of eye strain due to prolonged use of the VR system. Note that these are not cutoff requirements as most have them are 'judged by a suitable pilot', hence they inherently have some subjectivity.

### 5.7.3. Sizing

Before starting to size the visual system, a simplified N<sup>2</sup> chart has been created to see the effects of possible design changes on other subsystems (Fig. 5.24). From the N<sup>2</sup> chart one can see that the structure and motion cueing (vestibular) are mainly affected by the visual

	- G-forces - Vibrations	- G-forces - Vibrations	- G-forces - Moment arms - Vibrations	- Power - Moving parts
- Mass - Mass moment of inertia	<b>Visual</b>	- Volume - Mass	- Mass	- Power
- Mass - Mass moment of inertia		<b>Cabin structure</b>	- Mass - Dimensions - Mass moment of inertia	
- Mass - Mass moment of inertia	- Cabin mass budget	- Cabin mass budget	<b>Outside structure</b>	- Moving parts
- Power budget	- Onboard power budget	- Power transfer	- Power transfer	<b>Power Supply</b>

Figure 5.24: N<sup>2</sup> chart containing only the subsystems that share an input/output with the visual system [2].

system's mass and size. This was a primary concern when large visual systems such as the colimated display with projectors were being considered. Now that the comparably light VR glasses have been chosen this concern is less of an issue. The same holds for the power budget, as VR glasses need far less power than large displays or projectors. Sizing the VR glasses will hence be more constrained by visual fidelity and immersiveness set by the requirements as by the mass and power budgets. The goal for this subsection should therefore be to find the VR glasses which can display the most realistic outside world and to reduce offset cues as much as possible to avoid nauseating effects.

**VR glasses** Now then, from the preceding discussion it can be concluded that the only budget that is relevant for the VR glasses anymore is the cost budget: its power draw and mass are not significant in the overall picture, and therefore it does not make sense to trade off either of those for an increase in cost. Additionally, the subjectivity of the relevant requirements (see Subsec. 5.7.2) means that no strict cut-off exists, and the best way to guarantee satisfactory compliance with these requirements is to find the "best" VR system in the given cost budget range. Hence, design turns from a trade-off in all three of the aforementioned budgets into an optimisation: which visual system performs the best within the given budget?

A short list of the high-end VR glasses which best fit this case is presented in Tab. 5.17. More familiar names like the Oculus Rift or the regular HTC Vive are not considered as they do not present the high-end performance that is sought after.

Table 5.17: VR glasses

	STARVR ONE <sup>113</sup>	VR-2 Pro <sup>114</sup>	Vive Pro Eye <sup>115</sup>	Pimax 8K PLUS <sup>116</sup>
<b>Eye-tracking</b>	Yes	Yes	Yes	Yes (optional module)
<b>Resolution per eye</b>	1830x1464	1920x1080	1440x1600	2560x1440
<b>Refresh rate</b>	90Hz	60 – 90Hz	90Hz	90Hz
<b>Field of view</b>	210° Hor. 130° Ver.	87° Hor. 87° Ver. <sup>117</sup>	150° Hor. 110° Ver. <sup>118</sup>	170° Hor. 130° Ver. <sup>119</sup>
<b>Price</b>	3200 USD <sup>120</sup>	5995 EUR	1439 EUR	1200 USD <sup>121</sup> 122

An additional concern in the immersion of the pilot might be the cables associated with today's VR headsets. While some wireless VR headsets do exist, those are not part of the high-end market and serve mostly as a platform for watching films rather than high-end gaming or simulation. While the lack of a cable means that the wearer is not bothered by it, it also introduces the problems of latency and battery life, meaning that a spare system must be bought so that systems can be used in rotation. Latency has the added negative of the possibility of motion sickness presenting itself as a side-effect, as well as generally making the experience less immersive. Through proper guiding of the cable and due to the limited pilot motion (within the cabin), it is also very much possible to mitigate the hindrance the cable causes. The added benefit of not needing batteries and not suffering from increased latency means that this mitigation strategy is preferred, and only cabled VR glasses are considered.

One way to differentiate between the VR-glasses is to decide to include eye-tracking technology that the instructor could use to assess the training. This technology can be a very useful addition to the instructor's training guide, as laid out in Subsec. 4.3.2. It allows the instructor to see in real time what the trainee is looking at, and complements the information given by the cameras present within the cabin to a great extent. This is done by feeding the position of the point that the pilot is focusing on to AR glasses that the instructor is wearing. A lot of effort is invested in the immersion of the pilot to trigger a startle effect. This effect occurs when a pilot is under physical and mental shock, as would be experienced in a real life upset. Under these high pressure scenarios, it

<sup>113</sup>STARVR ONE

[cited 2020-06-11]

<sup>114</sup>VR-2 Pro

[cited 2020-06-11]

<sup>115</sup>Vive Pro Eye

[cited 2020-06-11]

<sup>116</sup>Oculus Rift S

[cited 2020-06-12]

<sup>117</sup>Field of view VR-2 Pro

[cited 2020-06-12]

<sup>118</sup>Field of view Vive Pro Eye

[cited 2020-06-12]

<sup>119</sup>What Makes Pimax So Immersive?

[cited 2020-06-12]

<sup>120</sup>STARVR ONE price

[cited 2020-06-11]

<sup>121</sup>Pimax 8kx

[cited 2020-06-12]

<sup>122</sup>Road to VR: Pimax Details Upcoming Accessories – Price, Launch Date & More

[cited 2020-06-12]

is important for the pilot to focus his attention on the instruments that are most relevant (dependent on the type of upset). When debriefing the pilot, the instructor can tell him where he should have looked at to react in the most appropriate way<sup>123</sup>. In a sense, eye-tacking technology improves the instructor's immersion during the training and one could argue that to provide the best possible feedback, the instructor needs to have good knowledge of what the pilot has been through during training. While the video feeds from the cabin to the IOS help build this knowledge, the eye tracking technology proves invaluable in the case of a virtual cockpit. As seen in Tab. 5.17, only VR-glasses that have the eye tracking technology implemented are considered, because the technology is deemed a valuable addition not just in upset recovery, but especially upset prevention. Much like student drivers are taught to check their mirrors often to prevent them from getting in accident scenarios in the first place, so too could this technology help teach pilots to check their instruments often and correctly to prevent an upset from every developing at all.

All VR-glasses compiled in Tab. 5.17 are compatible with the eye tracking technology and have high screen resolutions (per eye) and refresh rates, so as not to amplify the nauseating effects. The VR-2 Pro has a comparatively small field of view compared to its counterparts which is deemed detrimental in this case, where immersion plays a central role, as the human field of vision covers approximately 188°, of which roughly 114° is binocular [53]. Hence, in order to display peripheral areas, one needs a larger field of view than the VR-2 offers. In terms of cost and performance, the logical choice are the Pimax 8K PLUS VR glasses because they are the cheapest without compromising any of the technical aspects. The STARVR ONE does outperform the Pimax 8K PLUS in terms of field of view but its price is not within the budget allocated to the visual system (Sec. 3.5). The Varjo VR-2 offers a denser resolution in the glasses' focus, but the Pimax offers roughly  $\frac{2 \cdot 2560}{170} \approx 31.1$  pixels per degree (PPD). It can thus be inferred that in the pilot's focus, at one metre of distance (roughly their distance to the instruments), they will be able to distinguish lengths of up to  $2 \tan\left(\frac{PPD}{2}\right) \approx 0.6$  mm, which should be sufficient to read the text on the displays. Hence, the reduced FOV<sup>2</sup> that the VR-2 offers is deemed more of a disadvantage than the advantage that the increased focal resolution offers.

In the interest of time, the visual systems for the IOS are not tackled in this report. Primarily because they are not very sensitive to design changes. The onboard systems are more critical and hence sizing is focused around these.

To conclude, mass and power were not parameters that were used to perform a trade-off; nevertheless, they will contribute to the respective budgets. The Pimax 8K Plus only weighs 0.5 kg<sup>124</sup> and consumes at most 24 W (the FCC test report describes using a 12 V, 2.0 A DC adapter<sup>125</sup>, while coming in at a price of 1200 USD; therefore roughly 1200 EUR is set aside for the glasses in the budget (to account for shipping etc.).

#### 5.7.4. RAMS

To ensure smooth operation of the visual system, a RAMS (Reliability, Availability, Maintainability, Manufacturability and Safety) analysis is presented hereby. In terms of reliability, the VR-glasses are consumer-grade which warrants at least two years of operation by European law. This is of course not guaranteed, but luckily it is easy to have spare VR-glasses ready to swap in case of a malfunction. The VR-glasses are relatively inexpensive compared to the entire simulator, hence having spare parts boils down to the availability of the Pimax 8K PLUS on the market. Note that a multitude of VR-glasses would be compatible with the flight simulator, hence its use does not depend on the availability of the Pimax 8K PLUS specifically; the VR-glasses can be readily swapped with other models at any given moment in time with a minimal amount of setup given the plug and play nature of such devices. The maintenance and manufacturing aspect of the visual system is greatly simplified by use of these same off-the-shelf components. Maintenance comes down to replacing the glasses with the spare model and manufacturing does not need to be done by this team. The safety aspect is mainly addressed in Subsec. 7.2.3; the biggest two concerns are the time delay caused by having to remove the VR-glasses and the resulting disorientation during a calamity and eye strain due to prolonged usage. The first can only be addressed through establishing proper safety procedures on the operator's side such that the pilot may be evacuated by the instructor even while incapacitated; the latter problem has been shown not to be an issue given the length of time for which continuous use of the system is allowed.

<sup>123</sup>Illustration of usefulness of eye tracking technology

<sup>124</sup>Mass Pimax 8k Plus

<sup>125</sup>FCC ID: P2 Pimax 8K Test Report Pimax Technology (Shanghai)

[cited 2020-06-12]

[cited 2020-06-12]

[cited 2020-06-12]

### 5.7.5. Verification

Now, then, it is important that both the calculations presented in this chapter and the requirements relating to the visual system are verified, such that the reader may trust that the requirements as presented are all met and that the calculations made to come to that conclusion are trustworthy.

**Calculation verification** As a relatively large amount of data required for the budgets is already provided directly by the manufacturer, only very little verification has to take place. The only calculation made is that for the required power, and therefore a quick verification of that data will be presented here. All other parameters are taken directly from the manufacturer and therefore only their validation remains.

The developer states that the device can even run on a 2 A, 5 V phone charger<sup>130</sup>. While they do not present a source for this figure, it does verify the 24 W figure presented by the FCC: the FCC report is deemed more reliable, however, and therefore that is the estimate used in the power budget.

**Requirement verification** To verify that the chosen VR system is indeed capable of meeting the requirements as set, a compliance matrix is provided in Tab. 5.18. In this table, the reader can find whether a given requirement is verifiable (i.e. can be verified using a prototype) or verified (i.e. the design has already been shown to meet the requirements): no requirements were evaluated to be unmet or unverifiable. As shown, a large amount of verification should still be performed through physical tests, as is expected for a system that is inherently subjective.

Table 5.18: Visual cueing requirements compliance

Identifier	Compliance	Rationale
UPaRTS-SYS-CUE-VIS-1	Verifiable	Verifiable by test: requires working prototype and testing with pilot.
UPaRTS-SYS-CUE-VIS-1.1	Verifiable	Verifiable by test: requires working prototype and testing with pilot.
UPaRTS-SYS-CUE-VIS-1.2	Verifiable	Verifiable by test: requires working prototype and testing with pilot.
UPaRTS-SYS-CUE-VIS-1.3	Verifiable	Verifiable by test: requires working prototype and testing with pilot.
UPaRTS-SYS-CUE-VIS-1.4	Verifiable	Verifiable by test: requires working prototype and testing with pilot.
UPaRTS-SYS-CUE-VIS-1.5	Verifiable	Verifiable by test: requires working prototype and testing with pilot.
UPaRTS-SYS-16-VIS	Verifiable	Verifiable by test: requires working prototype and testing with multiple pilots.
UPaRTS-RSK-SAF-3-VIS	Verified	Verified by analysis: VR systems do not appear to induce statistically significant, lasting health effects[54].
UPaRTS-RSK-SAF-3.1-VIS	Verifiable	Verifiable by test: requires working prototype and testing with multiple pilots.

### 5.7.6. Validation

To show that the presented numbers as used in the budgets make sense, some validation is required. Part of this, of course, is physical testing, though as no Pimax 8K model is currently at hand this is delayed to a later design stage. To still allow for some early-stage validation, however, comparisons are made to other modern VR devices.

In terms of power, the Oculus Rift draws its power from two USB-3.0 ports<sup>126</sup> and can therefore only draw a maximum of 9 W<sup>127</sup>. The given 24 W then seems reasonable in terms of power consumption; it is in the same rough order of magnitude as this power consumption, though slightly higher as is to be expected from a higher-end headset.

As for the mass of the device, the Oculus Rift weighs in at most 0.380 kg and the VR Gear at roughly 0.310 kg<sup>128</sup>: for more comparable high-end headsets, the StarVR ONE has a mass of 0.450 kg, though that does not take straps and cables into account. The VR-2 Pro weighs in at roughly 0.855 kg, though a large part of that can be attributed to the counterweight it needs<sup>129</sup>. Hence, the 0.5 kg stated by Pimax is comparable to similar devices and, at the very least, does not seem to be unrealistic.

<sup>126</sup>Digital Trends: Spec Showdown: Oculus Rift vs. Samsung Gear VR

[cited 2020-06-21]

<sup>127</sup>Universal Serial Bus 3.0 Specification, pages 9-9 and 11-6

[cited 2020-06-15]

<sup>128</sup>Digital Trends: Spec Showdown: Oculus Rift vs. Samsung Gear VR

[cited 2020-06-21]

<sup>129</sup>Varjo: Varjo VR-2 Pro

[cited 2020-06-21]

<sup>130</sup>OpenMR PimaxVR forum: developer comment on Pimax power usage

[cited 2020-06-12]

### 5.7.7. Sensitivity analysis

The visual system is not reliant on most of the other subsystems. It is subjected to change if the headset for aural cueing changes, as both VR glasses and headset need to fit on top of each other. It is also prone to change if certain certification (such as Level D) want to be obtained: VR glasses are currently not an acceptable means of compliance (AMC) for Level D certification, which would mean that an entirely different system would have to be chosen. The current requirements are subject to a significant amount of subjectivity, which means that there are no cut-offs that can lead to sensitivity issues. One of the logical next steps would be to add or research a requirement in terms of pixel density, in which case the VR-2 might gain preference. Due to the low mass and power requirements of all of the described headsets, the impact this has on other systems is minimal to negligible, though, and therefore this point of sensitivity does not pose a risk. It can thus be concluded that there exists no points of sensitivity for the visual system that pose a critical risk.

## 5.8. Haptic Cueing

One of the other senses that should be fooled is the pilot's sense of touch: while the "feel" of the plane should accurately reflect the real case in an aerodynamical and mechanical sense, which can be achieved through properly reconstructing the feel of the controls, it is also important (due to the use of VR) that the *actual* feel of the aircraft is reflected well, i.e. the pilot feels the things he or she expects to feel in a tactile sense. How this is achieved for both of these interpretations of the word "feel" is described in this chapter.

### 5.8.1. Functional Analysis

In terms of functions, the haptic cueing system (trivially) satisfies function 2.3.2 (provide haptic cues). The main goal here is to provide the pilot with a convincing sensation of touch that does not clash with his or her other senses (such as vision or proprioception). Quite some functions are related to force feedback (2.3.2.1) and the environmental haptic cues (2.3.2.2) to simulate full aircraft integration. At last, by providing haptic sensations the pilot feels while pressing buttons should be able to be reflected in the visual systems (2.3.2.3). Lower levels of these functions can be found in page 34.

### 5.8.2. Requirement Analysis

To provide the functions as specified in Subsec. 5.8.1, a set of requirements was compiled that the haptics system must adhere to. These are:

- UPaRTS-CUE-HAP-1** The system shall provide realistic haptic cues equivalent to an EASA Level D flight simulator, as judged by a suitable pilot
- UPaRTS-CUE-HAP-1.1** The haptic system shall provide force feedback on the main controller
- UPaRTS-CUE-HAP-1.2** The haptic system shall provide vibrational feedback on the main controller
- UPaRTS-CUE-HAP-1.3** The haptic system shall provide force feedback on the thrust lever
- UPaRTS-CUE-HAP-1.4** The haptic system shall provide vibrational feedback on the thrust lever
- UPaRTS-CUE-HAP-1.5** The haptic system shall provide force feedback on the pedals
- UPaRTS-CUE-HAP-1.6** The haptic system shall provide vibrational feedback on the pedals
- UPaRTS-CUE-HAP-1.7** The system shall provide accurate haptic representations of buttons/switches relevant during the training exercise as judged by a suitable pilot
- UPaRTS-CUE-HAP-1.8** The haptic system shall provide data on the position of the pilot's and copilot's hands at a rate higher than the visual system refresh rate

A system which adheres to these requirements can fulfil functions 2.3.2.1.1-3, 2.3.2.2 and 2.3.2.3 described in Subsec. 5.8.1 and provides satisfactory haptic representation of the environment that is to be simulated, in that manner aiding the overall mission of providing effective and especially representative training of the pilot. It should be noted, then, that the choice was made to pursue an A320 simulator rather than a B737 or a general or interchangeable system. This means that no motorised force feedback is present in the aircraft that is to be simulated, and therefore that this need also not be present in the simulator. The reader should not confuse this, however, with redundancy of requirements UPaRTS-CUE-HAP-1.1-6: the provided feedback should still be a representation of the real aircraft, and controls in the A320 family are not fully 'lame': the stick, for example, does still contain springs to provide feedback, and this should also be reflected in the simulator. Additionally, to reflect the choice for a VR system, another haptic aspect must be reflected: the position of both pilots' hands, which is accounted for by the addition of requirement UPaRTS-CUE-HAP-1.8, resulting from function 2.3.2.3: it has been shown that it is possible to achieve latency

less than the refresh rate of modern VR visual systems before [55], which eliminates the effects of latency in this aspect of haptics entirely and therefore does not break immersion. As the position of the pilot's hands as shown must be congruent with the haptic environment presented through reproduction of the cockpit instruments, it was decided to incorporate this requirement and function in the haptic system rather than the visual system, though its primary function is to provide data that the visual system may use to show the pilot their hand/arm position as well as that of their partner.

### 5.8.3. Sizing

To provide haptic cueing, a multitude of systems is required. Maintaining the proprioceptive illusion is done through use of sensor gloves that feed location and orientation data of the pilot's hand and fingers to the processing systems which converts this to an image in the visual system, and the required tactile feedback for dials and buttons is provided through use of actual (tactile) replicas of these instruments. Hence, these two parts of the haptic systems shall be considered separately: lastly, the control instruments (sidestick, pedals and throttle) will also be sized.

**Gloves** A quick foray onto the consumer VR market shows that a wide array of gloves are already available that can provide accurate orientation data: when equipped with a proper tracker, some can also relay hand position. To satisfy the cueing requirements as described previously, both must be presented at the required frequency, which leaves only some high-end devices, shown in Tab. 5.19. Other (cheaper) devices exist, but they don't provide the data at the required rate or are not accurate enough. A quick note must be made that while haptic gloves traditionally refer to gloves that provide tactile feedback, the term has started to find more general use in reference to gloves that are used to provide tracking data for the location and orientation of the user's hand and fingers in virtual reality. Hence, throughout this report, the terms haptic gloves and tracking gloves (or simply gloves) are used interchangeably, and it should be understood that this strictly refers to tracking gloves and not to gloves that provide tactile feedback.

Table 5.19: VR gloves

Name	Battery life	Latency	Accuracy (angular)	Accuracy (translational)	Price (EUR)
<b>Manus Prime One</b> <sup>56</sup> [56]	3 hours	< 5 ms	7 degrees	4 cm (using VIVE tracker)	3700
<b>Captogloves</b> <sup>46</sup>	10 hours	N/A; "very low"	N/A	N/A	600
<b>Hi5 VR</b> <sup>137</sup>	3 hours	< 5 ms	1-2 degrees	N/A	1000

The major factor differentiating these three gloves is the translational accuracy of each of them: the Manus Prime One, used for motion capture for films alongside its use as VR gloves, can be equipped with the HTC VIVE tracker to allow for accurate position data, which is required to be able to relay hand position data to the pilot visually; the other two gloves, for which no translational data is known, do not seem to have the ability to do this convincingly, which is reflected in their lower price. As hand-eye coordination is essential in allowing the pilot to turn dials and press buttons, this translational context is essential to allowing the pilot to feel immersed. Hence, the Manus Prime is deemed to be the only acceptable choice. Another choice might be to design new gloves, though the additional time and monetary investment required was not deemed to be worth the potential long-term savings, as buying off-the-shelf gloves also provides other benefits. Sizing is therefore relatively simple as the required properties (mass, power and cost) are all straightforwardly provided by the manufacturer: as the gloves work on a battery they do not provide a contribution to the on-board power budget, though this does mean that an additional pair is required to allow for rotation and backup in case of failure. The mass of the device is given by the manufacturer as 0.064 kg, and the cost including the translational tracker comes down to 3700 euros per unit (rounded up), meaning that a total amount of 7400 euros must be reserved in the budget for the gloves. These same numbers should also be accounted for in the offboard budget, as the offboard pilot receives identical gloves (that could serve as spares if necessary).

**Instruments** The pilot must also be presented with the proper tactile feedback from his or her instruments, as reflected in requirements UPARTS-CUE-HAP-1.1-7. The choice for an Airbus A320-system greatly reduces the required equipment, as no force feedback has to be provided in the

instruments. This does not mean, however, that design of this subsystem is trivial: the instruments must still feel as they do in the aircraft, down to the buttons. While normally this is done through providing complete replicas of the actual cockpit, the use of VR and the light-weight design required mean that it is not that simple in this simulator. Luckily, the use of VR also means that none of the visual systems need be present, which means that a great deal of weight could potentially be saved in the choice of instruments. There is a set of three instrument panels that must be present in the cockpit, comprising the overhead panel, front panel and the central pedestal. Additionally, the sidestick, throttle and pedals must be present and respond as in the real aircraft, though those matters are discussed as part of the control instruments, discussed in Subsubsec. 5.21.

**Overhead panel** For the overhead panel, only the forward section need be present: the circuit breakers are not normally relevant in flight. As the overhead panel does not contain visual displays, it must be present in its entirety: a full simulation overhead panel weighs roughly 25 kg and would sell for roughly 4150 euros<sup>140</sup>, and these are thus the numbers budgeted for: in terms of power, the full overhead panel is given by the supplier to be capable of operating at 5 V and a current of 2 A, which means it can draw at most 10 W.

**Front panel** While the front panel contains many important instruments, a great deal of them are visual displays, and are therefore made redundant by the use of VR. This does not mean that all instruments are redundant: Tab. 5.20 presents the instruments present in a normal simulator front panel as sold by Opencockpits<sup>141</sup>, which would normally have a mass of 100 kg: additionally, it is determined which of those should be present in the front panel in this simulator based on whether the instrument is visual or also has tactile interaction. Using this, an estimate is made of the fraction of mass that should be on board the simulator, accounting for both redundant (visual) instruments and those that would normally be present once for each pilot. From this, it is found that only roughly 43% of all instruments need be present: by assuming that each of the required instruments is of equal mass, an estimate is found of 42.86 kg for the front panel. As this panel is normally encompassed by a large structure to contain and support it as well as the screens, it is assumed that another 10 kg (10% of the normal, total mass) can be shaved off by integrating these instruments in the cabin structure, which means a total front panel mass of 32.86 kg is found.

Now for the cost, buying a front panel would normally cost roughly 6239 euros<sup>141</sup>: while a large part of the instruments normally present in such a panel need not be present now, for the sake of being conservative this is the cost that is used now. As all 6 required instruments can operate using a single USB connection when bought separately, an upper bound for the power consumption of the combined devices is 27 W<sup>131</sup>, though this is almost sure to be an overestimate.

**Centre pedestal** As with the front panel, not all instruments in the pedestal need be present: to be able to estimate the costs in terms of mass anyways, a fractional approach like with the front panel is used to arrive at an estimate of 81.25% of the mass normally present in a replica centre pedestal (see Subsec. 5.21). Tab. 5.21 details the instruments that should be present in the centre pedestal off which this mass fraction is based.

Table 5.20: Front panel instruments; included components taken from Opencockpits S.L.

Instrument	Amount normally present	Amount required
FCU	1	1
EFIS	2	1
Autoland panel	2	1
Terrain panel	1	0
Landing gear panel	1	1
Chrono panel	1	1
Brake panel	1	1
Gauge accu-press	1	0
Pilot display	1	0
Engine monitor	1	0
Central display	1	0
<b>Total</b>	14	6

Table 5.21: Centre pedestal instruments; included components taken from Opencockpits S.L.

Instrument	Amount normally present	Amount required
MCDU	2	1
Radio panel	2	1
Audio panel	2	1
Radar panel	1	1
ATC panel	1	1
Engine start panel	1	1
Speed brake panel	1	1
Flaps panel	1	1
Cockpit door panel	1	1
Parking brake panel	1	1
Rudder trim dial	1	1
Switching panel	1	1
ECAM panel	1	1
<b>Total</b>	16	13

Hence, a total mass of roughly 40.63 kg is found. It should be noted that the centre pedestal normally also contains the throttle, but as this is discussed in control loading it is not taken into account here. Additionally, as the pedestal is already a flat board and does not contain a major structural component, it is assumed that no mass can be saved by integrating it in the structure of the cabin. As only a few instruments could potentially be removed from the centre pedestal, it is

<sup>131</sup>Universal Serial Bus 3.0 Specification, pages 9-9 and 11-6

[cited 2020-06-15]

assumed that the cost of these instruments is equal to that of a replica pedestal without throttle, as the throttle shall be discussed separately. This cost is given by Opencockpits as 4337 euros<sup>142</sup>. As the centre pedestal should be bought in a combination with the throttle and trim wheel (as those are not offered separately by Opencockpits), the power discussion for the centre pedestal is provided in detail in the discussion on the throttle in Subsec. 5.21. The result of that discussion is that 9 W of power is set aside for the pedestal as an upper bound.

Concluding, one then finds masses of 40.63, 32.86 and 25 kg for the centre pedestal, front panel and overhead panel, respectively, which makes for a total instrument mass of roughly 99 kg. In terms of costs, a total of 15000 euros must be set aside for the instruments, and for power consumption a total of 46 W presents a strict upper bound.

### Control instruments

The control instruments, being so vital to the job of the pilot, will be considered separately. Whereas the feel of other instruments does not affect training negatively, the feel of the control instruments can severely diminish the value of training. A discrepancy in the force required to press a button will not throw a pilot off, whereas a stick that feels "lame" or is too sensitive to inputs might negatively affect transfer of training or pilot immersion. Hence, these instruments must be of the highest quality and preferably exact replicas of the in-aircraft instruments. Luckily, the choice for an Airbus system does mean that no motorised force feedback is required.

**Pedals** As the pedals need to be fully convincing and accurate to the real thing, a high-cost professional replica is required. To get an estimate of the cost and mass associated with such a replica, Opencockpits was consulted as with the other instruments, where it was found that the price can be estimated to be roughly 2860 euros and the mass comes to roughly 15 kg<sup>132</sup>. In terms of power, the supplier provides a manual in which it is stated that for installation the consumer need only connect the pedals to a computer through USB, from which it can be gathered that the maximum power consumption is the maximum of 4.5 W provided by the 5 V and 0.9 A a USB 3.0-connection can provide<sup>133</sup>.

**Sidestick** Opencockpits also sells a replica of an A320 sidestick with proper tension loading representative of the A320<sup>134</sup>. One sidestick weighs around 12 kg and will cost roughly 931 euros: as with the pedals, a single USB-connection is required and therefore an upper bound of 4.5 W can be given on the power consumption of this device.

**Throttle** Opencockpit sells a throttle as part of a fully assembled pedestal. This pedestal exists in two versions, one with<sup>135</sup> and one without throttle<sup>136</sup>. Hence, the throttle is budgeted as 15 kg of mass and 2692 euros (both of which are the difference between the full pedestal and the light pedestal, the latter of which lacks the throttle and motorised trim). As the motorised trim wheel is attached to the throttle, it is included in this estimate as well. It should be noted that this differentiating between the throttle and the remainder of the pedestal is only done to allow for accurate budgeting: in the real case, the full package of pedestal and throttle and motorised trim wheel will be bought. In terms of power, it is harder to differentiate between the two: the full pedestal requires three USB connections and is therefore assumed to have at most a power consumption of 13.5 W<sup>137</sup>: to allow for separate budgeting, it is assumed that a third of this can be attributed to the throttle and trim wheel, while the remaining two-thirds are attributed to the pedestal, as the pedestal without throttle and trim wheel also requires three USB connections to function. This split is simply an administrative trick to allow for structured budgeting, and it should be understood that the pedestal comes as a full package drawing (at most) 13.5 W.

**IOS control instruments** Control instruments for the second pilot located outside of the cabin also need to be considered. However, since the second pilot is not the one being trained and since these instruments do not contribute to the onboard power or mass budgets, they are less crucial to the design. The second pilot is going to be equipped with exactly the same control instruments as the main pilot. Although cheaper, non-replica instruments would suffice, having these instruments as duplicates has the advantage that if an instrument fails in the cabin, it can be immediately replaced by using the instrument of co-pilot, meaning that the simulator can still be operated normally while a replacement part is underway.

<sup>132</sup>A320 Professional pedals

[cited 2020-06-12]

<sup>133</sup>Universal Serial Bus 3.0 Specification, pages 9-9 and 11-6

[cited 2020-06-15]

<sup>134</sup>A320 SideStick Captain side

[cited 2020-06-12]

<sup>135</sup>A320 Pedestal fully assembled complete version

[cited 2020-06-12]

<sup>136</sup>A320 Pedestal fully assembled light version

[cited 2020-06-12]

<sup>137</sup>Universal Serial Bus 3.0 Specification, pages 9-9 and 11-6

[cited 2020-06-15]

In conclusion, the total contribution to the onboard power and mass budgets due to control instruments are 18 W and 42 kg respectively, 46 W and 99 kg due to the other instruments (overhead panel, front panel and centre pedestal): these same contributions are made to the offboard power and mass budget by the instruments present on the IOS as well as the offboard charging of the haptic gloves, though those are less significant as the overall design is less sensitive to changes in the offboard systems, and the emphasis should therefore be placed on the onboard budgets. The haptic gloves contribute 0.064 kg in terms of mass and nothing in terms of power to the onboard budget, as they are battery powered. The instruments of the co-pilot are mainly reflected in the cost budget which amounts to a total of 13000 euros for all control instruments (onboard and offboard) and 30000 euros for the other instruments that are included as well as a total of 14800 euros for four pairs of tracking gloves: one for each pilot and two spares to allow for charging in rotation even after failure of one pair of gloves.

#### 5.8.4. RAMS

While the haptic systems are now sized, it is also important to show that these systems can satisfy the requirements in a reliable manner, being available when required and being straightforward to maintain and manufacture if necessary, all while being safe in use. Hence, a short RAMS (Reliability, Availability, Maintainability, Manufacturability and Safety) analysis is provided in the following. In terms of reliability, the haptic systems consist of consumer-grade components that are required by European law to have a warranty of at least two years. The modularity of the instruments means that if failure does occur it is localised and only partial replacement of the system is necessary; the gloves have to be replaced fully, however. As the instruments are exactly those used for fixed-base or home simulators, those will be available so long as that market exists, which is of course guaranteed over the length of the aircraft family lifetime. The tracking gloves are standard gloves for use in motion capture or virtual reality; as the latter becomes more commonplace, it can be expected that these gloves or comparable will only become more and more available. In terms of safety, the majority of issues are covered in the more general risks presented in Ch. 8; one more specific risk though is related to the fabric of the haptic gloves. As they are polyester gloves, they are at risk of melting in a fire which can cause severe burns. To prevent this from being an issue, the pilot should be briefed on this before the exercise and proper instruction should be given to immediately remove the gloves in case of a calamity (i.e. if any form of alarm is sounded). Of course, the necessary steps as described in Ch. 8 are also taken to prevent a fire from occurring in the first place.

#### 5.8.5. Verification

As no high-level mathematical analysis was presented here, there is no need for verification of calculations: the reliability of the calculations that were presented in this chapter can only be verified through real-life validation, at this point. Hence, all that remains is the verification of the requirements presented for this subsystem. Tab. 5.22 details each requirement and whether it is already verified by the design or at the very least verifiable through prototype tests at a later stage. No requirements were shown to be unverifiable.

Table 5.22: Haptic cueing requirements compliance

Identifier	Compliance	Rationale
UPaRTS-CUE-HAP-1	Verifiable	Verifiable by test: requires working prototype and testing with pilot.
UPaRTS-CUE-HAP-1.1	Verified	Verified by analysis: no force feedback required due to the choice for an Airbus system.
UPaRTS-CUE-HAP-1.2	Verified	Verified by analysis: no force feedback required due to the choice for an Airbus system.
UPaRTS-CUE-HAP-1.3	Verified	Verified by analysis: no force feedback required due to the choice for an Airbus system.
UPaRTS-CUE-HAP-1.4	Verified	Verified by analysis: no force feedback required due to the choice for an Airbus system.
UPaRTS-CUE-HAP-1.5	Verified	Verified by analysis: no force feedback required due to the choice for an Airbus system.
UPaRTS-CUE-HAP-1.6	Verified	Verified by analysis: no force feedback required due to the choice for an Airbus system.
UPaRTS-CUE-HAP-1.7	Verifiable	Verifiable by testing: requires working prototype and testing with pilot.

Identifier	Compliance	Rationale
UPaRTS-CUE-HAP-1.8	Verified	Verified by analysis: the latency of the chosen tracking gloves is lower than the refresh rate of the chosen headset.

### 5.8.6. Validation

As all described systems can be readily bought, the primary method of validation of the given numbers for mass, cost and power shall be simply buying and testing physical prototypes. Unfortunately the novel design choices mean that no comparable simulator exists to validate the numbers at this stage: the DLR Robotic Motion Simulator, while comparable in terms of system architecture, only has the control instruments (side-stick, throttle and pedals) and primary flight display, lacking all other instruments [9]. As exact mass and power estimates (the latter in terms of upper bounds) are already available through the supplier, this does not provide any new or more reliable information to validate with. To validate the mass of the instruments, it is also possible to contact the supplier and acquire information on the mass of each component, as it is known exactly which components each instrument consists of. As the amount of components required counts in the tens if not hundreds, the additional level of certainty acquired through this method was not deemed worth the time it takes for now, and this validation is left to a later design stage: indeed, it might even be easier to simply order the instruments and weigh them than to obtain an estimate through this method. The information for the tracking gloves is supplied directly from the supplier and thus no more reliable information is available. Hence, the main method of validation shall be physical testing as prototypes become available, which is not feasible at the current time.

### 5.8.7. Sensitivity analysis

The biggest threat in terms of sensitivity for the haptic system is if the customer decides to switch to a Boeing cockpit. In that case, control loading would have to be implemented in input controls which is likely to lead to a significant cabin weight increase. This has an effect on the remainder of the system, causing structural changes but also changes related to kinematics. As described in requirement UPaRTS-CUE-HAP-1.8, the haptic system must provide hand position data at a rate higher than the visual system refresh rate such as to prevent motion sickness and incongruency within the pilot's sense of proprioception and hand-eye coordination. It will thus speak to reason that a change in the visual system might result in a changed requirement: fortunately, the Manus Prime gloves already have a latency lower than 5 ms which means that a visual system with a frequency higher than 200 Hz would be required to warrant a change: this is not within the feasible range of current-generation headsets and indeed even high-end monitors currently only go up to 144 Hz. Therefore it is not expected that this will ever feasibly pose a problem. It can thus be concluded that the haptic systems are only sensitive to changes in the type of aircraft that is to be simulated.

## 5.9. System Overview

The previous sections detail the sizing of the subsystems, from which the system budgets have been affected. This section reiterates the mass estimations relative to the second iteration budget, showing whether there exists additional margin to continue the work in the future. From there, the verification of the training, system, and stakeholder requirements from the baseline report [1] is conducted. Given the verification of the system, a validation discussion is presented for future work.

**Preliminary Mass Estimation** The detailed sizing of the subsystems performed in the previous sections result in a new mass estimation which can be seen in Tab. 5.23. Looking at the budgeted and estimated mass of the cabin, there can immediately be concluded that the cabin will be lighter than initially thought. This is beneficial because there is even more, and therefore enough, slack to perform future design iterations. The mass estimation of the motion system remains the same and the floor loading determined in Subsec. 5.1 does not endanger the floor loading constraint. Since this floor loading will be the limiting case for our simulator, the mass estimation of the IOS and the off-board cabin was developed in less detail during this phase of the design and will be dealt with later on.

<sup>137</sup> Noitom Hi5

<sup>138</sup> bestware.com: Manus Prime One

<sup>139</sup> CaptoGlove: Buy CaptoGlove

<sup>140</sup> Opencockpits: A320 OVH FWD fully assembled

<sup>141</sup> Opencockpits: A320 Double seat trainer structure + components

<sup>142</sup> Opencockpits: A320 Pedestal assembled light version

[cited 2020-06-10]

[cited 2020-06-10]

[cited 2020-06-10]

[cited 2020-06-10]

[cited 2020-06-11]

[cited 2020-06-11]

Table 5.23: Preliminary design mass estimation

Category	Sub-Category	Budgeted Mass	Estimated Mass
Cabin	1 Structure and Shell	235 kg	69 kg
	1 Pilot	100 kg	100 kg
	1 G-seat	50 kg	45 kg
	1 Aural System	10 kg	9.8 kg
	1 Visual System	2 kg	1.5 kg
	1 Haptic System	80 kg	141 kg
	1 Power System	30 kg	30 kg
	<b>Total Mass</b>	<b>507 kg</b>	<b>396 kg</b>
Motion System	11 Rail	1025 kg m <sup>-1</sup>	1025 kg m <sup>-1</sup>
	1 Robotic Arm	12500 kg	12500 kg
	13 Energy Chain	5.7 kg m <sup>-1</sup>	5.7 kg m <sup>-1</sup>
	1 Carriage	2460 kg	2460 kg
	4 Brake	39 kg	39 kg
	<b>Total Mass</b>	<b>26166 kg</b>	<b>26166 kg</b>
IOS and Infrastructure	1 Instructor/Operator	100 kg	100 kg
	1 Station	150 kg	150 kg
	1 Operator Seat	7 kg	7 kg
	1 Main Processing Unit	30 kg	30 kg
	1 Emergency Computer	- kg	30 kg
	<b>Total Mass</b>	<b>287 kg</b>	<b>317 kg</b>
Off-board Cabin	1 Pilot	100 kg	100 kg
	1 Seat	40 kg	40 kg
	1 Aural System	10 kg	9.8 kg
	1 Visual System	2 kg	2 kg
	1 Haptic System	30 kg	42 kg
	1 Power System	30 kg	30 kg
	<b>Total Mass</b>	<b>212 kg</b>	<b>224 kg</b>
<b>System Total Mass</b>		<b>27172 kg</b>	<b>27103 kg</b>

**Preliminary Power Estimation** The power estimation due to the detailed subsystem sizing performed in the previous sections can be seen in Tab. 5.24. The onboard subsystems individual power usages are estimated to be lower than the maximum of 4kW determined in Subsec. 5.3.6. Even the total onboard power usage is currently estimated to be lower than 4kW, which for now results in a need for a single power cable up to the cabin. If due to future iterations, the onboard power usage exceeds the 4kW, a simple solution will be adding another power cable.

Table 5.24: Preliminary design power estimation

Category	Sub-Category	Budgeted Power	Estimated Power
Cabin	1 Structure and Shell	20 W	20 W
	1 G-seat	3000 W	3000 W
	1 Aural System	75 W	150 W
	1 Visual System	20 W	25 W
	1 Haptic System	660 W	74 W
		<b>Total Power</b>	<b>3775 W</b>
Motion System	1 Rail	4800 W	4800 W
	1 Robotic Arm	8000 W	8000 W
	4 Brake	130 W	130 W
	<b>Total Power</b>	<b>13320 W</b>	<b>13320 W</b>
IOS and Infrastructure	1 IOS Computer	90 W	90 W
	2 Monitor	12 W	12 W
	1 Aural System	150 W	150 W
	1 Main Processing Unit	589 W	589 W
	1 Emergency Computer	- W	15 W
	<b>Total Power</b>	<b>853 W</b>	<b>931 W</b>
Off-board Cabin	1 Aural System	75 W	150 W
	1 Visual System	20 W	25 W
	1 Haptic System	660 W	28 W
	<b>Total Power</b>	<b>755 W</b>	<b>203 W</b>
<b>System Total Power</b>		<b>18723 W</b>	<b>17723 W</b>

**Preliminary CO<sub>2</sub> Emission Estimation** In order to determine the CO<sub>2</sub> emission reduction of the simulator compared to in-aerobatic-aircraft training, the same assumptions as in the midterm are used [2].

- Only operational CO<sub>2</sub> emissions are compared.

- In-aircraft training also includes a facility building.
- The power of the in-aircraft training facility building is equal to the power of the simulator facility building during (de)briefing and flight
- Simulator training efficiency is 1.5 times in-aircraft training [1].
- CO<sub>2</sub> emissions per generated kWh are equal to the Dutch level in February 2019 (Dutch CO<sub>2</sub> emission factor) (0.4 kg kW<sup>-1</sup> h<sup>-1</sup>).<sup>143</sup>
- The pilot must drive an extra 120 kilometres to be able to train 1 hour in the simulator, at an emission level of 120.4 g of CO<sub>2</sub> per kilometre (resulting in 14.4kg CO<sub>2</sub> per hour).<sup>144</sup>.

With these assumptions, the CO<sub>2</sub> emissions can be calculated for the preliminary design in the same way as done in the midterm. The average power consumption of the simulator will be 18.5kW, the Dutch CO<sub>2</sub> emission factor is equal to 0.4 kg kW<sup>-1</sup> h<sup>-1</sup> and the CO<sub>2</sub> emission due to travel to the simulator is equal to 14.4 kg h<sup>-1</sup>. With this, the CO<sub>2</sub> emission of the simulator can be calculated and results in 21 kg h<sup>-1</sup>. To compare this emission with the emission of in-aerobatic-aircraft training, the CO<sub>2</sub> emission of the aerobatic aircraft must be calculated first. This is done with the fuel consumption of the aircraft (60 l h<sup>-1</sup>), the AvGas density (0.7185 kg l<sup>-1</sup>) and the AvGas emission factor (3.1 kg CO<sub>2</sub> kg<sup>-1</sup> AvGas<sup>-1</sup>)<sup>145</sup><sup>146</sup><sup>147</sup>. This results in a CO<sub>2</sub> emission of in-aerobatic-aircraft training of 134 kg h<sup>-1</sup>. With this emission and the training efficiency factor of 1.5, it can be concluded that the simulator will cause a CO<sub>2</sub> emission reduction of 89% compared to in-aircraft training.

### 5.9.1. Requirement Compliance

This section provides verification of the requirements of the system as a whole as established in the baseline report [1]. Given that certain requirements are encompassed within other subsections, this section deals with training requirements, system requirements, and stakeholder requirements. To maintain coherency of the provided tables, there exists a slight overlap in requirements.

Table 5.25: Training requirements compliance

Identifier	Requirement	Compliance	Rationale
UPaRTS-SYS-TRN-REC-1	The system shall be capable of recording the pilot during training	Verifiable	Verifiable by test when operational prototype developed
UPaRTS-SYS-TRN-REC-2	The system shall be capable of recording the system state	Verifiable	Verifiable by test when operational prototype developed
UPaRTS-SYS-TRN-IOS-1	The IOS shall be capable of logging performance and administrative information	Verifiable	Verifiable by test when system performance data and administrative information processing software is developed
UPaRTS-SYS-TRN-IOS-2	The IOS shall provide briefing possibility	Verifiable	Verifiable by analysis when IOS procedures are completely defined
UPaRTS-SYS-TRN-IOS-3	The IOS shall have access to system state information	Verifiable	Verifiable by test when the system state software is developed
UPaRTS-SYS-TRN-SAF-1	The operator shall have access to a communication line with the pilot at all times and vice versa	Verified	Initially verified by analysis of the aural system. Requires further verification by test when testing when product prototype is developed
UPaRTS-SYS-TRN-SAF-2	The operator shall have access to safety measures	Verifiable	Verifiable by demonstration when working prototype is developed
UPaRTS-SYS-TRN-SAF-3	The pilot shall have access to safety measures	Verifiable	Verifiable by demonstration when working prototype is developed

Table 5.26: System requirements compliance

Identifier	Requirement	Compliance	Rationale
UPaRTS-SYS-01	The system shall provide for pilot upset prevention training.	Verifiable	Verifiable by analysis when numerical extended envelope aircraft model is available
UPaRTS-SYS-02	The system shall provide for pilot upset recovery training.	Verifiable	Verifiable by analysis when numerical extended envelope aircraft model is available
UPaRTS-SYS-03	The system shall allow for simulating a single aisle aircraft to the extent required for upset prevention and recovery training.	Verifiable	Verifiable by analysis when numerical extended envelope aircraft model is available

<sup>143</sup>Renewable Energy in the Netherlands, slide 15

<sup>144</sup>Average CO<sub>2</sub> emissions from newly registered motor vehicles

<sup>145</sup>Pilotmix.com: Giles G202

<sup>146</sup>skydemon.aero: W&B - what does AVGAS weigh?

<sup>147</sup>verifavia.com: How are aircraft CO<sub>2</sub> emissions calculated?

<sup>148</sup>cbs.nl: Greenhouse gas emissions down

[cited 2020-05-27]

[cited 2020-05-27]

[cited 2020-05-27]

[cited 2020-06-18]

[cited 2020-06-18]

[cited 2020-06-18]

Identifier	Requirement	Compliance	Rationale
UPaRTS-SYS-04	The system shall provide for a means of simulating in-aircraft operations.	Verified	Verified by analysis: provided by haptic, visual and audio subsystems
UPaRTS-SYS-05	The system shall capture aircraft properties within an extended training envelope.	Verifiable	Verifiable by analysis when numerical aircraft model is developed or purchased
UPaRTS-SYS-06	The system shall provide for instructor/operator interference during operation.	Verifiable	Verifiable by test once working prototype is completed
UPaRTS-SYS-07	The system shall provide for pilot monitoring during operation.	Verifiable	Verifiable by test once working prototype is completed
UPaRTS-SYS-08	The system shall provide a dedicated instructor and operator station (IOS).	Verified	Verified by inspection of design decisions: IOS example presented in Fig. 5.3.2
UPaRTS-SYS-09	The system shall provide for briefing and debriefing capabilities.	Verifiable	Verifiable by analysis when briefing and debriefing procedures are defined by checking for possible communication
UPaRTS-SYS-10	The system shall provide measures of pilot performance relevant to upset prevention and recovery during training.	Verifiable	Verifiable by analysis when data processing is defined
UPaRTS-SYS-11	The system shall be maintainable throughout a lifetime of 20 years.	Verifiable	Verifiable by analysis when contractors are consulted for repair costs and if major components will operate 100000 hours without failure
UPaRTS-SYS-12	The system shall allow for upgradeability with new technologies.	Verified	Verified by analysis of design decisions: Haptic, visual and aural subsystems upgradable, robot system and cabin interchangeable
UPaRTS-SYS-13	The system shall provide a representative cabin environment as judged by a suitable pilot.	Verifiable	Verifiable by test when operational prototype is ready
UPaRTS-SYS-14	The system shall utilise equipment representative to a A320.	Verified	Verified by inspection of design decisions: internal configuration shown in Fig. 5.3.2 uses the A320 layout, and equipment shown in TABLE BLABLA uses A320 equipment.
UPaRTS-SYS-15	The system shall not cause physical injuries to the pilot or the instructor.	Verifiable	Verifiable by analysis if visual and aural system will not cause injuries when systems are prototyped
UPaRTS-SYS-16	The system shall not cause more motion sickness than an equivalent upset in a real aircraft.	Verified	Verified by analysis: simulator motion will be less violent than in real aircraft
UPaRTS-SYS-17	The training shall be representative of the simulated manoeuvres as determined by a suitable pilot.	Verifiable	Verifiable by demonstration when operational prototype is ready
UPaRTS-SYS-18	The simulator shall allow full operation by a single instructor.	Verifiable	Verifiable by demonstration when operational prototype is ready
UPaRTS-SYS-19	The system shall be composed of components sourced from contractors adhering to ISO-standard 14001.	Verified	Verified by analysis: Rail system, robotic arm are from certified contractors
UPaRTS-SYS-20	The system shall be composed of components sourced from contractors adhering to ISO-standard 26000.	Verified	Verified by analysis: Rail system, robotic arm are from certified contractors
UPaRTS-SYS-21	The system shall be composed of components sourced from contractors adhering to ISO-standard 45001.	Verified	Verified by analysis: Rail system, robotic arm are from certified contractors
UPaRTS-SYS-22	The system shall keep the cabin between 19 and 28°C.	Verifiable	Verifiable by demonstration when operational prototype is ready
UPaRTS-SYS-23	The system shall allow for cabin temperature changes in increments of at most 2.8°C.	Verifiable	Verifiable by demonstration when operational prototype is ready

Table 5.27: Stakeholder requirements compliance

Identifier	Requirement	Compliance	Rationale
UPaRTS-SH-SO-01	The simulator shall function continuously throughout the day with at most an hour of rest.	Verifiable	Visual, haptic and aural system verified by analysis, motion system is verifiable by analysis when motion system maintenance is defined
UPaRTS-SH-SO-02	The simulator shall be able to function throughout the whole year with at most two non-consecutive weeks of maintenance per year.	Verifiable	Verifiable by analysis when maintenance schedule is defined
UPaRTS-SH-SO-03	The total acquisition cost shall be no more than 25 M€.	Verifiable	Verifiable by analysis when exact part list and operational procedures are defined
UPaRTS-SH-SO-04	Hourly operational price shall be at most 1200€excluding the flight instructor.	Verified	Verified in Sec. 3.5.3

Identifier	Requirement	Compliance	Rationale
UPaRTS-SH-SO-05	The simulator facility area shall not exceed 20 × 20 meters	Verified	Verified by analysis: rail system, robot arm, IOS and both cabins all fit in the shown area.
UPaRTS-SH-SO-06	The lifetime of the simulators major components shall be at least 20 years.	Verifiable	Major components will operate 100000 hours without failure, hence verifiable by analysis when contractors are consulted for repair costs
UPaRTS-SH-SO-07	The simulator shall represent a two-pilot single aisle airliner of comparable specifications as a Boeing 737 or Airbus A320.	Changed	Changed to UPaRTS-SH-SO-23 as discussed in an individual meeting with the client
UPaRTS-SH-SO-08	The power budget of the on-board of the system shall not exceed 2 kW.	Changed	Changed to UPaRTS-SH-SO-24 as discussed in [6]
UPaRTS-SH-SO-09	The simulator shall reduce CO <sub>2</sub> emissions by 80% compared to real in-aircraft training	Verified	Reduction of CO <sub>2</sub> emissions by 89%, verified by analysis as shown in Subsec. 5.9
UPaRTS-SH-SO-10	The simulator shall provide a platform for incorporation of new and upgraded technology.	Verified	Verified by analysis of design decisions: Haptic, visual and aural subsystems upgradable, robot system and cabin interchangeable
UPaRTS-SH-SO-11	The mass of the cabin section of the simulator shall not exceed 3000 kg.	Verified	Cabin mass is estimated on 396 kg, verified by analysis as can be seen in Subsec. 5
UPaRTS-SH-SO-12	The simulator shall comply with EN 81-20:2020* safety certification standards.	Verifiable	Verifiable by demonstration when operational prototype is ready
UPaRTS-SH-SO-13	The simulator shall provide a platform for pilots to train upset prevention.	Verifiable	Verifiable by demonstration when operational prototype is ready
UPaRTS-SH-SO-14	The simulator shall provide a platform for pilots to train upset recovery.	Verifiable	Verifiable by demonstration when operational prototype is ready
UPaRTS-SH-SO-15	The simulator shall provide an accurate representation of the multi-crew coordination aspect of upset prevention and recovery as judged by a suitable pilot.	Verifiable	Verifiable by test when operational prototype is ready
UPaRTS-SH-SO-16	The simulator shall be able to provide the pilot with visual, audible, vestibular and haptic cues.	Verified	Verified by analysis of design decisions: cues are provided by the visual, aural, haptic and motion systems
UPaRTS-SH-SO-17	The simulator shall be equipped with an Instructor and operating Station (IOS).	Verified	Verified by inspection of design decisions: IOS example presented in Fig. 5.3.2
UPaRTS-SH-SO-18	The simulator shall provide the instructor and pilot a platform such that briefing can take place before, during and after the training.	Verifiable	Verifiable by test once audio system is implemented by checking if communication is possible
UPaRTS-SH-SO-19	The simulator floor loading shall not exceed 12kN/m <sup>2</sup> .	Verified	Simulator floor loading estimated on 7.6kN/m <sup>2</sup> , verified by analysis as seen in Subsec. 5.1
UPaRTS-SH-SO-20	The simulator shall provide cueing performance equivalent to a EASA FSTD(A) Level D simulator as judged by a suitable pilot	Verified	Verified by analysis on compliance to [29]
UPaRTS-SH-SO-21	The simulator shall provide onset g-forces at 70% of the real aircraft.	Changed	Changed to UPaRTS-SH-SO-22 due to [5].
UPaRTS-SH-SO-22	The simulator shall provide onset g-forces at 70% of 2.5g and -1g	Verified	Verified by analysis of design decisions: The robot arm can generate cues up to 1.3g, while the g-seat complements this with a minimum additional onset cue upwards of 0.7g (see Subsecs. 5.5.2, 5.5.3)
UPaRTS-SH-SO-23	The simulator shall represent a two-pilot single aisle airliner of comparable specifications as an Airbus A320.	Verified	Initially verified by inspection of design decisions: internal configuration shown in Fig. 5.3.2 uses the A320 layout. Further Verification required by demonstration for numerical aircraft model
UPaRTS-SH-SO-24	The power delivered to the onboard cabin shall be feasible regardless of the amount.	Verified	Onboard power estimated on 3269 W, verified by analysis as seen in Ch. 5.3.6

### 5.9.2. Validation

Given that the system has not been prototyped nor fully sized, the system cannot be validated. This is part of a future activity, with validation of the system possible once an initial working prototype is available as it is a stakeholder-oriented assessment. The stakeholders that will be required to be presented are: relevant authorities, the customer, and suitable pilots. The relevant authorities are required to note whether the system is compliant with regulations. The customer is required to note whether the system meets their expectations, and suitable pilots are required to note whether the cueing matches with their real-aircraft experience.

### 5.9.3. Sensitivity Analysis

To get an idea of how sensitive the simulator is to design- and requirement changes, a sensitivity analysis is performed based on the (key) stakeholder requirements which were not yet (entirely) covered in the subsystem sensitivity analyses performed in Subsec. 5.3.10, Subsec. 5.5.13, Subsec. 5.6.7, Subsec. 5.7.7 and Subsec. 5.8.7.

The total acquisition cost of the simulator was set by the customer to a maximum of 25 million euros, as noted in requirement UPaRTS-SH-SO-03. The current cost estimation (including 20% error margin) of the total system is 11.2 million euros (Sec. 3.5), this means that there is either a margin greater than 50% for a customer budget change or a margin of almost 14 million euros for future design iterations. However, one should aim for as low an acquisition cost as possible to remain relevant to the market.

Requirement UPaRTS-SH-SO-09 states that the CO<sub>2</sub> reduction of the simulator compared to in-aircraft training should be reduced with 80%, the CO<sub>2</sub> reduction estimated in Subsec. 5.9 is currently 89%. The CO<sub>2</sub> emission of the simulator is related to the power consumption of the simulator (33%), but most of the CO<sub>2</sub> emission (67%) is caused by the extra travel by car to the simulator. This implies that if the extra travel to the simulator is kept equal, the maximum average power consumption of the simulator can be 63 kW (currently estimated on 18 kW in Subsec. 5.24) while still complying with UPaRTS-SH-SO-09. This will most likely never be exceeded, which results in the advantage of even more allowable extra travel distance (up to 270 km per hour of training) compared to in-aircraft training.

Requirements UPaRTS-SH-SO-13, UPaRTS-SH-SO-14 and UPaRTS-SH-SO-20 are related to some degree. The first two requirements reflect the mission need statement: providing a platform for upset prevention and recovery training. The third requirement contains the customer's demand for cueing performance equivalent to EASA level D (but no certification necessary). However, if the customer demands EASA level D certification, (major) changes must be applied to the design (discussed in Sec. 4.4), requiring redistribution of the budgets. Furthermore, this will not necessarily contribute to higher cueing performance, but it will contribute to a larger market share. This is mainly due to the fact that the simulator will not only be suitable for the need described in UPaRTS-SH-SO-13 and UPaRTS-SH-SO-14 but also for nominal envelope pilot training. Note that this will also apply the other way around: if the customer additionally demands nominal envelope pilot training, EASA level D certification will be required.

Lastly, if requirement UPaRTS-SH-SO-23, which states that the simulator shall represent a two-pilot, single-aisle airliner of comparable specifications as an Airbus A320, is changed to another type of aircraft or even another type of vehicle, large parts of the simulator can remain the same. However, the haptic instruments almost certainly have to be replaced by more appropriate instruments as described in Subsec. 5.8.7. Furthermore, the numerical aircraft model (if already purchased) must be checked whether it is still useful and suitable for the new vehicle. If not, a new model should be developed or purchased which will take up a significant amount in the cost budget, but which will be still attainable within requirement UPaRTS-SH-SO-03.

# 6 System Logistics

This previous chapter oversaw the design of the product, from which the system logistics can be built upon. This chapter details the process involved and shows the system production plan, alongside giving an operation and logistic description.

## 6.1. Production Plan

To verify that the simulator is producible and to show how the production process is envisioned, a production plan was set up. The goal of this plan is to outline the sequential structuring of the production process and show which parts must be present when and where: it should be noted that this is thus not limited to manufacturing, but assembly and integration with the existing environment are also considered.

The steps within the production plan are visualised in Fig. 6.1.2, with the horizontal axis presenting a rough timeline of the events that occur. This diagram shows that the pilot cabin and secondary pilot station are assembled separately in a factory and shipped to the customer. The rest of the system, i.e. the robot arm, and the proper simulator environment, are assembled or integrated directly at the customer's location. For each assembly or major component, separate component groups listing the manufactured parts and/or off-the-shelf parts used are provided.

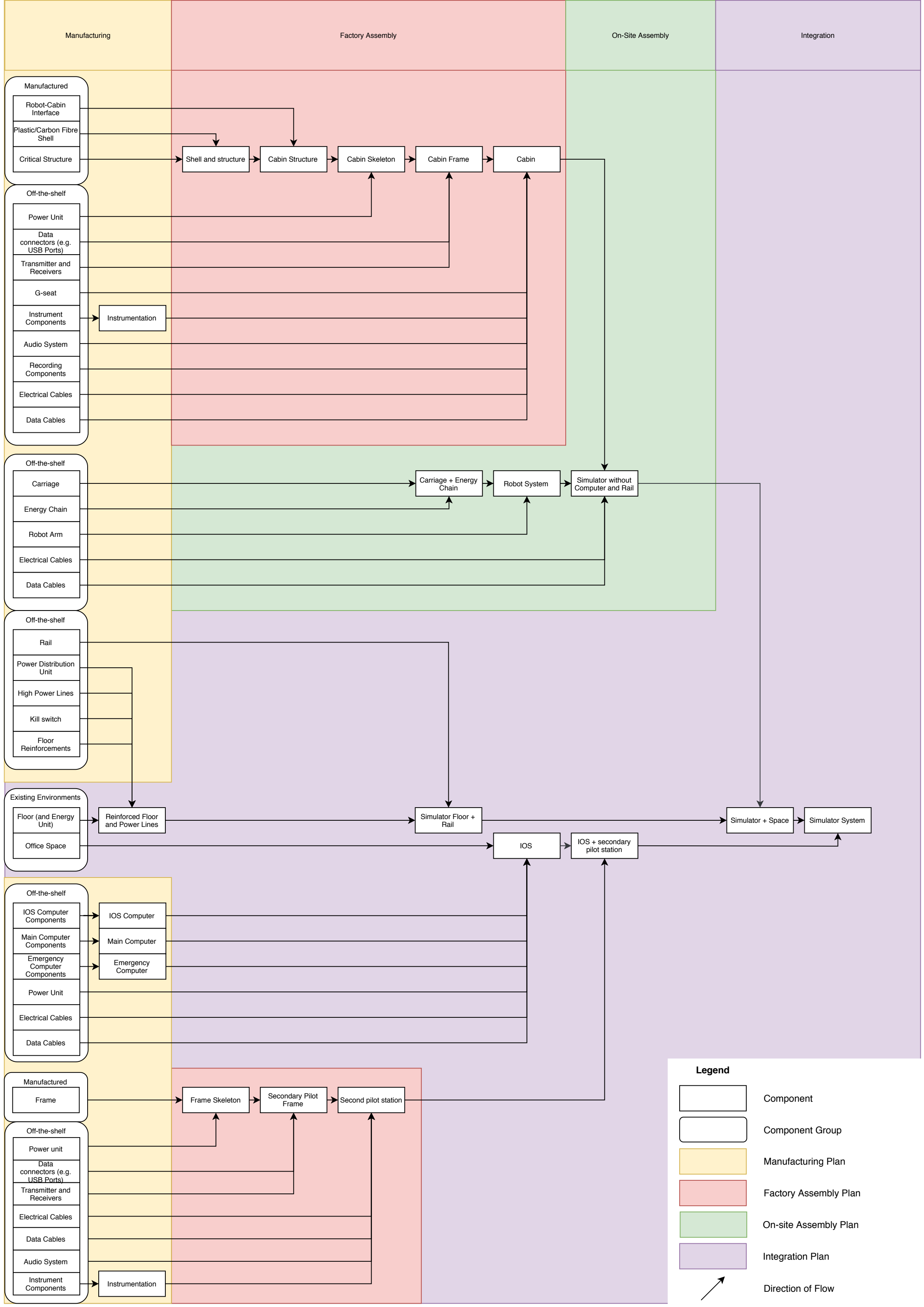
### 6.1.1. Integration

An aspect that must be highlighted in the case of the simulator, then, is integration. To be able to safely install the simulator, the environment in which it must be installed has to be adapted to the simulator: one cannot just place a simulator in any office building and assume that that will do. Some fundamental changes have to be made to the location of installation such that it can handle the loads imposed upon the floor by a heavy simulator and industrial-grade electrical power lines must be available. Hence, such changes have to be made on the customer's side before any type of delivery is even possible, which is reflected in the integration preparations that have to be made as shown in the production plan.

### 6.1.2. Sustainability

The production plan aims to reduce the impact of the process on all three forms of sustainability (environmental, economic and social) as much as possible: this is ensured in several ways. Firstly, only a relatively small amount of parts have to be manufactured in-house or specifically ordered from a third party: all other parts are more generic components bought off-the-shelf from a supplier. The parts that have to be made specifically are also non-type specific, generic parts (the cabin shell, cabin structure, cabin-robot interface and the frame for the secondary pilot position), meaning that this same production line could be used for any possible variants of the simulator for other aircraft families in the future. This means that the investment in such a production line would be a safe and cost-effective one, but also that it is relatively easy to ensure that the full manufacturing and assembly process is sustainable: all suppliers of off-the-shelf parts can be selected for compliance with ISO 14001, ISO 26000 and ISO 45001 (ensuring an environmentally and socially sustainable workplace), while only a relatively small process must be designed from the ground up to be sustainable.

To prevent any parts from travelling unnecessarily, assembly is done on-site wherever possible: by doing this, both the economic and environmental costs are kept to a minimum. This also means that the logistic burden on-site is lightened: while the parts are still of a significant size, they are not as big as a fully assembled simulator. Hence, chances of having to deconstruct part of the building to allow for moving in of the simulator are minimised, resulting in lower environmental costs but also potentially avoiding health hazards that can be a result of building demolition (consider asbestos, for example). This on-site assembly also has the advantage of ensuring that the parallel production lines only meet up very late, meaning that delays are unlikely to cause a delay in the final product, minimising economic losses for all parties.



## 6.2. Operations and Logistics

In this section, considerations on the operation and logistics of the system will be made. This is relevant for the customer and, eventually, the operator, in order to get an overview not only on the extent of training that can be performed with the system, but also the logistical constraints attached to it. Firstly, in Subsec. 6.2.1 the operations will be discussed, and in Subsec. 6.2.2 the logistics.

### 6.2.1. Operations

A full flight simulator system such as the one described in this report will very likely integrate a vast array of tools available to a training operator, each with the aim of improving flight safety in a specific way. The design presented in this report aims to be an overarching system, with capabilities not only in terms of UPRT scenarios but also standard training exercises, replacing to some extent current FSTD's in use around the world. While the basic principles of this new systems are very comparable to those of simulators in use today, its form factor and certain technological changes will pose challenges to its integration in an operator's training flow. Furthermore, when the system is in use, it is of high importance to the operator that the training is not only safe and effective, but that a high number of pilots can be trained over a certain period of time, decreasing running costs and allowing the operator to achieve healthy profit margins. Both of these factors will be considered in this subsection. This subsection ties in directly with Ch. 4, as the day-to-day operations of the system must fully support the goals described by Training Systems.

**Integration in current operations** To consider the challenges involved in integrating the new system in a customer's operations, some differences between the simulator presented in this report and conventional FSTD's in use today will be highlighted.

Firstly, we have the form factor of the system. Conventional FSTD's are very often 1-to-1 cabin replicas on a Stewart's platform, and although large in volume, their floor print is minimised. There is also no need for a separate IOS, as this is most often included within the cabin itself, making the system self-contained. Briefing and debriefing rooms are required in order to optimise pilot throughput, but no strict requirements exist for them. The system presented in the report will require a much larger floor print, as well as occupy more space in general when compared to the conventional solution, largely because of the reach of the robot arm and additional margins that must be kept free. The IOS must also be placed outside of the cabin, in close proximity to the simulator itself, which further extends the required space for the system. Immediately, this indicates that within the same physical space, fewer systems can be placed, and that (re-)construction of part of the client's facilities might be required.

The marked differences in the technologies used in this new system also carry other difficulties in terms of integrating the simulator in current operations. The simulator operators, for example, in this case also acting as instructors, will require a certain amount of training before being able to carry out training exercises independently. Other supporting staff such as in-house maintenance technicians will also require extensive training, as the motion system and its working is fundamentally different from the conventional solution.

Finally, due to the extended training capabilities of the system, especially in terms of UPRT, the training curricula used by the operator will have to be substantially updated in order to reflect the training envelope of the new simulator. While basic training curricula ship with the system (see Sec. 4.3), these need to be adapted in order to fully reflect the desires of the ATO and any additional regulations set by local authorities.

In general, these differences and the difficulties that arise from them indicate that the integration of the system in the operations of a customer already using conventional FSTDs will not be completely seamless. The difficulties arising from personnel education and training curricula can be accounted for in advance and should not impact the operation start date as set by the customer. These difficulties are also only applicable when the first of this type of system is bought, as subsequent purchases will benefit from the framework already in place. As for the space constraints, these will require planning in much longer-term, and can present a challenge to some less flexible or smaller customers. This can present a threat to the strong marketability desired for the system, and so all measures should be taken to streamline the order process and support the customer with the integration of the newly-purchased system in their operations. Considerations on the actual delivery and installation processes are made in Subsec. 6.2.2.

**Training throughput** The training throughput of the system is understood to mean the number of pilots that can effectively be trained in a certain time frame. This specification is very important, as operators rely on a very high throughput of pilots (and almost continuous usage) in order to ensure profitability. Not only that, but when the customer is also an Approved Training Organisation (ATO),

the number of systems they will have at their disposal is limited, and so a high throughput is required in order to train all the pilots within a company in a timely manner.

Throughput is directly tied to two factors: simulator occupancy time per training session and schedule and unscheduled downtime for maintenance or other repair activities. While the first factor can easily be estimated with high accuracy, maintenance times are strongly dependent on the overall reliability of the system and ease of repair of certain system, for which little data is available at this stage of the design. More information on maintenance is given in Subsec. 6.2.2

In current FSTDs in use for recurrent training and proficiency checks, the standard simulator occupancy time for such activities falls around 4 hours per pilot per session<sup>149</sup>. For formative training activities, simulator time usually falls short of these 4 hours, as retention abilities decrease in longer sessions. To obtain an estimate of the pilot throughput, the 4 hours per training session will be assumed as the standard value for the system. A note must be made, however, concerning the particularities of the system and their effect on the pilot's well-being, in particular the prolonged use of VR glasses. These effects are discussed in Subsec. 7.2.3, and in order to minimise them as much as possible, a recommendation is made to adjust the maximum continuous time in the simulator to be 2 hours. This means that a 4 hour session is then divided into two portions of equal length, with a section of off-board theoretical learning as a break. While this decreases pilot availability due to overall longer training periods, pilot comfort and attention in the simulator will remain high for the entire duration of the session. The pilot throughput is virtually the same despite this recommendation, and so the system's profitability isn't directly affected. For a 4 hour training session, with a 23/7 up-time of the simulator (as per requirement UPaRTS-SH-SO-1), the system is expected to have a throughput of 40 pilots trained per week. Over an entire year, considering 50 weeks of up-time, a total of 2000 individual training session can be achieved considering nominal operations. This value can increase substantially if the focus is shifted to formative training, where 2 hour sessions are very common.

### 6.2.2. Logistics

For the logistics part of the simulator a distinction can be made between three phases. The first phase will take place before the simulator is in operation. This phase will include the transportation and delivery of the different components of the simulator and also the on-site installation. The second phase runs for the entire operational lifetime of the simulator and includes maintenance and possible upgrades. When the end of the operational lifetime is reached, the last phase of the simulator logistics will begin. This end-of-life phase will include the disassembly and disposal of the simulator.

**Transportation and Delivery** To be sure that the installation of the simulator can take place without any problems, it is of great importance that the transportation and delivery of the simulator parts are thoughtfully planned. Simulator parts that will arrive too late will cause installation delays. Also, parts that arrive early can cause temporary on-site storage problems which will affect the installation efficiency. To correctly plan the transportation and delivery of the simulator parts, the delivery time and transportation method must be defined for all the different parts. The simulator will consist of both custom-made and off-the-shelf parts, all of which supplied by different contractors. These contractors will have distribution centres located in different places around the world, leading to different delivery times and transport methods. During this design stage, a distinction is made between (semi) made-to-order parts, specialised parts and widely available parts.

Made-to-order parts are only made when ordered, such as the motion system of the simulator but also custom made parts. For these parts, additional time is required before the part can be dispatched. According to FANUC Europe, which uses a distribution centre in Europe and also uses order prediction, this will take about four weeks<sup>150</sup>. After these four weeks, the part is ready for delivery. Heavy transport in Europe can take up to two weeks and must be planned in advance.

Specialised parts are intended for a small target group; the simulator replica instruments are an example of these parts. Because there is not much demand for these parts, they must most likely be ordered from abroad. Fortunately, specialised parts are often available from stock and can be dispatched in few days<sup>151</sup>. Parcel delivery times in Europe are between one and two weeks. As a result of this, specialised parts will be received in approximately two weeks. The parcel delivery costs between countries in Europe range from 10 to 50 euros depending on size and weight.

Widely available parts are used in a wide variety of applications, examples of this used in the simulator are among others VR glasses and aural system components. Like specialised parts, widely available parts are available from stock. In addition, these parts can be ordered from within the

<sup>149</sup>Finnair Pilot Training Summary

[cited 2020-06-16]

country. This will result in a total delivery time of maximum one week. Domestic delivery for normal parcels is usually reimbursed by the seller and can be neglected for now.

With the delivery times for the different parts known, rough planning can be made. However, in order to determine the exact order and delivery plan, the installation of the simulator must be defined first. After this, the point of time of installation is known for the different parts and the exact order and delivery sequence can be determined.

**Installation** As mentioned in the previous section, the installation plan of the simulator is required to determine the delivery sequence. Furthermore, it is important to determine requirements that the building must meet, what equipment and labourers are needed on which day and the total duration of the installation. At this stage of the design, it is not possible to determine the installation procedures in detail. However, a first approximation can be made. For this, a distinction is made between the simulator foundation, the cabin and the peripherals.

The foundation of the simulator will mainly consist of the motion system of the simulator. The cabin will be mounted on the robotic arm and this robotic arm will be mounted on the rail system, which will be mounted to the factory floor. The installation of the simulator will, therefore, start with preparing the factory floor, after that, the rail system can be delivered and installed. Either a crane or a heavy forklift is needed to put the rail in place, furthermore, specialised workmen able to install the rail and to control the crane or forklift are required. The rail system will be delivered in multiple 4 m long parts and this must certainly be taken into account when checking the accessibility of the building. As soon as the installation of the rail system is finished, the robotic arm can be installed, for this, also the crane or heavy forklift is needed. To keep the costs low, it is important to plan this tightly after each other. The robotic arm will also have large dimensions during transport and installation up to 4.1 m in height, which again must be taken into account for checking the accessibility of the building. In this design stage, an installation time of 2/3 days is assumed for the foundation of the simulator.

After the rail and robotic arm of the simulator are installed, the cabin can be mounted. However, before the cabin will be mounted to the robotic arm, the cabin must be produced, assembled and the cabin equipment must be installed, which can be done before and sequentially with the instalment of the simulator foundation. For the cabin mounting, again the crane or heavy forklift will be used. For now, an installation time (time to mount it to the robotic arm) of 1 day is set for the cabin.

Installation of the peripherals used in the IOS (Computers, speakers, desks, etc.) can already start during the instalment of the simulator foundation. However, the peripherals used in other parts of the simulator will most likely not be installed until the foundation and cabin are installed. Therefore, another 3 days is taken into account for finishing the simulator in this stage.

This together will result in a rough estimate of a total installation duration of 7 days, but due to unforeseen circumstances, it is possible that it will take up to 10 days. In this stage of the design, it is not yet possible to give a useful cost estimate of only the installation. This is due to not knowing the exact equipment needed and the complete component list. Furthermore, the rail system and robotic arm will most likely be installed under the supervision of the contractors.

**Maintenance** As mentioned earlier, the simulator will be able to operate 23 hours per day, seven days per week with two non-consecutive maintenance weeks per year. This means that in addition to the two weeks of offline maintenance, there is also an hour per day that can be used for daily maintenance to the simulator.

A large part of the daily maintenance will consist of cleaning, which will be cleaning of the simulator and cabin itself but also the IOS and the rest of the building. This will most likely be outsourced to an external cleaning company, allowing the instructor to perform other maintenance such as described in Subsec. 5.3.7. There will also be periods when additional maintenance is required during this hour of downtime, for which additional labourers will be hired. Such tasks can include changing small parts such as switches or knobs or performing the continuous maintenance activities required to keep the robot arm, linear track and the system in good working order.

For offline maintenance, a distinction can be made between planned and unforeseen maintenance. If unforeseen maintenance is not taken into account, there is a chance that training sessions that are cancelled due to malfunctioning of the simulator cannot be caught up on. For issues arising during the training hours of the simulator which can be quickly fixed, an on-site technician should be present to ensure that the downtime is as small as possible in these situations. For more serious issues that may require the simulator to be out of operation for a longer period of time, external technicians might be needed, and the downtime will most likely be substantial. To avoid situations

<sup>150</sup>fanuc.eu: Centralisation of European Product Customisation activities

[cited 2020-06-17]

<sup>151</sup>Opencockpits.com: Conditions of Use

[cited 2020-06-17]

like these, it is essential to compile and adhere to strict maintenance programs that keep the system in good working order at all times, decreasing the chances of unexpected severe failures. The compilation of such programs should be done in cooperation with the supplying partners and is left to a later stage of the project.

**Upgradability** Upgradability is of great interest to the operator, and being one of the customer set requirements (UPaRTS-SH-SO-10), has been an important driver in the development of the design. Upgradability translates to the ease with which technological advancements and layout changes in the real aircraft can be taken into account in the simulator, or even how the simulator can be changed to support a completely different aircraft type. High upgradability means that not only does this pliancy exist, but that changes can be made in a quick and economic way, providing the operator with a lot of flexibility,

The most common changes that can happen during the operating life of the system are small updates brought out by the aircraft's manufacturer that impact operations, which can be divided into software and hardware changes.

Software changes pertain to any rework of the on-board computers, flight envelope protection logic, automation improvements or similar. This sort of upgrades are overall very easy to implement in the system, and even though they require extensive rework of the flight models and simulation software, this can be done by dedicated engineers concurrently with training operations. Implementing them in the actual system is just a matter of updating the simulators software during the 1 hour downtime at the end of the day, for example. Software upgrades to the real aircraft are thus of minimal impact to the system and should present no issue to either the manufacturer or operator.

Hardware changes to the real aircraft, however, pose bigger challenges in terms of the system's upgradability. These can be changes in terms of additional switches, new systems, and upgrades to the cockpit layout that must be reflected in the simulator to ensure the training remains transferable and up-to-date. While such upgrades are considered extensive in the past, in the case of the system presented in this report, many of the difficulties are overcome by the fact that the cockpit is represented in a virtual way to the pilot, facilitating changes to a great extent. In fact, most of the physical changes that can be made by the real aircraft's manufacturer could be incorporated in the simulator by means of a rework to the virtual cockpit, which does not require simulator downtime. Some changes, especially with regards to any new/removed switches or actuators, do require a physical change in the simulator's cabin in order to preserve the 1-to-1 haptic cueing. As in the real aircraft, the interior layout is modular (see page 47), allowing certain panels to be easily removed and either upgraded or swapped. This does impact the operation of the simulator of course, and thus it must be carried out either in the daily 1 hour downtime (most likely for a panel swap) or during the bi-yearly 1 week maintenance period (in case of more in-depth upgrades e.g. a new input control column).

For much larger upgrades, it is not possible to estimate their feasibility as each upgrade would have a very specific set of changes. The specific case of upgrading the simulator to represent a fully different aircraft within the Airbus A3XX family, however, is a good proof of concept to demonstrate the flexibility of the system. Given the Airbus Cockpit Philosophy [57] which extends throughout their A3XX family concept, the interchangeability of the simulator is largely increased between the different aircraft. Most changes between aircraft types within this family occur in certain sections of the overhead panel, with the rest of the cockpit being largely unchanged. Depending on the aircraft, the systems and their nuanced operation can change significantly, but those changes are reflected in the software of the simulator and don't require additional downtime. For this specific case, it is expected that such an upgrade could be carried out in one of the 1 week downtime periods, alongside other maintenance, giving the operator extreme flexibility and the possibility of looking at the system not as a simulator for a specific aircraft, but as a platform capable of high fidelity simulation of an entire family.

Overall, the system's upgradeability is superior to that of conventional FSTDs. While some physical changes to the cabin may be required in certain upgrades, these can be carried out faster and more economically than its conventional counterpart, as the parts to be replaced (switches, knobs, etc.) are the amongst the cheaper in a simulator cabin. Given the use of VR devices to generate the remainder of the cockpit to the pilot-in-training, such as screens, instruments, and overall layout of the cockpit, a much higher level of flexibility is achieved. Limiting downtime and costs allows the customer to more easily maintain the system's training currency throughout its lifetime, and adapt it to newer technological standards should this be desired.

**End of Life** End-of-life processes are an essential part of the product's life cycle, and can represent a significant financial and logistical burden to the customer if not dealt with appropriately in advance. The end of life flow begins with disassembly, and then moves onto disposal, either recycling, reusing

or eliminating certain parts. The entire end of life process has a cost associated to it, the end of life cost.

Disassembly occurs in the opposite order of that of installation, as the cabin and peripherals are first detached from the robot arm, then the arm is disassembled, with finally the foundation being dealt with. The interior of the cabin should first be stripped to its primary "skeleton", with all instruments, inputs, and cueing systems removed in order to facilitate the removal of the cabin. The cabin can then be removed by making use of a crane or heavy forklift as done for installation. As for the robot arm, no disassembly of the arm itself will occur, and more insight into its disposal is given in the next paragraph. The robot arm should be disconnected from the rail track, again using a crane or heavy forklift. Finally, the linear rail must be disassembled, either completely or leaving only the floor attachments in case a new system will be installed. The disassembly process is carried out by certified maintenance technicians, and is expected to be completed within a week. The cost for disassembly cannot be estimated at this stage, but an estimation should be given to the customer as the design progresses to a more detailed phase.

After disassembly, the separate components must be either re-purposed or disposed of, depending on how feasible recycling is for a certain part. At this stage of the design, the main components of the system can be looked at, and a preliminary disposal strategy can be given. The cost of these actions is, once again, not defined this early in the process, and can only be estimated in close collaboration with all the chosen supplying partners. The sustainability aspects of the disassembly cycle is given in Subsec. 7.2.3. Starting with the linear rail, given its working condition is still acceptable, it is possible that this component could be re-purposed for non-human rated uses, such as an assembly line, for example. Should the economic benefit of this be deemed insufficient, then the metal components of the structure should be recycled, and the electronics completely disposed of. The robot arm, being the most intricate and expensive component of the motion system, can be re-purposed using FANUC's Robot Reapplication Services<sup>152</sup>, converting the robot for other (production line) applications, and thus recuperating some of its value. The cabin itself is divided into two parts, the shell and the instrumentation. As for the shell, given it is a custom made part with a very specific application, it must be recycled taking into account correct procedures for the chosen material. The instruments, on the other hand, given correct maintenance procedures throughout the system's lifetime, can be re-purposed for other training purposes that are not so strictly regulated, such as ground school mock-up training devices. If the operator in questions owns such devices, these can easily be re-purposed within the same company, reducing costs and waste. Finally, the IOS, given its much less intensive use when compared to the simulator itself, can even be used for a new system to be installed, reducing its acquisition costs. If this is not possible, components such as computers can be re-purposed within the company, with the remaining materials of the IOS recycled.

---

<sup>152</sup>FANUC Robot Enhancement and Reapplication Services

[cited 2020-06-18]

# 7 Sustainability

A large part of this project revolves around taking sustainability a step further: a flight simulator is inherently more sustainable than alternatives (aerobatic aircraft), and this project aims to take that fact and add to it. It should then be clearly explained what one means when talking about a term as vague as sustainability, though. In this project, sustainability is considered to be composed of three aspects, being environmental, social and economic sustainability. Environmental sustainability concerns the well-being of the natural world and therefore the minimisation of the impact on nature and its resources. Social sustainability concerns the physical and mental well-being of all stakeholders at all stages of the product's life, while economic sustainability ensures the product has value and presents an economically feasible and attractive concept for all stakeholders. The sum of these three then forms the totality of sustainability, and it is then immediately clear where the sustainable advantages of a simulator over in-aircraft training lay: simulators are inherently safer than aircraft and also offer potential savings both in terms of environmental impact and economic cost compared to their flying counterparts. By identifying this early on and implementing it as an intrinsic part to the approach [1, 2], the team has hoped to fully and positively exploit the potential for sustainability in this project, which will be detailed here both through the manner in which sustainable development was approached and implemented but also by covering the contributions and improvements this product makes in terms of sustainability in a concrete manner.

## 7.1. Implementation of Sustainability

To properly tackle the concept of sustainability, it is important that it is properly treated as part of the process. While it might be tempting to simply introduce extra constraints or requirements related to the subject, that does not fully capture the nuances and nature of sustainability: sustainability is a sliding scale, not a yes-or-no question, and by treating it as such it becomes an obstacle rather than a goal. By describing an approach to sustainability that is continuously, integrally and intrinsically part of the design process, it is hoped that this nuance of sustainability can be fully captured without sacrificing the qualities of the design. Additionally, product life cycle phases critical to sustainability in all its senses were identified early on to ensure proper allocation of resources to the areas where the largest amount of sustainable progress can be made.

### 7.1.1. Approach to Sustainability

A suitable approach to strive for a product which is sustainable in every sense of the term was already recognised during the early phases of this project. In the Project Plan this approach was described as follows: "First the goals with respect to sustainability are defined, then the impact on environmental, social and economic sustainability is measured, and finally compliance checks are performed at a regular interval" [3]. In hindsight, this is exactly what has been done. Most noticeably, this can be illustrated with requirement UPaRTS-SH-SO-9, which turned out to be a driving force throughout the design. This requirement dictates that the CO<sub>2</sub> emissions of the flight simulator should be at least 80% lower than the ones of comparable in-aircraft aerobatic training. This and many other goals with respect to sustainability were defined early [1]. The next step is to evaluate the impact of the goal with respect to environmental, social and economic sustainability. This was also done for UPaRTS-SH-SO-9. In the midterm report (Subsec. 6.4.2 [2]) detailed calculations on the implications of 80% reduction in carbon dioxide emissions have been performed. This led to the upper bound for power consumption of 43 kW and allowed to compare the different design in a quantitative way. The difficulty of quantifying aspects related to sustainability was also recognised early on [3]. As expected it has been easier to attach importance to UPaRTS-SH-SO-9, because it was possible to put a number on it. The power consumption played a defining role in the design trade-off process, eliminating the true-to-life concept for its excessive CO<sub>2</sub> emissions despite the ease of producing sustained motion cues. The last part described as 'compliance checks' was achieved by raising awareness of the team on the scope of sustainability early on and translating the goals which are most difficult to achieve into risks. These actions made sustainability a recurrent topic of conversations during meetings as it was in the back of everyone's head. The requirements allow the sustainability officers then to check for compliance in a more formal way: as shown in Tabs. 8.2 and 5.27, the sustainability requirements are indeed already satisfied or satisfiable in the current design. It should be emphasised though, that complying with all requirements does not immediately imply that the product is itself sustainable: as described before, sustainability cannot and should

not be boiled down to a set of requirements, but rather should be encapsulated in an approach and mindset. As the approach described seems to have given all the team members a sense of responsibility and as the topic of sustainability is addressed in meetings, this approach is also used in the final phase of the project.

### 7.1.2. Life Cycle Phases

Then, to ensure that no aspects of sustainability are forgotten or overlooked, the life cycle phases most critical to sustainability were identified in [1]. Out of the traditional life cycle phases of design, testing, production, operation, maintenance and end-of-life, it was identified that production, operation and end-of-life would have the highest economic, environmental and social impacts in terms of sustainability. During production, the majority of material resources are consumed and a great deal of energy and natural resources and therefore money are spent on transport, resource acquisition or manufacturing. By carefully considering this stage of the product (described in Sec. 6.1), a lot of gains can be made that do not necessarily (negatively) impact the end-product in terms of cost or quality: whether a part is sourced from halfway across the world or from one town over makes a great deal of difference in terms of sustainability, though it need not impact its quality or price. Hence, for example, the choice to assemble as much of the simulator on-site rather than shipping everything in one piece. Economically, this is also where a large part of the costs associated with the product are made and can thus be reduced. In operation, a large amount of social sustainability aspects can be impacted both positively and negatively: this is where training, the purpose of the simulator, is realised and therefore where it can be affected. Additionally, this phase is where user interactions with the device take place and thus also where one could see adverse effects in that regard popping up. Furthermore, this is also where the emissions related to operation of the simulator are made and therefore where they could be mitigated. Lastly, at the end of the simulator's life, it must be disposed of. This is of course not just the case at the end of the life of the entire simulator, but also throughout as parts are replaced. Disposal, of course, presents a large environmental and societal concern, but it also provides an economic problem as disposal can often be a costly process, especially when hazardous materials are involved. All this is not to say that the aspects of sustainability related to design, testing and maintenance must be overlooked: those are simply less significant, not irrelevant. If possible, sustainability should still be an aspect taken into account in those areas and, all else equal, it still speaks to reason to choose more sustainable options: the major gains can be made in the aforementioned phases, though. The majority of the contributions, as detailed in Sec. 7.2, must be and were made in the areas of production, operation and end-of-life.

## 7.2. Contribution of the product to Sustainability

In this section, the aspects of the flight simulator that contribute towards a more sustainable product are presented. At this stage, it is important to look back and to explain how the risks related to sustainability [1, 2] have been mitigated through design changes. The contributions of the product towards the three pillars of sustainability are presented below.

### 7.2.1. Environmental Sustainability

Environmental sustainability is for most people the first thing to come to mind when thinking of sustainability. While it is not the only aspect relevant in sustainability, it is very much an important one: even more so in the case of a UPRT simulator. One of the issues plaguing current UPRT is the fact that representative training comes at a tremendous environmental cost in terms of emissions, be the training in an aerobatic aircraft or in one of the few simulators that are currently suited for high-level UPRT such as Desdemona or the Kraken. This is therefore an area not only where the customer stipulates that the design must make big leaps (as determined in requirement UPaRTS-SH-SO-9) but also one where big leaps can be made regardless. Environmental sustainability is not limited to (CO<sub>2</sub>) emissions and though no stakeholder requirements are bound to waste production or recyclability, these are still areas where possibilities for improvement exist and hence where improvements were sought and implemented, as will be detailed in the following.

**Emissions** In Subsec. 7.1.2 it was explained that production and operation were counted among the sustainability-critical life phases: one reason for that is that this is when the majority of emissions related to the product take place. As explained previously, one customer requirement concerned the emissions associated with the use of the simulator: the customer wanted a simulator that produced CO<sub>2</sub> emissions at a level 80% lower than equivalent in-aircraft training. In Sec. 5.9 it was shown that this corresponds to an upper limit of roughly 43 kW in terms of allowable power usage, and this simulator is well below that with its estimated power use of 19 kW, which achieves a reduction in CO<sub>2</sub> emissions of roughly 89%. A remark that must be made, then, is that the possibil-

ity exists of the simulator being fully operationally carbon-neutral if the customer decides to make use of a fully green power supply, though that is in control of the customer and not of the design team.

For completeness' sake, then, it must be noted that harmful emissions are not just limited to CO<sub>2</sub>: among others, NO<sub>x</sub> is another source of environmental problems which has been the cause of recent controversy in Dutch politics. This is, like CO<sub>2</sub>, a combustion gas, which means that in switching to simulator training its emission is bound to fall: exact numbers are hard to come by, however, and therefore no attempt is made to provide an estimate of the decrease in NO<sub>x</sub>-emissions.

Additionally, by sourcing parts from ISO 14001-compliant companies, the emissions related to manufacturing can be further reduced without added cost or loss of quality: even major components like the robotic arm can be sourced from suppliers that adhere to this, as market leaders in that sector such as KUKA and FANUC adhere to those standards already<sup>153</sup> <sup>154</sup>. By assembling as much of the robot as possible on-site (see Sec. 6.1), unnecessary travel of parts as massive as the robot arm is prevented and transport-related emissions are reduced. This has the added benefit of reducing economic costs, too, of course. While one might ask whether it is then not more sustainable to have an arm be custom-made closer to or in the factory, this has implications for the reusability of the arm as explained in recyclability and reusability; a custom-made arm does not offer the benefit of an existing repurposing programme such as the one offered by FANUC.

Lastly, the choice was made to step off the original idea of using braking to produce high g-loads and rather supplement the accelerations produced by the robotic arm with a g-seat inside the cabin (described in Subsec. 5.5.3). This reduces the particulate matter emitted by the simulator (significantly), which provides less of an environmental and health hazard and also lessens waste production due to the comparatively lower rate of part replacement needed.

**Waste production** Another aspect that is important environmentally is the production of waste: by minimising the amount of waste resulting from the product, the long-term environmental impact of the product can be reduced. In this aspect production and end-of-life play an important role, as this is where the majority of the waste associated with the product is produced.

Firstly, use of parts from ISO 14001-compliant companies means that waste produced by parties and production not under control of the team is minimised; by applying waste-conscious and efficient manufacturing techniques in the manufacturing that is done in-house, it is then ensured that waste produced by components under control of the team is also minimised: due to the relatively low amount of parts manufactured in-house, the manufacturing approach can be carefully tailored to achieve this (see Sec. 6.1).

Then, to ensure that waste is also minimised during end-of-life, several measures are implemented in the design: the conscious choice for a light-weight system, which, for example, uses VR-glasses rather than a large, heavy mirror means that a smaller cabin is necessary and therefore that the overall amount of waste produced, all else equal, is lower. The lifetime of the device, coupled with its modularity and versatility mean that the risk of the device being disposed of by the consumer prematurely, quickly or unnecessarily is lower. Additionally, the use of off-the-shelf, standardised parts in a modular fashion whenever possible means that waste related to maintenance or broken parts is minimised: when something breaks, it is only that single part that has to be replaced and thrown out, not the entire subsystem. Additionally, this means that disposal procedures already exist for a lot of the parts that are used: the chosen VR glasses, instruments and tracking gloves, for example, are all consumer-grade products and therefore their disposal is safe and should not present a big issue in terms of hazardous materials or non-recyclable materials. This latter property warrants a more in-depth discussion, then, and so it shall be explored in further detail.

**Recyclability and reusability** Closely tied to waste production, though not entirely the same thing, is recyclability but also reusability of the product. As with waste production, significant opportunities exist and were exploited in the production and end-of-life phases, though one should be careful not to be blind to possibilities that exist in the operations phase.

In terms of production, the modularity of the system and use of standardised parts means that the possibility exists to refurbish used parts of scrapped simulators, though only to a limited degree, seeing as the system must be human-rated. Sustainability-conscious manufacturing and supplier choices as discussed in Sec. 6.1 means that waste produced during production can be partially recycled, reducing overall waste production as discussed in the previous paragraph.

During operation of the simulator, another form of reusability comes into play. The versatility of the simulator, means that it is possible to quickly and relatively cheaply repurpose the simulator in case of changes in fleet composition: as the cabin is normally only installed on the arm on-site (for more

<sup>153</sup>KUKA AG: Reports, guidelines, certificates

[cited 2020-06-17]

<sup>154</sup>FANUC: Sustainability at FANUC

[cited 2020-06-17]

details, the reader is referred to Sec. 6.1, installing an alternate cabin on an arm is no different than the install process on normal installation. In this manner, an entire simulator could essentially be "recycled". This also has added economic benefits for the customer, being that they do not need to buy an entirely new simulator with all the associated costs and logistical problems, but in terms of environmental benefits this means that no unnecessary environmental costs are made. On a similar note, upgrading the simulator in case of technology or regulation changes also does not require a fully new simulator.

By sourcing products and parts from recycling-minded suppliers, one can guarantee that the parts used do not need to be disposed of even at the end of the lifetime of the device: the use of modular, standardised off-the-shelf parts means that a wide choice of suppliers is available and therefore that the freedom exists to make this choice. An example is the robotic arm, which is currently proposed to be a FANUC model: as the arm is used for human transport, it is paramount that it outlives the simulator. It would then be a waste to dispose of such a large part of the product even though it may still be very well-suited for other (non-human rated) tasks after this lifetime. FANUC offers a programme to repurpose used robotic arms<sup>155</sup>, which means that a very large part of the simulator (roughly three-quarters in terms of the moving mass) can outlive the simulator by a large margin. Through careful selection of parts sourced from partners in the post-DSE phase, this may be extended to other parts of the design, too.

### 7.2.2. Economic Sustainability

Economic sustainability is quintessential to the customer. Projects that do not guarantee to generate revenue in due time are not economically attractive and hence less likely to survive. This subsection highlights the aspects of economic feasibility that are discussed in the market analysis (Ch. 3) and dives into the costs related to the critical life cycle phases presented in Subsec. 7.1.2.

In the market analysis, it was observed that the concept of a UPRT-specific simulator in terms of marketability relies heavily on regulation changing in favour of more advanced UPRT. To mitigate this and other problems, the training curriculum for the simulator was designed to encompass more than simply upsets, as described in Subsec. 4.1.3. Additionally, through upgradability, the device hopes to reduce this niche role that the simulator might otherwise be perceived to have by customers, as such a flexible system in turn enhances the flexibility of the customer economically. Changes in fleet composition from the A320 to another aircraft or changes in training requirements then need not require a full or partial replacement of the customer's simulator fleet, and the effective lifetime of the simulator can be longer. Hence, depreciative costs are lower and the customer pays a lower amount of money over the lifetime of the simulator.

**Acquisition cost** The customer has a number of cost to cover before the flight simulator is fully operational. One main advantage of the robotic arm is that its parts are relatively small and most them are off-the-shelf. Having large parts can have big implications in terms of cost as transport might have to be done in expensive large containers and walls of the facility might have to be deconstructed to install the part. Another advantage is that buying the robotic arm off-the-shelf allows for high investment certainty as the exact price is known. It is much harder to estimate the price of designing, testing and producing a robotic arm from scratch. Money and time is also saved as off-the-shelf robotic arms already have sustainability and safety certifications which shortens the time it takes until the product is operational and can generate revenue.

**Operation and maintenance cost** Over the lifetime of the simulator, the customer will also incur costs both to operate the simulator and to keep it operational. It is also in this area that the robotic arm provides a set of advantages: firstly, the simulator draws a relatively low amount of power compared to high-end UPRT simulators, and therefore does not incur large power consumption costs. Additionally, it can be operated by a only single operator and, if necessary for the scenario, a single second pilot. Due to the use of standardised, consumer-grade parts not too much specialist knowledge is required in terms of maintenance which means maintenance costs can be kept relatively low, too. This same fact also guarantees that replacement parts are readily available at acceptable price levels at all times. By dropping the idea of using braking to achieve high loads, maintenance need not be as frequent as would otherwise have been the case.

**End-of-life cost** Lastly, the robotic arm offers great advantages for the last life cycle phase. As the arm has to support a human it is likely to structurally last much longer than its intended lifetime for safety reasons. As mentioned under Environmental Sustainability, the FANUC programme to repurpose used robotic arms<sup>156</sup> can be chosen. The alternative is to dispose the flight simulator. As the use of toxic materials is limited to (possible) braking fluids, disposal cost is also reduced.

<sup>155</sup>FANUC: Robot Reapplication (Redeployment) Services

[cited 2020-06-17]

<sup>156</sup>FANUC: Robot Reapplication (Redeployment) Services

[cited 2020-06-17]

### 7.2.3. Social Sustainability

Making a product socially sustainable involves assuring safe use of the device at all times, usefulness of the device but also user-friendliness. A flight simulator that is dangerous to use, does not improve pilot skills and is not enjoyable to use does not fulfil its intended purpose. The following analysis addresses the weak points of the final design with respect to these three categories.

**Safety** As explained the midterm report [2], flight simulators can be considered inherently more socially sustainable than aerobatic training as training pilots for upsets in real aircraft presents a greater risk in terms of safety for the pilot, instructor and bystanders. However, care should be taken not to neglect the safety aspects of robotic arms. In the case of the final design a number main safety aspects have been addressed and mitigated since the midterm report. These are: eye strain due to prolonged use of VR-glasses, the robotic arm crashing into anything surrounding it (bystander, floor, wall, ceiling or the robot arm itself), physical injuries due to abrupt g-forces, the evaporation of toxic gasses due to fluids used in the robotic arm, fire outbreak and privacy breach. The risk of eye strain is mitigated by limiting the amount of time the pilot spends continuously in the simulator to 120 min as described in Subsec. 6.2.1. In order to prevent collisions with anything that is within the robotic arm's reach the motion of the robotic arm is restricted to so-called 'feasible states'. When generating these states the physical constraints of the robot arm, but also the boundaries of the motion space are defined. This mitigation solution is described in Subsec. 5.5.7. Since an upside-down orientation is part of the feasible states, there is a safety risk related to the robotic arm stopping in a position that makes egress dangerous for the pilot. A mitigation solution for this exact risk is presented in Sec. 8.3 (R-SAF-2). The section on Robotic Motion Kinematics (Sec. 5.5) also provides a mitigation plan for the risk of physical injuries due to abrupt g-forces. This is tackled by obtaining the acceleration profile of the intended motion. This profile is based on predefined velocity and acceleration bounds which prevent the robotic arm from accelerating excessively. For the possible health hazards related to evaporation of toxic gasses (or possible fine particles), it was decided to check with the suppliers for compliance with safety standards such as ANSI/RIA R15.06-1999<sup>157</sup>. This American safety standard assesses safety requirements related to the use of robotic arms, exposure to hazardous materials being one of the points of concern. A similar approach is taken to mitigate the risk of fire outbreaks. ISO standard ISO45001<sup>158</sup> encapsulates social sustainability and fits this case, as the KUKA robotic arm also uses this standard. On top of having to comply with these standards, the hatch of the cabin was designed with safety in mind. During training the hatch is electronically locked, in case of power outage, it can still be opened using an emergency release button. In addition, all participants (pilot, instructor and co-pilot) have an emergency button within arm's reach that is connected to an independent computer, capable of stopping the flight simulator's motion (See pages 40-41). Finally, the hatch is designed in such a way that if the spring loaded system (which allows to automatically open the hatch) does not work it can still be opened manually by the pilot (See Subsec. 5.3.7). The last safety concern is the risk of privacy breach. Data about the pilot's performance and privation information are likely to be stored in the main computer. To reduce to probability and impact of a possible data breach the personal data of each pilot should not be attached to the training data or it should be encrypted in a decentralized data storage. This can be done by storing training performance data anonymously. The only way to associated this data with the pilot's personal information would be by using a key. On top of that, data that does not need to be stored will not be stored. It is important to keep an eye on current data protection regulations<sup>159</sup> such that the provided platform allows users to easily comply with these.

**Usefulness** The second aspect of social sustainability is the product's usefulness. A flight simulator only adds societal value if society proves to benefit from it. In the case of the robotic arm, this is achieved by providing a platform to improve pilot skills for LOC-I. The identified knowledge gap is split up into three aspects, a pilot's emotional response, training for disorientation and providing continuous UPRT throughout a pilot's career. These aspect are described in detail under Subsec. 4.1.2. From this knowledge gap, clear system objectives in terms of training value are presented in Subsec. 4.1.3. Usefulness cannot be quantified easily, hence it boils down to trying to make the product as useful as possible. Identifying the knowledge gap and translating it into training objectives are logical first steps, but there are other difficulties to overcome. The risk of negative pilot training is a risk that all flight simulator manufacturers need to account for. Efforts are made to make the robotic arm's motion as similar to the aircrafts motion as possible. Aircraft data on real life accident such as the Airbus A330-202 (2009-06-01) (See Subsec. 5.4.1) has been gathered and will drive the design to improve the fidelity of the robotic arm.

<sup>157</sup>ANSI: ANSI/RIA R15.06-2012

<sup>158</sup>KUKA AG: Reports, guidelines, certificates

<sup>159</sup>EU data protection rules

[cited 2020-06-16]

[cited 2020-06-16]

[cited 2020-06-17]

**User-friendliness** The last pillar of social sustainability is user-friendliness. A product can be considered user-friendly if it is efficient to use, intuitive to learn and enjoyable to use. A flight simulator is inherently more efficient to use than aerobatic aircraft for multiple reasons. Training does not depend on weather conditions or air traffic, the time needed to lead up to an upset is much shorter for a flight simulator as you do not need to take-off and climb and the flight simulator can be stopped at any time to brief to pilot. It is important to not lose this advantage that flight simulators have over aerobatic aircraft by overloading the instructor with work. The instructor's workload should be viable in a way that allows him to single-handedly operate the simulator. This has been taken into account by compiling the necessary steps an instructor needs to follow in an instructor's guide which is presented in Subsec. 4.3.2. The second facet of user-friendliness relates to the ease with which the user learns to operate the device. In an ideal world, the interface is so intuitive that the user does not need a manual to figure out which action to take. At this stage of the project it is difficult to concretely make the device intuitive. The interface of the robotic arm needs to be iterated based on user studies during later design stages. Finally, to ensure the well-being of the pilot, temperature control has to be taken into account as the cabin's temperature is prone to climb due to the electronic components and it being a confined space with a person sitting in it (see Subsec. 5.3.5). In addition, motion sickness has to be kept to a minimum by improving model fidelity and reducing the offset between the different cues. At this stage of the design it is hard to guarantee perfect synchronisation of the cues: a mitigation solution for future design stages is proposed in the Tab. 8.3. In the same context of well-being, technicians and manufacturers need to work in an environment that promotes their well-being. To make sure that a healthy work environment can be guaranteed at all times, social sustainability standards can be enforced in a similar way as suggested under safety.

Through continuous assessment of the different aspects that contribute to environmental, economic and social sustainability, this product has been designed in the most possible sustainable way. By analysing each life cycle phase one can make sure to not leave out contributions that would otherwise be forgotten. Throughout the design process, the sustainable development strategy has already proven its effect. Concerns with regards to sustainability which had been identified during the early phases of this project have now been completely mitigated through specific design changes. It is noteworthy that significant leaps have been made and opportunities were identified and taken advantage off. This is reflected in a higher than expected reduction in CO<sub>2</sub> emissions and in the possibility of refurbishing the robotic arm which encompasses three quarters of the entire flight simulator's mass.



# Technical Risk Assessment

Any project eventually will, in one way or another, be exposed to some sort of risk(s) at any moment in the project timeline. It is of importance that potential risks are identified, assessed, and if possible mitigated before these risks could harmfully impact the progression of the project. To facilitate the method which the risk managers utilise to tackle the risk assessment process, a framework for risk management has been set up in Sec. 8.1. The risk managers will take responsibility for identifying the most impactful potential risks, labelling and categorising these according to their risk type, and consequentially establish mitigation plans for each risk identified.

The results of this process are summarised in Sec. 8.3 in which the risks are presented in a risk matrix complemented with their causes, impacts, risk levels, and mitigation plans. The technical risk assessment performed for this document is a follow-up of the assessments performed in [1] and [2] and delves deeper into the design specific risks that have been encountered in these final stages of the design process. It is important to note that in general, the risk management process is continuously evolving and therefore risks need to be constantly monitored throughout the entire project. Therefore, the risks are constantly subject to change implying that risks may be removed, added, or regraded whenever necessary. Risk management strives to minimise the number of significant risks that the project is exposed to.

One of the major risks that the system is continuously exposed to during the design process is the risk of not meeting requirements that have been set from the start of the project. To facilitate a managerial way of keeping in track of the requirement compliance, all requirements that have been proposed in [1] are listed throughout the report in their corresponding sections. In this chapter, the compliance of the requirements regarding risk is presented and elaborated on in Sec. 8.2.

## 8.1. Framework for Risk Management

To be able to manage, identify, assess, and mitigate potential risks involved in the project, a framework for risk management has been established which aids the risk managers in fulfilling their task. Additionally, adherence to top-level requirements will continuously be checked to ensure compliance, and if compliance is not met, a plan can be set in motion to tackle this issue immediately. Especially in this final stage of the design process, now that the design has been finalised, it is essential that the identified risks are analysed thoroughly as in this stage all risks should be mitigated to a risk level that allows the design to be deemed feasible, reliable, and convincing by the customers.

The risk assessment is initialised through the identification process of potential risks resulting in a clear overview of the risks that ought to be assessed by the risk managers. The identification of new risks will be done in close collaboration with all the different departments. Meetings will be organised to discuss new risks that arise from subsystem design changes, possible risk level changes for and/or removal of existing risks. Whenever a risk has been edited, added or removed, the rationales for the action that has been taken will be noted down and added to the rationale list as presented in Sec. 8.3.1.

Following up on the identification process, the risks will then be categorised according to their risk type and subsequently quantified by grading each specific risk based on their likelihood of occurrence and their magnitude of impact on the design. The grading process is based on the grading scheme as presented in Tab. 8.1. Based on the analysis of the risks on their causes, impact, and their grades, mitigation plans will carefully be established by the risk managers to reduce risk levels to acceptable standards which will be realised by lowering the likelihood of occurrence, reducing the magnitude of impact or better yet, decreasing both. Whenever the situation occurs that issues related to risk arise despite the risk management procedures, risk managers will initiate discussion with the responsible design team to evaluate the issue at hand and to minimise its impact on the progress of the project. It is important to note that neither party possesses the authority to overrule the counterparty; a common agreement must be established.

Table 8.1: Risk map for severity vs. probability

Probability	Severity			
	1—Catastrophic	2—Critical	3—Marginal	4—Negligible
A—Very probable	1A (r)	2A (r)	3A (o)	4A (g)
B—Probable	1B (r)	2B (r)	3B (o)	4B (g)
C—Occasional	1C (r)	2C (o)	3C (o)	4C (w)
D—Remote	1D (o)	2D (o)	3D (g)	4D (w)
E—Improbable	1E (g)	2E (g)	3E (g)	4E (w)

## 8.2. Risk requirement compliance

This section presents the requirements that have been defined as risk related requirements in [3] and shows the compliance of the requirements in Tab. 8.2. The compliance is either verified, verifiable, non-verifiable or not verified and corresponding rationales are provided as well. With verified it is meant that the requirement has been deemed as complied with based on findings that have been referenced in the rationales. Verifiable indicates that the requirement can certainly be verified but not yet in the current design phase; in essence, more data is needed. Non-verifiable implies that the requirement cannot be verified at this point and will also not be verifiable in a later stage, and finally not verified suggests that the requirement could be verified at this stage of the design but has not (yet) been done due to some reason that will be stated as a rationale.

Table 8.2: Risk requirements compliance

Identifier	Requirement	Compliance	Rationale
<b>UPaRTS-RSK-SYS-1</b>	The system shall use, where applicable, components that are standardised and used in other applications. [UPaRTS-SH-SO-10]	Verified	Verified by analysis: robot arm, structures and interface are off-the-shelf/standardised
<b>UPaRTS-RSK-SYS-1.1</b>	The system shall use standardised electrical interfaces to allow for upgradability in the foreseeable future. [UPaRTS-SH-SO-10]	Verified	Verified by analysis: for aural, visual, and haptic cueing off-the-shelf systems will be used (Sec. 5.6, Sec. 5.7, Sec. 5.8). Same holds for cables and e-chain (Sec. 5.3.6).
<b>UPaRTS-RSK-SYS-2</b>	The system shall use generalised instruments that can be adapted to cover most single aisle aircraft of the past 30 years. [UPaRTS-SH-SO-10]	Verified	Verified by analysis: the system utilises VR in combination with position tracking gloves and physical instruments, which are all replaceable.
<b>UPaRTS-RSK-SYS-3</b>	The system's software shall be upgradable. [UPaRTS-SH-SO-10]	Verified	Verified by analysis: standard programming languages and techniques will be used, which can be readily upgraded.
<b>UPaRTS-RSK-SYS-4</b>	The system shall substitute infeasible model response inputs with their closest feasible counterparts	Verified	Verified by analysis: the motion cueing algorithm does not allow for infeasible motion, and only cues the closest feasible motion by design.
<b>UPaRTS-RSK-SYS-5</b>	The system shall make provisions to prevent physical injury at every system action.	Verified	Verified by analysis: in Sec. 5.5 it is explained that possible physical injuries would most likely arise from abrupt g-forces which have been mitigated in this section by defining the acceleration profile of the cabin based on a maximum acceleration and velocity. Additionally, requiring adherence to strict safety specifications also verifies this requirement.
<b>UPaRTS-RSK-SYS-6</b>	The system shall inform the IOS of any safety interventions.	Verifiable	Verifiable by analysis: data processing has not been completed yet.
<b>UPaRTS-RSK-MNT-1</b>	The system shall be proven to endure 48 hours of consecutive operation. [UPaRTS-SH-SO-1]	Verifiable	Verifiable by testing: this can be shown once the system (or a prototype) is produced and tested.

Identifier	Requirement	Compliance	Rationale
UPaRTS-RSK-MNT-2	The system's maintenance schedule shall be adaptive and dependent on the hours and type of operation	Verifiable	Verifiable by analysis: this will be possible once structural testing (simulations or otherwise) and maintenance planning design has started.
UPaRTS-RSK-MNT-3	The system shall be proven to withstand in excess of 200% of the maximum design loads after 6 months of reference operations. [UPaRTS-SYSSTR-INT-1.4]	Verifiable	Verifiable by testing: this will be possible once structural testing (simulations or otherwise) and maintenance planning design has started.
UPaRTS-RSK-MNT-4	The system's principal structural components shall be stress and fatigue tested to demonstrate their design capabilities of lifetime and maximum allowable stress. [UPaRTS-SH-SO-6]	Verifiable	Verifiable by testing: as elaborated on partly in Sec. 5.3, as well as through additional structural testing and simulations later in the design process.
UPaRTS-RSK-MNT-5	The system shall be disposable at rate of at most 1% of the purchase price.	Verifiable	Verifiable by analysis: this can be done by considering the material composition of the structure and the cost depreciation of components, but was not done in the interest of time.
UPaRTS-RSK-MNT-6	The system shall be assemblable on-site by a crew of trained technicians.	Verifiable	Verifiable by demonstration: this will be possible once the assembly design (or a prototype) is produced.
UPaRTS-RSK-MNT-7	The system shall limit the use of hazardous materials, except for cases where there are no other options.	Verified	Verified by analysis: care has been taken to use only recyclable and environmentally friendly materials, which excluded the use of hazardous substances. This, however, does not apply to necessary protective coatings and braking fluids.
UPaRTS-RSK-MNT-8	The system components shall fit in standard shipping containers.	Verifiable	Verifiable by analysis: the assembly of components and packing sizes can be analysed, but were not studied at this stage due to time constraints.
UPaRTS-RSK-SAF-1	The system's abort function shall be independent from the main systems in terms of its infrastructure.	Verified	Verified by analysis: as shown in the hardware diagram on p. 39.
UPaRTS-RSK-SAF-1.1	The system's abort function shall be operable in the case of a power outage.	Verified	Verified by analysis: shown in the hardware diagram on p. 39.
UPaRTS-RSK-SAF-2	The system shall allow egress and access in the case of a power outage.	Verifiable	Verifiable by demonstration: this has been partially shown in Sec. 5.3; care has been taken to use non-flammable materials to aid in emergency egress safety.
UPaRTS-RSK-SAF-3	The system shall not induce adverse health effects due to prolonged use.	Verified	Verified by analysis: VR systems do not appear to induce statistically significant, lasting health effects[54]
UPaRTS-RSK-SAF-3.1	The system shall keep unintentional nauseating effects to a minimum.	Verifiable	Verifiable by testing: can only be verified through testing of the system
UPaRTS-RSK-TRN-1	The system shall allow for the IOS to set termination and restart conditions if degradatory conditions arise.	Verifiable	Verifiable by demonstration: this will be verifiable once the specifics of the motion planning algorithm are developed.
UPaRTS-RSK-AM-MOD-1	The numerical aircraft model shall account for, and mitigate erroneous model parameters.	Verified	Verified by analysis: this function has been taken over by the motion planning algorithm, to ensure that this safety-critical functionality lies at a single system.

As observed from the table, most of the requirements are either verified or verifiable which indicates that during the design process the majority of the requirements concerning risk have been taken into consideration. For the requirements that have not (yet) been verified it is safe to say that

these will also pose no issues in further stages as the verification can be done with certainty. The rationale for not having verified the two requirements UPaRTS-RSK-MNT-5 and UPaRTS-RSK-MNT-8 is solely due to time constraints but will be considered as post-DSE activity. Finally, none of the requirements regarding risk as represented in the table is labelled as non-verifiable which implies that these specific requirements have been continuously met and will also be met in later stages. Hence it can be concluded that the risk requirements are fully adhered to by the system.

### 8.3. Risk Analysis

In this ending stage of the design process the main objective of risk analysis is to re-evaluate the risks that were identified in [2] as the design has now been finalised. As budgets become tighter and design choices more and more specific, it is to no surprise that existing risk levels will fluctuate and additional risks will emerge. These additional risks will be analysed and assessed to ensure that the exposure of any of the subsystems to their most critical risks, is minimised. In the following, the risk managers adhere to the framework as proposed in Sec. 8.1, namely, the process of identifying, assessing, and mitigating risks. The result of this analysis will drive the final design considerations and will serve as an additional check for the feasibility of the system.

Similar to the risk analysis done in [2], this document will logically also solely focus on the design risks associated with the robotic arm design concept. However, unlike the analysis proposed in [2], this analysis will delve deeper into the risks that arise from the subsystem designs and especially the risks derived from the robotic kinematics, training systems and structures departments will play a major role in this risk analysis as these form the foundation of the entire system.

#### 8.3.1. Risk Matrix

In order to facilitate categorising and tracing the risks, each risk is assigned a unique code which encompasses its risk type and number. The risks are categorised into the following groups: System (S), Maintenance (M), Safety (SAF), Design (D), Training systems (TS), Sustainability (SUS) and Motion Kinematics (MK). As an example, the first identified risk that belongs to the system group will be denoted as R-S-1. In this subsection, the most prominent identified risks will be presented in Tab. 8.3 together with their corresponding causes, impacts, risk levels before and with mitigation (RBM, RWM), and mitigation plans. Finally, the subsection concludes with an elaboration on the rationales behind the grading of each risk that is mentioned in the proposed risk matrix. The risk matrix that is presented in Tab. 8.3 uses colours to indicate the risk levels which are additionally labelled with the first letter of the colour given to that specific cell. White (w) is associated with the least concerning risk based on its risk level, followed by green (g), orange (o), and red (r) representing the highest-concerning risk level as defined in Tab. 8.1.

Table 8.3: Risk matrix

Risk	Cause	Impact	RBM	Mitigation	RWM
R-S-1. Negative pilot training	Low training fidelity, cues provided to the pilot differ too much from real-life cues causing the pilot to train in unrealistic scenarios	Simulator does not fulfil its purpose of filling the gap in LOC-I. Erroneous muscle memory can possibly cause a dangerous situation in a real aircraft	1B (r)	Restrict training curriculum to high fidelity motions. Validate cues by letting an experienced pilot test the simulator	3C (o)
R-S-2. Non-compliance of lifetime requirement UPaRTS-SH-SO-06	Current lifetime specifications of robot arm are not specific enough. Requirement not verifiable at this stage	Violation of stakeholder requirement, possible cancellation of the project	1B (r)	Testing the robotic arm, contact supplier to get more accurate information on the lifetime. Possibly reinforcing robot arm	3D (g)
R-S-3. Numerical model development/procurement resource deficit	Insufficient research on model availability and detailed requirements	Non-compliance with model-related requirements	1B (r)	Detailed study as part of post-DSE activities	3C (o)
R-M-1. System is not able to function 23/7	Not enough time for maintenance, choice of robotic arm does not meet the uptime requirement	Top-level requirement violated, simulator downtime leading to less training flight hours per day	2B (r)	Perform adaptive maintenance (based on usage of simulator), find a robotic arm that guarantees 48 hours of continuous operation	3C (o)

Continued on next page

Risk	Cause	Impact	RBM	Mitigation	RWM
R-SAF-1. Fire outbreak in cabin	Overheating of electrical component, short circuit, abrasive nature of cables and fatigue causing brushing	Safety hazard, large damage and downtime for repairs	1B (r)	Fire retardants, testing components under high temperatures, cable management and insulation, fire extinguishers, emergency exit	2E (g)
R-SAF-2. Cabin state hindering egress	Power outage in combination with extreme robot arm state	Unsafe egress procedure, possible injury	1C (r)	Preventing extreme positions, emergency equipment (aerial work platform)	3D (g)
R-D-1. Cabin mass too high	To meet the acceleration requirements a different robotic arm with smaller payload has to be chosen, unexpected weight increase after iteration of the design	Robot arm cannot perform desired motion, cabin instruments might have to be left out, possible failure	2B (r)	Cut the cabin weight, find a different robotic arm	3D (g)
R-D-2. Failure of robotic arm due to insufficient stiffness	Cabin weight too high, off-the-shelf robotic arm is not fit for purpose	Structural failure, pilot injury, lower acceleration range	1B (r)	Lower cabin mass, find a stiffer robotic arm	2D (o)
R-D-3. Carriage is unfeasible or has to be adapted	Sizing of carriage has not been done yet	Design concept might have to be adapted, jeopardising use of linear rail, structural uncertainty	1B (r)	Size carriage as soon as possible (post-DSE activity). (In a similar way as risk management pushed the sizing of the linear rail in the beginning of the second iteration)	3C (o)
R-TS-1. Not being able to reach level-D certification	The concept might not be flexible enough or too novel to comply with the current (strict) regulations (Subsec. 4.1.3)	Marketability impacted as product could not legally perform proficiency checks in order to implement UPRT as described in Subsec. 4.1.3	2C (o)	Analyse requirements before committing, leave room for flexible design	3D (g)
R-SUS-1. Motion sickness	Discrepancies between different cues, low model fidelity	Training might have to be interrupted or cannot be completed, impact marketability of product	2A (r)	Look into system to synchronise motion cueing and visual buffer, test system	3C (o)
R-RK-1. Low motion cueing fidelity	Due to compounded effect of the physical robot arm cues and illusion of g-force of g-seat	Less immersion, might not meet the desired sensation of 1.75g	2B (r)	Testing to fine tune / define a way of using the g-seat in combination with the robot arm	3D (g)
R-RK-2. Disparity between numerical model and commanded cue	Path planning is not fast enough and might skip motion cues	Discontinuous and incomplete motion cues	2C (o)	Performance testing of the code using Monte Carlo techniques, defining a maximum execution time	4D (w)

The reasons behind the probability and severity gradings given to each risk in Tab. 8.3 are provided below.

- R-S-1** The risk of negative pilot training remains highly relevant as it is a risk that all flight simulators face. The severity of this risk is deemed 'catastrophic' (1) as in a worst case scenario, wrong muscle memory could lead to a dangerous situation in a real aircraft. If not enough effort is put into improving the fidelity of the flight simulator this risk is 'probable' (B) to happen.
- R-S-2** The severity of not meeting the lifetime requirement of 20 years is 'catastrophic' (1) as a top-level stakeholder requirement would be violated. It is hard to determine its likelihood as the reason for which this risk is listed in Tab. 8.3 is that a lot of uncertainty is linked to it. It is estimated that if not properly addressed, not reaching the intended lifetime is 'probable' (B) to happen.
- R-S-3** Not evaluating the resources needed to purchase or develop a numerical model can have severe consequences in terms of project feasibility, hence this risk is rated as 'catastrophic' (1). If no detailed study is performed in the post DSE-activities, it is 'probable' (B) that implementing the numerical model won't be possible.
- R-M-1** The impact of not meeting the uptime requirement is deemed 'critical' (2) as it would lead to non-compliance of a top-level requirement. However, this does not mean that the simulator cannot be used at all to train for UPRT. The structures department deems that this is a

hard requirement to achieve as a lot of uncertainty is linked to it. Hence, this risk is graded as 'probable' (B).

- R-SAF-1** In a worst case scenario a fire would endanger the life of a person, hence it is clear that this risk needs to be graded as 'catastrophic' (1). If no precautions are taken it is deemed 'probable' (B) for a fire to start due to the large amount of electronics close together.
- R-SAF-2** If egress is not guaranteed in a safe way for all possible training scenarios, the pilot's safety is jeopardised, hence this risk is deemed 'catastrophic' (1). The probability that the arm stops in a state that does not allow egress and that the arm cannot be moved is deemed 'occasional' (C).
- R-D-1** Not managing to have a light enough cabin would drastically limit the accelerations that can be achieved during training hence it is ranked as 'critical' (2). The probability of not finding a robotic arm that can carry the current cabin while providing the needed acceleration profile is deemed 'probable' (B).
- R-D-2** Low stiffness can lead to system failure and pilot injury, hence this risk is ranked as 'catastrophic' (1). If stiffness is not analysed in enough detail accidents are 'probable' (B) to happen.
- R-D-3** The impact of not determining the feasibility of the carriage can have drastic effects on the entire design philosophy (possibly not allowing the use of the linear rail) hence this risk is deemed 'catastrophic' (1). If this risk is not tackled in the next design phase it is 'probable' (B) that implementation of the carriage will be problematic.
- R-TS-1** If the product is not designed around the strict regulations for Level-D certification it is 'probable' (B) that despite design adaptations the certification cannot be obtained. This would negatively impact its marketability, which is deemed 'critical' (2).
- R-SUS-1** Motion sickness does not necessarily prevent the pilot from being trained, but inhibits the training curriculum, hence this risk has the severity 'critical' (2). If nothing is done to mitigate the nauseating effects of the simulator it is 'very probable' (A) to constitute a problem.
- R-RK-1** The choice of combining the illusion of g-forces provided by the g-seat and the 'real' g-forces from the other motion systems creates the risk that motion cueing fidelity is too low. This would negatively impact the training quality and is hence given the rating 'critical' (2). If the combination of these different motion systems is not properly studied it is 'probable' (B) that the cueing fidelity will be affected.
- R-RK-2** The method developed for motion planning needs to be tested as it might turn out to not be feasible. The severity would then be 'critical' (2) as adaptation would have to be made such that smooth robot arm movements can be obtained. If this is not tested the probability of this risk occurring is deemed 'occasional' (C).

Compared to the risk assessment in [2], some identified risks are omitted from the risk matrix (Tab. 8.3). Based on new design choices these risks either became less likely to happen or their severity was drastically reduced. The exact rationales for omitting these are given below.

**Not able to obtain certification for emergency system** - As presented in Subsec. 7.2 (Social sustainability - Safety) it is common for off-the-shelf robotic arms to have safety related certifications. Hence it is deemed that not obtaining such certification is less likely to occur.

**Tangled cables** - Proper cable management has been addressed in Subsec. 5.3.6. It is deemed that if enough thought is put into path planning and arrangement of cables, this risk can be completely mitigated.

**Breakage of energy chord alongside rail track** - Similarly to the previous risk, the movement of the energy chord is highly predictable as it follows the robotic arm along the rail system. It is deemed that the risk of breaking this chord due to the movement of the robotic arm has a too low likelihood to be included.

**Cabin crashing into surrounding objects, floor, person or wall** - The mitigation solution for this risk has been addressed in Sec. 5.5 and Subsec. 7.2 (Social sustainability - Safety). The motion of the robotic arm is going to be restricted to exclusively feasible points in the motion space. Through testing and validation of this solution, the risk of crashing can be completely mitigated.

**Training instructors is too resource intensive** - Attention has been paid to make the job of the instructor viable by coming up with a clear instructor guide to perform the training (See Subsec. 7.2, Social sustainability - User-friendliness). Hence it is believed that this risk is less likely to happen.

**System is not assemblable** - As the entire robot arm is bought off-the-shelf, assembly is reduced to connecting the arm to the rail system and mounting the cabin. This is far less complex than

the assembly for other design options that were considered in [2], hence the likelihood of this risk occurring is lower and it is omitted.

**Deformation/jamming of wheel and rail system** - It is deemed that the rail and the wheels supporting the robot arm can easily be oversized to make sure that these sustain the loads without compromising the rest of the design. Hence the likelihood of this risk is now lower.

**Failure of system due to poor maintenance** - This risk has been omitted because it is deemed more likely that there is not enough time for maintenance (reflected in risk R-M-1) than that maintenance is not done properly. Hence the issue of maintenance is entirely reflected in risk R-M-1.

**Adverse health effects and/or injury of pilot** - This risk has been omitted for multiple reasons. The cause for adverse health effects was prolonged use of the VR glasses. In Sec. 5.7 it is shown that VR systems do not appear to cause lasting health effects with enough statistical significance to be cause for concern. The cause for injuries was due to abrupt g-forces, which has been mitigated in Sec. 5.5 by defining the acceleration profile of the cabin based on a maximum acceleration and velocity. On top of that, the system will have to obtain strict safety certifications which will have to show that the probability of this risk is close to zero.

**Short circuiting of electronics** - The risk of a short circuit already has to be mitigated in R-SAF-1 to prevent fire outbreaks. Since these two risks are so interrelated this one has been omitted.

### 8.3.2. Risk Maps

The risks that have been identified and graded as shown in Tab. 8.3 are compiled in this subsection and presented in risk matrices that show the risk grades before and with mitigation. It can clearly be seen that before mitigation, most of the risks were found to be of high risk level (red). However, with the current mitigation plans that have been established, from Tab. 8.5 it can be observed that all risks have been moved over from high risk levels to acceptable risk levels (orange, green). This indicates that the mitigation plans that have been set up are likely to be effective.

Table 8.4: Risk map before mitigation

Probability	Severity			
	1 - Catastrophic	2 - Critical	3 - Marginal	4 - Negligible
A - Very probable	- (r)	R-SUS-1 (r)	- (o)	- (g)
B - Probable	R-S-1/2/3/SAF-1/D-2/3 (r)	R-M-1/D-1/RK-1 (r)	- (o)	- (g)
C - Occasional	R-SAF-2 (r)	R-TS-1/RK-2 (o)	- (o)	- (w)
D - Remote	- (o)	- (o)	- (g)	- (w)
E - Improbable	- (g)	- (g)	- (g)	- (w)

Table 8.5: Risk map after mitigation

Probability	Severity			
	1 - Catastrophic	2 - Critical	3 - Marginal	4 - Negligible
A - Very probable	- (r)	- (r)	- (o)	- (g)
B - Probable	- (r)	- (r)	- (o)	- (g)
C - Occasional	- (r)	- (o)	R-S-1/S-3/M-1/D-3/SUS-1 (o)	- (w)
D - Remote	- (o)	- R-D-2	R-S-2/SAF-2/D-1/TS-1/RK-1 (g)	R-RK-2 (w)
E - Improbable	- (g)	R-SAF-1 (g)	- (g)	- (w)

Finally, although a number of safety-related risks have been mitigated through implemented design changes, new risks have emerged at this stage of the project. These new risks have been included because of the uncertainty linked to them. It is likely that through thorough analysis in the post-DSE activities, these risks would pose less of a threat. It can be noted that the risk of negative pilot training (R-S-1) was treated in every risk assessment so far. This recurrent risk is likely to be a challenge until the very end of the design. The same goes for the risk of motion sickness (R-SUS-1), which can only be fully mitigated once the system can be tested. While these risks have to be worked on continuously, this risk assessment shows what the next important steps are in the design process. Research has to be put into finding or developing a suitable numerical model (R-S-3), through contact with suppliers and testing one hopes to get rid of the uncertainty linked to the uptime and lifetime requirements (R-S-2, R-M-1), preliminary sizing of the carriage needs to be performed as soon as possible (R-D-3) and a trade-off between high robotic arm accelerations and high cabin mass needs to be performed.

# 9 Future Plans

This section will discuss all logic and considerations beyond this report, describing future timelines and packages for the design as well as the business aspect of the product. It will first have a look at how the design deficiencies will be filled up in Sec. 9.1. This will be followed up by the business flow in Sec. 9.2. At last, the whole section will be visualised in Sec. 9.3. The future timeline consists of four discrete phases, these being the detailed phase (52 weeks), testing phase (52 weeks), production phase (25 weeks) and the delivery phase (4 weeks).

## 9.1. Design Considerations

During this report, and previous works [1–3], multiple functions and requirements were created. However, not all of these were taken into account due to the preliminary nature of this design phase. In this report the driving functions and requirements were taken into account to a sufficient level of detail. This was done with tools that are readily available, such as the NASA GTM aircraft model. The goal of the post-DSE phase from the technical perspective is to succeed and exceed in fulfilling the functions as described in page 34. This will all start with making decisions and keeping contact with producers for standard products, such as a relevant vehicle model from the OEM or the visual cueing provider. Besides, in the current design level, the fidelity quality of the simulation programs are reasonable but not design ready and should be increased. Besides, integration between the subsystems will be increased. This is done by means of testing, such as testing the acoustic position of the audio system. Although the inputs and outputs were described in this report, literal integration between all subsystems (Aural cueing and Aeromechanics) should be considered. Lastly, and maybe most importantly, based on stakeholder requirements, Level D certification or equivalent level D training capabilities should be met to create a meaningful training tool.

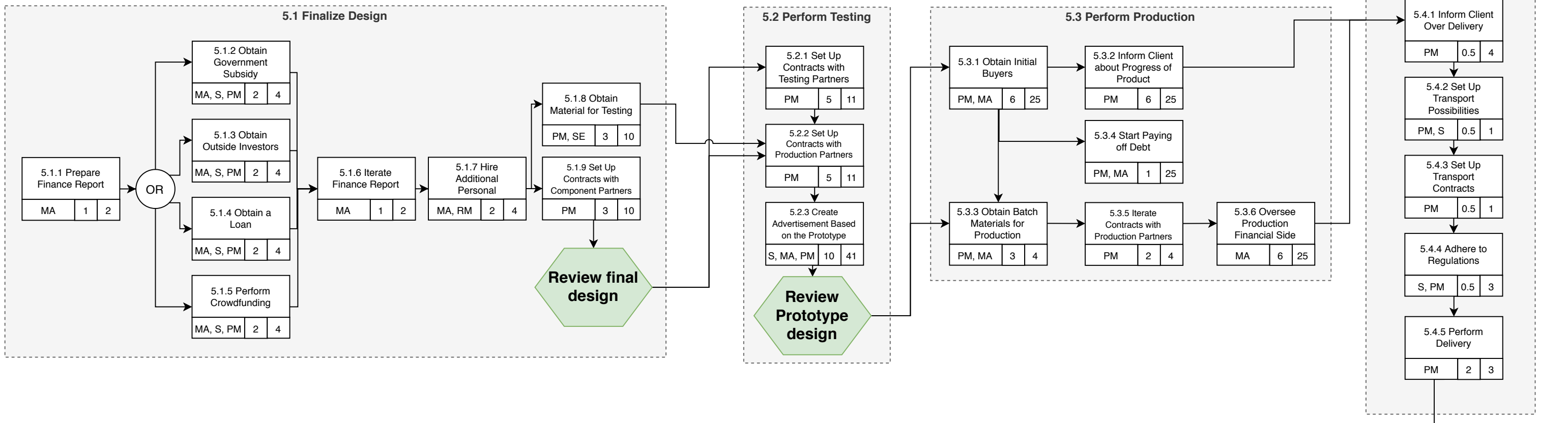
## 9.2. Business Considerations

Although a lot has been tackled in Ch. 3, this section describes the future on the business, administrative front. First, upfront additional investments have to be made to cover future costs (approximately 11.5 million euros) to cover the expanses before the first unit is sold. This money will cover the Finalise Design and Perform Testing phases, good for 104 weeks (2 years) where a feasible first product will be created and proved. Customers have to be persuaded to buy the simulator, which is done during the Perform Testing phase where the simulator prototype will be used to create advertisement for future customer interest. Another aspect of the business is hiring additional personnel to accompany the current group later on in the design, these are more detailed focus and needed to finish the overall design. Also do note that for every action (production, testing, personnel), contracts have to be set-up to determine criteria with the partners. Also, this category is responsible for the contact with the customer and all the administrative tasks connected with delivery.

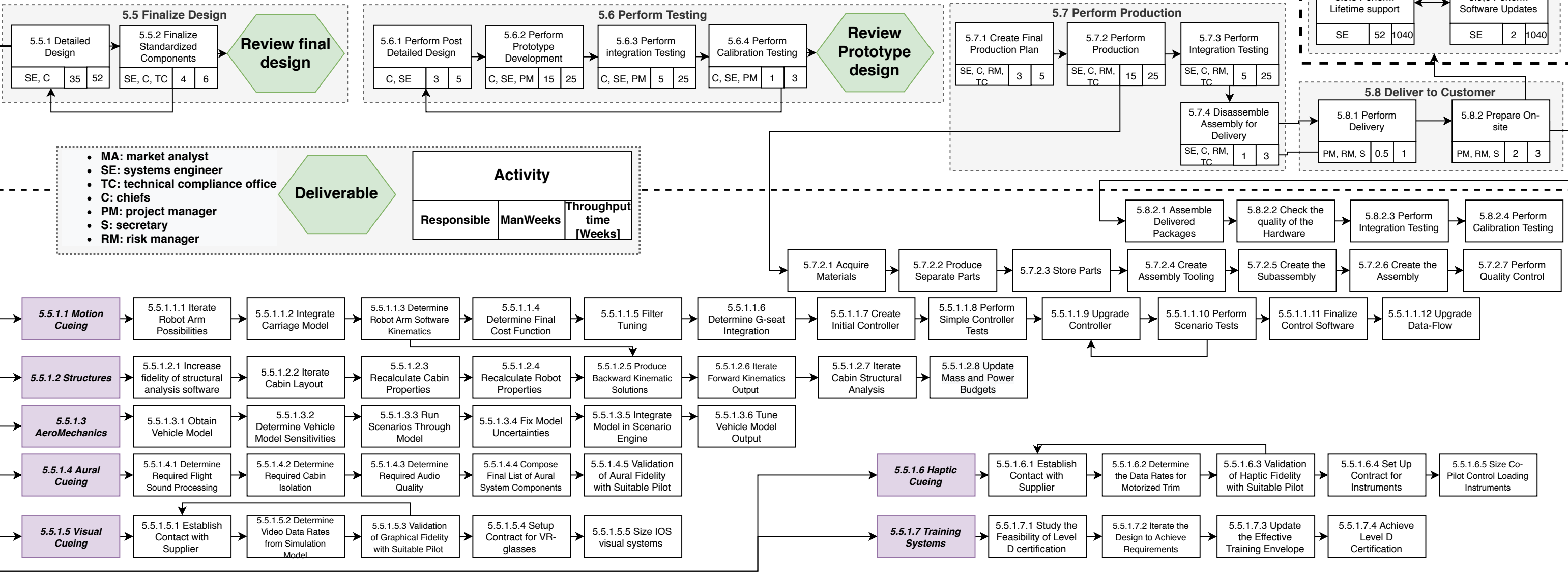
## 9.3. Future Project Logic

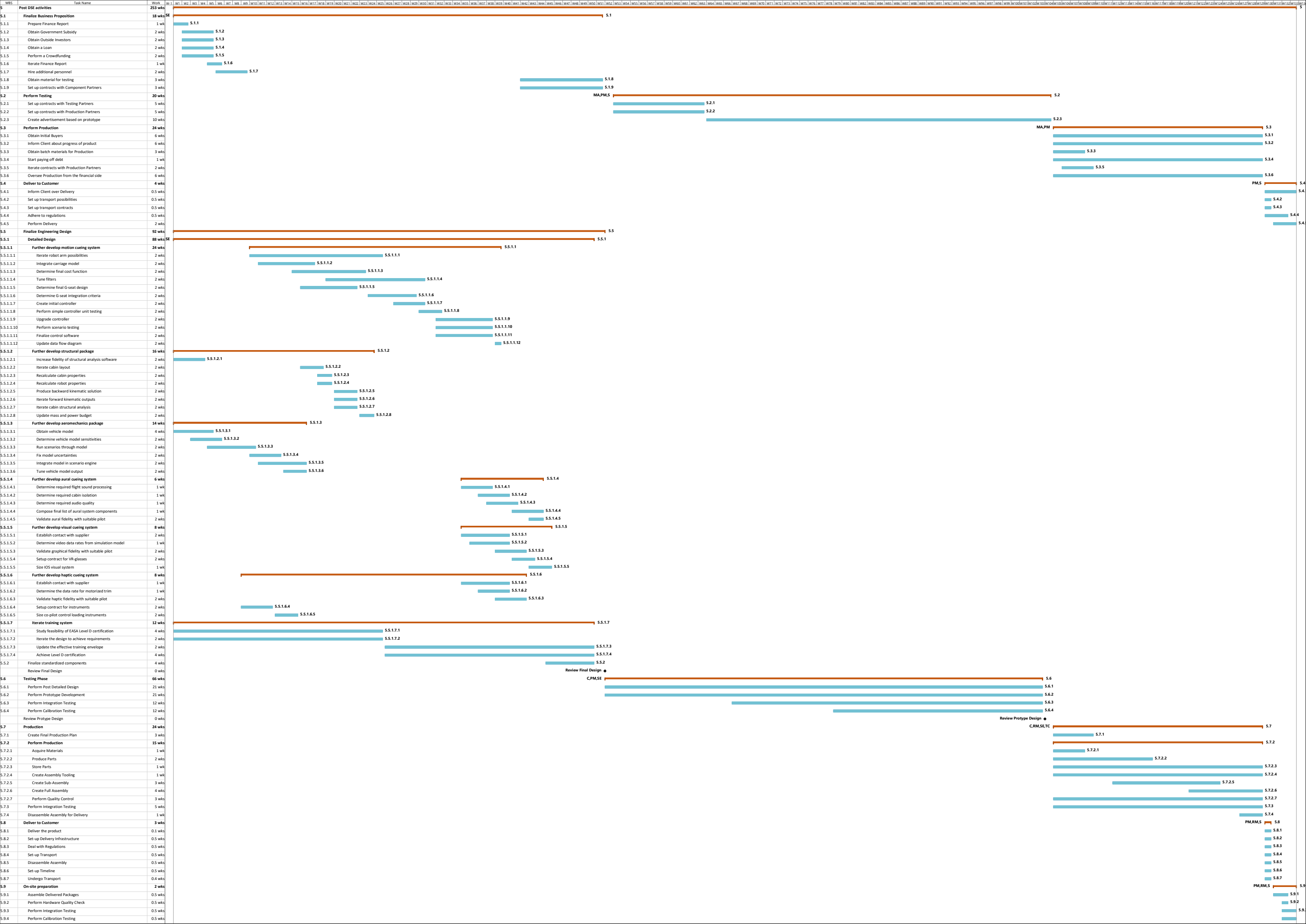
Taking all of the previous statements into account, project logic diagrams can be made consisting of a Gantt Chart Fig. 9.3, and a Project Design and Development Logic chart Fig. 9.3. Also the product lifetime is taken into account here. This is 20 years, 1040 weeks in total. This will include customer support as well as continues software updates related to security updates and glitch fixes. Besides, combined with the production lifetime of 20 years, and the design lifetime, the total project time equates to

## 5.0 Post DSE Business Flow Chart



## 5.0 Post DSE Design Flow Chart





# 10 Conclusion

At the start of this project, a mission need statement (MNS) was defined. To examine whether a device can be made that fulfils this defined need, a project objective statement (POS) was defined as a result of which several analyses were then performed. Following an initial consideration of the possibilities, a trade-off concluded that a robotic arm-based motion system had the best chance of successfully filling this need. A second iteration then found that the robotic arm mounted on a linear rail would be the most promising option.

Based on a market analysis, a market of at least seven UPRT simulators per year was found to exist. A regulation change will be critical in determining how successful this simulator could become in the market. Despite these risks, there is potential for this simulator to succeed in the market.

Having found a potential market, the pilot training curriculum is expanded upon to aid in the design of the subsystems. Several gaps in existing training curricula were identified: the limited inclusion of emotional response in training, no UPRT continuity throughout a pilot's career, and other limitations relating to the used flight simulation training devices. To cover these gaps adequately, goals were set for the system, including the possibility of simulating both upsets and normal operations, thereby ensuring the introduction of emotional response and facilitating training continuity. From these goals, a general training envelope was presented, alongside a proof-of-concept training guide for both the pilot and the instructor. From the analysed training constraints, it became apparent that in order to fully achieve the goals defined previously, a Level D certification should preferably be pursued in the future. This remains the greatest limitation of the system in its current iteration. With the training curriculum established, the subsystem design began, which serves to provide credibility to the design choices, showing that a system designed based on the deduced requirements is indeed feasible.

From a structural perspective, a cabin structure consisting of two parallel, hollow, aluminium beams, a connection to the robot arm and a carbon fibre shell, sized at 69 kg was found to be a possible solution. It is also confirmed that aluminium light weight bolts are sufficient to attach the cabin to the robot arm. The structure was found not to exceed floor loading limitations. However, due to sensitivity to assumptions a more thorough analysis of this floor loading is required. Finally, power- and data cables can be facilitated with off-the-shelf cable carriers. After deriving a number of motion cueing requirements from various sources (such as the NASA GTM model and crash data of the Airbus A330-203 crash on 2009-06-01), bounds were established on the capabilities of the motion cueing hardware and a promising motion cueing algorithm was set up. Through these analyses, more confidence was built up as to the feasibility of a real-time upset motion cueing system for a system utilising a linear rail, robotic arm, and g-seat. As for the aural, visual and haptic cueing systems, an analysis of existing devices shows that the required capabilities are well within the reach of current-generation audio systems, VR headsets and position tracking gloves. Possible existing solutions for each of these are an Ethernet-based audio system, the Pimax 8K PLUS VR headset and the Manus Prime motion capturing gloves.

Following the system sizing, the logistics revolving the production and operations of the simulator were given. A preliminary production plan showed that the simulator cabins can be produced in a separate factory and then shipped to the customer to be assembled. Considering the operations, it is understood that some preparations must be made by the customer in order to properly integrate the system, but the expected pilot throughput is in line with that of conventional simulators. As for logistics, the transportation, delivery, installation, and maintenance are covered, and none of these pose an added difficulty for the system. Upgradability was also covered, being a significant advantage associated with a VR cockpit, and finally the end-of-life processes for the system were described.

An analysis of the described design shows that this simulator can exist in a sustainable manner in all three senses of the word (environmental, economic and social). Continuous assessment throughout the project allowed for mitigation of a number of sustainability concerns and provided the possibility of making even greater contributions than expected: CO<sub>2</sub> emissions were cut by 89% in this iteration rather than the required 80%. Additionally, careful selection of the robotic arm manufacturer can allow for reuse of at least 75% of the simulator mass after the end of its lifetime.

In terms of risk analysis, the current remaining risks chiefly centre around the market and its compatibility with a non-Level D simulator, negative pilot training, the development of a suitable numerical model, the feasibility of low downtime operation, the stiffness of the robotic arm, the

development of a suitable carriage and prevalence of motion sickness. Because there are mitigation solutions available (that have been planned for implementation in the next stage of the project) however, these risks are not deemed critical to the mission.

Concluding, this project has ventured to design a market-viable flight simulator training device capable of meeting an ever-growing need for upset prevention and recovery training. This project objective was indeed met through a rigorous conceptual design process, taking into account the many aspects surrounding the market, training systems, cueing, and structural and environmental safety. While there remain tasks that are to be completed in later stages of the project, such as detailed system design and a more in-depth market analysis, it is safe to conclude that there are ample prospects to meet the mission need in the future.

## 11 Recommendations

In the past ten weeks, the initial subsystem design resulted in multiple recommendations for future design purposes. These recommendations span both the administrative aspect as well as the design aspect of the product. This section will quickly summarise points worth taking into account for future developers.

The administrative side spans the market analysis, risk analysis and sustainability. The focus for the market analysis is to manage the acquisition price of the product, manage the demand of the product and manage the product investment. The goal, in other words, is to have a vendable product and make sure that the design can continue without hindrances. The risk department should continue managing risks as well as continuously check for new risks that might arise during design. Besides, risk managers should check if the design requirements will be met as well as manage them if not. At last, the main recommendations for sustainability are to explore repurposing and recycling programs for components other than the robot arm, such that an end-of-life plan can be established. On the social sustainability side, user friendliness and motion sickness research should be performed.

To further develop the training systems, a few points are recommended. Firstly, the proof-of-concept training guides should be expanded to include all key exercises within the training curriculum, taking into account the achieved fidelity in further iterations of the design. Secondly, the Level D qualification objective must be further explored, and in case this proves unfeasible, a contingency should be drawn. It is beneficial both from a training and a marketing perspective if a market group for which a Level D qualification would not be required is identified. Adapting the training curricula from requirements that may result from this study will increase the product's value and marketability.

Structures should increase the fidelity of the analysis software as well as have a better integration with the robot motion kinematics. Besides, detail in the overall analysis is needed to present a realistic, ready-for-production system; bolt placement is an example of such detail. Aeromechanics should, in the future, look at integration with an OEM vehicle model and analyse the performance that flows from that model. Besides, it should expand upon the numerical model that currently is in place and add representative visual graphics to accompany the aircraft state. For Robot Motion Kinematics, it is recommended to start developing controller mathematics and controller software, focusing on integrating the proposed mathematical scheme with the dynamics of the robot arm. Besides, bigger emphasis should be placed on integration with the rail and the sustained motion cueing seat. A recommendation for the aural system is to start exploring the possibilities on (semi) custom made speakers, providing more accurate sound distribution. Besides, onboard isolation should be a greater part of the design, to mute noise from outside sources. For this, great strides can be expected by replacing the ventilation holes by an onboard air-conditioning system. For both visual cueing and haptic cueing the hardware is final. Recommendations are made to integrate it with other subsystems. On the visual side, the software capabilities should be explored while on the haptic side calibration should be performed. For haptic cueing, research could be done on the idea of a robotic sleeve (an robot integrated system on the pilot's arm/hand), moving away from the haptic gloves idea.

# Bibliography

- [1] Roemer Bakker, Andrea Bettini, Max Bouwmeesters, Hamza El-Kebir, Kaj Hoefnagel, Kevin Kho, Sebastien Origer, Afonso Tuna, Jacques Weijers, and Quirijn van Woerkom. DSE Group 11 Baseline Report: Flight Simulator for Upset Prevention & Recovery Training. Technical report, Delft University of Technology, Delft, The Netherlands, May 2020.
- [2] Roemer Bakker, Andrea Bettini, Max Bouwmeesters, Hamza El-Kebir, Kaj Hoefnagel, Kevin Kho, Sebastien Origer, Afonso Tuna, Jacques Weijers, and Quirijn van Woerkom. DSE Group 11 Midterm Report: Flight Simulator for Upset Prevention & Recovery Training. Technical report, Delft University of Technology, Delft, The Netherlands, May 2020.
- [3] Roemer Bakker, Andrea Bettini, Max Bouwmeesters, Hamza El-Kebir, Kaj Hoefnagel, Kevin Kho, Sebastien Origer, Afonso Tuna, Jacques Weijers, and Quirijn van Woerkom. DSE Group 11 Project Plan: Flight Simulator for Upset Prevention & Recovery Training. Technical report, Delft University of Technology, Delft, The Netherlands, April 2020.
- [4] IATA. Loss of Control In-Flight Accident Analysis Report. Technical report, IATA, Montreal, Canada, 2019.
- [5] Olaf Stroosma and DSE Group 11. Acceleration Loading Meeting June 04, 2020. June 2020.
- [6] Olaf Stroosma and DSE Group 11. Notes Tutor Meeting and presentation May 28, 2020. May 2020.
- [7] Laurens van Horssen, Coen C. de Visser, and Daan M. Pool. Aerodynamic stall and buffet modeling for the cessa citation II based on flight test data. In *2018 AIAA Modeling and Simulation Technologies Conference*. American Institute of Aeronautics and Astronautics, January 2018. doi: 10.2514/6.2018-1167. URL <https://doi.org/10.2514/6.2018-1167>.
- [8] H Kingma. Thresholds for perception of direction of linear acceleration as a possible evaluation of the otolith function. *BMC Ear, Nose and Throat Disorders*, 5(1), June 2005. doi: 10.1186/1472-6815-5-5. URL <https://doi.org/10.1186/1472-6815-5-5>.
- [9] Yuanbo Nie, Tobias Bellmann, Andreas Labusch, Gertjan Looye, Erik-Jan Van Kampen, and Q. Ping Chu. Aircraft upset and recovery simulation with the DLR robot motion simulator. In *AIAA Modeling and Simulation Technologies Conference*. American Institute of Aeronautics and Astronautics, January 2015. ISBN 9781624103438. doi: 10.2514/6.2015-1142.
- [10] Tobias Bellmann, Johann Heindl, Matthias Hellerer, Richard Kuchar, Karan Sharma, and Gerd Hirzinger. The DLR robot motion simulator Part I: Design and setup. In *2011 IEEE International Conference on Robotics and Automation*, pages 4694–4701. IEEE, May 2011. ISBN 9781612843865. doi: 10.1109/icra.2011.5979913.
- [11] *Determining Electric Motor Load and Efficiency Load Ranges*. U.S. Department of Energy.
- [12] *Robocoaster Specification*. KUKA Roboter GmbH, February 2003.
- [13] Tan Kiat Wee, Eduardo Cuervo, and Rajesh Balan. FocusVR. *Proceedings of the ACM on Interactive, Mobile, Wearable and Ubiquitous Technologies*, 2(3):1–25, September 2018. ISSN 2474-9567. doi: 10.1145/3264952.
- [14] Olaf Stroosma and DSE Group 11. Status Meeting June 06, 2020. June 2020.
- [15] Adrian Kampa. The review of reliability factors related to industrial robots. *Robotics Automation Engineering Journal*, 3(1):145–149, November 2018. doi: <http://dx.doi.org/10.19080/RAEJ.2018.03.555624>. URL <http://dx.doi.org/10.19080/RAEJ.2018.03.555624>.
- [16] Olaf Stroosma and DSE Group 11. Tutor feedback on the final report June 23, 2020. 2020.
- [17] Manual on Aeroplane Upset Prevention and Recovery Training. Technical Report Doc 10011, ICAO, Montreal, Canada, 2014.
- [18] Stephen P. Creamer. *Airplane Upset Prevention and Recovery Training Aid*. International Civil Aviation Organization, revision 3 edition, February 2017.
- [19] ICAO. *Document 9868 - Procedures for Air Navigation Services Training*. 2 edition, 2015. ISBN 978-92-9249-874-0. URL [www.icao.int](http://www.icao.int).
- [20] ICAO. Upset Prevention and Recovery Training (UP&RT) Provisions: What do they say and why? Mexico City, Mexico, January 2015.
- [21] Guidance Material and Best Practices for the Implementation of Upset Prevention and Recovery Training. Technical Report 2, IATA, Montreal, Canada.
- [22] Part-FCL. Technical Report 2, European Aviation Safety Agency, June 2016.
- [23] Seidl Helga. Pilot Training In Spatial Disorientation, Upset Prevention & Recovery: Appendix 2-Syllabus. Technical report, AMST-Systemtechnik, July 2015.
- [24] Annemarie Landman, Annemarie Van Den Hoed, Dirk Van Baelen, Olaf Stroosma, René Van Paassen, Eric Groen, and Max Mulder. A Scenario for Inducing the Leans Illusion in a Hexapod Motion Simulator. Unpublished.
- [25] John S. Duncan. Advisory Circular 120-111 - Upset Prevention and Recovery Training. Technical report, Federal Aviation Administration, January 2017.
- [26] Monica Martinussen. *Aviation psychology and human factors*. CRC Press/Taylor & Francis, Boca Raton, 2010. ISBN 9781439808436.
- [27] John S. Duncan. Advisory Circular 120-109A - Stall Prevention and Recovery Training. Technical report, Federal Aviation Administration, November 2015.
- [28] *A320 FCOM - Flight Controls*. Airbus, Blagnac Cedex, France, 36 edition.
- [29] Certification Specifications for Aeroplane Flight Simulation Training Devices. Technical Report 2, European Aviation Safety Agency, Cologne, Germany, May 2018.
- [30] C. A. Balafoutis and R. V. Patel. *Dynamic Analysis of Robot Manipulators*. Springer US, 1991. doi: 10.1007/978-1-4615-3952-0.
- [31] FANUC. Datasheet M-2000iA/1700L. Brochure, 2019. MDS-03833-EN.
- [32] Kevin Cunningham, David Cox, Daniel Murri, and Stephen Riddick. A piloted evaluation of damage accommodating flight control using a remotely piloted vehicle. In *AIAA Guidance, Navigation, and Control Conference*. American Institute of Aeronautics and Astronautics, August 2011. doi: 10.2514/6.2011-6451. URL <https://doi.org/10.2514/6.2011-6451>.
- [33] Sunjoo Advani and Joris Field. Upset prevention and recovery training in flight simulators. In *AIAA Modeling and Simulation Technologies Conference*. American Institute of Aeronautics and Astronautics, August 2011. doi: 10.2514/6.2011-6698. URL [www.nlr.nl](http://www.nlr.nl).
- [34] Final Report on the accident of flight AF 447. Technical report, The BEA: the French Civil Aviation Safety Investigation Authority, July 2012. URL [www.bea.aero](http://www.bea.aero).
- [35] Stefan Schuet, Thomas Lombaerts, Vahram Stepanyan, John Kaneshige, Kimberlee Shish, Peter Robinson, and Gordon Hardy. Vertical Motion Simulator Experiment on Stall Recovery Guidance. 2017. URL <http://www.sti.nasa.gov>.
- [36] Thomas Jordan, William Langford, Christine Belcastro, John Foster, Gautam Shah, Gregory Howland, Reggie Kidd, and Lockheed Martin. Development of a Dynamically Scaled Generic Transport Model Testbed for Flight Research Experiments. Technical report, NASA Langley Research Center, Hampton, Virginia, 2004. URL [www.larc.nasa.gov](http://www.larc.nasa.gov).
- [37] Tail strike on takeoff involving Airbus A320, VH-VGF. Technical report, Australian Transport Safety Bureau, May 2016. URL [www.atsb.gov.au](http://www.atsb.gov.au).
- [38] Jared A. Grauer, Eugene A. Morelli, and Daniel G. Murri. Flight-test techniques for quantifying pitch rate and angle-of-attack rate dependencies. *Journal of Aircraft*, 54(6):2367–2377, November 2017. doi: 10.2514/1.c034407. URL <https://ntrs.nasa.gov/search.jsp?R=20170001231>.
- [39] Tilbe Mutluay. The Development of an Inertia Estimation Method to Support Handling Quality Assessment. Technical report, Delft University of Technology, September 2015. URL <http://repository.tudelft.nl/>.
- [40] Richard M. Hueschen. Development of the Transport

- Class Model (TCM) Aircraft Simulation From a Sub-Scale Generic Transport Model (GTM) Simulation. Technical Report NASA/TM-2011-217169, Hampton, Virginia, 2011.
- [41] Torbjørn Cunis. *Modeling, Analysis, and Control for Upset Recovery - from System Theory to Unmanned Aircraft Flight*. PhD thesis, ISAE - Institut Supérieur de l'Aéronautique et de l'Espace, September 2019. URL <https://tel.archives-ouvertes.fr/tel-02555908>.
- [42] A. Da Ronch, D. Vallespin, M. Ghoreyshi, and K. J. Badcock. Evaluation of dynamic derivatives using computational fluid dynamics. *AIAA Journal*, 50(2):470–484, February 2012. ISSN 00011452. doi: 10.2514/1.j051304.
- [43] George E. Cooper and Jr. Harper, Robert P. Technical Report NASA TN D-5153, Moffett Field, California, April 1969.
- [44] Frank M. Cardullo, William J. Hewitt, and Gerald J. Kron. Advanced g-seat for aircraft simulation, October 1976.
- [45] Tobias Bellmann, Martin Otter, and Gerd Hirzinger. The DLR robot motion simulator part II: Optimization based path-planning. In *2011 IEEE International Conference on Robotics and Automation*, pages 4702–4709. IEEE, May 2011. ISBN 9781612843865. doi: 10.1109/icra.2011.5979914.
- [46] Y. Bar-Yam. When systems engineering fails-toward complex systems engineering. In *SMC'03 Conference Proceedings. 2003 IEEE International Conference on Systems, Man and Cybernetics. Conference Theme - System Security and Assurance (Cat. No.03CH37483)*. IEEE, doi: 10.1109/icsmc.2003.1244709. URL <https://doi.org/10.1109/icsmc.2003.1244709>.
- [47] Roy Featherstone. *Rigid Body Dynamics Algorithms*. Springer US, 2008. doi: 10.1007/978-1-4899-7560-7. URL <https://doi.org/10.1007/978-1-4899-7560-7>.
- [48] Rafał Lewkowicz and Grzegorz Kowaleczko. An inverse kinematic model of the human training centrifuge motion simulator. *Journal of Theoretical and Applied Mechanics*, 57(1):99–113, January 2019. doi: 10.15632/jtam-pl.57.1.99. URL <https://doi.org/10.15632/jtam-pl.57.1.99>.
- [49] Pyung Hun Chang. Analysis and control of robot manipulators with redundancy. Technical report, MIT Artificial Intelligence Laboratory, February 1988.
- [50] Olaf Stroosma. Project Guide Design Synthesis Exercise: Flight Simulator for Upset Prevention and Recovery Training. Technical report, Delft University of Technology, Delft, 2020.
- [51] Pernilla Ulfvengren. *Design of natural warning sounds in human-machine systems*. PhD thesis, Royal Institute of Technology, Stockholm, Sweden, 2003.
- [52] Bakker Stroosma. RE: Aural system questions June 12, 2020. June 2020.
- [53] Ian P. Howard and Brian J. Rogers. *Binocular Vision and Stereopsis*. Oxford University Press, February 1996. doi: 10.1093/acprof:oso/9780195084764.001.0001.
- [54] Jason Jerald. *The VR Book: Human-Centered Design for Virtual Reality*. Morgan & Claypool Publishers-ACM, 2015. ISBN 1970001127. URL [https://www.ebook.de/de/product/25202396/jason\\_jerald\\_the\\_vr\\_book.html](https://www.ebook.de/de/product/25202396/jason_jerald_the_vr_book.html).
- [55] J. Torres-Sanchez, S. Tedesco, and B. O'Flynn. A 3d hand motion capture device with haptic feedback for virtual reality applications. In *2018 IEEE Games, Entertainment, Media Conference (GEM)*, pages 232–238, 2018.
- [56] Susanne van der Veen, Martine Bordeleau, Peter Pidcoe, Christopher France, and James Thomas. Agreement analysis between vive and vicon systems to monitor lumbar postural changes. *Sensors*, 19(17):3632, August 2019. ISSN 14248220. doi: 10.3390/s19173632.
- [57] Airbus. Flight Operations Safety Awareness Seminar (FOSAS). Technical report, Nairobi, Kenya, 2017.